UNIVERSITÀ DEGLI STUDI DI MILANO

Facoltà di Medicina e Chirurgia

Dipartimento di Biotecnologie Mediche e Medicina Traslazionale
(BIOMETRA)

Dottorato di Ricerca in Medicina Sperimentale e Biotecnologie Mediche
XXX Ciclo

ATP-gated P2X7 receptor as a novel checkpoint molecule in T effector/memory cell function

Tesi di Dottorato di:

Elsa ROTTOLI

Matr. n. **R10997**

Tutor: **Prof. Fabio GRASSI**

Coordinatore del dottorato: **Prof. Massimo LOCATI**

Anno Accademico 2016 - 2017

TABLE OF CONTENTS

ABSTRACT

Adenosine triphosphate is an ubiquitous extracellular messenger, which activates P2 purinergic receptors in the plasma membrane of eukaryotic cells. Activation of P2 receptors regulates many cellular functions ranging from survival and proliferation to apoptosis. The final effect of extracellular ATP on a cell depends on the composition of P2 receptor expressed on its surface. We showed that T effector/memory (TEM) cells express high levels of *P2rx7* encoding for the ATP-gated ionotropic P2X7 receptor subtype. The deletion of the gene in these cells results in increased survival and cell proliferation both *in vitro* and in an *in vivo* model of homeostatic expansion. *P2rx7*$^{-/-}$ TEM cells are characterized by a bioenergetic advantage with respect to wild-type (WT) cells and morphometric analysis of mitochondria revealed that *P2rx7*$^{-/-}$ TEM cells are characterized by a fused mitochondria network, while WT TEM cells have more fissed mitochondria. Microarray gene expression analysis showed that *P2rx7*$^{-/-}$ TEM cells clustered together and separately from WT cells. Among differentially expressed genes we identified cyclin-dependent kinase inhibitor 1A (*Cdkn1a*), encoding for *p21*$^{Waf1/Cip1}$, as a transcript upregulated in WT cells. P21 inhibits progression through G_1 to S phase in mammalian cells and it is upregulated in senescent cells. We demonstrated that P2X7 signaling directly upregulated *Cdkn1a* in TEM cells and this resulted in a block in cell cycle progression. We hypothesize that P2X7 receptor could induce premature senescence in TEM cells. Accordingly, the analysis of β-galactosidase, a marker of senescence, revealed that P2X7 induces an increase in the enzyme activity in TEM cells. Moreover, WT TEM cells stimulated with a pharmacological agonist of P2X7 are characterized by increased in *Trp53* and *Gadd45b* expression as well as p38 MAPK phosphorylation. Moreover, P2X7 stimulation induces an increase in mitochondrial ROS and an increase in histone H2AX phosphorylation as a marker of DNA damage and cellular senescence. The tumor microenvironment is reach in extracellular ATP; we hypothesized this feature could affect TEM cells survival and function. In fact, we show that lack of P2X7 promoted expansion and accumulation of both CD4 and CD8 tumor infiltrating lymphocytes in a melanoma mouse model, thus favoring the control of tumor

size. Altogether our results point to P2X7 as a checkpoint for limiting CD4 TEM cells expansion in inflammatory environments that might be targeted to implement cytotoxic T cell responses in cancer immunotherapy.

INTRODUCTION

In mammals, the protection of the organism from invasion by pathogens is mediated by the two branches of the immune system. Innate immunity provides the early response against infections whereas adaptive immunity subsequently contributes the pathogen-specific immune response. Innate immunity consists of cellular and biochemical defense mechanisms that are in place also before infection and respond as soon as in contact with the pathogen. The principal components of the innate immune system are physical and chemical barriers, phagocytic cells (neutrophils and macrophages), dendritic cells and natural killer cells and other innate lymphoid cells, blood proteins including proteins of the complement system and other mediators of inflammation. In contrast to innate immunity, adaptive immunity is stimulated by protracted exposure to infectious agents, enhances the efficacy of the immune response and confers specific memory. In fact, the most important characteristics of the adaptive immune system are the specificity of the response, and the ability to respond more vigorously to repeated exposures to the same microbe (i.e. memory). T and B lymphocytes are the cellular components of the adaptive immune system.

1.T lymphocytes

1.1 T cell development in the thymus

T cell development begins in the bone marrow from a common lymphoid hematopoietic progenitor that migrates to the thymus. The thymus supports multistage lineage commitment and differentiation steps to yield mature and self-tolerant T cells. Thymopoiesis is initiated and maintained during fetal and neonatal life. In adulthood the thymus is smaller and possess limited T cell developmental potential (Donskoy and Goldschneider, 1992). In the thymus, T cell sub-lineages can be divided into two large classes, namely αβ and γδ T cells, which are distinguished on the basis of the T cell receptor (TCR). The choice between αβ and γδ fates is likely the first lineage decision made by progenitors and is instructed by TCR signaling. Stronger TCR signaling favors

γδ whereas weaker signaling favors αβ lineage development (Haks et al., 2005; Hayes et al., 2005); (Kreslavsky and von Boehmer, 2010). Thymocytes development proceeds through a series of steps that are broadly characterized by coreceptor expression, by TCR gene rearrangement and expression, and by expression of other markers such as cytokine receptors or activation molecules. Immature thymocyte precursors do not express either CD4 or CD8 coreceptor molecule and are defined as double negative (DN). At this stage, TCR genes rearrangement is initiated and cells become committed either to the αβ or γδ T cell lineage (Petrie et al., 1992). Development of αβ T cells is characterized by expression of the pre-TCR, which induces differentiation to the early CD4/CD8 double positive (DP) stage. Upon rearrangement of the TCR α-chain gene, the αβ TCR is expressed on the cell surface and the interaction with self-MHC molecules expressed on cortical thymic epithelial cells (cTECs) will determine the thymocyte fate. Initial TCR stimulation would eventually lead to downregulation of CD8 (CD4+8^{int} stage) and upregulation of the TCR. Modulation of CD8 would allow the thymocyte to detect whether its TCR is restricted by MHC class I (MHCI) or MHC class II (MHCII) molecule. Loss of signal strenght would implement the differentiation program related to MHCI restriction, whereas sustained signaling would result in differentiation of MHCII restricted CD4 cells (Singer et al., 2008). A TCR signal above a certain threshold induces thymocyte survival and differentiation, referred to as positive selection (Starr et al., 2003), whereas a strong signal causes activation-induced cell death (apoptosis), leading to negative selection of potentially self-reactive cells (Gascoigne et al., 2016; Palmer, 2003; Stritesky et al., 2012).

In the thymus we can distinguish four sequential phenotypes within DN cells; stages DN1 to DN4 based on expression of CD44, CD25 and CD117 (c-kit) (Godfrey et al., 1992). The DN1 subset (CD44+c-kit+CD25-) has high proliferative capacity and is able to give rise to both αβ and γδ cells. DN1 thymocytes differentiate into DN2 cells (CD44+c-kit+CD25+) that migrate outwards the thymus in the perimedullary cortex to the inner cortex (Lind et al., 2001). At this stages thymocytes can still be diverted to become dendritic cells (DCs) or natural killer cells (NKs). After migration in the outer cortex, they further differentiate into the DN3 cells (CD44-c-kit-CD25+). These cells are characterized by large-scale rearrangement of TCRβ, TCRγ and TCRδ loci,

orchestrated by non-redundant recombinase activating genes (RAG1 and RAG2) (Godfrey et al., 1994). Only cells that efficiently rearrange TCR genes proceed throughout the differentiation process, while those that fail to do so die (Michie and Zuniga-Pflucker, 2002). Some DN3 cells differentiate into γδ T cells, whereas other DN3 cells intensely proliferate and generate αβ lineage committed CD4+CD8+ double positive (DP) thymocytes (Ciofani et al., 2006), which are the most abundant cells in the thymus. Double positive thymocytes initiate the rearrangement of the TCRα locus and are selected based on the specificity of their clonotypic TCR. MHCI and MHCII specific T cells will develop into CD4 and CD8 single positive (SP) immunocompetent T cells, respectively, that will leave the thymus to seed the periphery (Petrie and Zuniga-Pflucker, 2007) (Bhandoola et al., 2007).

1.2 T cell activation

Mature T cells that have differentiated in the thymus are released into the bloodstream. These cells are considered immunologically naïve and are characterized by the high expression of L-selectin (CD62L) and chemokine receptor CCR7, both key molecules for the entry of T cells into lymph nodes through high endothelial venules (HEVs) (Berard and Tough, 2002). In lymph nodes, naïve T cells become activated and start to proliferate and differentiate upon antigen recognition. This occurs as a result of the interaction between the TCR and CD4 as coreceptor with peptide-MHC II complex presented by antigen presenting cells (APCs). TCR activation promotes a number of signaling cascades that ultimately determine cell fate through regulating cytokine production, cell survival, proliferation and differentiation into effector cells. The differentiation process is influenced by the cytokine milieu, the type of APC, the strength of TCR interaction and the nature of costimulatory molecules, which drive and control T cell number and fate. One of the most important costimulatory molecule identified in the early 1980s is the membrane receptor CD28. It was found to enhance TCR-induced proliferation and differentiation of naïve T cells. B7-1 (CD80) and B7-2 (CD86), the ligands of CD28, are expressed at high levels by activated professional APCs (Lenschow et al.,

1996; Pages et al., 1994). Other important costimulatory molecules are represented by the CD28 homologous inducible costimulatory (ICOS) and the members of the TNF receptor family (CD27, 4-1BB, and OX-40) (Coyle et al., 2000; Hutloff et al., 1999). T cells also express co-inhibitory molecules and one of the most studied is cytotoxic T lymphocyte antigen 4 (CTLA-4), which also binds to CD80 and CD86. CTLA-4 is induced following T cell activation and suppresses T cell responses. When CTLA-4 is upregulated, the T cell downregulates CD28 by exocytosis (Rudd et al., 2009). Expression of CD80 and CD86 is modulated by the activation state of the APC. CD86 is constitutively expressed on APCs at low levels; infections, stress and damage recognition by innate receptors activate APCs and induce increased expression of both CD80 and CD86 on the cells surface (Hathcock et al., 1994; Inaba et al., 1994). The modulation of receptors and ligands on T cells and APCs provides multiple levels of regulation for T cell activation (Flies and Chen, 2003). The earliest event in TCR activation is the phosphorylation of immunoreceptor tyrosine-based activation motif (ITAMs) on the cytosolic side of the TCR/CD3 complex by Src-like protein tyrosine kinases (PTK) lck and/or fyn. The phosphorylated ITAM is recognized by Src homology (SH) 2 domain of the Syk (spleen tyrosine kinase)-family kynase zeta-chain associated protein-70 (ZAP-70) PTK, which in turn is activated by Lck-mediated phosphorylation. ZAP-70 phosphorylates a number of downstream target sites, including tyrosines on the transmembrane adapter protein LAT and the cytosolic adapter protein src homology 2 (SH2) domain-containing leukocyte phosphoprotein of 76 kDa (SLP-76) (Iwashima et al., 1994; Zhang et al., 1999; Zhang et al., 1998). These adaptor proteins are fundamental for the correct activation of multiple signaling pathways. LAT is characterized by the presence of nine distinct tyrosines, which become phosphorylated upon TCR activation. LAT then functions as a scaffold for the recruitment and activation of several different SH2-domain-containing signaling proteins, such as phospholipase Cγ1 (PLCγ1), phosphoinositide 3-kinase (PI3K) and the cytosolic adapter/linkers proteins GRB2 and Gads (Sommers et al., 2004; Zhang et al., 1999). SLP-76 itself has three modular domains: an amino (N)-terminal acidic region with three tyrosine phosphorylation motifs, which interact with the SH2 domains of Vav1, Nck and IL-2 induced tyrosine kinase (Itk), a central proline-rich domain and a carboxy

(C)-terminal SH2 domain. The result of SLP-76 interactions is the stabilization of PLCγ1 (Koretzky et al., 2006). PLCγ1 activity is important for the activation of different signaling pathways such as Ca^{2+} influx, rearrangements of the cytoskeleton, interaction with integrins and DAG-induced responses. Activated PLCγ1 hydrolyzes phosphatidylinositol-4,5-bisphosphate into inositol-1,4,5-triphosphate (IP_3) and diacylglycerol (DAG), fundamental messengers to sustain T cell activation (Beach et al., 2007). Ltk that has been recruited to the membrane by SLP-76 interacts with PIP_3 that has been generated by PI3K (Berg et al., 2005) and is phosphorylated by lck. DAG generation is important for the activation of PKCθ and the activation of RAS/RAF/ERK through RAS-GTP. Two Ras GEFs are presents in T cells, son of sevenless (SOS) and Ras guanyl nucleotide-releasing protein (RasGRP). RasGRP appears to be important for early activation of Ras, as SOS cannot compensate for its deficiency (Dower et al., 2000; Ebinu et al., 2000). PKCθ activates the NFκB transcription factor that translocates to the nucleus where it activates genes involved in T cell functions (Schulze-Luehrmann and Ghosh, 2006) (Figure 1).

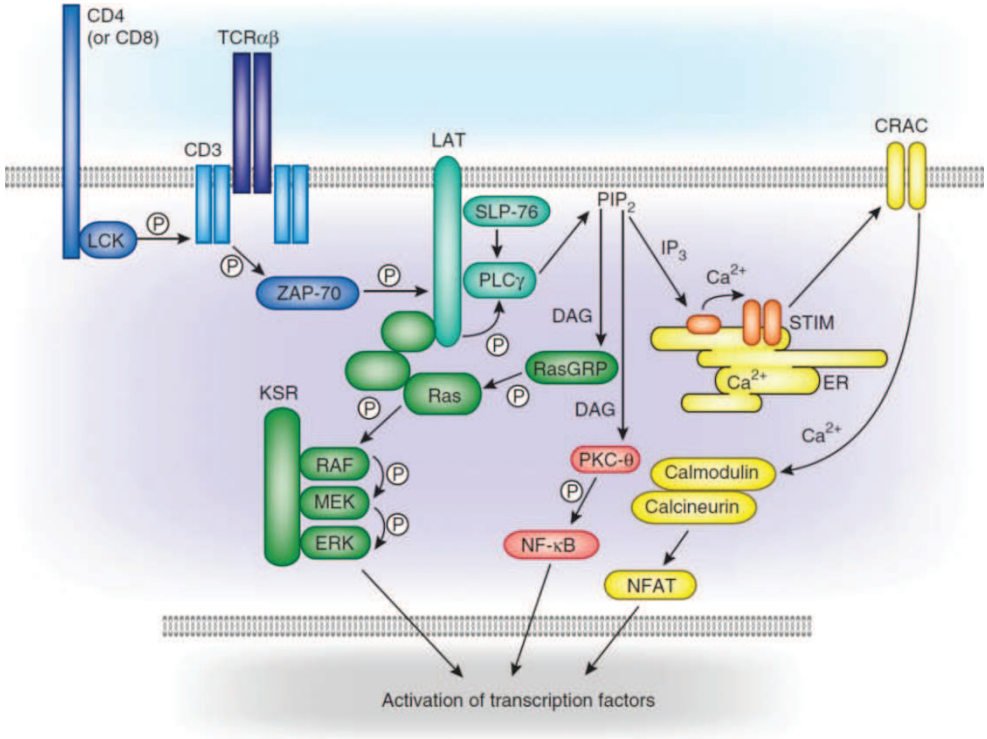

Figure 1: TCR signaling pathway. The recognition of the MHC-peptide complex by the TCR leads to a signaling cascade that involves the phosphorylation of proximal TCR components (blue), signaling by the Ras-Erk pathway (green), activation of the transcription factor NFκB (pink) by PKCθ, and Ca^{2+} flux-mediated signaling (yellow). These pathways activate transcription factors that mediate a variety of T cell developmental and effector programs (Morris and Allen, 2012).

TCR-induced increases in intracellular calcium and the activation of MAPK are critical for the activation of T cells. IP_3, generated by PLCγ1, binds to IP_3 receptor on the endoplasmic reticulum (ER) membrane, resulting in the release of Ca^{2+} from ER. The depletion of Ca^{2+} from the ER results in the opening of Ca^{2+} channels in the plasma membrane, triggered through the sensor STIM1 that participates to the generation of CRAC channels (Hogan et al., 2010). The influx of Ca^{2+} ions leads to the activation and nuclear translocation of NFAT through calcineurin and calmodulin (Kannan et al., 2012; Smith-Garvin et al., 2009). This results in the transcription of IL-2 and other genes important for regulating T cell activation (Dolmetsch et al., 1997; Wu et al., 2006). Nuclear translocation of NFAT determined by increase of cytosolic Ca^{2+} in the absence of the concomitant activation of the MAPK pathway results in T cell anergy.
Interaction with costimulatory molecules is necessary for T cell activation. CD28 plays a major role in cytokine production, cell survival and metabolism. CD28 ligation alone activates the PI3K pathway because it induces the phosphorylation of the kinases glycogen synthase kinase 3α (GSK3α) and GSK3β. This requires PIP_3-activated AKT kinase and is sensitive to pharmacological inhibition of PI3K (Appleman et al., 2002). This also implies PI3K-dependent activation of AKT by upstream PDK1. Activation of AKT is important not only for NFκB and NFAT pathways, but also for the expression of the anti-apoptotic protein BCL-X_L (Acuto and Michel, 2003; Beals et al., 1997).

1.3 T cell subsets

CD4+ T cells play a fundamental role by helping B cells to produce antibodies, but also orchestrating CD8 T cells and macrophages functions against a wide variety of microorganisms (Zhu et al., 2010). CD4+ T helper (Th) cells can be subdivided into heterogeneous subsets on the basis of their immunological functions, which are supported by the expression of well-defined profiles of specific transcription factors, cytokines and homing receptors. For many years the heterogeneity of CD4+ Th cells has been limited to Th1 and Th2 cells, which have been considered responsible for different types of protective responses and for the pathogenesis of many disorders. The identification of

new cytokines has allowed to enlarge the series of functional subsets of CD4+ Th effector cells. In particular, CD4+ Th cells producing IL-17 and IL-22, named Th17, have been implicated in the pathogenesis of many chronic inflammatory disorders. More recently, two other subsets of Th cells, namely Th9 and Th22 cells, have been described, even if their role in physiology and pathophysiology is still unclear (Annunziato and Romagnani, 2009; Romagnani, 1994). Another subset constituted by T follicular helper cells, is important for antibody responses, while regulatory T cells constitute a population whose function is to control immune reactions to self and foreign antigens.

1.3.1 Th1 cells

Th1 cells produce high levels of IFN-γ and are responsible for both phagocyte activation and production of opsonizing and complement-fixing antibodies. This subset is responsible for the protection against intracellular pathogens (Romagnani, 1994). IL-12 is the key factor needed to generate Th1 cell differentiation, but also IFN-γ plays an important role, as shown by the fact that its neutralization during IL-12 driven Th1 differentiation partially diminishes this polarization (Bradley et al., 1996). During Th1 differentiation both IL-12 though STAT4 and IFN-γ through STAT1, promote the activation of the master regulator transcription factor of Th1 subset, T-bet. T-bet activation causes a feedback which ends in the increased production of IFN-γ and higher T-bet expression, amplifying Th1 differentiation (Yamane and Paul, 2012). At later stages, IL-12/STAT4 signaling induces the upregulation of IL-18Rα. IL-18 and IL-12 together induce IFN-γ production by Th1 cells in the absence of TCR receptor stimulation, amplifying Th1 responses (Annunziato and Romagnani, 2009). In addition to their protective functions from pathogens, Th1 cells also play a role in the development of autoimmune diseases and chronic disorders such as experimental autoimmune encephalomyelitis (EAE), collagen-induced arthritis and inflammatory bowel disease (IBD) (Cosmi et al., 2014; Hirahara et al., 2013) (Figure 2).

1.3.2 Th2 cells

Type 2 immune response confers protection against infection by extracellular parasites, like helminths, but can also promote acute and chronic inflammatory responses against allergens (Pulendran and Artis, 2012). Th2 cells regulate type 2 responses through the secretion of various type 2 cytokines, including IL-4, IL-5, IL-9 IL-13, IL-10, IL-25 and amphiregulin. Th2 polarization from naïve CD4 T cell is achieved because of the early production of IL-4 during the primary response (Parronchi et al., 1992). IL-4 and IL-13 regulate the production and secretion of IgE by B cells during allergic responses. IgE binds to low affinity Fc receptor for IgE (FcεRI) on basophils and mast cells and their interaction with a multivalent ligand induces cross linking of FcεRI. This leads to the secretion of mediators such as histamine and serotonin and the production of several cytokines such as IL-4 and IL-13. IL-5 positively regulates different eosinophils functions, such as eosinophilopoesis, bone marrow release and survival (Coffman et al., 1989). IL-9 production contributes to mast cell and IgE response. Moreover, it induces mucin production in epithelial cells (Faulkner et al., 1998; Longphre et al., 1999).

As a consequence to IL-4 production and binding to its receptor, Th2 cells activate STAT6, which in turn upregulates GATA-binding protein-3 (GATA3). This transcription factor is the master regulator of Th2 development and is fundamental for the production of IL-13 and IL-4 (Kaplan et al., 1996). GATA3 alone, however, is not sufficient to induce IL-4 production. IL-2 mediated activation of STAT5 plays a critical role and the collaboration of STAT5 and GATA3 accounts for full differentiation of Th2 *in vitro* (Zhu et al., 2006).

Importantly, there is a mutual regulation of Th1 and Th2 polarization induced by IL-4 and IFN-γ, respectively, as well as Th1-specific and Th2-specific transcription factors. It was shown that GATA3 can downregulate STAT4, while strong activation of STAT5 inhibit T-bet expression. On the other hand, T-bet can suppress GATA3 expression (Usui et al., 2003; Usui et al., 2006; Zhu et al., 2003) (Figure 2).

1.3.3 Th17 cells

The Th17 subset is primarily involved in recruiting leukocytes and inducing inflammation. This reaction is critical for destroying extracellular bacteria, fungi and contribute to inflammatory diseases. Th17 have been also implicated in the pathogenesis of most common autoimmune diseases such as rheumatoid arthritis (RA), inflammatory bowel disease (IBD) and multiple sclerosis (MS) (Annunziato et al., 2007). Th17 cells produce main effector cytokines as IL-17A (referred to as IL-17), IL-17F, IL-22, and IL-21. Their differentiation requires retinoid-related orphan receptor (ROR)γt, a transcription factor induced by TGF-β in combination with the pro-inflammatory cytokines IL-6, IL-21 and IL-23, all of which activate STAT3 phosphorylation (Chen et al., 2007). Despite TGFβ is the critical signaling cytokine necessary for Th17 differentiation (Veldhoen et al., 2008; Volpe et al., 2008), is now clear that TGF-β can also induce the differentiation of inducible T regulatory (iTreg) cells depending on the cytokine milieu. The balance between Th17 and iTreg could be influenced by the ability of natural Treg (nTreg) cells to produce TGF-β, but in the presence of inflammatory cytokines naïve T cells differentiate into Th17 cells (Veldhoen et al., 2006; Zhou et al., 2009). Mice lacking TGF-β are depleted of both Th17 and Foxp3+ Treg cells and develop autoimmunity caused by uncontrolled Th1 cell activity (Li et al., 2006). TGF-β signaling seems to play an important role in STAT3 stabilization by inhibiting IL-6/IL-21-induced expression of suppressor of cytokine signaling 3 (SOCS3), which negatively regulates STAT3 signaling (Qin et al., 2009). Several other transcription factors have been implicated in modulating the RORγt/Foxp3 balance during T helper cell differentiation. IRF4 is essential for Th17 differentiation both i*n vitro* and *in vivo* (Brustle et al., 2007). Mice lacking *Irf4* are characterized by reduced RORγt and increased Foxp3 expression as well as lack of IL17 production. They are protected from experimental autoimmune encephalomyelitis (EAE). *Irf4* was also identified as a direct target of Foxp3 and its selective loss in Treg cells impairs the suppression of Th2 cells response (Zheng et al., 2009). Another transcription factor important for Th17 differentiation is Runx1, which was shown to form a complex with RORγt to promote Th17 cell differentiation (Zheng et al., 2008). However, in Treg cells, Runx1 interacts with Foxp3 and suppresses the production of IL-2

and IFN-γ, thus promoting Treg cells suppressive activity (Ono et al., 2007). Runx1 is also required to maintain Foxp3 expression in nTreg and in TGF-β induced Foxp3 iTreg cells. Thus, the ability of Runx1 to cooperate with both RORγt and Foxp3 maintains the functional plasticity of Th17 and iTreg. Th17 cells, moreover, selectively express the aryl hydrocarbon receptor (AHR), a ligand-dependent transcription factor. The activation of AHR results in the expression of IL-22, promoting Th17 development and related cytokines. Mice lacking AHR are still able to develop Th17 cell responses, but they are unable to produce IL-22 and show defective Th17 cells differentiation (Veldhoen et al., 2008). As previously discussed, the amplification process is necessary to mount a correct immune response and T cell differentiation program. IFN-γ and IL-4 are the main amplifying cytokines for the generation of Th1 and Th2 cells, respectively, while IL-21 plays this role for Th17 cells polarization. IL-21 with TGF-β amplifies Th17 cells differentiation. IL-6 is not required in this phase that is therefore independent from TCR signaling (Korn et al., 2007). IL-23, another fundamental cytokine, acts together with IL-1β to induce $Tbet^{+}ROR\gamma t^{+}$Th17 cells independently of TGF-β (Ghoreschi et al., 2010) (Figure 2).

1.3.4 Th22 cells

Beyond Th17 cells, a subset referred to as Th22 cells is an important source of IL-22. In humans, Th22 cells are characterized by the production of IL-22 with little or no IL-17 and have been observed in healthy caecum, where they play an important role in maintaining mucosal barrier function (Wolff et al., 2012).

1.3.5 Th9 cells

Th9 lymphocytes are a pro-inflammatory subset of T helper cells, which are involved in different inflammatory conditions, including autoimmune diseases and allergic reactions. They are primed in response to TGF-β and IL-4. Th9 development depend upon IL-4 activated transcription factor STAT6 (Veldhoen et al., 2008). It is still not clear if Th9 cells are required as a source of IL-9 during autoimmunity and how they cooperate with Th2 in promoting inflammation (Jabeen and Kaplan, 2012).

1.3.6 T follicular helper (Tfh) cells

T cell help to B cell is fundamental for adaptive immunity and generation of immunological memory. Bcl6 is the master regulator transcription factor of Tfh cells (Johnston et al., 2009; Nurieva et al., 2009). Tfh cells are characterized by the expression of CXCR5, PD1, SAP (SH2D1A), IL-21, ICOS and absence of the transcription factor Blimp1. They express high levels of Bcl6, while non-Tfh cells express high levels of Blimp1. Blimp1 suppresses the expression of Bcl6 and, on the contrary, Bcl6 suppresses the expression of Blimp1 (Crotty, 2011). Tfh cells are fundamental for the formation and maintenance of germinal center (GC), the regulation of B cell differentiation into plasma cells and memory B cells (Crotty, 2011). CXCR5 is the canonical marker of Tfh and is necessary for the migration of Tfh cells in response to CXCL13 (Schaerli et al., 2000). The migration of Tfh cells to the T-B border allows Tfh differentiation thanks to the expression of ICOSL by B cells. ICOS engagement in Tfh cells activates PI3K and leads to the production of IL-21 (Rolf et al., 2010). To induce GC formation, Tfh cells must drive GC B cell differentiation by stimulating the expression of Bcl6 in activated B cells. Once the GC is formed, Tfh cells provide the signals necessary for the survival and the proliferation of GC B cell, promote somatic hypermutation and select proficient GC B cells (Allen et al., 2007). There are different pathways through which Tfh cells stimulate B cells, including CD40L, IL-4, IL-21, PD1 and BAFF, which compete with Fas-FasL interaction. In the absence of pro-survival stimuli, GC Tfh cells promote GC B cells death through Fas-FasL. The final result of GC reaction is the production of functional memory B cells and high affinity plasma cells. The production of high affinity antibodies is a fundamental process necessary to block the spread of pathogens in the body, so a large proportion of Tfh cells functions is dedicated to B cell survival and proliferation. However, Tfh and GC B cell processes must be tightly regulated in order to avoid the development of autoimmunity and lymphoma (Crotty, 2011) (Figure 2).

1.3.7 Treg cells

T regulatory (Treg) cells, which constitutively express the transcription factor Foxp3, are indispensable for the maintenance of immune self-tolerance and homeostasis by suppressing aberrant or excessive immune responses that might be harmful to the host (Rudensky, 2011; Sakaguchi et al., 2008). The majority of natural Foxp3+ T reg (nTreg) cells are produced by the thymus as antigen-primed mature T cells. Another subset differentiates in the periphery from naïve cells and is defined inducible Treg (iTreg). nTerg cells migrate into inflammation sites and suppress effector lymphocytes (Chaudhry et al., 2009; Chung et al., 2011). Treg cells produce IL-10, TGF-β and IL-35. IL-10 is a potent inhibitory cytokine, which suppresses inflammatory responses and limits tissue damage (Asseman et al., 1999; Ouyang et al., 2011). IL-10 and TGF-β exert a potent anti-allergic action and suppress the production of IgE (Jutel and Akdis, 2008). TGF-β is the central cytokine that promotes iTreg cell lineage commitment (Chen et al., 2003). TGF-β signaling activates Smad2 and Smad3, which are upstream of Foxp3 expression (Takimoto et al., 2010). However, it was demonstrate that Smad2 and Smad3 can also induce Treg cells differentiation via a Foxp3-independent pathway. Smad3 inhibits Th17 developmental program by blocking RORγt (Martinez et al., 2009). STAT5 is another important transcription factor that enhances Foxp3 expression. The target DNA sequence of STAT5 and STAT3 is represented by a common multiple site across the IL-17 locus. The two transcription factors function closely and antagonize each other. Defective STAT5 signaling impairs Treg cells differentiation and favors polarization to Th17 (Laurence et al., 2007) (Figure 2).

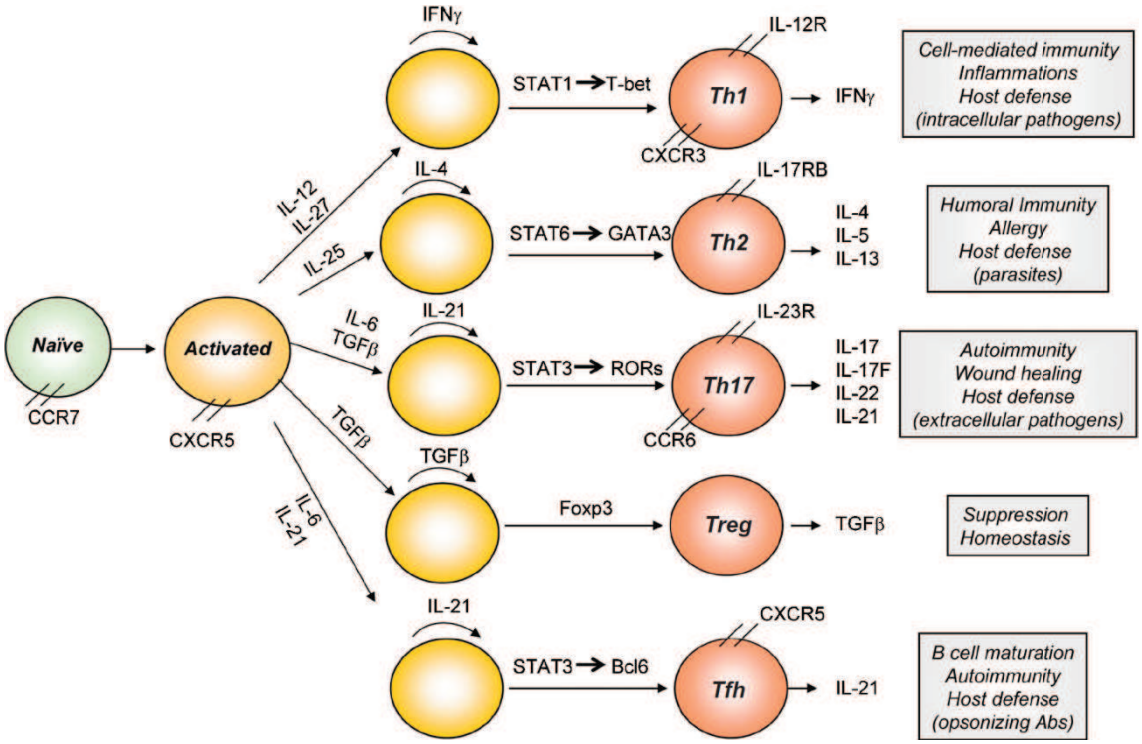

Figure 2: Effector Th cell differentiation. Upon encountering antigen presented by professional APCs, naive CD4 T cells differentiate into effector subsets (Th1, Th2, Th17, Treg and Tfh) that are characterized by specific cytokine production, expression of transcription factors and chemokine receptors, and immune regulatory functions (Nurieva and Chung, 2010).

1.4 Memory T cells

T cell mediated immune responses result in the generation of antigen specific memory T cells, which may persist for years, even a lifetime. They are able to migrate to peripheral tissues and rapidly respond to antigen stimulation. Memory T cells are classified depending on their homing ability and effector functions. Until recently, memory T cells were divided in central memory T cells (TCM) which are restricted to secondary lymphoid tissues and blood, and have little or no effector function; effector memory T (TEM) cells, which migrate between peripheral tissues, blood and spleen, and display immediate effector functions (Sallusto et al., 1999). A third subset of memory T cells has been recently described, namely tissue resident memory T (TRM) cells (Mueller et al., 2013). TCM cells constitutively express CCR7 and CD62L, that are also expressed by naïve T cells and are necessary for adhesion to high endothelial venules (HEV) and migration to secondary lymphoid organs (Campbell et al.,

1998; Forster et al., 1999). Compared to naïve T cells, TCM are more sensitive to antigenic stimulation, less dependent on co-stimulation and upregulate CD40L, thus providing more effective feedback to dendritic cells (DC) and B cells. TCM cells produce IL-2 after antigen stimulation, and when they differentiate to effector cells, they produce large amount of IFN-γ and IL-4. TEM cells have extinguished CCR7 expression, are heterogeneous for CD62L expression levels, and display chemokine receptors and adhesion molecules required for the homing to inflamed tissues. They are characterized by rapid execution of effector functions and produce IFN-γ, IL-4 and IL-5 following antigen stimulation (Sallusto et al., 2004). There are mechanisms such as competition for cytokines and other survival factors, expression of anti-apoptotic genes such as BclXL and availability of space at a given site, that play a fundamental role in the generation of proper adaptive immune memory (Di Rosa and Santoni, 2003). TCR signal strength is another important factor in determining T cell differentiation. The strength of signaling that T cells receive can depend on the antigen concentration, the presence of costimulatory molecules and the duration of the interaction between T cells and APC (Iezzi et al., 1998; Valitutti et al., 1995; Viola et al., 1999). DC/T cell interactions are very dynamic and different levels of stimulation may be delivered at different times. At early stages, a high number of DC with a large dose of antigen and secreting a large amount of cytokines would promote a massive proliferation of antigen-specific T cells, which become effector cells and some of them will persist as TEM. At later time points, fewer DC are recruited, carrying lower amount of antigen with exhausted cytokine-production capacity (Langenkamp et al., 2000). This condition may lead to the expansion of non-effector cells, some of which will persist as TCM. According to this model, TEM cells are generated at early stages, whereas TCM cells at later stages of the immune response. The strength of TCR signal and intensity of cytokine receptors stimulation drive T cells through hierarchical thresholds of differentiation (Lanzavecchia and Sallusto, 2002). These are stochastic events, meaning that not all the cells will receive the same strength of signal. As a consequence, primed T cells reach different stages that contain both effector cells and cells that have been arrested at intermediate levels of differentiation and are retained into lymph

nodes. This spectrum can be simply resolved into distinct subsets of TCM and TEM surviving after antigen clearance (Figure 3).

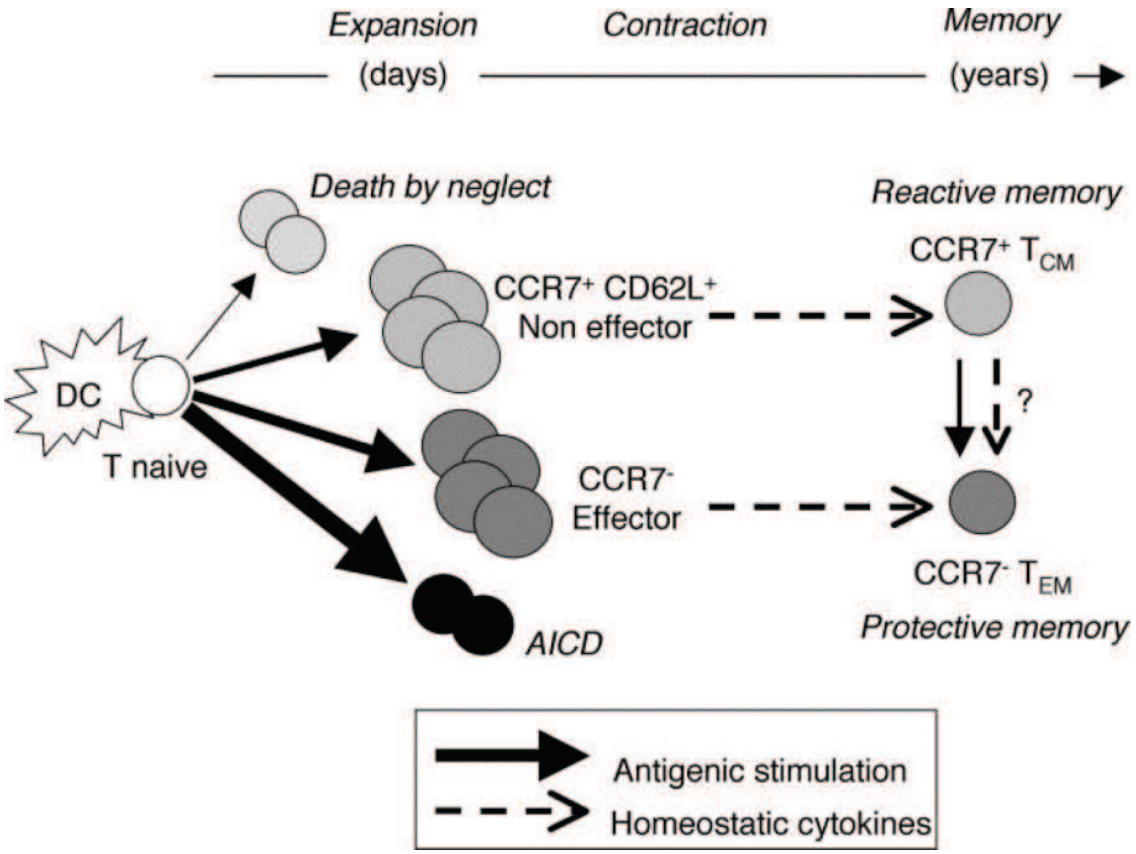

Figure 3: A signal strength model for T cell differentiation and memory generation. The progression follows a sequence of proliferation, preceding the acquisition of fitness, effector function and death. The duration and intensity of antigenic stimulation is indicated by the length and thickness of the solid arrow. Antigen-independent events leading to T cell proliferation and differentiation are indicated by the dotted lines. AICD, activation-induced cell death (Sallusto et al., 2004).

2.Regulatory mechanisms of T cell functions

2.1 T cell exhaustion

T cell exhaustion is considered a state of T cell dysfunction that arises during chronic infections, cancer, autoimmunity and chronic inflammation. Exhausted T cells are defined as effector T cells with decreased cytokine expression and effector functions, and resistant to reactivation. They are characterized by

sustained expression of inhibitory receptors and have a distinct transcriptional profile compared to effector or memory T cells. T cells that become exhausted are not able to control infections and tumors (Wherry, 2011). Loss of function of exhausted T cells occurs in a hierarchical manner, meaning that some functions are lost before others. Three immunoregulatory inducers are involved in T cell exhaustion: cell surface inhibitory receptors (such as PD1), soluble factors (such as IL-10) and immunosuppressive cell types (such as Treg and other cells). T cells can transiently express inhibitory receptors during activation, but the prolonged expression of multiple inhibitory receptors is a key features of exhausted T cells (Virgin et al., 2009). Inhibitory receptors are important in different aspects of adaptive immunity, including self-tolerance and prevention of autoimmunity (Freeman et al., 2006). The PD1/PD-L1 axis is one of the major pathway involved In T cell exhaustion and blocking this pathway during infections increases T cell responses against pathogens. This means that T cell exhaustion is an active process that could be reversed in order to improve T cell function (Barber et al., 2006). Other cell surface inhibitory receptors, such as LAG3 CD244 (2B4), CD160, TIM3, CTLA-4, are involved in T cell exhaustion (Crawford and Wherry, 2009). In addition to cell surface inhibitory receptors, Foxp3+CD4+Treg cells can affect immune responses during chronic infections and in tumors (Penaloza-MacMaster et al., 2014; Virgin et al., 2009). Their suppressive activity in the presence of immuneregulatory cytokines, such as IL-10 and TGF-β, are involved in the induction of T cell exhaustion (Brooks et al., 2006; Tinoco et al., 2009). The molecular pathways of exhausted T cells are TCR dependent, such as SPRY2 and NFAT (Agnellini et al., 2007; Martinez et al., 2015). Chronic antigen stimulation induces NFATc1 translocation to the nucleus and as a consequence the upregulation of PD1 (Oestreich et al., 2008). Both CD4 and CD8 exhausted cells are characterized by a specific transcriptional profile that include major changes in the expression of costimulatory and inhibitory molecules, signaling molecules, transcription factors, cytokine and chemokine receptors and gene involved in cellular metabolism (Crawford et al., 2014; Doering et al., 2012; Wherry et al., 2007) (Figure 4).

2.2 T cell anergy

T cell anergy is defined as a state of induced hyporesponsiveness characterized by low IL-2 secretion, which is induced in naïve T cells following low co-stimulatory and/or high co-inhibitory stimulation. It serves to induce tolerance in the periphery and protect the host from developing autoimmune diseases (Schwartz, 1990, 2003). This state of anergy can be induced by a strong TCR signal in the absence of co-stimulation or by stimulation with low affinity ligand in the presence of co-stimulation (Mirshahidi et al., 2001). All of these conditions result in a weak or incomplete activation of the cell, but sufficient to induce de novo protein synthesis to maintain the anergic state (Quill and Schwartz, 1987). The principal signaling pathway that seems to be involved in the induction of anergy is NFAT translocation into the nucleus. In fact, around 40 years ago it was shown that cyclosporine A, a selective inhibitor of NFAT, could block anergy induction (Jenkins et al., 1990). In some cases the anergic state seems to be determined by excessive calcium/NFAT signaling that results in transcriptional enhancement of negative regulatory elements of TCR/CD28 signaling (Telander et al., 1999).

Anergy in T cells is characterized by an unusual pattern of cytokines expression in response to TCR stimulation, that suggests a state of resistance to proliferation (Jenkins et al., 1987; Mueller et al., 1991). When the T cell is restimulated by APCs and the antigen, IL-2 production is mostly affected, but also IL-4 and IFN-γ production are compromised. Inflammatory chemokine production is unaffected. These anergic T cells are characterized by the block in the activation of the Ras/MAP kinase pathway (Fields et al., 1996; Li et al., 1996). Both the ERK and JNK pathways are inhibited and there is one report of a block in the p38 pathway (DeSilva et al., 1997). Importantly, when anergic T cells are transduced with constitutively active MAP kinase, IL-2 activity is restored (Zha et al., 1996). Diacylglicerol kinase-α (DGK-α) plays a central role in the induction of anergy as a negative regulator of the TCR signal (Zha et al., 2006). DGK-α phosphorylate DAG, converting it into phosphatidic acid and depleting available DAG that otherwise could activate RASGRP1 (Tognon et al., 1998). Future studies are directed at developing pharmacological approaches to

promote anergic state in autoimmunity and transplantation as well as to restore T cell function in cancer and chronic infections (Figure 4).

2.3 T cells senescence

Cellular senescence was first described in fibroblasts where the erosion of telomeres at each cell division initiates a cascade of events which lead to growth arrest (Akbar and Henson, 2011). The process of cellular senescence can also be independent of telomeres shortening, when there is an accumulation of DNA damage anywhere in the genome that leads to the upregulation of p53 gene transcription. P53 in turn induces the transcription of the cyclin dependent kinase inhibitors (CDKN) 1A (also known as p21) and 2A (p16) (Campisi and d'Adda di Fagagna, 2007) and, as a consequence, prolonged arrest of the cell cycle (Di Leonardo et al., 1994). Long-term activation of the checkpoint gene CDKN1A creates a feedback inducing mitochondrial dysfunction and production of reactive oxygen species (ROS) through serial signaling through GADD45-MAPK14(p38MAPK)-GRB2-TGFBR2-TGFβ. These ROS in turn replenish short-lived DNA damage foci and maintain an ongoing DNA-damage response (DDR) (Passos et al., 2010). DNA damage induces the recruitment of ATR and ATM kinases, which phosphorylate the histone H2AX on Serine 139 (γH2AX), a key step for the recruitment of DDR. The intracellular sensing of DNA damage activates the machinery of DNA repair, which, if successful, enables the cell to survive. If DNA cannot be repaired, DNA damage repair foci persist within the nucleus, leading ultimately to growth arrest and senescence (d'Adda di Fagagna, 2008). The accumulation of senescent cells is associated with aging of tissues (van Deursen, 2014).

Immunosenescence is defined as the overall decline of immune function during ageing that involves both innate and adaptive immune system (Franceschi et al., 1999). T cell senescence refers to low proliferative activity, which could result from excessive telomeres erosion due to the induction of proliferative activity, or to DNA damage due in part to mitochondrial dysfunction leading to increased production of ROS (Henson et al., 2014). For T cells in peripheral blood, there is a correlation between the sequential loss of costimulatory

receptors and telomeres erosion. Senescent T cells with the shorter telomeres are characterized by lack of the expression of CD27 and CD28 (Plunkett et al., 2007). These cells are also found in young individuals, especially if they have genetic defects that lead to excessive proliferation after T cell activation (Plunkett et al., 2005). Until now it was not clear if senescent phenotypes after activation was a passive or an actively maintained process involving the activation of inhibitory pathways. It was demonstrated that both senescent fibroblasts and T cells are characterized by the constitutive activation of p38 MAPK (Davis et al., 2010; Henson et al., 2015; Lanna et al., 2014).

Molecular Feature[b]	Fibroblast[c]	T Cells[c]
Proliferation	↓	↓
Telomere length	↓	↓
Telomerase activity	↓	↓
Apoptosis	↓	↑
β-Galactosidase	↑	?
γH2AX	↑	↑
p16	↑	?
p53	↑	↑
p38	↑	↑
Cytokine production	↑	↑

Table 1: Characteristics of fibroblast and T cell senescence. The majority of data on cellular senescence are derived from experiments on fibroblasts. While T cells also undergo senescence, some of the molecular features are different. The key features of senescence phenotype are common to fibroblasts and T cells, such as lack of proliferation, short telomeres and the inability to upregulate telomerase. However, a major difference is susceptibility to apoptosis with fibroblasts being long-lived and T cells succumbing to death. Furthermore, it is not known whether senescent T cells express high levels of β-galactosidase or γ-H2AX (Akbar et al., 2016).

Two separate pathways have been described for p38 MAPK activation in T cells. The canonical MAPK cascade activated by cytokines or costimulatory receptors, that culminates in p38 activation (Lanna et al., 2014) and an alternative pathway where TCR ligation induces p38 autophosphorylation independently of upstream canonical MAPK activity (Patterson et al., 2014). However, it was observed that senescent T cells do not express several kinases and scaffold molecules that are involved in this alternative p38 activation pathway, and are thus unlikely to engage this second pathway for p38 activation (Lanna et al., 2014; Salvador et al., 2005). This suggested the existence of a

third unique mechanism for the activation of p38 in senescent T cells. This third p38 activation pathway in T cells was identified recently; it involves the activation of a molecular complex that contains AMP-responsive protein kinase (AMPK, a sensor activated by low nutrient and energy availability), the scaffold molecule TAB1 (TGF-β-activated kinase 1 and MAP3K7-binding protein 1), and p38 itself. This complex induces p38 activation through autophosphorylation. The key point is that AMPK in T cells is activated not only by low intracellular glucose but also by endogenous DNA damage (i.e. senescence). This suggests that there is a convergence of senescence and nutrient-sensing pathways in T cells to activate p38 via AMPK/TAB1. Correspondingly, inhibition of either AMPK, TAB1, or p38 itself reconstitutes proliferation as well as telomerase activity in the senescent T cell population (Lanna et al., 2014) (Figure 4).

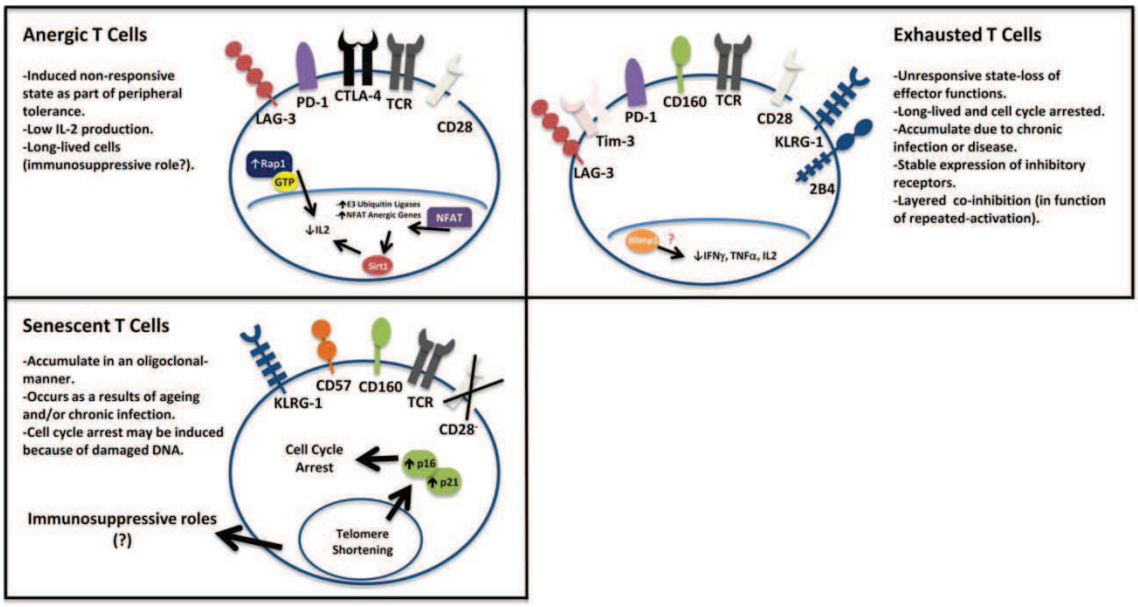

Figure 4: General characteristic for anergic, exhausted and senescent T cells. Anergic T cells are T cells stimulated with low co-stimulatory and/or high co-inhibitory signaling. These cells are unresponsive to subsequent activating conditions with limited IL-2 expression. Exhausted T cells are effector T cells that have lost their effector functions including effector cytokine expression due to repeated stimulation. These cells express multiple regulatory receptors. Senescent T cells are described as unresponsive/terminally differentiated T cells. The hallmark is their cell cycle arrest along with limited CD28 expression and/or high levels of regulatory receptor expression (modified from (Crespo et al., 2013).

2.4 T cell metabolism

The regulation of T cell metabolism is fundamental in order to mount a correct immune response and to develop memory. When T cells are activated, they go through as series of modifications in their metabolism in order to meet the increased metabolic demands of cell growth. In T lymphocytes, glucose is a critical substrate for adenosine triphosphate (ATP) production (Greiner et al., 1994). During glycolysis the glucose is broken down into two molecules of pyruvate. This process that does not require oxygen gives rise to two molecules of reduced nicotinamide adenine dinucleotide (NADH) and two molecules of ATP per molecule of glucose. The pyruvate can enter into the tricarboxylic acid (TCA) cycle in the mitochondria and generates NADH and reduced flavin adenine dinucleotide ($FADH_2$), which the cell can use to fuel oxidative phosphorylation (OXPHOS), an oxygen dependent process that produces up to 36 ATP molecules per molecule of glucose. Alternatively, pyruvate can be transformed into lactate, regenerating NAD^+ to be used in glycolysis (Vander Heiden et al., 2009).

Resting naïve T cells, which never encountered the antigen, maintain low rate of glycolysis and utilize predominantly OXPHOS or fatty acid oxidation (FAO) to produce ATP, accordingly with their non-proliferative state (Figure 5). Upon antigen recognition, T cells have to face a massive proliferation and become metabolically activated. They switch to a program of anabolic growth and biomass accumulation to generate daughter cells, which increase the need of ATP and metabolic resources (Pearce et al., 2013) (Figure 5). TCR signaling directs the metabolic reprogramming of T naïve cells, promoting the upregulation of glucose and amino acids transporters (Frauwirth et al., 2002; Sinclair et al., 2013) in order to facilitate nutrients uptake. TCR activation induces the upregulation of c-Myc and estrogen related receptor α (EERα) (Wang et al., 2011), which enhances the expression of genes of the metabolism and suppress the catabolic pathways of ATP. Activated T cells then use aerobic glycolysis and convert pyruvate into lactate despite the availability of oxygen for complete glucose oxidation. This process is known as Warburg effect in cancer biology and is a common trait of proliferating cells (Vander Heiden et al., 2009).

When the antigen is cleared, the majority of T effector cells die, but a subset of long-lived memory T cells (TM) persists. TM cells are a quiescent population and, as a consequence, they adopt a metabolic profile similar to that of naïve (a catabolic metabolism characterized by increased OXPHOS and low nutrients uptake compared to T effector cells) (Figure 5). However, T memory cells are characterized by increased mitochondrial mass and as a consequence increased spare respiratory capacity (SRC) (van der Windt et al., 2012). These characteristics of TM cells allow for a rapid mitochondrial ATP production upon TCR engagement, conferring a bioenergetic advantage to TM cells when exposed to the antigen a second time and for this reason they are viewed as metabolically primed (van der Windt et al., 2013).

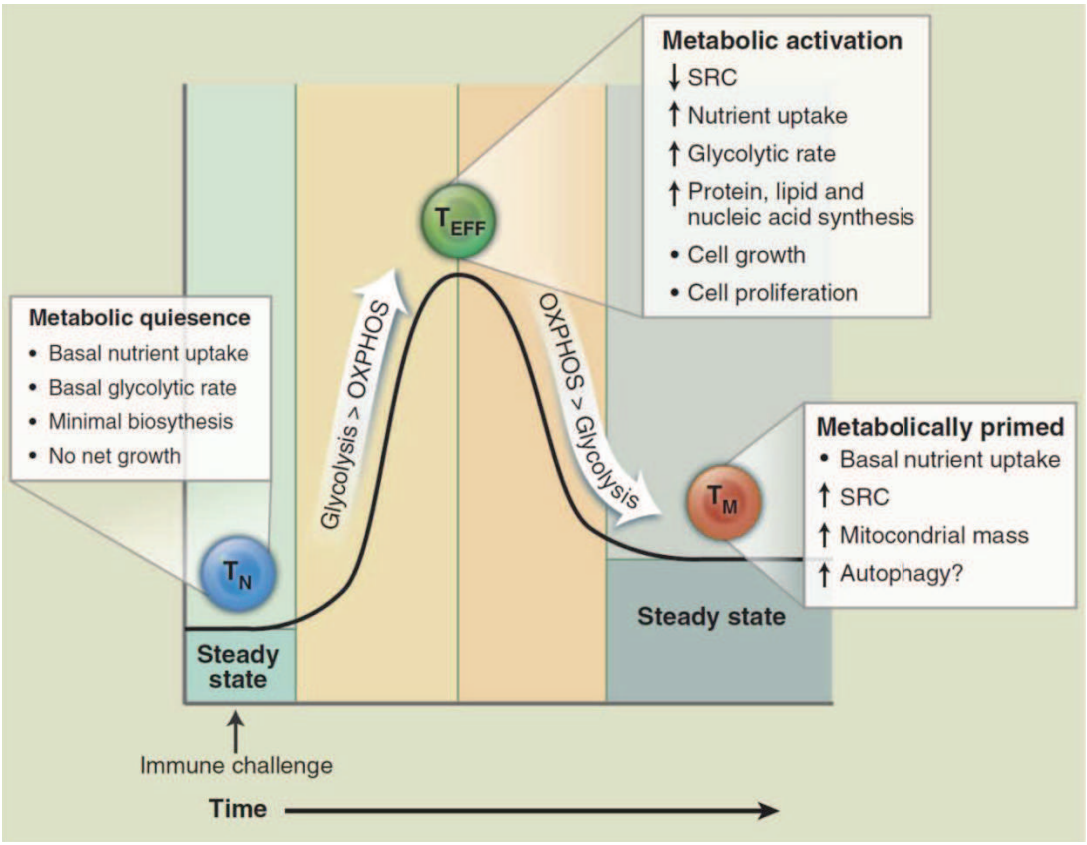

Figure 5: T cell metabolism changes over the course of an immune response. T cells display distinct metabolic profiles depending on their state of activation. Naïve T cells (TN, blue) are metabolically quiescent; they adopt a basal level of nutrient uptake and use OXPHOS as their primary pathway of ATP production. Upon immune challenge, TEFF (green) cells shift to a state of metabolic activation characterized by increased nutrient uptake, elevated glycolytic and glutaminolytic metabolism, biomass accumulation, and reduced mitochondrial SRC. TEFF cells preferentially use glycolysis over OXPHOS for ATP production. Transition to the TM (orange) stage is characterized by a quiescent metabolism, with increased reliance on FAO to fuel OXPHOS. Mitochondrial mass and SRC are elevated in TM cells, suggesting that these cells are metabolically primed to respond upon reinfection (Pearce et al., 2013).

Several transcription factors and signaling pathways support these changes in T cell metabolism after activation. IL-2 and ligation of costimulatory molecules promote the switch to glycolysis through the increase of nutrient transporter expression and the activation of the key metabolic regulator mTOR (Frauwirth et al., 2002; Jones and Thompson, 2007; Kolev et al., 2015). The ligation of CD28 enhances PI3K activity, which phosphorylates PDPK1. PDPK1 itself phosphorylates Akt, which activates mTORC1. Both Akt and mTOR promote aerobic glycolysis and support effector T cell differentiation and function (Delgoffe et al., 2011; Pollizzi et al., 2015). HIF1α, a transcription factor that responds to oxygen level, also increases glucose uptake and catabolism through glycolysis (Kim et al., 2006). Mitochondrial are fundamental for the regulation of metabolic activity of T cells, antiviral responses and cell death. They constantly remodel their structure via nuclear-encoded GTPase (Nunnari and Suomalainen, 2012). Recently, it was shown that mitochondrial dynamics (fusion and fission) can control T cell fate through metabolic reprogramming (Buck et al., 2016). Fissed mitochondria increase reactive oxygen species (ROS) production (Yu et al., 2006), facilitate mitophagy (Frank et al., 2012), accelerate cell proliferation (Taguchi et al., 2007) and mediate apoptosis (Youle and Karbowski, 2005). Mitochondrial fusion, instead, is considered a survival mechanism in response to stress and starvation and it is linked to longevity (Friedman and Nunnari, 2014; Gomes et al., 2011; Rambold et al., 2011). T memory cells are characterized by fused mitochondria with tight cristae, while mitochondria in T effector cells are fused and characterized by more separated cristae (Buck et al., 2016). Without tight cristae, the electron transport chain (ETC) of the mitochondria is less effective and electrons may loiter in the complexes causing an increase in ROS production (Sena et al., 2013). The protein optic atrophy 1 (Opa1), responsible for inner mitochondrial membrane fusion, is necessary for the generation of T memory cells, but not T effector cells. Moreover, enforcing fusion in T effector cells improves adoptive therapy against tumors, because T cells are characterized by increased longevity and persistence, without affecting the ability of producing cytokines (Buck et al., 2016).

3. T cell in the tumor

T cells are recruited in the tumor as a defense mechanism against it. In the past years, the presence of T cells in the tumor has been correlated with a favorable prognosis in patients with melanoma (Clark, 1991) and in more recent years in patients with ovarian cancer (Sato et al., 2005), bladder cancer (Sharma et al., 2007), renal cell carcinoma (Nakano et al., 2001) and others solid tumors. It seems that the capacity of the immune system to respond against the tumor is directly correlated to the amount of tumor infiltrating lymphocytes (TILs). Over the past years, TILs has been identified in the primary tumor, tumor draining lymph nodes and metastases of numerus cancer types. Depending on the type of tumor, TILs can highly or poorly infiltrate it. However, cancers that express weakly immunogenic antigens evade killing and this can be a primary mechanism of tumor progression (Vesely and Schreiber, 2013). Tumors are also known to escape immunity via T cell dysfunction or hyporesponsiveness, as exhaustion, anergy and senescence, which have been all described in cancer patients (Crespo et al., 2013; Wherry, 2011) .

3.1 Anti-tumor activity of CD4 and CD8 T cells

TILs comprise a heterogeneous group of lymphocytes that differ in their ability to potentiate the anti-tumor immune response. Both CD4+ and CD8+ T cells were found in tumors and in vitro experiments showed that CD4+ TILs produce cytokines after stimulation with the tumor and CD8+ TILs exert an anti-tumor cytolytic activity (cytotoxic T lymphocytes, CTLs) and are dependent on CD4+ T helper activity (Goedegebuure and Eberlein, 1995). However, the role of CD4+ T cells seems to be more complicated and controversial. In particular, CD4+ T cells are characterized by plasticity that might results in switching from anti-tumor to tumorigenic function (Sorensen et al., 2012). CD4+ Treg cells are present in the tumor and exert an immunosuppressive function. On the contrary, Th1 cells would play a positive role in tumor rejection through the secretion of IFN-γ. IFN-γ has an important role in increasing the density of major histocompatibility complexes (MHC) I and II in tumor cells and APCs, increasing

the ability of T cells to reject the tumors. The lack of expression of MHC II is one of the causes of variable efficacy of CD4+ T cells to exert an anti-tumor function (Donia et al., 2013). However, IFN-γ is considered a double edged sword because it selectively enhances responses to tumor-associated antigens and reduces tumor cells susceptibility to immune-mediated cytotoxicity (Donia et al., 2013; Zaidi and Merlino, 2011). CD4 cells can exert a direct anti-tumor activity by recognizing endogenously processed antigens followed by secretion of type 1 cytokines or by providing help to CD8+ T cells (Friedman et al., 2012; Quezada et al., 2010). TILs are characterized by the expression of different co-inhibitory receptors, which downregulate lymphocyte activation and effector function. Both CD4 and CD8 express CTLA-4, which, as described above, shares the CD80 and CD86 ligands with CD28, but with higher affinity and may therefore out-compete it (Collins et al., 2002). CTLA-4 is a negative regulator of CD28-dependent T cell responses and, as a consequence, it contrasts anti-tumor responses of TILs. This has been demonstrated in many pre-clinical models of cancer, thus suggesting that interfering with this pathway in patients may also result in improved survival (Quezada and Peggs, 2013). Another co-inhibitory molecule expressed by TILs is PD1. Its ligand, PD-L1, is expressed by a variety of tumors such as melanoma, glioblastoma and different types of carcinomas (mammary, ovarian, lung, cervical, colon and renal) (Blank et al., 2004) (Quezada and Peggs, 2013). Unlike CTLA-4, which downmodulates T effector responses during early phases of T cell priming, PD1 inhibits T cell activation at the time of an ongoing effector response (Greenwald et al., 2005). Immunotherapies targeting these T cell inhibitory checkpoints in recent years obtained dramatic results in controlling incurable melanoma. The effect of PD1 blockade would be promoting TILs expansion within the tumor and increase of IFN-γ production.

3.2 Tumor antigens and immunological tolerance

The fact that endogenous T cells can antagonize tumor growth in the context of cancer immunotherapy implicates that T cells can recognize tumor antigens presented by MHC on the surface of cancer cells (Tumeh et al., 2014). These

antigens can derive from normal non-mutated self-proteins, to which T cell tolerance is impaired or alternatively they can derive from the product of DNA mutations that results in the generation of tumor specific neo-antigens. Mice cured by surgical tumor resection become resistant to subsequent tumor reinjection, suggesting the presence of immunological memory toward cancer cells (Gross et al., 1943). Tumor antigens can be divided into two categories: tumor specific antigens (TSAs), which are antigens expressed solely by tumor cells, and tumor associated antigens (TAAs), which are mostly expressed in tumors cells but can also be found in normal cells (Rosenberg, 1999). TAAs in melanoma include a group of antigens involved in melanoma differentiation, aptly named melanoma differentiation antigens (MDAs). TSAs are also called neo-antigens and are in fact mutated self-antigens (Schumacher and Schreiber, 2015). Given their absence from the human genome, neo-antigens theoretically exhibit increased immunogenicity, because T cells directed against these molecules are unaffected by central tolerance. The evidence of their immunogenicity has only begun to surface due to technological advances in different domains of experimental cell biology. Recent studies have suggested that neo-antigens may mediate clinical responses to immune checkpoint inhibitors, such as antibodies directed against CTLA-4 or PD1 (Lee et al., 2016). Tumors possess different mechanisms to evade the anti-tumor immune response (Figure 6). In metastatic melanoma and in aggressive recurrent melanoma TAAs are often downregulated (Khong et al., 2004; Maeurer et al., 1996). Moreover, aggressive melanoma cells express decreased levels of MHC I as a mechanism to avoid recognition by CTLs. In addition, tumor cells also express death signals, such as Fas ligand (Fas-L), and utilize Fas signaling to induce apoptosis in T cells (Hahne et al., 1996). Another mechanism to induce immunological tolerance is the secretion of inhibitory signaling molecules, such as the immunosuppressive cytokines TGF-β and prostaglandin E2 (PGE2) (Gorelik and Flavell, 2001; Nicolaou et al., 2004). Tumor cells can escape the immune system also through the alteration of expression of co-stimulatory and co-inhibitory molecules. Immunological tolerance can be induced when dysfunctional APCs are not able to transmit positive costimulatory signals while presenting TAAs to T cells (Sotomayor et al., 2001), or when tumor cells express co-inhibitory or immune check point molecules that protect them from

the attack of T cells. Melanoma cells express PD-L1, which binds to PD1 on T cells and resist CTL-mediated cells lysis (Hirano et al., 2005). Tumors also recruit tolerogenic CD4+CD25+Foxp3+ Treg cells to evade anti-tumor immunity. CTLA-4 and PD1 also enhance Treg cell immunosuppressive function (Jacobs et al., 2012; Wing et al., 2008). Thus, cancer cells exploit immune checkpoints, not only to suppress tumor-specific T effector responses, but also to induce immunosuppressive Treg cells in order to facilitate tumor immune escape.

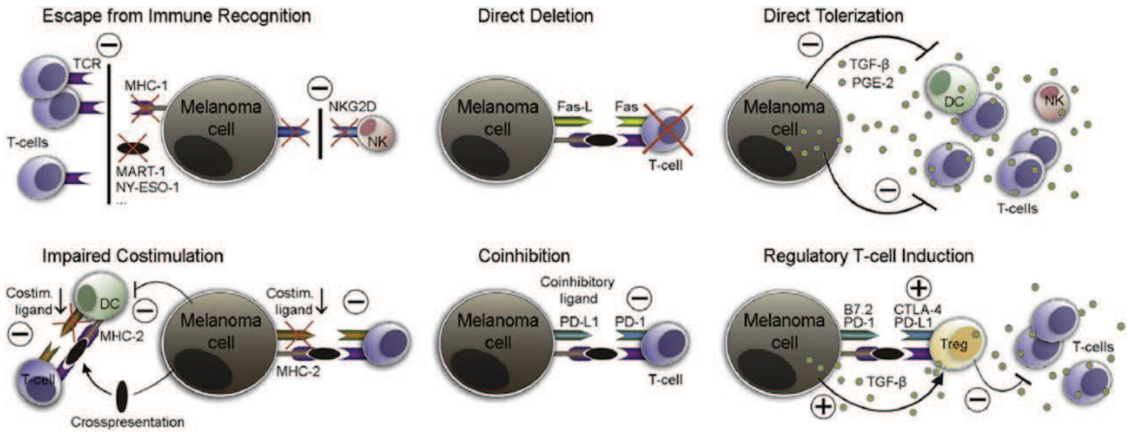

Figure 6: Immunological mechanisms underlying melanoma immune evasion. Melanomas can evade rejection by CTLs by downmodulating expression of MHC class I or melanoma-associated antigens (MAAs) on the cell surface. Melanoma cells may also evade natural killer (NK)-mediated cytotoxicity by down-modulating their expression of activating NK receptor ligands or by inducing a decrease in expression of activating receptors on NK cells. Melanoma cells can also overexpress Fas Ligand (Fas-L) and induce apoptosis of T-effector TILs, or directly tolerise immune effector populations by secreting immunosuppressive factors (e.g., TGF-β or PGE-2). Cross-presentation of MAAs by DCs incapable of adequate co-stimulation can render tumor-specific T cells anergic. Additionally, MHCII-expressing melanoma cells might function as antigen presenting cells (APCs) that could tolerise tumor-reactive TILs through lack of co-stimulation, or by delivering a co-inhibitory or immune checkpoint signal. Finally, melanoma cells can actively induce and/or recruit Treg cells via the secretion of soluble mediators (e.g., TGF-β) or by engaging with Treg-expressed immune checkpoints (e.g., B7/CTLA-4, PD-1/PD-L1) to mitigate the anti-tumor immune response (Lee et al., 2016).

3.3 Immunoregulatory mechanisms in the tumor microenvironment

TILs effector functions are strongly influenced by the tumor microenvironment (TME). Apart from tumor cells, TME comprises blood vessels, immune cells, fibroblasts, bone marrow-derived inflammatory cells, TILs and the extracellular matrix (ECM). The tumor can influence the microenvironment by releasing extracellular signals, promoting angiogenesis and inducing peripheral immune tolerance. On the contrary, immune cells in the microenvironment can influence the growth of the tumor. In 2001, it was shown that the immune system can control not only the magnitude, but also the quality of tumor by influencing tumor immunogenicity via immunoediting (Dunn et al., 2002; Shankaran et al., 2001). This study revealed that tumors formed in mice that lacked an intact immune system were, as a group, more immunogenic (classified as unedited) than similar tumors derived from immunocompetent mice (termed edited). The immune system not only protects the host against tumor formation, but also shapes tumor immunogenicity. This hypothesis is the basis for cancer immunoediting, which stresses the dual host-protective and tumor-promoting actions of immunity on developing tumors (Schreiber et al., 2011). The principal mechanisms through which the tumor can influence T cell effector functions are T cell anergy, exhaustion and senescence. In particular, an unbalance between inhibitory and stimulatory B7 family members in the tumor could be responsible for the induction of anergy (Pardoll, 2012; Zou and Chen, 2008). However, cellular and molecular mechanisms controlling T cell anergy are insufficiently understood. T cell exhaustion in tumor could be the result of the persistent exposure to tumor antigens. They are described as effector cells with decreased cytokine expression and effector function, and resistant to reactivation (Wherry, 2011). Exhausted CD8+ T cells were found in patients with melanoma, hepatocellular carcinoma, and ovarian cancer (Baitsch et al., 2011; Curiel et al., 2003). Senescent T cells are characterized by telomeres shortening, phenotypic changes, like loss of CD28 expression of CD28 and cell cycle arrest (Adibzadeh et al., 1995; Effros, 1998). p21 and p53 expression increases in senescent cells (Beausejour et al., 2003; Passos et al., 2010). In

addition to phenotypic alteration, senescent T cells show defective killing abilities and the development of negative regulatory functions (Akbar and Henson, 2011). Beside T cell anergy, exhaustion and senescence, another important aspect to consider is how immune cell metabolism is altered by the tumor microenvironment. Tumors are a major disturbance to tissue homeostasis, because they create a metabolically demanding environment that affects the metabolism and functions of infiltrating immune cells. Cancer cell growth is often supported by aerobic glycolysis which is the optimal pathway to support effector functions of many immune cells (Pearce et al., 2013). This similarity generates a competition for substrates between tumors and immune cells. The demand of nutrients, metabolites and oxygen imposed by proliferative cancers cells, in combination with their immunosuppressive action, create harsh environmental conditions in which immune cells must navigate and adapt (Buck et al., 2017). During tumor growth, regions of hypoxia are established and HIF-1α is induced and intensifies cancer cell glucose utilization and lactate release (Eales et al., 2016). How this metabolic heterogeneity in tumor cells relates to immune cell function has not been well elucidated, but exposure of NK and T cells to high concentrations of lactate impairs the activation of the transcription factor NFAT and production of IFN-γ (Brand et al., 2016). Lactic acid also disrupts T cell motility and causes loss of cytolytic function in CD8 T cells (Haas et al., 2015). Moreover, it was shown that decreasing conversion of pyruvate to lactate by genetic targeting of lactate dehydrogenase A (LDHA) in tumors helps to restore T cell infiltration and function, linking lactate production to immunosuppression (Brand et al., 2016). Hypoxia also has drastic effects on TIL function, proliferation and migration (Vuillefroy de Silly et al., 2016). HIF-1α induces the expression of PD-L1 in tumor cells (Noman et al., 2014), which leads to TILs suppression via PD1.

A recent work by Scharping et al., has shown that CD8 TILs lose mitochondrial mass, membrane potential, and oxidative capacity, which lead to a block in their proliferation and IFN-γ production (Scharping et al., 2016). From these observations it is possible to conclude that cells intrinsically more effective in competing for nutrients would have increased possibilities to survive in the tumor microenvironment. Therefore, restoring metabolic fitness and remodeling

hypoxic tone in tumors are promising strategies to implement the anti-tumor T cell effector response.

4. Purinergic signaling in the immune system

The ability of rapidly sensing signs of distress is one of the main feature of a homeostatic system. This is especially important in living organisms that are characterized by a continuous exchange of information with the outside and continuous processes of self-renewal. It is important for such a homeostatic system to be able to constantly monitor the internal environment in order to detect any signs of injury or distress. Accordingly, a homeostatic system should be able to release a series of intracellular signaling molecules to report cell or tissue damage. One of the simplest way to signal distress is the presence of receptors that sense in the extracellular space molecules that normally reside intracellularly. ATP is one of the most important signal of distress and damage (Di Virgilio and Vuerich, 2015). Physiologically, ATP is almost exclusively present intracellularly, at several millimolar concentration, while in the extracellular space the concentration of ATP is in the low nanomolar range (Burnstock, 2007). ATP is the energetic currency of the cell, but it can be released in the extracellular space by dying cells and act as a danger associated molecular pattern (DAMP). In the immune system, ATP plays an important role in controlling both activation and differentiation of different immune cell types. For example, in the initial phase of inflammation, DAMP signaling is needed to activate DCs and to modulate the ensuing immune response. ATP can also be released by living cells, in a regulated fashion, through vesicles or specific channels such as connexin and pannexin (Bodin and Burnstock, 2001), to act as an autocrine/paracrine signal. In the extracellular space, ATP is sensed by purinergic P2 receptors. The P2 receptor family is further subdivided into P2Y and P2X receptors (Abbracchio et al., 2006; Ralevic and Burnstock, 1998). The P2Y receptors are G protein-coupled receptors and are stimulated by nucleotides such as ATP, ADP, UTP, UDP, UDP glucose and UDP galactose. There are eight known P2Y receptors in humans: P2Y1, 2, 4, 6, 11, 12, 13, 14. The P2X ionotropic receptors are ligand-

gated non-selective ion channels and seven members have been described in mice and humans: P2X1, 2, 3, 4, 5, 6, 7. Both P2Y and P2X receptors are expressed by immune cells, in a cell type- and differentiation-dependent manner; the activation of these receptors controls different cellular processes ranging from survival, proliferation and cell death (Rayah et al., 2012). The effect of ATP on a given cells depends on the concentration of ATP in the extracellular space, the duration of stimulation and the level of expression and the composition of P2 receptors on the cell surface. In particular, ATP in the extracellular space can be degraded to adenosine by specific enzymes such as ectoapyrase (e.g. CD39) and ecto-5'-nucleotidase (CD73) (Yegutkin, 2008).

Beside its role as DAMP for the innate immune system, the role of ATP in the adaptive immune system has been extensively studied in the latest years. The importance of ATP/P2XR signaling axis at the immunological synapse has been recently unraveled. Upon contact of the TCR with cognate MHC/peptide complex, T naïve cells release ATP through pannexin 1 hemichannels during the capacitive calcium entry (CCE) phase of T cell activation. The ATP released binds to P2X receptors on the T cells in an autocrine fashion and promotes the activation of the MAPK pathway and the translocation of NFAT into the nucleus. This leads to the expression of IL- 2 and pro-inflammatory T cell activation. In the absence of ATP/P2XR signaling and MAPK activation, the translocation of NFAT in the nucleus induces a transcriptional program characteristic of T cell anergy (Schenk et al., 2008) (Fig. 7).

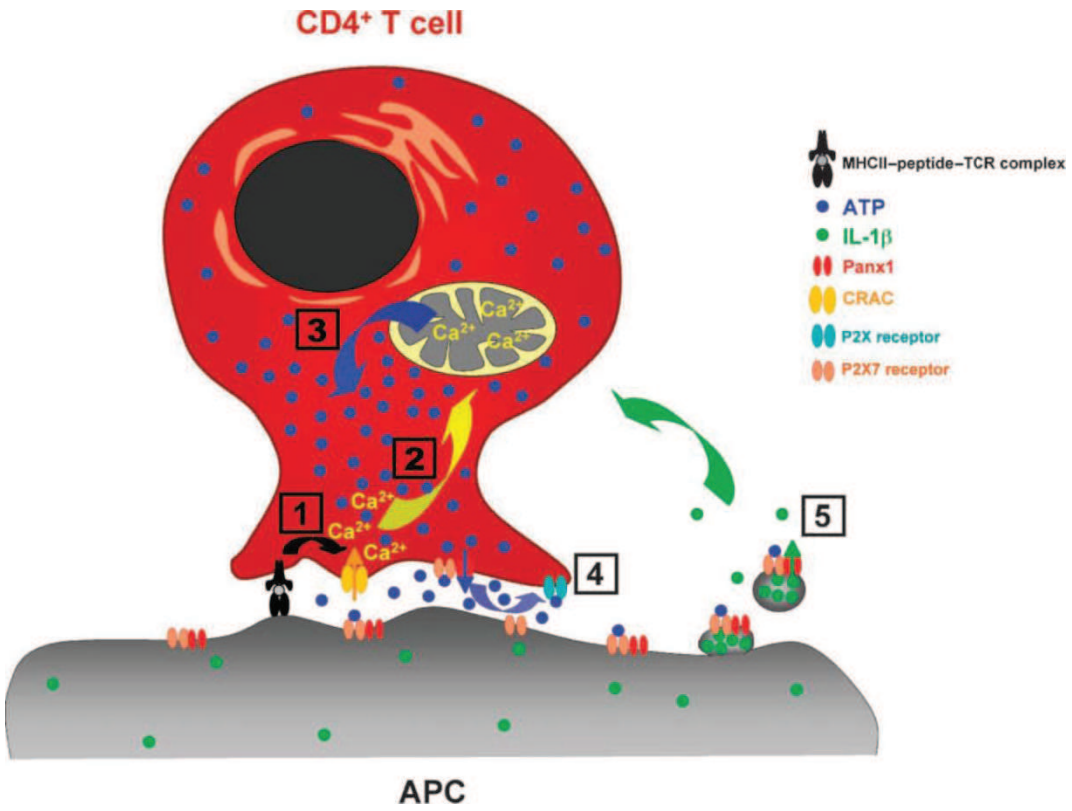

Figure 7: Purinergic control of T cell activation. Schematic representation of a T cell (red) interacting with an APC (gray). The early phase of T cell activation, which is triggered by the interaction of the TCR with the MHC–peptide complex, is characterized by CCE (step 1), which is accompanied by mitochondrial uptake of Ca2+ (step 2) and Ca2+-dependent stimulation of ATP synthesis (step 3). ATP is released from activated T cells through pannexin hemichannels, which open when the cytosolic [Ca2+] is elevated. This mechanism guarantees a high concentration of pericellular ATP, which by binding to P2XRs, serves as an indispensable autocrine costimulus for productive T cell activation (step 4). Finally, ATP released from activated T cells might also modulate APC function, such as secretion of IL-1β (step 5) (Schenk et al., 2008).

4.1 The P2X7 receptor

The P2X7 receptor is an ATP-gated cation channel and the only member of the P2X receptor family characterized by low affinity for ATP, meaning that it requires high concentration of ATP to be activated. The P2X7 monomer has a short intracellular N-terminal residue, a bulky extracellular domain, two transmembrane helices and a long cytoplasmic carboxy-terminal tail (Surprenant et al., 1996), fundamental for mediating P2X7 signaling. At physiological concentrations of ATP in the extracellular space, the P2X7 receptor is not active, but when the concentration of ATP increases it opens a channel permeable to cations such as Na^+, K^+, Ca^{2+}. In the presence of high

concentrations of ATP or after a prolonged stimulation, the P2X7 receptor forms a cytolytic pore that allows the passage of molecules with a molecular weight up to 900 Da, including ATP itself (Scheuplein et al., 2009). P2X7 can also be stimulated in an ATP-independent fashion. The mechanism involves the ecto-ADP-ribosyltransferase ARTC2.2, which, in the presence of nicotinamide adenine dinucleotide (NAD+), catalyzes ADP-ribosylation of P2X7 at an arginine residue at position 125 at the edge of the ATP-binding pocket in the extracellular domain of the protein (Adriouch et al., 2008; Seman et al., 2003). Interestingly, NAD+ dependent activation of P2X7 by ADP-ribosylation provides a long lasting activation signal, while P2X7 activation by the non-covalent binding of ATP necessitates the continuous presence of ATP in the extracellular milieu at sufficient concentration (Scheuplein et al., 2009). At the moment ADP-ribosylation of P2X7 has been shown only in murine cells, therefore the possible significance of this activation mechanism in humans is not known. One of the consequences of P2X7 activation is the modification of cell volume and plasma membrane composition. For example, T cells respond to ATP stimulation with rapid sequential shrinkage and swelling and externalization of phosphatidylserine (PS) onto the outer membrane leaflet of the plasma membrane (Adriouch et al., 2001; Taylor et al., 2008). Externalization of PS is considered as an early indicator of the induction of apoptosis and is related to the influx of both Na^+ and Ca^{2+}. Interestingly, PS exposure after ATP stimulation is reversible if ATP is removed within the first 30 minutes of exposure (Mackenzie et al., 2005), while PS exposure after ADP-ribosylation is not reversed after removal of NAD+ (Seman et al., 2003). The formation of the membrane pore is another important characteristic of P2X7 receptor activation and it has been functionally linked to the long intracellular C-terminus region of the receptor (Becker et al., 2008). However, whether the formation of the pore is mediated by P2X7 itself and/or by other P2X7-associated proteins such as pannexin 1 is still unclear. Another non-selective cation channel, the phospholipid scramblase anoctamin 6 (ANO6), has been recently identified as an important element in the formation of the membrane pore following P2X7 activation in macrophages (Ousingsawat et al., 2015). P2X7 receptor is highly expressed in cells of the innate immune system, and its function has been extensively studied. In particular, P2X7 receptor has a fundamental pro-

inflammatory role. During inflammations, ATP activates P2X7 receptor, which mediates the efflux of K^+, the opening of pannexin 1 channels and the activation of NLRP3 inflammasome. This leads to the processing by caspase 1 of pro-IL1β to the mature form, which is then released (Ferrari et al., 2006). The role of P2X7 receptor in the adaptive immune system has been investigated more and more in the latest years. Regarding T cells, the expression of P2X7 depends on the stage of maturation and differentiation. It was shown that the ATP/P2X7 axis plays a role in thymocytes death by neglect and in thymic differentiation of γδ T cells by promoting ERK phosphorylation (Frascoli et al., 2012). Moreover, mature peripheral CD4+ T cells display higher surface levels of P2X7 compared to CD8+ T cells. Interestingly, P2X7 surface expression also seems to be regulated by T cell activation. T cells expressing more activation markers show lower P2X7 surface levels compared to the resting counterpart (Adriouch et al., 2007). The P2X7-dependent cell death is very important in regulating the homeostasis of different T cell populations both at steady state and in pathophysiological contexts. *In vivo* studies has shown that Treg and NKT cells are characterized by high sensitivity to ATP- and NAD+ mediated cell death (Hubert et al., 2010; Kawamura et al., 2006; Rissiek et al., 2014). *P2rx7* knock out mice exhibit a higher number of Treg cells in the spleen compared to wild-type (WT) mice. Moreover, it has been shown that P2X7 receptor in Tfh cells is important in regulating the composition of the gut ecosystem. Tfh cells in the Payer's Patches (PPs) of the small intestine express high levels of P2X7 receptor, which regulates their survival and function. *P2rx7* knock out mice are characterized by expansion of PPs at steady state, due to increased number of Tfh cells and germinal centers. This leads to enhanced production of high-affinity IgA that results in alteration of the microbiota composition (Proietti et al., 2014). Very recently, it was shown that the binding of retinoic acid through retinoic acid receptor α induces the upregulation of P2X7 in CD4+ T effector cells in the gut. The intestinal effector T cells are effectively deleted by P2X7 activation-dependent apoptosis (Hashimoto-Hill et al., 2017). It has become clear that ATP can be released from living cells in different physiological and pathophysiological conditions. Pellegatti et al. demonstrated the presence of ATP in the tumor microenvironment at a millimolar range (Pellegatti et al., 2008). The role of P2X7 receptor in tumors has been recently investigated in

P2rx7-deficient mice. The pharmacological or genetic ablation of P2X7 results in the increase of tumor development in a model of colitis-associated cancer, due to accumulation of Treg cells in the tumor microenvironment (Hofman et al., 2015). Another important mechanism of P2X7 activity in tumors could rely on the more efficient priming of anti-tumor CD8+ T cells in WT mice due to a more efficient DC maturation through the NLRP3-P2X7 axis, thus leading to a more effective-tumor antigens presentation to CTLs and more favorable T effector/Treg ratio for the organism (Adinolfi et al., 2015; Ghiringhelli et al., 2009). These studies reveal the important role of P2X7 in the tumor microenvironment. It cannot be excluded that inhibition of P2X7 activity in other cell subsets could be beneficial for the anti-cancer immune response. It is important to consider that besides Treg cells other mature T cells subsets express high level of P2X7 receptor. It seems reasonable to envisage that blockade of P2X7 receptor concomitant with immunotherapy could be beneficial in promoting accumulation of pro-inflammatory T cells within the tumor, contributing to its rejection. In summary, it has become clear that P2X7-mediated cell death constitutes a crucial factor for the homeostatic regulation of different T cell subsets and play essential role in the regulation of immune responses. Depending on the amount of extracellular ATP or NAD+ and/or the expression level of P2X7, the receptor may regulate T cell activation and function. Short pulse and low concentration of ATP or its restricted presence at only one side of the cells (for example at the immunological synapse) might promote T cell activation (Rissiek et al., 2015) (Figure 8). In contrast, long-lasting whole-cell activation of P2X7 by high concentrations of ATP or NAD+ in cells expressing high levels of P2X7 might promote cell death.

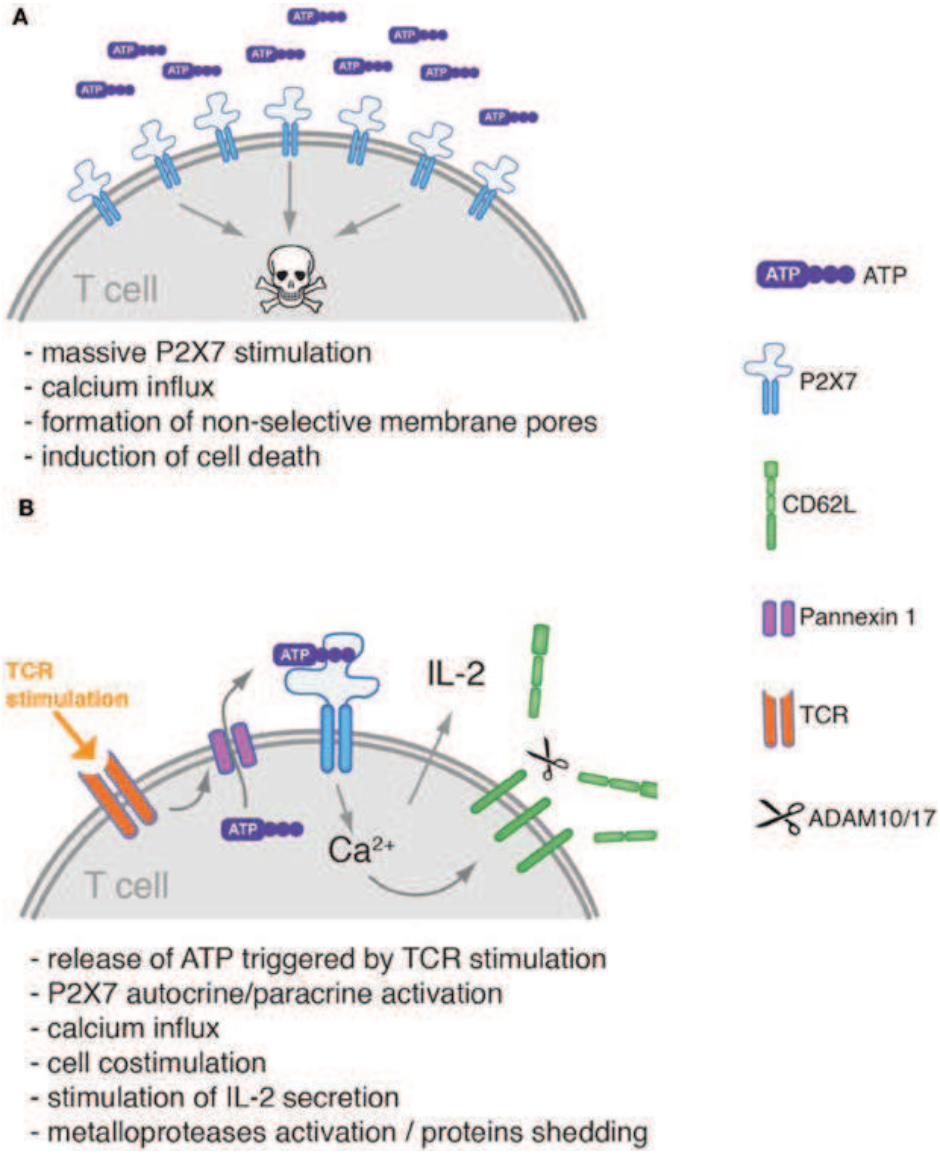

Figure 8: P2X7 mediated cell death and role of P2X7 in T cell activation. P2X7 stimulation can have different consequences in T cells. The extracellular concentration of ATP, the density of P2X7, the concomitant expression of ATP degrading ectoenzymes, the T cell subset and the activation status of the cell are all important elements in shaping the response to extracellular ATP. (A) High concentrations of extracellular ATP culminate in cell death through the induction of massive membrane depolarization and permeabilization. (B) At lower ATP concentrations and P2X7 expression levels or in the presence of ATP-catabolizing enzymes, P2X7 stimulation promotes T cell activation by enhancing cytosolic Ca2+ concentration. This may result in the stimulation of NFAT and MAPK, and IL-2 secretion as well as in the activation of a metalloprotease that catalyzes the shedding of CD62L and possibly other cell surface proteins (modified from (Rissiek et al., 2015).

AIM OF THE STUDY

The ATP-gated ionotropic P2X7 receptor is expressed by a number of mammalian cell types. In the innate immune system the ATP/P2X7 axis has a fundamental role during inflammation, as it is responsible for the release of mature IL-1β in the extracellular space. P2X7 receptor is a signature gene also of effector T cell subsets, however, its role in the adaptive immune system has to be investigated more thoroughly. Our lab previously demonstrated that P2X7 receptor influences T follicular helper cells survival in the gut associated lymphoid tissue. The aim of this study was to characterize P2X7 receptor function in T effector memory (TEM) cells. We used *P2rx7*$^{-/-}$ mice to analyze the effect of P2X7 activation on T cell proliferation and survival both *in vitro* and *in vivo*. We analysed transcriptional, metabolic and signaling profiles controlled by P2X7 activity in order to understand the effect of extracellular ATP (eATP) on TEM cells via P2X7. Since the tumor microenvironment is very rich in eATP, we addressed whether P2X7 could condition tumor infiltrating lymphocytes (TILs). In a chimeric model of melanoma we adoptively transferred WT or *P2rx7*$^{-/-}$ T cells in order to understand whether lack of P2X7 could endow TILs with functional advantages with respect to WT cells. Finally, we performed morphological analysis of TEM cells in electron microscopy to characterize possible mitochondria features that could correlate with improved bioenergetics of P2*rx7*$^{-/-}$ cells.

MATERIAL AND METHODS

Mice

C57/BL6J, *P2rx7*$^{-/-}$ (B6.129P2-*P2rx7*^{tm1Gab}/J), UBC and *Cd3ε*$^{-/-}$ mice were bred in specific pathogen-free (spf) facility at the Institute for Research in Biomedicine, Switzerland. Genotyping was accomplished by the polymerase chain reaction (PCR) method according to the manufacturer's protocol. Mice were housed, five per cage, in ventilated cages under standardized conditions (20 ± 2ºC, 55 ± 8% relative humidity, 12 h light/ dark cycle). Food and water were available ad libitum, and mice were examined daily.

Cell isolation from mice organs

For *in vitro* experiments and adoptive transfer CD4 or CD8 T naïve and T effector/memory (TEM) cells were sorted at FACSAria (BD Biosciences) from pooled cell suspensions of spleen, inguinal, axillary, brachial, cervical and mesenteric lymph nodes collected from C57BL/6J and *P2rx7*$^{-/-}$ mice. T Naïve cells were sorted as CD4 or CD8 +/-, CD62L+, CD44- and CD25-, while TEM cells were sorted as CD4 or CD8 +/-, CD62L-, CD44+ and CD25-. Magnetic Cell Sorting (MACS, Miltenyi Biotec) with anti-CD4 and anti-APC mAbs were used to purify cell subsets from complex cell mixtures.

B16 and HeLa cell lines

B16 cells were cultured in RPMI-1640, while HeLa cells were cultured in DMEM. Both media were supplemented with 10% heat-inactivate fetal bovine serum, 100 U/mL penicillin/streptomycin and 100 U/mL kanamycin. Cells were maintained in 5% CO_2 at 37°C. Tumor cells at 70-80% confluency were harvested by diluting them 1:5 in 0.25% trypsin.

In vivo experiments

To analyse in vivo homeostatic expansion, CD4 T naïve cells were sorted from spleen and secondary lymph nodes of UBC and *P2rx7*$^{-/-}$ mice as described above. 1x10^6 total cells were injected into 8 week old *cd3ε*$^{-/-}$ mice. Recipient mice were sacrificed four weeks after reconstitution and spleen, Peyer's patches and mesenteric lymph nodes were analyzed at FACS. To analyse anti-tumor response, CD4 or CD8 T naïve cells and CD4 TEM cells were sorted from C57/BL6J and *P2rx7*$^{-/-}$ mice as described above. 2.5x10^5 T naïve or TEM cells were injected into *cd3ε*$^{-/-}$ mice. Melanoma B16 cells were harvested at exponential growth. After five days from reconstitution with T cells, melanoma cells were resuspended in PBS at a concentration of 5x10^6 cells/mL and a volume of 0.1 mL (5x10^5 tumor cells) was injected subcutaneously into the back of recipient *cd3ε*$^{-/-}$ mice. Tumor growth was scored with a caliper by measuring the greatest tumor diameter and its perpendicular to determine an average and then the area was calculated as: $(\text{average}/2)^2\pi$. Tumor-bearing animals were sacrificed after 20 days or earlier when showing any sign of discomfort.

Cell isolation from tumor tissue

Tumors were cut in small pieces and resuspended in RPMI-1640 with 1.5 mg/mL type I collagenase (Sigma), 100 µg/mL DNase I (Roche) and 5% FBS, digested for 45 minutes at 37°C under gentle agitation. The digestion product was then passed through a 70 µm cell strainer to obtain a single cell suspension. Lymphocytes were then enriched by Percoll density gradient following manufacturer's protocol.

Antibodies and flow cytometry

Anti-mouse antibodies

The following mAbs were purchased from BD Bioscience: APC conjugated anti-CD62L (clone: MEL-14, Cat.#: 17-0621-83, working dilution 1:200), PE conjugated anti-Ki-67 (clone: SolA15, Cat.#: 12-5698-80, working dilution

1:100), APC conjugated anti-CD8α (clone: 53-6.7 Cat.# 17-0081-83, working dilution 1:200). The following mAbs were purchased from BioLegend: PE conjugated anti-CD44 (clone: IM7, Cat.#: 103008, working dilution 1:200), PE/Cy7 conjugated anti-CD25 (clone: OC61, Cat.# 102016, working dilution 1:200), APC/Cy7 conjugated anti-CD4 (clone: RM4-5, Cat.#: 100526, working dilution 1:200), Pacific Blue conjugated anti-CD8α (clone: 53-6.7, Cat.# 100725, working dilution 1:200), FITC conjugated anti-TCRβ (clone: H57-597, Cat.# 109215, working dilution 1:200). APC conjugated anti-CD8α (clone: 53-6.7, Cat.# 17-0081-83, working dilution 1:200).

Anti-human antibodies

The following mAbs were purchased from Life Technologies: PE-Texas Red conjugated anti-CD4 (clone: S3.5, Cat.# MHCD0417, working dilution 1:1000), QD655 conjugated anti-CD45RA (clone: MEM-56, Cat#. Q10069, working dilution 1:1000). The following mAbs were purchased from BioLegend: PE conjugated anti-CCR7 (clone: G043H7, Cat#. 353204, working dilution 1:600), PE/Cy5 conjugated anti-CD25 (clone: BC96, Cat.#: 302608, working dilution 1:20), PE/Cy5 conjugated anti-CD8 (clone: HIT8a, Cat.#: 300909, working dilution 1:20).

Samples were acquired on a LSRFortessa (BD Bioscience) flow cytometer. Data were analyzed using FlowJo software (TreeStar) or FACS Diva software (BD Bioscience).

Real-time PCR

Total RNA from FACS sorted cells was precipitated in Trizol (Invitrogen) and reverse transcribed to cDNA using Random hexamers (Roche, Cat.#: R 15504) and M-MLV reverse-transcriptase (Invitrogen, Cat.#: 28025-013) following manufacturer's protocol. mRNA samples were treated with 2 U/sample of DNase (Applied Biosystems). Transcripts were quantified by real-time PCR on an ABI PRISM 7700 Sequence Detector with predesigned TaqMan Gene Expression Assays and reagents according to the manufacturer's instructions (https://www.lifetechnologies.com). The following probes were used for mouse

cells: *Cdkn1a* (Mm00432448_m1), *Cdkn1b* (Mm00432448_m1), *P2rx1* (Mm00435460_m1), *P2rx2* (Mm01202368_g1), *P2rx3* (Mm00523699_m1), *P2rx4* (Mm00501787_m1), *P2rx5* (Mm00473677_m1), *P2rx6* (Mm00440591_m1), *P2rx7* (Mm01199500_m1), *trp53* (Mm01731290_g1), *Gadd45b* (Mm00435123_m1). The following probes were used for human cells: *CDKN1A* (Hs00355782_m1), *P2RX7* (Hs00175721_m1).
All reactions were performed in triplicate. The relative amounts of mRNAs were calculated by the ΔCT method. *Hprt* for mouse cells and *TBP* for human cells were used as internal housekeeping genes.

Time monitoring of DAPI uptake

Purified T naïve or TEM cells were resuspended at $1x10^6$ cells/mL and loaded with DAPI (1 µg/mL). After 30 seconds of measurement for DAPI basal level, cells were stimulated with BzATP (100µM) and DAPI uptake was monitored over time (250 seconds) at LSRFortessa and the kinetics analyzed using FlowJo software.

Microarray data analyses

All microarray data analyses were performed in R (version 3.2.0) using Bioconductor libraries (BioC 3.1) and R statistical packages. Probe level signals were converted to expression values using robust multi-array average procedure RMA of Bioconductor *affy* package. Differentially expressed genes were identified using Significance Analysis of Microarray (SAM) algorithm coded in the *samr* R package. In SAM, we estimated the percentage of false positive predictions (i.e. False Discovery Rate, FDR) with 100 permutations. To identify genes associated with *p2rx7* deletion, we compared the expression levels of WT and *p2rx7*$^{-/-}$ TEM cells and selected those probe sets with absolute fold change larger than a selected threshold (e.g. ≥ 2 or ≤ -2) and FDR ≤ 5% in all comparisons. To functionally annotate differentially expressed genes and identify de-regulated signaling pathways, we performed over-representation analysis using Fisher test and Gene Set Enrichment Analysis on gene sets derived from previously published gene signatures and from gene set

databases. GSEA software (http://www.broadinstitute.org/gsea/index.jsp) was applied on log2 expression data of WT and *P2rx7*$^{-/-}$ cells. Genes were considered significantly enriched at FDR ≤ 5% when using Signal2Noise as metric and 1,000 permutations of gene sets. Finally, we investigated the average expression was calculated as the standardized average expression of all signature genes in sample subgroups (e.g. WT/*P2rx7*$^{-/-}$).

Ki-67 staining

For detection of nuclear antigen Ki-67, sorted TEM cells or purified tumor infiltrating lymphocytes (TILs) were fixed and permeabilized using the BD Cytofix/Cytoperm Fixation/Permeabilization Solution Kit (BD Biosciences) according to the manufacturer's recommendations, followed by staining with Ki-67 mAb.

***In vitro* monitoring of cell survival and proliferation**

T naïve or TEM cells were grown in a 96 flat-bottom well plate in RPMI-1640 supplemented with 10% heat-inactivated fetal bovine serum, 100 U/mL penicillin/streptomycin and 100 U/mL kanamycin and maintained in 5% CO_2 at 37°C. Cells were labeled with CellTrace violet (Thermo Fisher, Cat.#: C34557) and stimulated by plate-bound anti-CD3ε mAb (2µg/mL) with co-immobilized anti-CD28 mAb (2µg/mL) (eBioscience); for stimulation with cytokines, cells were cultured with IL-2 at 50 U/mL. CellTrace dilution was measured in viable cells through the exclusion of dead and apoptotic cells by electronically gating PI and Annexin V negative cells. FACS acquisitions were standardized by fixed numbers of calibration beads (BD Biosciences). Half-life and cell cycling activity was calculated as previously described (Hawkins et al., 2007).

Quantification of β-galactosidase and mitochondria-associated ROS

To measure cellular senescence, purified TEM cells were stimulated for 3 days with anti-CD3ε and CD28 mAbs in the presence or absence of 70 µM BzATP. Cells were then harvested and incubated for 2 h with 100 nM bafilomycin A1 to

inhibit lysosomal β-galactosidase before adding the β-galactosidase substrate C_{12}FDG (Thermo Fisher). Relative β-galactosidase activity was assessed as fluorescence emission at FACS (with 488 nm laser). Mitochondria-associated ROS levels were measured by staining cells with MitoSOX red (Molecular Probes/Invitrogen) at 5 µM for 40 min at 37ºC. Cells were then washed and resuspended in PBS for FACS analysis (with laser for PE).

Transmission electron microscopy

WT and *P2rx7*$^{-/-}$ TEM cells were stimulated 3 days with anti-CD3 and anti-CD28 antibodies and then fixed in 2% paraformaldehyde and 2% glutaraldehyde in sodium cacodylate 0.1 M. Following fixation, samples were washed in cacodylate buffer and post fixed in 1% osmium tetroxide. After extensive washing in H_2O, samples were stained with uranyl acetate saturated in ethanol 20% for 1 hour and then washed again. Samples were then dehydrated in increasing concentration of ethanol (70%, 80%, 90%, 100%) and propylene oxide and embedded in Eponate 12 resin (Ted Pella). The resin-embedded samples were cut using an ultramicrotome (Leica Microsystem) with a diamond knife (DiATOME, Switzerland), collected on copper grids (EMS), and counter-stained with uranyl acetate solution for 20 minutes, and 1% lead citrate (EMS) for seven minutes, before being observed through a transmission electron microscope (Philips) equipped with a digital camera (Morada, Olympus). The area, perimeter and circularity of about 100 mitochondria per sample were measured on electron micrographs acquired at 10500x using ImageJ64 software.

Seahorse metabolic analysis

WT and *P2rx7*$^{-/-}$ TEM cells were stimulated 3 days with anti-CD3 and anti-CD28 antibodies, then collected and plated on Seahorse 96 well plate coated with Cell-Tak (Corning, Cat# 354240) and analyzed with Seahorse XF Cell Mito Stress kit (Seahorse Bioscience). Oxygen consumption rate (OCR) was measured in XF media (non-buffered RPMI-1640 supplemented with 10mM glucose, 2mM L-glutamine and 1mM sodium pyruvate) under basal condition

and in response to 1 µM oligomycin, 1.5 µM fluoro-carbonyl cyanide phenylhydrazone (FCCP) and 100 nM rotenone + 1 µM antimycin A, using a 96 well XF or XFe Extracellular Flux Analyzer (EFA) (Seahorse Bioscience). Data were analyzed with Wave software.

Western blotting

For western blot analysis TEM cells were washed with ice cold PBS and lysed with RIPA buffer 1x (Sigma) or with Urea 9 M to detect nuclear protein, both supplemented with phosphatase inhibitor cocktail (Sigma-Aldrich) and protease inhibitor cocktail (Roche). Samples were centrifuge at 14.000 rpm for 10 min at 4°C and snap frozen. Cleared protein lysate was denatured with loading buffer supplemented with DTT 0.1 µM for 10 min at 65°C. Samples were run on precast 4-12% bis-tris protein gels (BioRad) and then transferred onto PVDF membranes using Trans-Blot Turbo Transfer System (BioRad). Membranes were blocked with 10% (wt/vol) nonfat dry milk (Bio-Rad) and 0.1% Tween-20 in TBS and incubated with appropriate antibodies in TBS with 0.1% Tween-20 for 16 h at 4°C. The following antibodies were purchased from Cell Signaling Technology: anti-p38 MAPK (rabbit, Cat. #9212), anti-phospho p38MAPK (T180/Y182) (rabbit, clone: D3F9, Cat. #4511), anti-phospho H2A.X (S139) (rabbit, clone: 20E3, Cat. #9718), anti-Opa1 (rabbit, clone: 2D6U6N, Cat. # 80471), anti-Drp1 (rabbit, clone: D6C7, Cat. # 8570). Anti-P2X7 antibody was purchased from Alomone Labs (rabbit, Cat. #APR-004); anti-actin antibody was purchased form Sigma (rabbit, Cat. #A2066); anti-GAPDH antibody was purchased form Millipore (mouse, clone: 6C5 Cat. #MAB374). All incubations with primary antibody were followed by incubation with secondary HRP-conjugated anti-rabbit (Cat. #7074, Cell Signaling Technology), or anti-mouse (Cat. #7076, Cell Signaling Technology) IgG antibodies in TBS with 0.1% Tween-20. Membranes were developed using the Pierce ECL Western blotting substrate (Thermo Scientific, Cat.# 32209), signals were detected with the ImageQuant LAS 4000 system in the standard acquisition mode (GE Healthcare Life Sciences), and bands were quantified using the Multi Gauge Analysis tool (Fujifilm).

Immunohistochemistry and digital image analysis

To assess the number of tumor infiltrating T cells, 4 µm sections from each sample were immunostained with a primary goat polyclonal antibody against CD3ε (Santa Cruz Biotechnology; #Sc-1127). For each sample, serial sections incubated with a 10% solution of normal rabbit serum served as negative controls. The number of $CD3\varepsilon^+$ cells per area of the tumor was evaluated using the ImageJ analysis program (http://rsb.info.nih.gov/ij/) in four 200X microscopic fields. The number of T cells per mm^2 of intestinal mucosa was then calculated.

Transfection of human TEM cells

Peripheral blood mononuclear cells (PBMCs) were isolated from blood by density-gradient centrifugation using Ficoll-Paque™ Plus gradient (GE-Healthcare). CD4+ T cells were enriched by positive selection using human CD4 MicroBeads (Miltenyi Biotec) and then CD4 TEM cells were sorted with a FACSAria (BD) as CD4+, CD8-, CCR7-, CD45RA-, CD25-. TEM cells were electroporated with Neon transfection kit and device (Invitrogen). A total of 5,0 $x10^5$ TEM cells were washed three times with PBS before resuspension in 10 µL of Buffer T (Neon kit, Invitrogen). 40 pmol of *P2RX7* Silencer Select Pre-designed siRNA (Ambion) or, as a control, siGLO Green Transfection Indicator (Dharmacon) were added to the cells to a final volume of 11 µL and mixed. 10 µL of the suspension was electroporated with Neon electroporation Device (Invitrogen; 2150 V, 30 ms, 1 pulse). Electroporated cells were then transferred in RPMI-1640 supplemented with 10% FBS and without antibiotics for 24 hours. For analysis of cell proliferation, electroporated TEM cells were labelled with CellTrace violet (Thermo Fisher, Cat.#: C34557) and plated on 96 well NUNC immunoplate coated with anti-CD3 (5 µg) and anti-CD28 (1 µg) antibodies for 5 days, with or without 300 µM BzATP.

Statistical analyses

Statistical analysis was performed with the Prism software (GraphPad). Comparisons of two groups were calculated using nonparametric Mann Whitney test or Student's unpaired t test. Comparisons for more than two groups were calculated using Kruskall-Wallis test followed by Dunn's multiple comparison test. Results are presented as mean values ± SEM of at least 5 mice per group from the same experiment and are representative of at least three independent experiments. Values of $P<0.05$ were considered significant.

RESULTS

P2X7 receptor regulates CD4+ TEM cell survival and proliferation both *in vitro* and *in vivo*

We previously reported that Tfh cells express high levels of *P2rx7* transcript, which influences Tfh cell proliferation and survival within the Peyer's patches (PPs) of the small intestine (Proietti et al., 2014). The data obtained in these cells prompted us to investigate *P2rx7* expression in other T cell subsets, including T naïve and effector memory (TEM) cells. Real-time quantitative reverse transcription PCR (qRT-PCR) for the different *P2rx* genes revealed that, in both naïve and TEM cells, *P2rx7* is the most expressed member of the P2X family (Figure 1A). Nevertheless, qRT-PCR and western blot revealed that TEM cells express significantly increased levels of both *P2rx7* transcript (Figure 1B) and P2X7 protein (Figure 1C) as compared to naïve cells. In order to correlate P2X7 receptor expression with its functionality, we tested DAPI permeability at FACS upon stimulation with the selective P2X7 agonist 3'-*O*-(4-benzoyl) benzoyl ATP (BzATP), as a measure of P2X7 receptor pore opening. These experiments showed that only a small fraction of T naïve cells is sensitive to P2X7-mediated DAPI uptake, while the majority of TEM cells were sensitive to BzATP stimulation (Figure 1D).

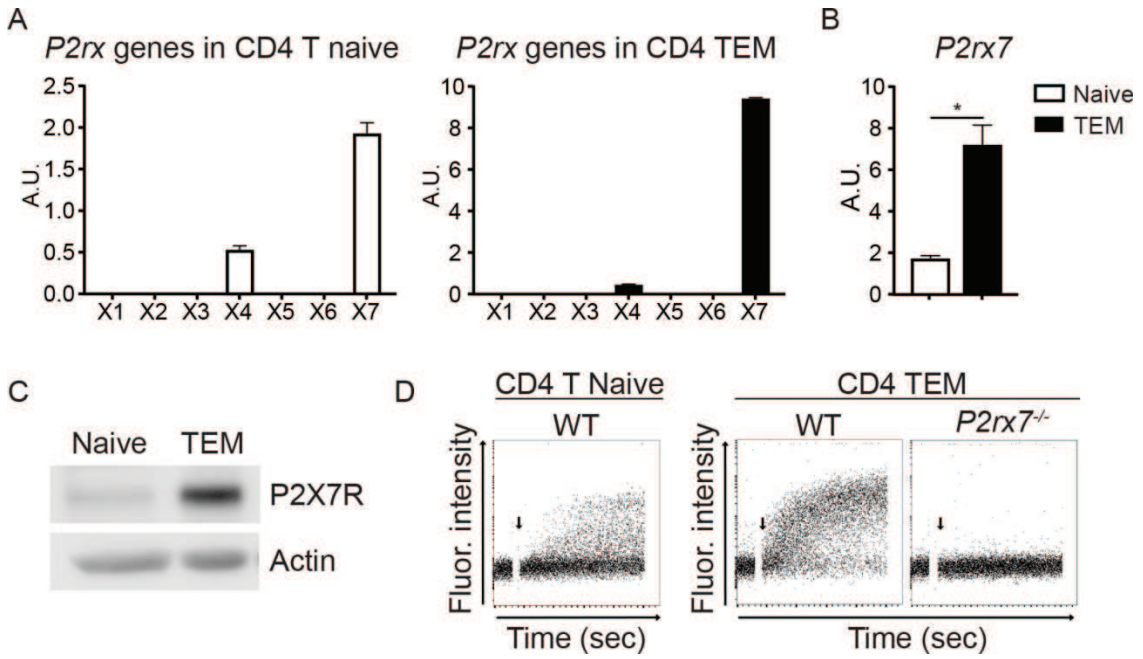

Figure 1: Effector memory express higher levels of *P2rx7* than naïve T cells. A) Quantitative Real-Time PCR (qRT-PCR) of the seven *p2rx* genes (X1-X7) performed in ex-vivo CD4+ T naïve cells (left, white) and CD4+ TEM cells (right, black). B) qRT-PCR of *P2rx7* transcript performed in ex-vivo CD4+ T naïve and TEM cells. Histograms show mean ± SEM. C) P2X7 receptor protein quantification by western blot in CD4+ T naïve and TEM cells. D) Time-monitoring of DAPI permeability at FACS after stimulation with BzATP of purified WT CD4+ T naïve and TEM cells. *P2rx7*$^{-/-}$ TEM cells were also tested as negative control. Data are representative results of at least three independent experiments with 3 to 5 mice for experiment. A.U., Arbitrary Unit. * $p<0.05$.

Therefore, we concentrated our efforts on the characterization of the function of P2X7 receptor in TEM cells. To address whether P2X7 activity affected TEM cell responsiveness, we analyzed *in vitro* cell proliferation and survival in response to anti-CD3 and anti-CD28 antibodies, using time series data obtained at FACS with CellTrace violet labeled WT and *P2rx7*$^{-/-}$ cells (Hawkins et al., 2007). As early as 24 hours after stimulation, a significant increase in the cell number and half-life of *P2rx7*$^{-/-}$ TEM cells with respect to WT cells was evident (Figure 2A). Moreover, the analysis of violet dilution showed that *P2rx7*$^{-/-}$ TEM cells progress earlier in the first cell division and require less time to enter subsequent cell divisions (Figure 2B). Interestingly, we observed a significant increase in the cell number of *P2rx7*$^{-/-}$ TEM compared to the WT counterpart also after stimulation with IL-2 (Figure 2C). All these data suggest that the absence of P2X7 receptor confers a proliferative advantage and an increased

survival to TEM cells *in vitro* when stimulated either with anti-CD3 and anti-CD28 antibodies or IL-2.

To evaluate whether these phenomena were a peculiarity of *in vitro* stimulation or could be observed also *in vivo*, we analysed homeostatic expansion of WT and *P2rx7*$^{-/-}$ mice. Naïve T cells injected into a lymphopenic host undergo extensive proliferation and acquire a phenotype similar to antigen-experienced memory T cells (Goldrath et al., 2004). We co-injected into *cd3ε*$^{-/-}$ mice CD4+ naïve T cells purified from *P2rx7*$^{-/-}$ and C57Bl/6-TgUBC-GFP mice, which express green fluorescent protein (GFP) under the control of the ubiquitin promoter (Figure 2D). After two weeks we collected spleens, mesenteric lymph nodes (MLNs) and PPs and analyzed at FACS the presence of memory-like CD4+ T cells originated from the different donors. The results showed that more than 90% of the memory cells that were recovered in the secondary lymphoid organs were negative for GFP, indicating they were from *p2rx7*$^{-/-}$ mice (Figure 2E). This result indicates that lack of P2X7 confers a proliferative and survival advantage to TEM cells, both *in vitro* and *in vivo*.

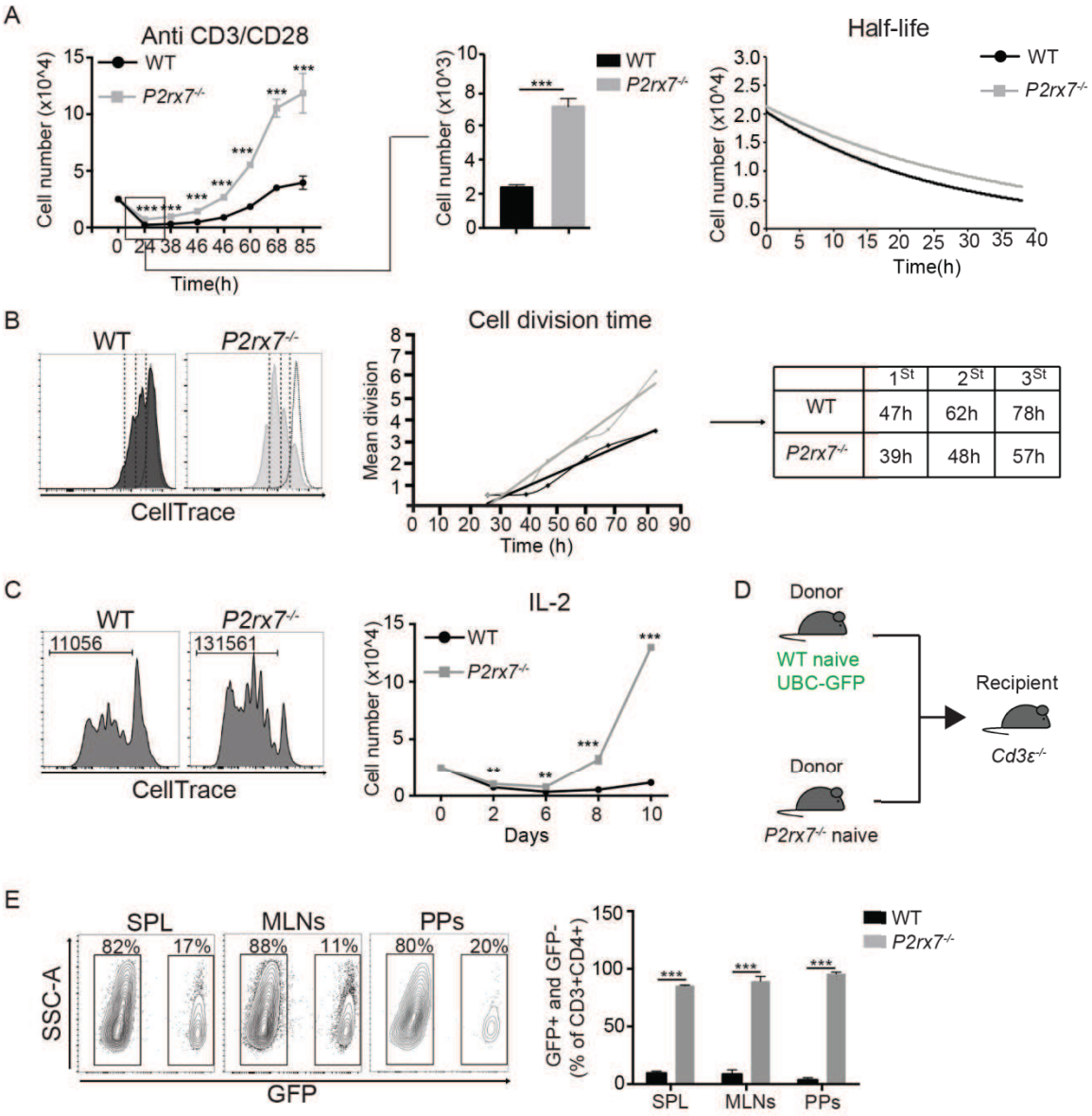
A
Anti CD3/CD28
WT
P2rx7-/-
Cell number (x10^4)
Time(h)
Cell number (x10^3)
Half-life
B
WT
P2rx7-/-
CellTrace
Cell division time
Mean division
Time (h)
1St
2St
3St
WT
47h
62h
78h
P2rx7-/-
39h
48h
57h
C
11056
131561
IL-2
Days
D
Donor
WT naive
UBC-GFP
Recipient
Cd3ε-/-
P2rx7-/- naive
E
SPL
MLNs
PPs
82%
17%
88%
11%
80%
20%
SSC-A
GFP
GFP+ and GFP- (% of CD3+CD4+)

Figure 2: *P2rx7*$^{-/-}$ TEM cells are characterized by increased survival and proliferation than WT cells both in vitro and in vivo. A) Left, cell number quantification at FACS of purified WT and *P2rx7*$^{-/-}$ TEM cells stimulated with anti-CD3 and anti-CD28 antibodies. In a separated histogram, the 24 hour time-point is shown in detail. Right, extrapolation for the rate of TEM cells death before entry into cell division. B) Left, representative CellTrace dilution of WT and *P2rx7*$^{-/-}$ TEM cells after 3 days of stimulation with anti-CD3 and anti-CD28 antibodies. Right, linear regression analysis of mean division number against harvest time. The table on the right shows the time taken for the cells to enter into each subsequent division (see Methods section). C) Representative CellTrace dilution of WT and *P2rx7*$^{-/-}$ TEM cells after stimulation with IL-2 for 10 days. In the left corner of the plot the cell number of dividing cells is represented. The graph on the right shows the cell number at different days of stimulation. D) Schematic representation of the experimental design: co-injection of T naïve cells from WT (in green) and *P2rx7*$^{-/-}$ mice (donors mice) into the same recipient *cd3ε*$^{-/-}$ mice. E) Dot plot (left) and statistical analysis of spleen (SPL), mesenteric lymph nodes (MLNs) and Peyer's patches (PPs) from *cd3ε*$^{-/-}$ mice reconstituted with purified WT (GFP+) and *P2rx7*$^{-/-}$ (GFP-) naïve CD4 cells at 1:1 ratio. Cells were gated for surface CD4 and CD3 and were analyzed for GFP expression. Histograms show mean percentages ± SEM. Data are representative results of at least three independent experiments with 3 to 5 mice for experiment. ** $p<0.01$, *** $p<0.001$.

P2X7 receptor activation induces upregulation of p21$^{waf1/cip1}$ and arrest of cell cycle progression

To better characterize the molecular pathway/s activated by P2X7 stimulation, we analysed the transcriptional profiles of *ex vivo* purified TEM cells from WT and *p2rx7*$^{-/-}$ mice with Affimetrix gene arrays. This analysis showed that *P2rx7*$^{-/-}$ TEM cells clustered together and separately from the WT counterpart (Figure 3A). Among the genes differently expressed by the two genotypes, we focused our attention on cyclin-dependent kinase inhibitor 1A (*Cdkn1a*), as one of the most downregulated transcripts in *P2rx7*$^{-/-}$ cells. *Cdkn1a* encodes for p21$^{Waf1/Cip1}$, which, together with the cyclin dependent kinase inhibitor p27^{Kip1}, regulates the progression through G1 to S phase of the cell cycle in mammalian cells (Coqueret, 2003). *In silico* analysis performed in publicly available datasets showed a positive correlation between the expression of *P2rx7* and *Cdkn1a* genes in T cells (Figure 3B). To directly correlate P2X7 activation with induction of *Cdkn1a* transcription, we stimulated WT TEM cells with BzATP and analysed *Cdkn1a* mRNA levels. QRT-PCR showed a significant increase of *Cdkn1a* transcripts in stimulated as compared to unstimulated cells. Moreover,

pretreatment of WT cells with the selective P2X7 antagonist A-438079 prevented *Cdkn1a* upregulation, indicating that P2X7 activation regulates *Cdkn1a* transcription (Figure 3C). The effect of BzATP was specific for p21 since the transcription of *Cdkn1b,* encoding for p27, was unaltered by P2X7 stimulation (Figure 3C).

We then analyzed the effect of BzATP on the cell cycling activity of TEM cells upon stimulation with anti-CD3 and anti-CD28 antibodies. The analysis of cell proliferation at FACS on cells labeled with CellTrace violet showed a block in the cell cycle progression of WT CD4+ TEM cells upon exposure to BzATP in a dose-dependent way, with a significant increase in the percentage of undivided cells. Pretreating cells with A-438079 antagonist prevented P2X7 mediated cell cycle block (Figure 3D). Data obtained at FACS by staining for the nuclear antigen Ki-67, a marker of proliferating cells, were in line with these results: WT TEM cells treated with BzATP showed a reduced percentage of Ki-67 positive cells compared to the untreated group and pretreatment with the antagonist A-438079 allowed the recovery of the proliferating phenotype (Figure 3E). We also confirmed that *ex vivo* isolated *P2rx7*$^{-/-}$ TEM cells proliferate more than WT cells (Figure 3E and 2B). Together, these data suggest that P2X7 activation in TEM cells induces a block in cell cycle progression through the upregulation of p21.

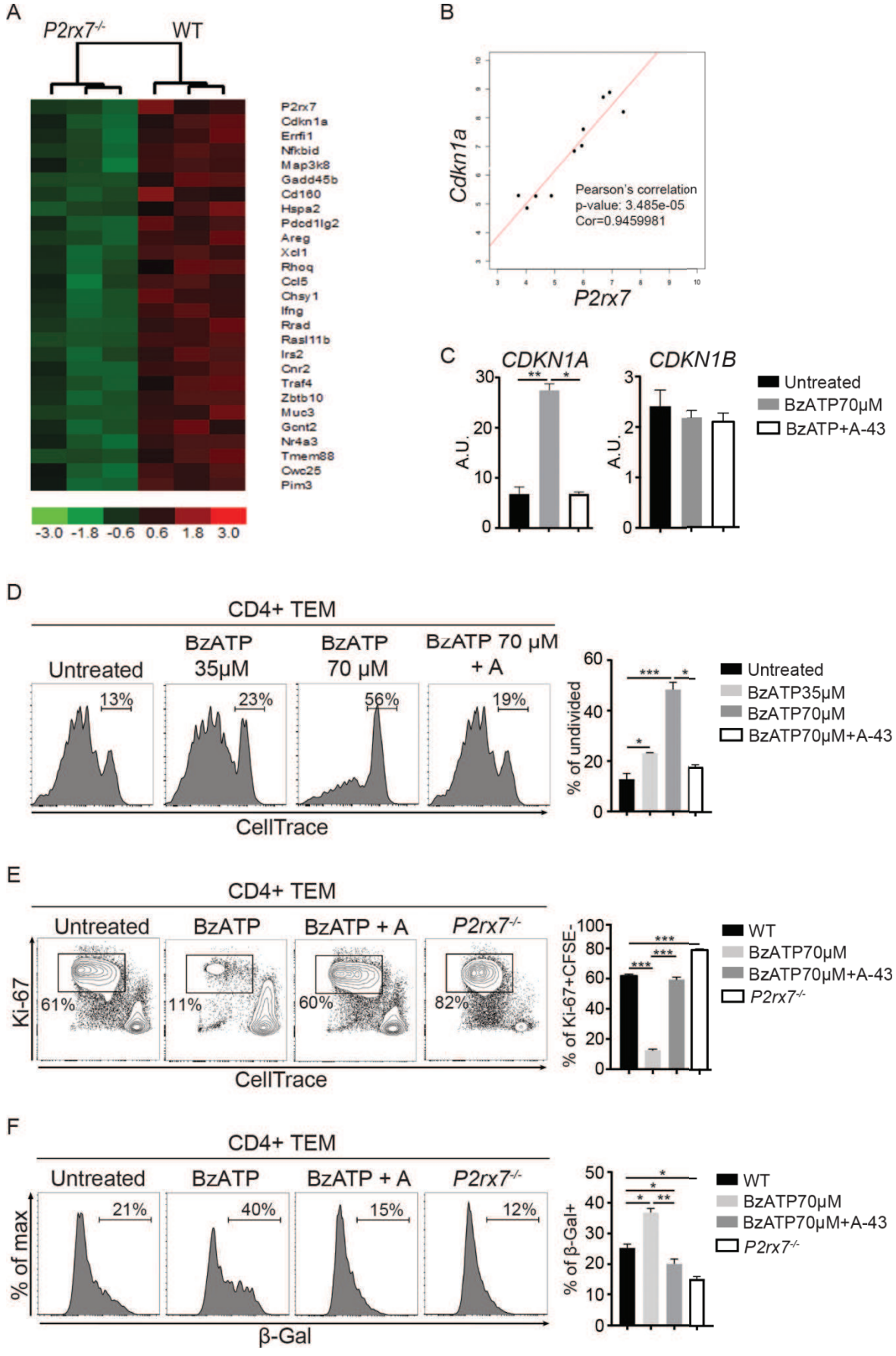
A
P2rx7-/-
WT
P2rx7
Cdkn1a
Errfi1
Nfkbid
Map3k8
Gadd45b
Cd160
Hspa2
Pdcd1lg2
Areg
Xcl1
Rhoq
Ccl5
Chsy1
Ifng
Rrad
Rasl11b
Irs2
Cnr2
Traf4
Zbtb10
Muc3
Gcnt2
Nr4a3
Tmem88
Owc25
Pim3
-3.0 -1.8 -0.6 0.6 1.8 3.0
B
Cdkn1a
P2rx7
Pearson's correlation
p-value: 3.485e-05
Cor=0.9459981
C
CDKN1A
CDKN1B
A.U.
Untreated
BzATP70μM
BzATP+A-43
D
CD4+ TEM
Untreated
BzATP 35μM
BzATP 70 μM
BzATP 70 μM + A
13%
23%
56%
19%
CellTrace
% of undivided
Untreated
BzATP35μM
BzATP70μM
BzATP70μM+A-43
E
CD4+ TEM
Untreated
BzATP
BzATP + A
P2rx7-/-
Ki-67
61%
11%
60%
82%
CellTrace
% of Ki-67+CFSE-
WT
BzATP70μM
BzATP70μM+A-43
P2rx7-/-
F
CD4+ TEM
Untreated
BzATP
BzATP + A
P2rx7-/-
% of max
21%
40%
15%
12%
β-Gal
% of β-Gal+
WT
BzATP70μM
BzATP70μM+A-43
P2rx7-/-

Figure3: P2X7 stimulation induces premature senescence in TEM cells through *Cdkn1a* upregulation. A) Differential gene expression between ex-vivo WT and *P2rx7*$^{-/-}$ TEM cells: heat map showing genes significantly downregulated (green) in *P2rx7*$^{-/-}$ compared to WT TEM cells (red). Each row represents one gene and each column one sample. B) Correlation analysis between *Cdkn1a* and *P2rx7* performed *in silico* for mouse T cells. C) Quantitative RT-PCR of *Cdkn1a* (left) and *Cdkn1b* (right) transcripts. The analysis was performed on purified WT TEM cells either untreated or stimulated with BzATP 70 μM or pretreated with A-438079 50 μM and then stimulated with BzATP. Histograms show mean ± SEM. D) Representative CellTrace dilution and statistical analysis of purified WT TEM cells stimulated with anti-CD3 and anti-CD28 antibodies for 3 days and treated with BzATP 35 or 70 μM, or pretreated with A-438079 50 μM. The numbers in the FACS plots and in the histogram represent the percentage of undivided cells. E) Dot plots of FACS staining and statistical analysis for the nuclear antigen Ki-67 performed on purified WT and *P2rx7*$^{-/-}$ TEM cells stimulated with anti-CD3 and anti-CD28 antibodies for 3 days and treated as indicated. The numbers in the plots and in the histogram represent the percentage of Ki-67 positive cells. F) β-galactosidase staining at FACS of WT and *P2rx7*$^{-/-}$ TEM cells stimulated with anti-CD3 and anti-CD28 antibodies for 3 days and treated as indicated. Numbers in the plot and in the histogram represent the percentage of β-galactosidase positive cells. Histograms shows mean percentages ± SEM. Data are representative results of at least three independent experiments with 3 to 5 mice for experiment. A.U., Arbitrary Unit. ** $p<0.01$, *** $p<0.001$.

P2X7 receptor induces premature senescence in CD4 TEM cells

High expression of p21 has been associated to senescent cells (Herbig et al., 2004). Thus, we investigated whether P2X7 receptor might induce premature senescence in T cells by measuring the presence of the well-known senescence-associated marker β-galactosidase (Akbar et al., 2016). FACS analysis revealed an increased percentage of β-galactosidase positive cells in *ex vivo* WT compared to *P2rx7*$^{-/-}$ TEM cells (Figure 3F). Moreover, treating WT cells with BzATP induced a significant increase in the percentage of β-galactosidase positive cells, which was abolished by the pretreatment with A-438079 antagonist (Figure 3F). These results prompted us to characterize the molecular pathway/s associated to the induction of senescence by P2X7 receptor activity in TEM cells.

Senescent T cells are characterized by constitutive activation of p38 MAPK (Davis et al., 2010). Accordingly, western blot analysis of TEM cells treated with BzATP revealed an increased phosphorylation of p38 MAPK at site

Thr180/Tyr182 (Figure 4A). Moreover, pretreating WT TEM cells with the p38 antagonists PD169316 and SB239063 prevented *Cdkn1a* upregulation mediated by P2X7 stimulation (Figure 4B). Next, we assessed the expression of other senescence-associated genes, including *trp53* and the growth arrest and DNA damage inducible 45 beta (*gadd45b*) (Akbar et al., 2016). qRT-PCR revealed a significant increase both in *trp53* and *gadd54b* transcripts in WT TEM cells treated with BzATP and, again, the pretreatment with A-438079 restored the basal transcriptional level (Figure 4C).

The increase of ROS production is often seen in prematurely senescent cells (Passos and Zglinicki, 2012). We measured mitochondrial ROS production at FACS in WT and *P2rx7*$^{-/-}$ TEM cells labelled with MitoSOX dye. *Ex vivo* WT cells produced higher levels of mitochondrial ROS compared to *P2rx7*$^{-/-}$ cells (Figure 4 D). When we stimulated WT cells with BzATP, we saw a significant increase in the percentage of MitoSOX positive cells that we prevented by pretreatment with A-438079 (Figure 4D). These data are consistent with the hypothesis that P2X7 receptor activity induces premature senesce in TEM cells. To further confirm this idea, we measured the phosphorylation of the histone H2AX at serine 139 (γ-H2AX) (Siddiqui et al., 2015). Western blot analysis revealed an increase in γ-H2AX at steady state in WT compared to *P2rx7*$^{-/-}$ TEM cells. Moreover, P2X7 stimulation with BzATP further increased the magnitude of γ-H2AX, while pretreatment with A-438079 abolished it (Figure 4E). All these results clearly show that the absence or pharmacological inhibition of P2X7 prevent the induction of premature senescence in TEM cells.

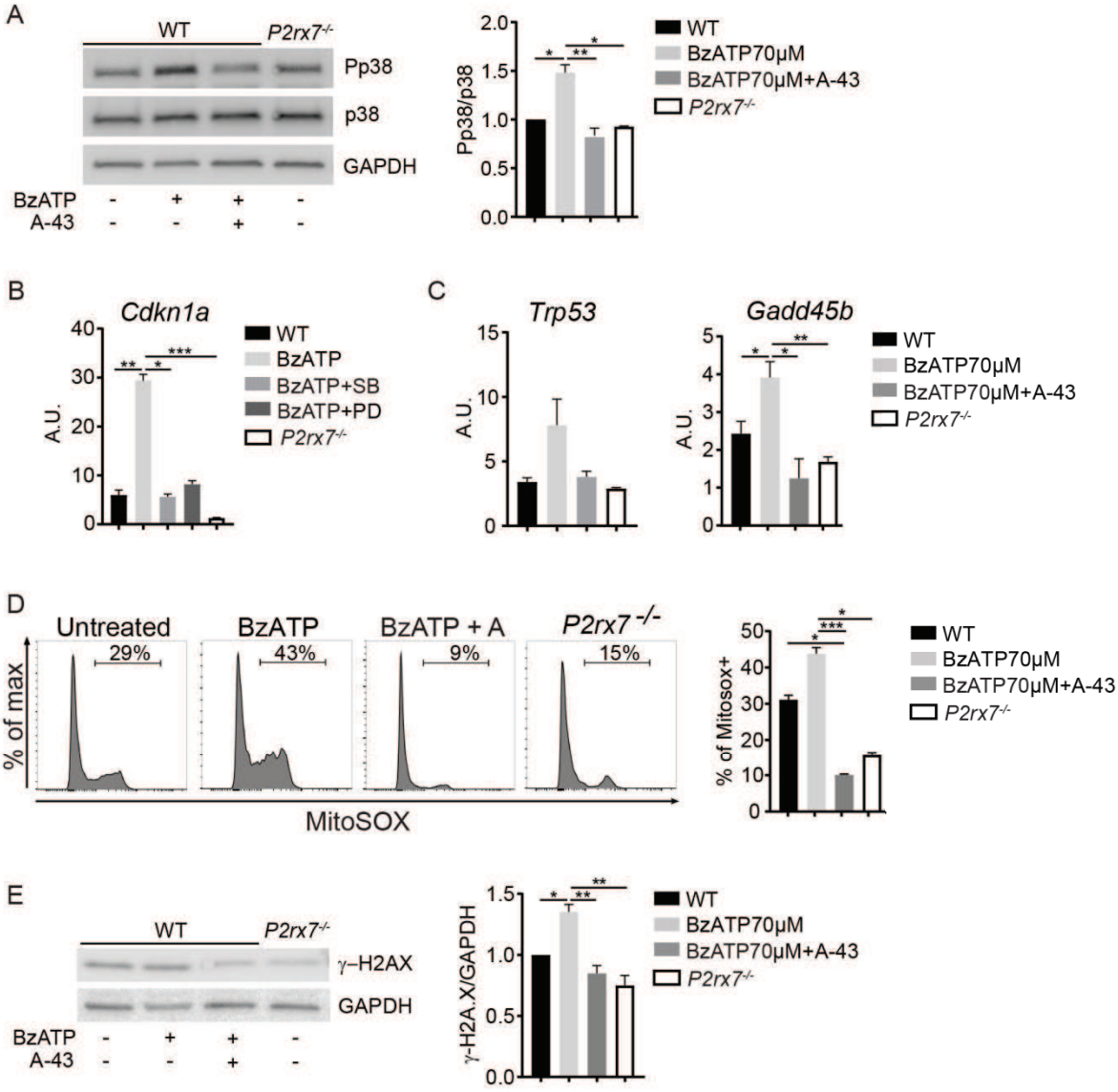
A
WT
P2rx7-/-
Pp38
p38
GAPDH
BzATP - + + -
A-43 - - + -
Pp38/p38
WT
BzATP70μM
BzATP70μM+A-43
P2rx7-/-
B
Cdkn1a
A.U.
WT
BzATP
BzATP+SB
BzATP+PD
P2rx7-/-
C
Trp53
Gadd45b
A.U.
WT
BzATP70μM
BzATP70μM+A-43
P2rx7-/-
D
Untreated
BzATP
BzATP + A
P2rx7 -/-
29%
43%
9%
15%
% of max
MitoSOX
% of Mitosox+
WT
BzATP70μM
BzATP70μM+A-43
P2rx7-/-
E
WT
P2rx7-/-
γ–H2AX
GAPDH
BzATP - + + -
A-43 - - + -
γ-H2A.X/GAPDH
WT
BzATP70μM
BzATP70μM+A-43
P2rx7-/-

Figure 4: P2X7 receptor signaling pathway. A) Western blot analysis on cell protein extracts from WT and *P2rx7*$^{-/-}$ TEM cells stimulated with anti-CD3 and anti-CD28 antibodies for 3 days and treated as indicated. Samples were probed for p38 MAPK phosphorylated at Thr180/Tyr182 (Pp38), p38 total protein and GAPDH. Histograms represent the densitometric analysis of Pp38 normalized on total p38. Histograms shows mean ± SEM. B) Quantitative RT-PCR of *Cdkn1a* transcript performed on WT TEM cells either untreated, treated with BzATP, or treated with BzATP together with PD 169316 and SB 239063 and on *P2rx7*$^{-/-}$ TEM cells. Histograms show mean ± SEM. C) Quantitative RT-PCR of *Trp53* and *Gadd45b* transcripts. The analysis was performed on purified WT and *P2rx7*$^{-/-}$ TEM cells stimulated as indicated. Histograms show mean ± SEM. E) Representative FACS plots and statistical analysis of WT TEM cells labelled with MitoSOX and stimulated with BzATP 70 μM or pretreated with A-438079 50 μM, and *P2rx7*$^{-/-}$ TEM cells. Numbers in the plots indicate the percentage of MitoSOX positive cells and the histogram shows percentage mean ± SEM. F) Western blot analysis on cell protein extracts from WT and *P2rx7*$^{-/-}$ TEM cells stimulated with anti-CD3 and anti-CD28 antibodies for 3 days and treated as indicated. Samples were probed for histone H2AX phosphorylated at serine 139 (γ-H2Ax), and GAPDH. Histogram represents densitometric analysis of γ-H2Ax normalized on GAPDH. Histograms show mean ± SEM. Data are representative results of at least three independent experiments with 3 to 5 mice per experiment. A.U., Arbitrary Unit. * $p<0.05$, ** $p<0.01$, *** $p<0.001$.

Deletion of P2X7 receptor in CD4 T cells results in their accumulation in the tumor microenvironment

The tumor microenvironment imposes metabolic restriction that can mediate hyporesponsiveness of TILs through different mechanisms, including T cell senescence (Crespo et al., 2013). It was demonstrated that the tumor microenvironment is rich in ATP (Pellegatti et al., 2008), so we hypothesized that P2X7-mediated premature senescence through the upregulation of p21 might limit TILs anti-cancer response. To address this, we reconstituted *cd3ε*$^{-/-}$ mice with CD4+ CD25- TEM cells deriving from WT or *P2rx7*$^{-/-}$ mice. After five days we injected subcutaneously B16 tumor cells and monitored the tumor growth for the next twenty days, when the mice were sacrificed (Figure 5A). FACS analysis of the tumor revealed a significant increase in the percentage of CD4+ TILs in mice injected with *P2rx7*$^{-/-}$ cells (Figure 5B). Histological analysis of tumor samples further confirmed an increased accumulation of *P2rx7*$^{-/-}$ than WT TEM cells in the tumor (Figure 5C), suggesting that the absence of the receptor confers a survival/proliferation advantage to TEM cells. Moreover,

FACS analysis of TILs showed a significant increase in the percentage of Ki-67 positive in mice adoptively transferred with *P2rx7*$^{-/-}$ T cells compared to WT cells (Figure 5E), indicating that lack of P2X7 endow TEM cells with increased expansion potential within the tumor. Consistent with these results, qRT-PCR revealed a reduced expression of *Cdkn1a* transcripts in *P2rx7*$^{-/-}$ compared to WT TILs (Figure 5D). Despite the significant advantage of *P2rx7*$^{-/-}$ over WT TEM in tumor infiltration, the tumor size was not different in *cd3ε*$^{-/-}$ mice reconstituted with TEM cells of the two genotypes (Figure 5F).

Reconstitution of *cd3ε*$^{-/-}$ mice with WT or *P2rx7*$^{-/-}$ CD4+ T naïve cells in the same experimental setting resulted in analogous outcome (Figure 5G). By FACS analysis we observed an increase in the percentage of CD4+ TILs in mice reconstituted with *P2rx7*$^{-/-}$ compared to WT cells (Figure 5H) and qRT-PCR showed a reduction in *Cdkn1a* transcripts in *P2rx7*$^{-/-}$ cells (Figure 5I). Our results suggest that lack of P2X7 receptor supports the survival and the accumulation of CD4 T cells in the tumor microenvironment. However, in spite of enhanced infiltration we could not detect any difference in tumor size between mice injected with *P2rx7*$^{-/-}$ or WT cells. We hypothesized this phenomenon could be due to the absence of a direct cytotoxic effect of CD4 T cells against the tumor.

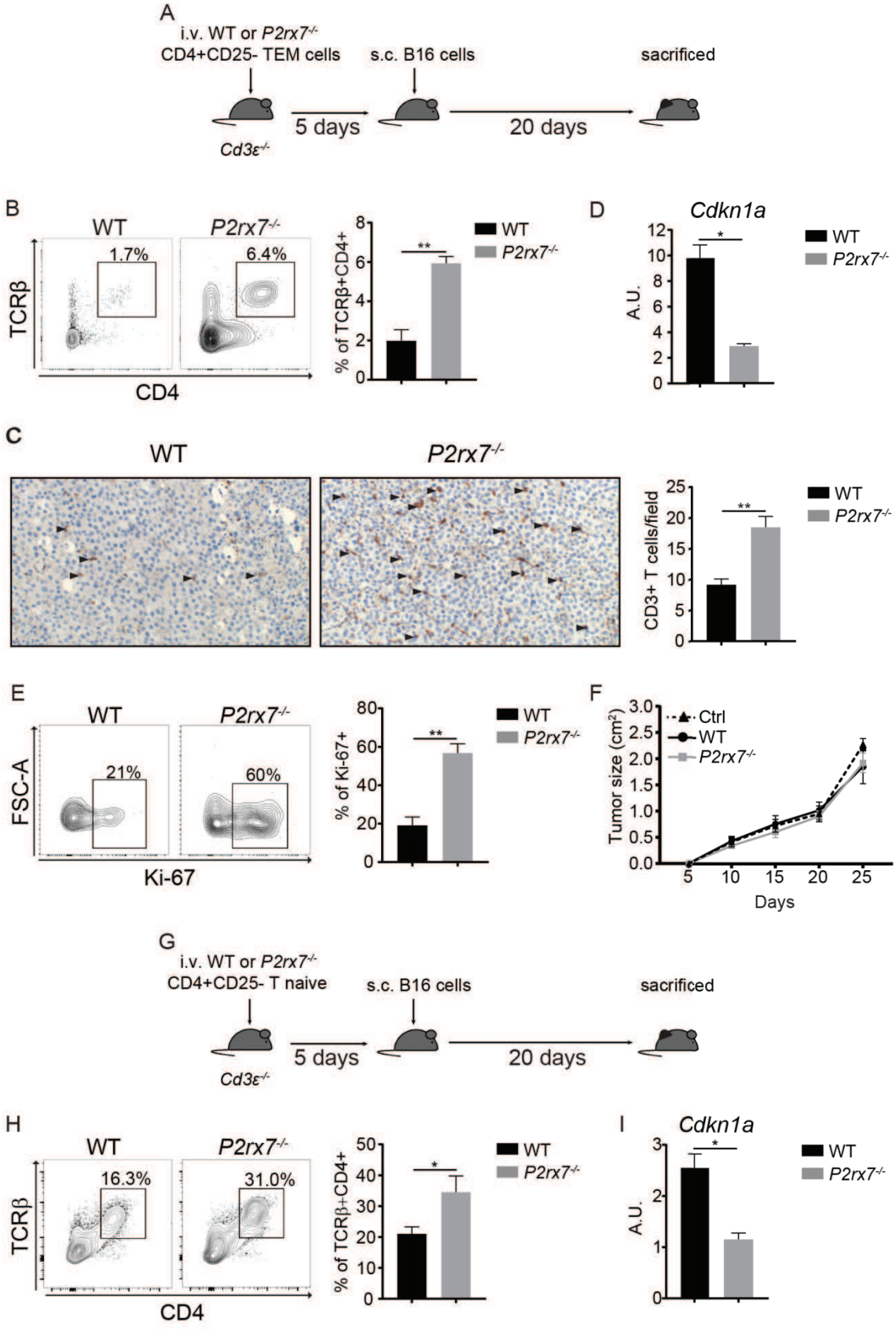
A
i.v. WT or P2rx7-/-
CD4+CD25- TEM cells
s.c. B16 cells
sacrificed
5 days
20 days
Cd3ε-/-
B
WT
P2rx7-/-
1.7%
6.4%
TCRβ
CD4
% of TCRβ+CD4+
**
WT
P2rx7-/-
D
Cdkn1a
A.U.
*
WT
P2rx7-/-
C
WT
P2rx7-/-
CD3+ T cells/field
**
WT
P2rx7-/-
E
WT
P2rx7-/-
21%
60%
FSC-A
Ki-67
% of Ki-67+
**
WT
P2rx7-/-
F
Ctrl
WT
P2rx7-/-
Tumor size (cm2)
Days
G
i.v. WT or P2rx7-/-
CD4+CD25- T naive
s.c. B16 cells
sacrificed
5 days
20 days
Cd3ε-/-
H
WT
P2rx7-/-
16.3%
31.0%
TCRβ
CD4
% of TCRβ+CD4+
*
WT
P2rx7-/-
I
Cdkn1a
A.U.
*
WT
P2rx7-/-

Figure 5: *P2rx7*$^{-/-}$ CD4 T cells survive and accumulate more within the tumor than WT CD4 T cells. A) Schematic representation of the experimental procedure: 250.000 WT or *P2rx7*$^{-/-}$ CD4+CD25- TEM were injected intravenously (i.v.) into *cd3ε*$^{-/-}$ mice. After 5 days, 500.000 B16 tumor cells were injected subcutaneously (s.c.) and after 20 days the mice were sacrificed. B) FACS plot for surface CD4 and TCRβ and statistical analysis of TILs from *cd3ε*$^{-/-}$ mice reconstituted with WT or *P2rx7*$^{-/-}$ CD4 TEM cells. Numbers in the plot represent the percentage of CD4, TCRβ positive cells within the tumor. Histogram shows percentage mean ± SEM. C) Immunohistochemistry of tumor samples from *cd3ε*$^{-/-}$ mice reconstituted with CD4 WT (left) or *P2rx7*$^{-/-}$ (right) TEM cells, labeled for CD3+ TILs (arrowhead). Histogram shows mean ± SEM of the number of CD3+ TILs per field analyzed. D) Quantitative RT-PCR for *Cdkn1a* transcript performed on CD4+ TCRβ+ TILs from *cd3ε*$^{-/-}$ mice reconstituted with CD4 WT or *P2rx7*$^{-/-}$ TEM cells. E) Dot plots of FACS staining and statistical analysis for the nuclear antigen Ki-67 performed on CD4, TCRβ positive cells in the tumor of *cd3ε*$^{-/-}$ mice reconstituted with CD4 WT or *P2rx7*$^{-/-}$ TEM cells. Numbers in the plot represent the percentage of Ki-67 positive cells. The histogram shows the mean percentage ± SEM. F) Analysis of tumor size (area in cm^2) over time in *cd3ε*$^{-/-}$ mice transplanted with 500.000 B16 tumor cells and injected with 250.000 CD4 WT or *P2rx7*$^{-/-}$ TEM cells. G) Schematic representation of experimental procedure: 250.000 WT or *P2rx7*$^{-/-}$ CD4+ CD25- T naive cells were injected intravenously (i.v.) into *cd3ε*$^{-/-}$ mice. After 5 days, 500.000 B16 tumor cells were injected subcutaneously (s.c.) and after 20 days the mice were sacrificed. H) FACS plot and statistical analysis for CD4 and TCRβ within the tumor of *cd3ε*$^{-/-}$ mice reconstituted with CD4 WT or *P2rx7*$^{-/-}$ T naive cells. Numbers in the plot represent percentage of CD4 and TCRβ positive cells. Histogram shows the percentage mean ± SEM. I) Quantitative RT-PCR for *Cdkn1a* transcript performed on CD4 TILs. Data are representative results of at least three independent experiments with 3 to 5 mice per experiment. A.U., Arbitrary Unit. * $p<0.05$, ** $p<0.01$.

The ablation of P2X7 receptor in CD8 T cells improves their accumulation in the tumor microenvironment and results in reduction of tumor size

Unlike CD4 T cells, CD8 T cells exert a direct cytotoxic effect against tumor cells and because of this function their accumulation in the tumor is beneficial (Sorensen et al., 2012). This prompted us to investigate whether deletion of *P2rx7* could contribute enhanced tumor infiltrating and cytotoxic activities to CD8 T cells.

First, we analyzed *P2rx7* expression in CD8 naïve and TEM cells. qRT-PCR revealed that both CD8 naïve and TEM cells express lower levels of *P2rx7* mRNA compared to CD4 TEM cells (Figure 6A). FACS analysis of DAPI permeability after stimulation with BzATP confirmed the reduced functionality of P2X7 receptor in CD8 compared to CD4 TEM cells (Figure 6B).

We measured cell proliferation at FACS after labelling cells with CellTrace violet and stimulating them with anti-CD3 and anti-CD28 antibodies. Interestingly, while 70 and 100 μM BzATP had no significant effects on the cell cycling activity of CD8 T cells, a higher concentration of BzATP (200 μM) induced a blockade in the cell cycle progression of CD8 TEM cells (Figure 6C), to a similar extent as lower concentrations in CD4 TEM cells (Figure 3D). Analysis of the expression of *Cdkn1a* by qRT-PCR showed a significant increase of transcripts when CD8 TEM cells were treated with high concentration of BzATP and the pre-treatment with P2X7 antagonist A-438079 restored the basal level (Figure 6D).

Thus, because the high concentrations of eATP present in the tumor microenvironment are compatible with inhibition of CD8 cells via P2X7, we repeated the adoptive transfer experiment on tumor bearing *cd3ε*$^{-/-}$ mice with naïve CD8 cells derived from either WT or *P2rx7*$^{-/-}$ animals. We injected B16 tumor cells 5 days after CD8 cells transfer and analyzed the tumor infiltrating cells 20 days later (Figure 6E). FACS analysis of the tumor revealed that the majority of TILs acquired a TEM-like phenotype. Moreover, we observed a significant increase in the percentage of tumor infiltrating CD8 T cells in mice reconstituted with *P2rx7*$^{-/-}$ cells as compared to those reconstituted with WT cells (Figure 6F). Interestingly, mice that received *P2rx7*$^{-/-}$ CD8 cells were able to control tumor growth with significantly increase efficacy than mice that received WT cells (Figure 6 G). These data suggest that, despite expression of lower levels of *P2rx7* transcripts in CD8 T cells, P2X7 receptor influences the survival and proliferation of CD8 cells in the tumor microenvironment, which is very rich in eATP, Lack of P2X7 in both CD4 and CD8 T cells is beneficial in adoptive cellular immunotherapy against tumor, suggesting that inhibition of P2X7 receptor might be exploited for enhancing tumoricidal effect of adoptively transferred T cells in cancer immunotherapy.

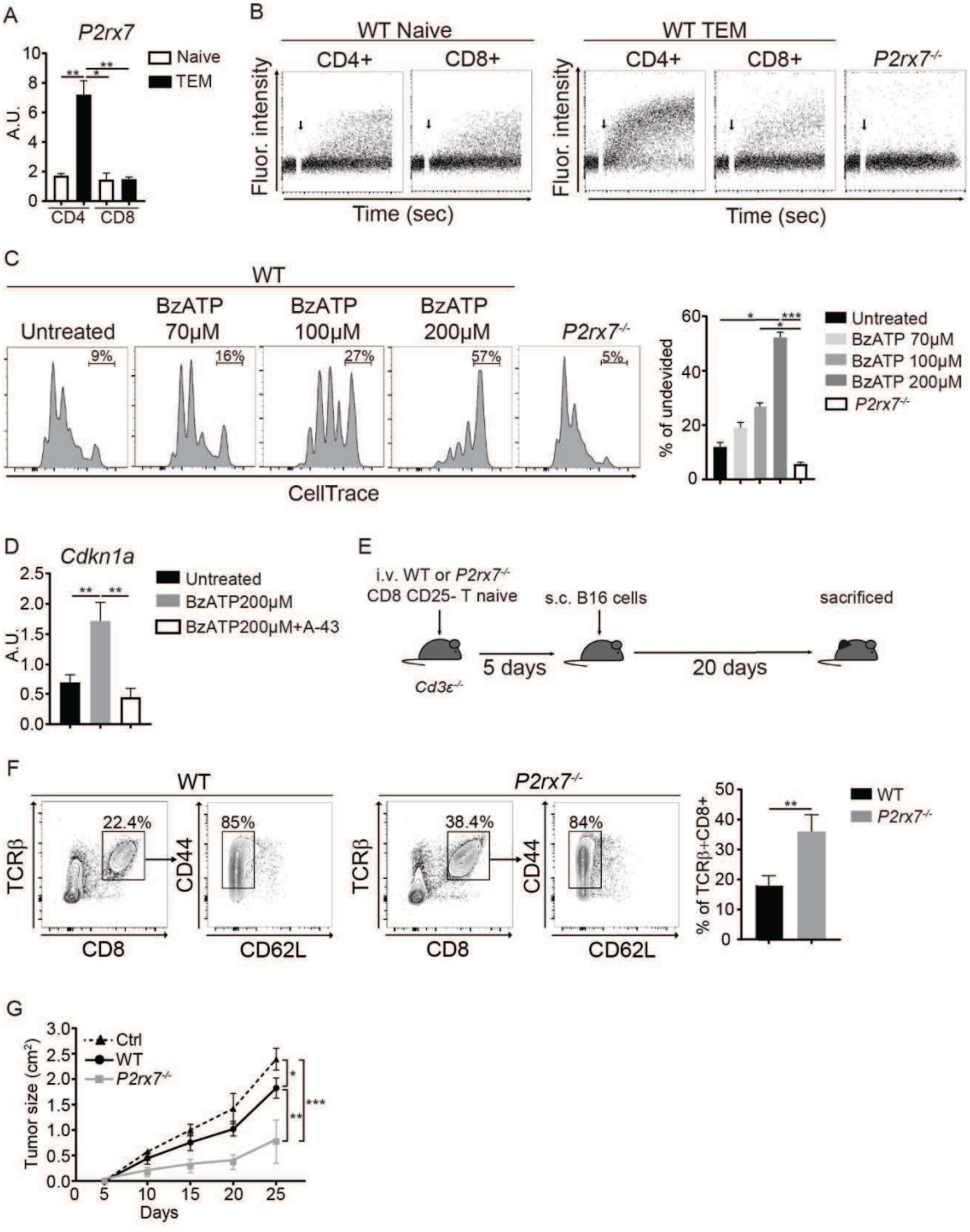
A
P2rx7
Naive
TEM
A.U.
CD4
CD8
B
WT Naive
WT TEM
CD4+
CD8+
P2rx7-/-
Fluor. intensity
Time (sec)
C
WT
Untreated
BzATP 70µM
BzATP 100µM
BzATP 200µM
P2rx7-/-
9%
16%
27%
57%
5%
CellTrace
% of undevided
D
Cdkn1a
Untreated
BzATP200µM
BzATP200µM+A-43
E
i.v. WT or P2rx7-/-
CD8 CD25- T naive
s.c. B16 cells
sacrificed
Cd3ε-/-
5 days
20 days
F
WT
P2rx7-/-
22.4%
85%
38.4%
84%
TCRβ
CD8
CD44
CD62L
% of TCRβ+CD8+
G
Ctrl
WT
P2rx7-/-
Tumor size (cm²)
Days

Figure 6: *P2rx7*$^{-/-}$ CD8 T cells exert enhanced control on tumor size than WT cells. A) Quantitative RT-PCR for *P2rx7* transcript performed on CD4+ and CD8+ T naïve and TEM cells. Histogram shows the mean ± SEM. B) Time-monitoring of DAPI permeability at FACS after stimulation with BzATP of purified WT CD4 and CD8 T naïve and TEM cells. CD8 *P2rx7*$^{-/-}$ TEM cells were also tested as negative control. C) Representative CellTrace dilution and statistical analysis of purified CD8 WT and *P2rx7*$^{-/-}$ TEM cells stimulated with anti-CD3 and anti-CD28 antibodies for 3 days. CD8 WT TEM cells were treated with increasing concentrations of BzATP (70 μM, 100 μM and 200 μM). The numbers in the FACS plots represent the percentage of undivided cells and the histogram shows the percentage mean ± SEM. D) Quantitative RT-PCR of *Cdkn1a* performed on CD8 WT TEM cells either untreated, treated with BzATP 200 μM or pretreated with A-438079 50 μM. E) Schematic representation of the experimental procedure: 250.000 WT or *P2rx7*$^{-/-}$ CD8+ CD25- T naive cells were injected intravenously (i.v.) into *cd3ε*$^{-/-}$ mice. After 5 days, 500.000 B16 tumor cells were injected subcutaneously (s.c.) and after 20 days the mice were sacrificed. F) Dot plots of FACS staining for CD8 and TCRβ positive cells in the tumor and distribution for CD44 and CD62L staining from *cd3ε*$^{-/-}$ mice reconstituted with CD8 WT or *P2rx7*$^{-/-}$ T naïve cells. Numbers in the plots represent the percentage of TILs and the histograms show the mean percentage ± SEM. G) Analysis of tumor size (area in cm^2) in *cd3ε*$^{-/-}$ mice reconstituted with CD8 WT or *P2rx7*$^{-/-}$ T naïve cells and injected with B16 tumor cells. Data are representative results of at least three independent experiments with 3 to 5 mice per experiment. A.U., Arbitrary Unit. * $p<0.05$, ** $p<0.01$ *** $p<0,001$.

P2RX7 silencing confers an advantage in cell proliferation and survival to human CD4 TEM cells

In order to see if P2X7 receptor has the same function in human T cells, we isolated human CD4 TEM cells and transfected them with *P2RX7* siRNA to silence its expression, and then analyzed cell proliferation. After siRNA transfection, we measured by qRT-PCR a partial but significant downregulation of *P2RX7* transcript in human TEM cells compared to cells transfected with a control siRNA (Figure 7A). Thus, we analyzed at FACS cell proliferation of transfected TEM cells labeled with CellTrace violet, after stimulation with anti-CD3 and anti-CD28 antibodies. After five days, CellTrace dilution clearly showed that TEM cells transfected with *P2RX7* siRNA proliferated significantly more than cells transfected with control siRNA (Figure 7B).

Thus, we measured *CDKN1A* expression by qRT-PCR and we observed a significant reduction of the transcript in TEM cells transfected with *P2RX7* siRNA compared to control cells (Figure 7C). Interestingly, when we stimulated

control TEM cells with BzATP we measured a significant increase in *CDKN1A* expression, as detected in mouse *P2rx7*$^{-/-}$ TEM cells (Figure 7C and 3C), suggesting that also in human cells P2X7 stimulation controls the transcription of *CDKN1A* and could be involved in the induction of premature senescence of T cells.

To see whether P2X7 activity could condition human TEM cells function in the tumor microenvironment, we cultured human TEM cells in medium conditioned with HeLa cells supernatant and measured the percentage of dead cells. FACS staining for annexin V and propidium iodide (PI) revealed a significant reduction in the double positive population in TEM cells transfected with *P2RX7* siRNA compared to TEM cells transfected with control siRNA (Figure 7D), indicating that silencing of *P2RX7* conferred resistance to cell death induced by ATP released by tumor cells. These data shows that inhibition of P2X7 activity confers a survival and cell proliferation advantage to human TEM cells, making P2X7 receptor a possible target to enhance tumor immunotherapy.

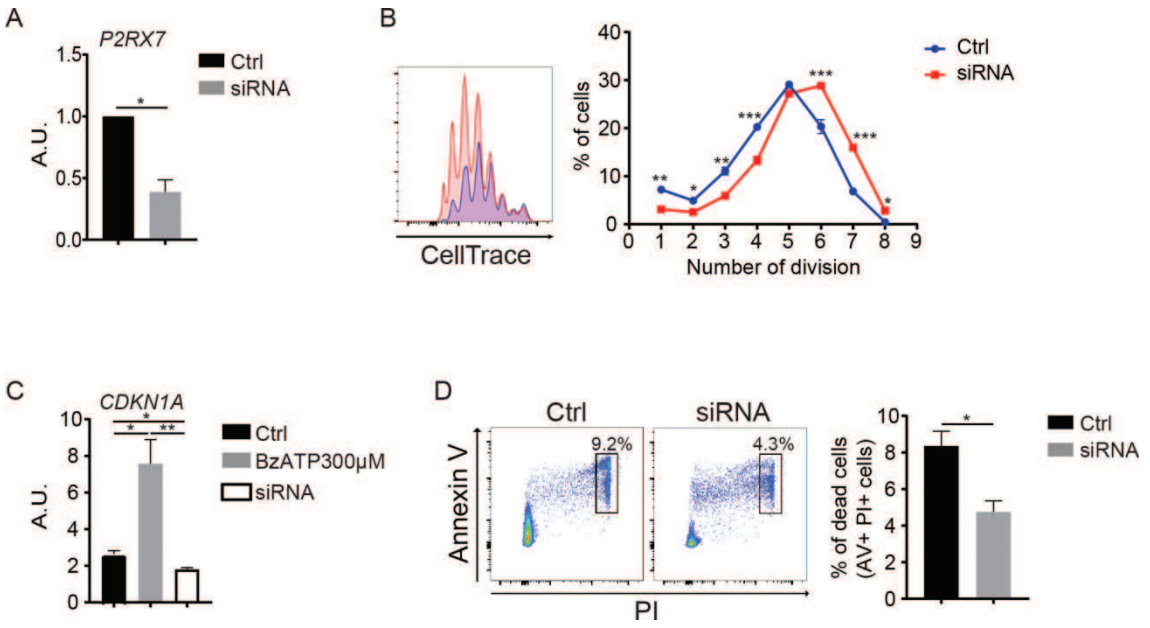

Figure 7: *P2RX7* silencing in human TEM cells promotes cell survival and proliferation. A) Quantitative RT-PCR for *P2RX7* transcript performed on human CD4 TEM cells transfected with *P2RX7* siRNA (siRNA) or with a control siRNA (Ctrl). Histograms show the mean ± SEM. All values were normalized on Ctrl values. B) Representative CellTrace dilution and statistical analysis of purified human TEM cells (transfected as indicated above) stimulated with anti-CD3 and anti-CD28 antibodies for 5 days. The graph represents means ± SEM (Y axis) of cell percentages within each cell division (X axis). C) Quantitative RT-PCR for *CDKN1A* transcript performed on Ctrl CD4 TEM cells with or without BzATP 300 µM, and TEM cells transfected with *P2RX7* siRNA. Histograms show the means ± SEM. D) FACS plot and statistical analysis of Annexin V and propidium iodide (PI) staining performed on human Ctrl and *P2RX7* siRNA TEM cells cultured with HeLa cells supernatant. Numbers in the plots represent the percentage of Annexin V and PI positive cells. The histograms show the percentage means ± SEM. A.U., Arbitrary Units. * p<0.05, ** p<0.01 *** p<0,001.

Lack of P2X7 receptor results in increased mitochondrial fusion and metabolic advantage of TEM cells

Morphological changes in mitochondria represent a primary signal in metabolic reprogramming during cellular quiescence or activation. In particular, mitochondrial fusion is considered a survival mechanism that enhances longevity in T cells (Gomes et al., 2011). This prompted us to characterize the morphology of mitochondria in TEM cells. Transmission electron microscopy performed on WT or *p2rx7*$^{-/-}$ TEM cells stimulated with anti-CD3 and anti-CD28

antibodies revealed significant differences in mitochondrial dimensions between the two genotypes (Figure 8A). We measured a significant increase in both the mitochondrial area and perimeter of *P2rx7*$^{-/-}$ TEM cells (Figure 8B and 8C), while no differences were seen in the circularity of the organelles (Figure 8D). We therefore analyzed by western blot the levels of mitochondrial inner membrane fusion protein Opa1, which was demonstrated to be fundamental for memory T cells generation (Buck et al., 2016), and fission protein Drp1. Consistent with morphological data, we detected an increase in Opa1 and a decrease in Drp1 levels in *P2rx7*$^{-/-}$ compared to WT TEM cells (Figure 8E). These data suggest that mitochondria are poised to fusing in *P2rx7*$^{-/-}$ TEM cells.
Recent work demonstrates that fused mitochondria are characterized by tighter cristae compared to fissed mitochondria. Tight cristae favor electron transport chain activity, therefore mitochondrial fusion favors oxidative phosphorylation (Sena et al., 2013). Given the different phenotype of mitochondria, we analyzed the bioenergetic profile of *P2rx7*$^{-/-}$ and WT TEM cells with the Seahorse technique in response to secondary stimulation with oligomycin (ATP synthase inhibitor), followed by FCCP (oxidative phosphorylation uncoupler) and rotenone with antimycin A (ETC complex I and III inhibitors), all drugs that stress the mitochondria. From the analysis of the metabolic profile we could reveal an increase in metabolic activity in *P2rx7*$^{-/-}$ compared to WT TEM cells, shown by the increased oxygen consumption rate (OCR) (Figure 8F). These data indicate that lack of P2X7 confers a metabolic advantage by using mitochondrial respiration over glycolysis.
Altogether these results unravel an inhibitory function for P2X7 receptor in TEM cells unraveling a novel role for P2X7 as a checkpoint inhibitor molecule.

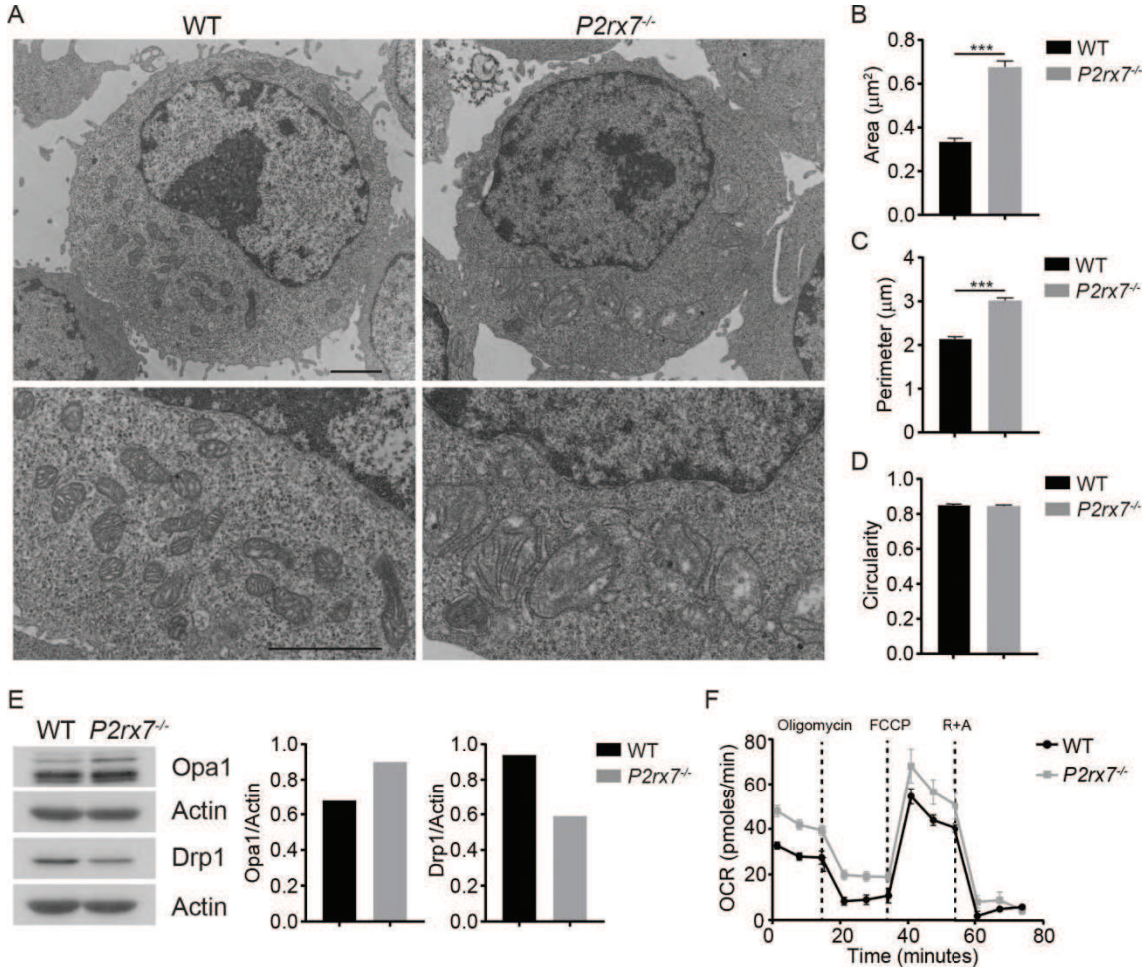

Figure 8: : *P2rx7*$^{-/-}$ TEM cells are characterized by fused mitochondria and metabolic advantage. A) Electron micrographs showing the entire cell (above) and a detail of mitochondria (below) of WT and *P2rx7*$^{-/-}$ TEM cells. Scale bars: 2 µm. B) Statistical analysis of area, perimeter (C) and circularity (D) of mitochondria in WT and *P2rx7*$^{-/-}$ cells. Histograms show the mean ± SEM. E) Protein quantification by western blot of inner membrane fusion protein Opa1 and fission protein Drp1. Histograms represent the densitometric analysis of the proteins normalized on GAPDH. F) Seahorse metabolic profile showing OCR measurement of WT and *P2rx7*$^{-/-}$ TEM cells at baseline, after stimulation with oligomycin, FCCP and rotenone plus antimycin A (R+A). Shown are means ± SEM. Data are representative results of two independent experiments with 5 mice for experiment. *** p<0,001.

DISCUSSION

Nucleotides such as ATP or UTP are mainly found inside cells, nevertheless they are also released in the extracellular space by different mechanisms and play important functions in intercellular communication. An important mechanism of nucleotide release is represented by cell damage and death: apoptotic and necrotic cells release ATP as a danger signal or damage associated molecular pattern (DAMP) (Idzko et al., 2007). In the absence of cell death, mechanical stimulation, hypoxia or pathogens invasion, or specific release pathways such as membrane channels, vesicular transport and exocytosis of granules, are involved in the secretion of ATP outside the cell (Burnstock and Boeynaems, 2014). ATP released during tissue damage acts as a DAMP for the cells of the innate immune system through stimulation of P2X7 receptor. *P2rx7*, which encodes for the P2X7 receptor, is a signature gene of effector T cell subsets (Choi et al., 2013 J of immunology; (Hale et al., 2013; Hashimoto-Hill et al., 2017; Hill et al., 2008), but its role in these cells has been poorly investigated. Early studies suggested that CD4 T cells in peripheral lymph nodes are sensitive to P2X7-induced cell death (Haag et al., 2002; Seman et al., 2003), but it is unclear whether there is any specificity in *P2rx7* expression for specific T cell subsets or differentiation stages. We have shown that *P2rx7* is the most expressed member of the *P2rx* gene family both in T naïve and T effector/memory (TEM) cells, but it is selectively and robustly upregulated in TEM cells. *P2rx7* expression correlates with its functionality. Indeed, TEM cells stimulated with a selective P2X7 agonist becomes permeable to DAPI, in agreement with the formation of a cytolytic pore, which is permeable to molecules with size up to 1.4 nm (Browne et al., 2013).

Effector memory T cells are generated following priming of naïve clones in secondary lymphoid organs by antigen presentation though class II major histocompatibility complex (MHC II) on antigen presenting cells (APC). Once the pathogen is cleared during primary response, the majority of effector cells are eliminated during the contraction phase of the adaptive immune response, but a small population of long-lived cells will constitute the memory pool of antigen experienced T cells. This pool of memory T cells can be classified as

TEM and T central memory (TCM) cells. TEM cells migrate to inflamed peripheral tissues and provide immediate effector response, while TCM cells home to secondary lymphoid organs and differentiate to effector cells in response to a second antigenic stimulation (Sallusto et al., 2004). Memory T cells differ from naïve cells because of their lower activation threshold and more vigorous expansion following antigen encounter. Moreover, TEM cells can proliferate in the absence of antigen in response to cytokines (Kondrack et al., 2003). Understanding cell intrinsic programs that regulate TEM cells lifespan and expansion have implications in both physiological and pathological conditions, such as autoimmune diseases, transplant rejection, cancer and aging of the immune system.

It was recently demonstrated that P2X7 receptor mediates cell death within the intestinal effector T cells pool, preventing aberrant buildup of activated T cells (Hashimoto-Hill et al., 2017). According to that, our results show that the absence of P2X7 receptor confers an increased half-life and survival to TEM cells *in vitro*. Moreover, we uncovered a role for P2X7 receptor in regulating T cell cycling activity. We found that both in antigen-driven and cytokine-driven expansion *P2rx7*$^{-/-}$ TEM cells are characterized by a proliferative advantage compared to WT TEM cells. This feature was also confirmed *in vivo* in a model of homeostatic expansion.

Interestingly, P2X7 activation promotes a block in the cell cycle progression in a dose dependent manner, while absence of P2X7 receptor or pharmacological antagonism unleashes TEM cells from the homeostatic control of survival and expansion. We demonstrated that P2X7 activation regulates the transcription of *Cdkn1a* as a key negative regulator of cell cycle progression and inducer of premature senescence in TEM cells. *Cdkn1a* encodes for p21$^{waf1/Cip1}$ protein and its expression correlates with *P2rx7* expression. The P21$^{waf1/Cip1}$ signaling pathway actively contributes to the stability of the G_0 arrest in senescent cells and is constantly upregulated after the induction of senescence (d'Adda di Fagagna et al., 2003). We found that P2X7 signaling results in the activation of p38 MAPK, the upregulation of *Trp53* and *Gadd45b* expression as well as in triggering of a DNA damage response induced by increased mitochondrial ROS production, all features associated to cellular senescence (Passos et al., 2010).

It is naturally thought that senescence is associated with the physiological aging process, however, tumor cells for example can induce premature T cell senescence. In addition to phenotypic changes, senescent T cells are characterized by defective cytotoxicity and development of immunosuppressive regulatory functions, thereby becoming less efficient in controlling tumor burden (Akbar and Henson, 2011; Appay et al., 2000). Senescent CD8 T cells were observed in patients with lung (Meloni et al., 2006) as well as head and neck cancers (Tsukishiro et al., 2003). The microenvironment of solid tumors is characterized by high levels of extracellular ATP (Pellegatti et al., 2008), which is important for the activation and the recruitment of immune cells and improves efficacy of chemotherapy (Michaud et al., 2011). Moreover, ATP activates NLRP3 inflammasome in tumor infiltrating DCs driving IL-1β secretion that in turn promotes the polarization of IFNγ-producing CD8 T cells, thus eliciting anti-cancer immune response (Aymeric et al., 2010). With a chimeric model of melanoma we demonstrated that adoptively transferred *P2rx7*$^{-/-}$ CD4 TEM or naïve cells, despite their lack of effect on the control of tumor size, proliferate more vigorously and accumulate to a greater extent within the tumor than WT cells. Notably, we showed that the adoptive transfer of CD8 T cells from *P2rx7*$^{-/-}$ mice, in addition to the increased infiltration of the tumor microenvironment, also resulted in a significant reduction of tumor size. CD8 TEM cells express a lower level of *P2rx7* transcripts and they are less sensitive to BzATP stimulation as compared to CD4 TEM cells. However, when stimulated with high amounts of BzATP, as found in the tumor microenvironment (Pellegatti et al., 2008), CD8 TEM cells upregulate *Cdkn1a*, which mediates a block in cell cycle progression. This evidence suggests that P2X7 is a general regulator of T cell senescence and function that might be targeted in cancer immunotherapy to achieve enhanced tumoricidal effect by TILs.

In the last years the function of P2X7 receptor in cancer biology has been intensively investigated (Di Virgilio and Adinolfi, 2017; Roger et al., 2015). Recently, it was proposed that cancer cells can undergo immunogenic cell death upon exposure to selected chemotherapeutic drugs or radiotherapy. This process would rely on the release by dying cells of factors that facilitate antigen presentation to T cells by DCs (Galluzzi et al., 2017). The immunogenicity of this kind of cell death depends on the release of intracellular molecules such as

different proteins and ATP (Ghiringhelli et al., 2009). Immunogenic cell death turned out to be important for understanding the mechanisms whereby the anti-cancer immune response could affect the outcome of anti-cancer therapy. Within this framework, the P2X7 receptor should have a prominent role in conditioning the host immune system towards a beneficial inflammatory response against the tumor. Our results show that the selective targeting of P2X7 in T cells infiltrating the tumor might avoid premature senescence and promote T cell anti-tumor response. Therefore, while contributing to tumor eradication by synergizing with chemotherapy, extracellular ATP might act in an opposite way on the adaptive branch of the anti-tumor response by limiting the lifespan and function of T cells.

Interestingly, human TEM cells, in which *P2RX7* is silenced, are characterized by increased proliferation and downregulation of *CDKN1A*. These data show that blocking P2X7 receptor in tumor infiltrating lymphocytes may be a translatable treatment for enhancing human cancer immunotherapy.

It was recently shown that metabolic programming in T cells is regulated in part by mitochondria remodeling. Memory T cells are characterized by fused mitochondria, which correlate with more efficient OXPHOS, thanks to a tighter cristae organization. This feature is associated to longevity and improves adoptive cellular immunotherapy against tumors (Buck et al., 2016; Klein Geltink et al., 2017). In line with this, we demonstrated that *P2rx7*$^{-/-}$ TEM cells are characterized by enlarged mitochondria as compared to WT TEM cells, likely due to increased expression of the mitochondrial fusion protein Opa1 and a decrease in the mitochondrial fission protein Drp1. This results in a more efficient OXPHOS as revealed by increased OCR in *P2rx7*$^{-/-}$ compared to WT TEM cells. Our data suggest a model where P2X7 receptor is an important molecule for the regulation of TEM cells survival and function. It is primarily involved in the activation of the p38 MAPK/p53/p21 signaling pathway and mediates the induction of premature senescence in TEM cells. All these features unravel a new role for P2X7 receptor as a check point inhibitor in TEM cells and a possible new target in cancer immunotherapy.

REFERENCES

Abbracchio, M.P., Burnstock, G., Boeynaems, J.M., Barnard, E.A., Boyer, J.L., Kennedy, C., Knight, G.E., Fumagalli, M., Gachet, C., Jacobson, K.A.*, et al.* (2006). International Union of Pharmacology LVIII: update on the P2Y G protein-coupled nucleotide receptors: from molecular mechanisms and pathophysiology to therapy. Pharmacol Rev *58*, 281-341.

Acuto, O., and Michel, F. (2003). CD28-mediated co-stimulation: a quantitative support for TCR signalling. Nat Rev Immunol *3*, 939-951.

Adibzadeh, M., Pohla, H., Rehbein, A., and Pawelec, G. (1995). Long-term culture of monoclonal human T lymphocytes: models for immunosenescence? Mech Ageing Dev *83*, 171-183.

Adinolfi, E., Capece, M., Franceschini, A., Falzoni, S., Giuliani, A.L., Rotondo, A., Sarti, A.C., Bonora, M., Syberg, S., Corigliano, D.*, et al.* (2015). Accelerated tumor progression in mice lacking the ATP receptor P2X7. Cancer Res *75*, 635-644.

Adriouch, S., Bannas, P., Schwarz, N., Fliegert, R., Guse, A.H., Seman, M., Haag, F., and Koch-Nolte, F. (2008). ADP-ribosylation at R125 gates the P2X7 ion channel by presenting a covalent ligand to its nucleotide binding site. FASEB J *22*, 861-869.

Adriouch, S., Hubert, S., Pechberty, S., Koch-Nolte, F., Haag, F., and Seman, M. (2007). NAD+ released during inflammation participates in T cell homeostasis by inducing ART2-mediated death of naive T cells in vivo. J Immunol *179*, 186-194.

Adriouch, S., Ohlrogge, W., Haag, F., Koch-Nolte, F., and Seman, M. (2001). Rapid induction of naive T cell apoptosis by ecto-nicotinamide adenine dinucleotide: requirement for mono(ADP-ribosyl)transferase 2 and a downstream effector. J Immunol *167*, 196-203.

Agnellini, P., Wolint, P., Rehr, M., Cahenzli, J., Karrer, U., and Oxenius, A. (2007). Impaired NFAT nuclear translocation results in split exhaustion of virus-specific CD8+ T cell functions during chronic viral infection. Proc Natl Acad Sci U S A *104*, 4565-4570.

Akbar, A.N., and Henson, S.M. (2011). Are senescence and exhaustion intertwined or unrelated processes that compromise immunity? Nat Rev Immunol *11*, 289-295.

Akbar, A.N., Henson, S.M., and Lanna, A. (2016). Senescence of T Lymphocytes: Implications for Enhancing Human Immunity. Trends Immunol *37*, 866-876.

Allen, C.D., Okada, T., and Cyster, J.G. (2007). Germinal-center organization and cellular dynamics. Immunity *27*, 190-202.

Annunziato, F., Cosmi, L., Santarlasci, V., Maggi, L., Liotta, F., Mazzinghi, B., Parente, E., Fili, L., Ferri, S., Frosali, F.*, et al.* (2007). Phenotypic and functional features of human Th17 cells. J Exp Med *204*, 1849-1861.

Annunziato, F., and Romagnani, S. (2009). Heterogeneity of human effector CD4+ T cells. Arthritis Res Ther *11*, 257.

Appay, V., Nixon, D.F., Donahoe, S.M., Gillespie, G.M., Dong, T., King, A., Ogg, G.S., Spiegel, H.M., Conlon, C., Spina, C.A.*, et al.* (2000). HIV-specific CD8(+) T cells produce antiviral cytokines but are impaired in cytolytic function. J Exp Med *192*, 63-75.
Appleman, L.J., van Puijenbroek, A.A., Shu, K.M., Nadler, L.M., and Boussiotis, V.A. (2002). CD28 costimulation mediates down-regulation of p27kip1 and cell cycle progression by activation of the PI3K/PKB signaling pathway in primary human T cells. J Immunol *168*, 2729-2736.

Asseman, C., Mauze, S., Leach, M.W., Coffman, R.L., and Powrie, F. (1999). An essential role for interleukin 10 in the function of regulatory T cells that inhibit intestinal inflammation. J Exp Med *190*, 995-1004.

Aymeric, L., Apetoh, L., Ghiringhelli, F., Tesniere, A., Martins, I., Kroemer, G., Smyth, M.J., and Zitvogel, L. (2010). Tumor cell death and ATP release prime dendritic cells and efficient anticancer immunity. Cancer Res *70*, 855-858.

Baitsch, L., Baumgaertner, P., Devevre, E., Raghav, S.K., Legat, A., Barba, L., Wieckowski, S., Bouzourene, H., Deplancke, B., Romero, P.*, et al.* (2011). Exhaustion of tumor-specific CD8(+) T cells in metastases from melanoma patients. J Clin Invest *121*, 2350-2360.

Barber, D.L., Wherry, E.J., Masopust, D., Zhu, B., Allison, J.P., Sharpe, A.H., Freeman, G.J., and Ahmed, R. (2006). Restoring function in exhausted CD8 T cells during chronic viral infection. Nature *439*, 682-687.

Beach, D., Gonen, R., Bogin, Y., Reischl, I.G., and Yablonski, D. (2007). Dual role of SLP-76 in mediating T cell receptor-induced activation of phospholipase C-gamma1. J Biol Chem *282*, 2937-2946.

Beals, C.R., Sheridan, C.M., Turck, C.W., Gardner, P., and Crabtree, G.R. (1997). Nuclear export of NF-ATc enhanced by glycogen synthase kinase-3. Science *275*, 1930-1934.

Beausejour, C.M., Krtolica, A., Galimi, F., Narita, M., Lowe, S.W., Yaswen, P., and Campisi, J. (2003). Reversal of human cellular senescence: roles of the p53 and p16 pathways. EMBO J *22*, 4212-4222.

Becker, D., Woltersdorf, R., Boldt, W., Schmitz, S., Braam, U., Schmalzing, G., and Markwardt, F. (2008). The P2X7 carboxyl tail is a regulatory module of P2X7 receptor channel activity. J Biol Chem *283*, 25725-25734.

Berard, M., and Tough, D.F. (2002). Qualitative differences between naive and memory T cells. Immunology *106*, 127-138.

Berg, L.J., Finkelstein, L.D., Lucas, J.A., and Schwartzberg, P.L. (2005). Tec family kinases in T lymphocyte development and function. Annu Rev Immunol *23*, 549-600.

Bhandoola, A., von Boehmer, H., Petrie, H.T., and Zuniga-Pflucker, J.C. (2007). Commitment and developmental potential of extrathymic and intrathymic T cell precursors: plenty to choose from. Immunity *26*, 678-689.

Blank, C., Brown, I., Peterson, A.C., Spiotto, M., Iwai, Y., Honjo, T., and Gajewski, T.F. (2004). PD-L1/B7H-1 inhibits the effector phase of tumor rejection by T cell receptor (TCR) transgenic CD8+ T cells. Cancer Res *64*, 1140-1145.

Bodin, P., and Burnstock, G. (2001). Purinergic signalling: ATP release. Neurochem Res *26*, 959-969.

Bradley, L.M., Dalton, D.K., and Croft, M. (1996). A direct role for IFN-gamma in regulation of Th1 cell development. J Immunol *157*, 1350-1358.

Brand, A., Singer, K., Koehl, G.E., Kolitzus, M., Schoenhammer, G., Thiel, A., Matos, C., Bruss, C., Klobuch, S., Peter, K.*, et al.* (2016). LDHA-Associated Lactic Acid Production Blunts Tumor Immunosurveillance by T and NK Cells. Cell Metab *24*, 657-671.

Brooks, D.G., Trifilo, M.J., Edelmann, K.H., Teyton, L., McGavern, D.B., and Oldstone, M.B. (2006). Interleukin-10 determines viral clearance or persistence in vivo. Nat Med *12*, 1301-1309.

Browne, L.E., Compan, V., Bragg, L., and North, R.A. (2013). P2X7 receptor channels allow direct permeation of nanometer-sized dyes. J Neurosci *33*, 3557-3566.

Brustle, A., Heink, S., Huber, M., Rosenplanter, C., Stadelmann, C., Yu, P., Arpaia, E., Mak, T.W., Kamradt, T., and Lohoff, M. (2007). The development of inflammatory T(H)-17 cells requires interferon-regulatory factor 4. Nat Immunol *8*, 958-966.

Buck, M.D., O'Sullivan, D., Klein Geltink, R.I., Curtis, J.D., Chang, C.H., Sanin, D.E., Qiu, J., Kretz, O., Braas, D., van der Windt, G.J.*, et al.* (2016). Mitochondrial Dynamics Controls T Cell Fate through Metabolic Programming. Cell *166*, 63-76.

Buck, M.D., Sowell, R.T., Kaech, S.M., and Pearce, E.L. (2017). Metabolic Instruction of Immunity. Cell *169*, 570-586.

Burnstock, G. (2007). Physiology and pathophysiology of purinergic neurotransmission. Physiol Rev *87*, 659-797.

Burnstock, G., and Boeynaems, J.M. (2014). Purinergic signalling and immune cells. Purinergic Signal *10*, 529-564.

Campbell, J.J., Bowman, E.P., Murphy, K., Youngman, K.R., Siani, M.A., Thompson, D.A., Wu, L., Zlotnik, A., and Butcher, E.C. (1998). 6-C-kine (SLC), a lymphocyte adhesion-triggering chemokine expressed by high endothelium, is an agonist for the MIP-3beta receptor CCR7. J Cell Biol *141*, 1053-1059.

Campisi, J., and d'Adda di Fagagna, F. (2007). Cellular senescence: when bad things happen to good cells. Nat Rev Mol Cell Biol *8*, 729-740.

Chaudhry, A., Rudra, D., Treuting, P., Samstein, R.M., Liang, Y., Kas, A., and Rudensky, A.Y. (2009). CD4+ regulatory T cells control TH17 responses in a Stat3-dependent manner. Science *326*, 986-991.

Chen, C.H., Seguin-Devaux, C., Burke, N.A., Oriss, T.B., Watkins, S.C., Clipstone, N., and Ray, A. (2003). Transforming growth factor beta blocks Tec kinase phosphorylation, Ca2+ influx, and NFATc translocation causing inhibition of T cell differentiation. J Exp Med *197*, 1689-1699.

Chen, Z., Tato, C.M., Muul, L., Laurence, A., and O'Shea, J.J. (2007). Distinct regulation of interleukin-17 in human T helper lymphocytes. Arthritis Rheum *56*, 2936-2946.

Chung, Y., Tanaka, S., Chu, F., Nurieva, R.I., Martinez, G.J., Rawal, S., Wang, Y.H., Lim, H., Reynolds, J.M., Zhou, X.H.*, et al.* (2011). Follicular regulatory T cells expressing Foxp3 and Bcl-6 suppress germinal center reactions. Nat Med *17*, 983-988.

Ciofani, M., Knowles, G.C., Wiest, D.L., von Boehmer, H., and Zuniga-Pflucker, J.C. (2006). Stage-specific and differential notch dependency at the alphabeta and gammadelta T lineage bifurcation. Immunity *25*, 105-116.

Clark, W.H. (1991). Tumour progression and the nature of cancer. Br J Cancer *64*, 631-644.

Coffman, R.L., Seymour, B.W., Hudak, S., Jackson, J., and Rennick, D. (1989). Antibody to interleukin-5 inhibits helminth-induced eosinophilia in mice. Science *245*, 308-310.

Collins, A.V., Brodie, D.W., Gilbert, R.J., Iaboni, A., Manso-Sancho, R., Walse, B., Stuart, D.I., van der Merwe, P.A., and Davis, S.J. (2002). The interaction properties of costimulatory molecules revisited. Immunity *17*, 201-210.

Coqueret, O. (2003). New roles for p21 and p27 cell-cycle inhibitors: a function for each cell compartment? Trends Cell Biol *13*, 65-70.

Cosmi, L., Maggi, L., Santarlasci, V., Liotta, F., and Annunziato, F. (2014). T helper cells plasticity in inflammation. Cytometry A *85*, 36-42.

Coyle, A.J., Lehar, S., Lloyd, C., Tian, J., Delaney, T., Manning, S., Nguyen, T., Burwell, T., Schneider, H., Gonzalo, J.A.*, et al.* (2000). The CD28-related molecule ICOS is required for effective T cell-dependent immune responses. Immunity *13*, 95-105.

Crawford, A., Angelosanto, J.M., Kao, C., Doering, T.A., Odorizzi, P.M., Barnett, B.E., and Wherry, E.J. (2014). Molecular and transcriptional basis of CD4(+) T cell dysfunction during chronic infection. Immunity *40*, 289-302.

Crawford, A., and Wherry, E.J. (2009). The diversity of costimulatory and inhibitory receptor pathways and the regulation of antiviral T cell responses. Curr Opin Immunol *21*, 179-186.

Crespo, J., Sun, H., Welling, T.H., Tian, Z., and Zou, W. (2013). T cell anergy, exhaustion, senescence, and stemness in the tumor microenvironment. Curr Opin Immunol *25*, 214-221.

Crotty, S. (2011). Follicular helper CD4 T cells (TFH). Annu Rev Immunol *29*, 621-663.

Curiel, T.J., Wei, S., Dong, H., Alvarez, X., Cheng, P., Mottram, P., Krzysiek, R., Knutson, K.L., Daniel, B., Zimmermann, M.C.*, et al.* (2003). Blockade of B7-H1 improves myeloid dendritic cell-mediated antitumor immunity. Nat Med *9*, 562-567.
d'Adda di Fagagna, F. (2008). Living on a break: cellular senescence as a DNA-damage response. Nat Rev Cancer *8*, 512-522.

d'Adda di Fagagna, F., Reaper, P.M., Clay-Farrace, L., Fiegler, H., Carr, P., Von Zglinicki, T., Saretzki, G., Carter, N.P., and Jackson, S.P. (2003). A DNA damage checkpoint response in telomere-initiated senescence. Nature *426*, 194-198.

Davis, T., Bachler, M.A., Wyllie, F.S., Bagley, M.C., and Kipling, D. (2010). Evaluating the role of p38 MAP kinase in growth of Werner syndrome fibroblasts. Ann N Y Acad Sci *1197*, 45-48.

Delgoffe, G.M., Pollizzi, K.N., Waickman, A.T., Heikamp, E., Meyers, D.J., Horton, M.R., Xiao, B., Worley, P.F., and Powell, J.D. (2011). The kinase mTOR regulates the differentiation of helper T cells through the selective activation of signaling by mTORC1 and mTORC2. Nat Immunol *12*, 295-303.

DeSilva, D.R., Jones, E.A., Feeser, W.S., Manos, E.J., and Scherle, P.A. (1997). The p38 mitogen-activated protein kinase pathway in activated and anergic Th1 cells. Cell Immunol *180*, 116-123.

Di Leonardo, A., Linke, S.P., Clarkin, K., and Wahl, G.M. (1994). DNA damage triggers a prolonged p53-dependent G1 arrest and long-term induction of Cip1 in normal human fibroblasts. Genes Dev *8*, 2540-2551.

Di Rosa, F., and Santoni, A. (2003). Memory T-cell competition for bone marrow seeding. Immunology *108*, 296-304.

Di Virgilio, F., and Adinolfi, E. (2017). Extracellular purines, purinergic receptors and tumor growth. Oncogene *36*, 293-303.

Di Virgilio, F., and Vuerich, M. (2015). Purinergic signaling in the immune system. Auton Neurosci *191*, 117-123.

Doering, T.A., Crawford, A., Angelosanto, J.M., Paley, M.A., Ziegler, C.G., and Wherry, E.J. (2012). Network analysis reveals centrally connected genes and pathways involved in CD8+ T cell exhaustion versus memory. Immunity *37*, 1130-1144.

Dolmetsch, R.E., Lewis, R.S., Goodnow, C.C., and Healy, J.I. (1997). Differential activation of transcription factors induced by Ca2+ response amplitude and duration. Nature *386*, 855-858.

Donia, M., Hansen, M., Sendrup, S.L., Iversen, T.Z., Ellebaek, E., Andersen, M.H., Straten, P., and Svane, I.M. (2013). Methods to improve adoptive T-cell therapy for melanoma: IFN-gamma enhances anticancer responses of cell products for infusion. J Invest Dermatol *133*, 545-552.

Donskoy, E., and Goldschneider, I. (1992). Thymocytopoiesis is maintained by blood-borne precursors throughout postnatal life. A study in parabiotic mice. J Immunol *148*, 1604-1612.

Dower, N.A., Stang, S.L., Bottorff, D.A., Ebinu, J.O., Dickie, P., Ostergaard, H.L., and Stone, J.C. (2000). RasGRP is essential for mouse thymocyte differentiation and TCR signaling. Nat Immunol *1*, 317-321.

Dunn, G.P., Bruce, A.T., Ikeda, H., Old, L.J., and Schreiber, R.D. (2002). Cancer immunoediting: from immunosurveillance to tumor escape. Nat Immunol *3*, 991-998.

Eales, K.L., Hollinshead, K.E., and Tennant, D.A. (2016). Hypoxia and metabolic adaptation of cancer cells. Oncogenesis *5*, e190.

Ebinu, J.O., Stang, S.L., Teixeira, C., Bottorff, D.A., Hooton, J., Blumberg, P.M., Barry, M., Bleakley, R.C., Ostergaard, H.L., and Stone, J.C. (2000). RasGRP links T-cell receptor signaling to Ras. Blood *95*, 3199-3203.

Effros, R.B. (1998). Replicative senescence in the immune system: impact of the Hayflick limit on T-cell function in the elderly. Am J Hum Genet *62*, 1003-1007.

Faulkner, H., Renauld, J.C., Van Snick, J., and Grencis, R.K. (1998). Interleukin-9 enhances resistance to the intestinal nematode Trichuris muris. Infect Immun *66*, 3832-3840.

Ferrari, D., Pizzirani, C., Adinolfi, E., Lemoli, R.M., Curti, A., Idzko, M., Panther, E., and Di Virgilio, F. (2006). The P2X7 receptor: a key player in IL-1 processing and release. J Immunol *176*, 3877-3883.

Fields, P.E., Gajewski, T.F., and Fitch, F.W. (1996). Blocked Ras activation in anergic CD4+ T cells. Science *271*, 1276-1278.

Flies, D.B., and Chen, L. (2003). A simple and rapid vortex method for preparing antigen/adjuvant emulsions for immunization. J Immunol Methods *276*, 239-242.

Forster, R., Schubel, A., Breitfeld, D., Kremmer, E., Renner-Muller, I., Wolf, E., and Lipp, M. (1999). CCR7 coordinates the primary immune response by establishing functional microenvironments in secondary lymphoid organs. Cell *99*, 23-33.

Franceschi, C., Valensin, S., Fagnoni, F., Barbi, C., and Bonafe, M. (1999). Biomarkers of immunosenescence within an evolutionary perspective: the challenge of heterogeneity and the role of antigenic load. Exp Gerontol *34*, 911-921.

Frank, M., Duvezin-Caubet, S., Koob, S., Occhipinti, A., Jagasia, R., Petcherski, A., Ruonala, M.O., Priault, M., Salin, B., and Reichert, A.S. (2012). Mitophagy is triggered by mild oxidative stress in a mitochondrial fission dependent manner. Biochim Biophys Acta *1823*, 2297-2310.

Frascoli, M., Marcandalli, J., Schenk, U., and Grassi, F. (2012). Purinergic P2X7 receptor drives T cell lineage choice and shapes peripheral gammadelta cells. J Immunol *189*, 174-180.

Frauwirth, K.A., Riley, J.L., Harris, M.H., Parry, R.V., Rathmell, J.C., Plas, D.R., Elstrom, R.L., June, C.H., and Thompson, C.B. (2002). The CD28 signaling pathway regulates glucose metabolism. Immunity *16*, 769-777.

Freeman, G.J., Wherry, E.J., Ahmed, R., and Sharpe, A.H. (2006). Reinvigorating exhausted HIV-specific T cells via PD-1-PD-1 ligand blockade. J Exp Med *203*, 2223-2227.

Friedman, J.R., and Nunnari, J. (2014). Mitochondrial form and function. Nature *505*, 335-343.

Friedman, K.M., Prieto, P.A., Devillier, L.E., Gross, C.A., Yang, J.C., Wunderlich, J.R., Rosenberg, S.A., and Dudley, M.E. (2012). Tumor-specific CD4+ melanoma tumor-infiltrating lymphocytes. J Immunother *35*, 400-408.

Galluzzi, L., Buque, A., Kepp, O., Zitvogel, L., and Kroemer, G. (2017). Immunogenic cell death in cancer and infectious disease. Nat Rev Immunol *17*, 97-111.

Gascoigne, N.R., Rybakin, V., Acuto, O., and Brzostek, J. (2016). TCR Signal Strength and T Cell Development. Annu Rev Cell Dev Biol *32*, 327-348.

Ghiringhelli, F., Apetoh, L., Tesniere, A., Aymeric, L., Ma, Y., Ortiz, C., Vermaelen, K., Panaretakis, T., Mignot, G., Ullrich, E.*, et al.* (2009). Activation of the NLRP3 inflammasome in dendritic cells induces IL-1beta-dependent adaptive immunity against tumors. Nat Med *15*, 1170-1178.

Ghoreschi, K., Laurence, A., Yang, X.P., Tato, C.M., McGeachy, M.J., Konkel, J.E., Ramos, H.L., Wei, L., Davidson, T.S., Bouladoux, N.*, et al.* (2010). Generation of pathogenic T(H)17 cells in the absence of TGF-beta signalling. Nature *467*, 967-971.

Godfrey, D.I., Kennedy, J., Mombaerts, P., Tonegawa, S., and Zlotnik, A. (1994). Onset of TCR-beta gene rearrangement and role of TCR-beta expression during CD3-CD4-CD8- thymocyte differentiation. J Immunol *152*, 4783-4792.

Godfrey, D.I., Masciantonio, M., Tucek, C.L., Malin, M.A., Boyd, R.L., and Hugo, P. (1992). Thymic shared antigen-1. A novel thymocyte marker discriminating immature from mature thymocyte subsets. J Immunol *148*, 2006-2011.

Goedegebuure, P.S., and Eberlein, T.J. (1995). The role of CD4+ tumor-infiltrating lymphocytes in human solid tumors. Immunol Res *14*, 119-131.

Goldrath, A.W., Luckey, C.J., Park, R., Benoist, C., and Mathis, D. (2004). The molecular program induced in T cells undergoing homeostatic proliferation. Proc Natl Acad Sci U S A *101*, 16885-16890.

Gomes, L.C., Di Benedetto, G., and Scorrano, L. (2011). During autophagy mitochondria elongate, are spared from degradation and sustain cell viability. Nat Cell Biol *13*, 589-598.

Gorelik, L., and Flavell, R.A. (2001). Immune-mediated eradication of tumors through the blockade of transforming growth factor-beta signaling in T cells. Nat Med *7*, 1118-1122.

Greenwald, R.J., Freeman, G.J., and Sharpe, A.H. (2005). The B7 family revisited. Annu Rev Immunol *23*, 515-548.

Greiner, E.F., Guppy, M., and Brand, K. (1994). Glucose is essential for proliferation and the glycolytic enzyme induction that provokes a transition to glycolytic energy production. J Biol Chem *269*, 31484-31490.

Haag, F., Freese, D., Scheublein, F., Ohlrogge, W., Adriouch, S., Seman, M., and Koch-Nolte, F. (2002). T cells of different developmental stages differ in sensitivity to apoptosis induced by extracellular NAD. Dev Immunol *9*, 197-202.

Haas, R., Smith, J., Rocher-Ros, V., Nadkarni, S., Montero-Melendez, T., D'Acquisto, F., Bland, E.J., Bombardieri, M., Pitzalis, C., Perretti, M.*, et al.* (2015). Lactate Regulates Metabolic and Pro-inflammatory Circuits in Control of T Cell Migration and Effector Functions. PLoS Biol *13*, e1002202.

Hahne, M., Rimoldi, D., Schroter, M., Romero, P., Schreier, M., French, L.E., Schneider, P., Bornand, T., Fontana, A., Lienard, D.*, et al.* (1996). Melanoma cell expression of Fas(Apo-1/CD95) ligand: implications for tumor immune escape. Science *274*, 1363-1366.

Haks, M.C., Lefebvre, J.M., Lauritsen, J.P., Carleton, M., Rhodes, M., Miyazaki, T., Kappes, D.J., and Wiest, D.L. (2005). Attenuation of gammadeltaTCR signaling efficiently diverts thymocytes to the alphabeta lineage. Immunity *22*, 595-606.

Hale, J.S., Youngblood, B., Latner, D.R., Mohammed, A.U., Ye, L., Akondy, R.S., Wu, T., Iyer, S.S., and Ahmed, R. (2013). Distinct memory CD4+ T cells with commitment to T follicular helper- and T helper 1-cell lineages are generated after acute viral infection. Immunity *38*, 805-817.

Hashimoto-Hill, S., Friesen, L., Kim, M., and Kim, C.H. (2017). Contraction of intestinal effector T cells by retinoic acid-induced purinergic receptor P2X7. Mucosal Immunol *10*, 912-923.

Hathcock, K.S., Laszlo, G., Pucillo, C., Linsley, P., and Hodes, R.J. (1994). Comparative analysis of B7-1 and B7-2 costimulatory ligands: expression and function. J Exp Med *180*, 631-640.

Hawkins, E.D., Hommel, M., Turner, M.L., Battye, F.L., Markham, J.F., and Hodgkin, P.D. (2007). Measuring lymphocyte proliferation, survival and differentiation using CFSE time-series data. Nat Protoc *2*, 2057-2067.

Hayes, S.M., Li, L., and Love, P.E. (2005). TCR signal strength influences alphabeta/gammadelta lineage fate. Immunity *22*, 583-593.

Henson, S.M., Lanna, A., Riddell, N.E., Franzese, O., Macaulay, R., Griffiths, S.J., Puleston, D.J., Watson, A.S., Simon, A.K., Tooze, S.A*., et al.* (2014). p38 signaling inhibits mTORC1-independent autophagy in senescent human CD8(+) T cells. J Clin Invest *124*, 4004-4016.

Henson, S.M., Macaulay, R., Riddell, N.E., Nunn, C.J., and Akbar, A.N. (2015). Blockade of PD-1 or p38 MAP kinase signaling enhances senescent human CD8(+) T-cell proliferation by distinct pathways. Eur J Immunol *45*, 1441-1451.

Herbig, U., Jobling, W.A., Chen, B.P., Chen, D.J., and Sedivy, J.M. (2004). Telomere shortening triggers senescence of human cells through a pathway involving ATM, p53, and p21(CIP1), but not p16(INK4a). Mol Cell *14*, 501-513.

Hill, J.A., Hall, J.A., Sun, C.M., Cai, Q., Ghyselinck, N., Chambon, P., Belkaid, Y., Mathis, D., and Benoist, C. (2008). Retinoic acid enhances Foxp3 induction indirectly by relieving inhibition from CD4+CD44hi Cells. Immunity *29*, 758-770.

Hirahara, K., Poholek, A., Vahedi, G., Laurence, A., Kanno, Y., Milner, J.D., and O'Shea, J.J. (2013). Mechanisms underlying helper T-cell plasticity: implications for immune-mediated disease. J Allergy Clin Immunol *131*, 1276-1287.

Hirano, F., Kaneko, K., Tamura, H., Dong, H., Wang, S., Ichikawa, M., Rietz, C., Flies, D.B., Lau, J.S., Zhu, G*., et al.* (2005). Blockade of B7-H1 and PD-1 by monoclonal antibodies potentiates cancer therapeutic immunity. Cancer Res *65*, 1089-1096.

Hofman, P., Cherfils-Vicini, J., Bazin, M., Ilie, M., Juhel, T., Hebuterne, X., Gilson, E., Schmid-Alliana, A., Boyer, O., Adriouch, S*., et al.* (2015). Genetic and pharmacological inactivation of the purinergic P2RX7 receptor dampens inflammation but increases tumor incidence in a mouse model of colitis-associated cancer. Cancer Res *75*, 835-845.

Hogan, P.G., Lewis, R.S., and Rao, A. (2010). Molecular basis of calcium signaling in lymphocytes: STIM and ORAI. Annu Rev Immunol *28*, 491-533.

Hubert, S., Rissiek, B., Klages, K., Huehn, J., Sparwasser, T., Haag, F., Koch-Nolte, F., Boyer, O., Seman, M., and Adriouch, S. (2010). Extracellular NAD+ shapes the Foxp3+ regulatory T cell compartment through the ART2-P2X7 pathway. J Exp Med *207*, 2561-2568.

Hutloff, A., Dittrich, A.M., Beier, K.C., Eljaschewitsch, B., Kraft, R., Anagnostopoulos, I., and Kroczek, R.A. (1999). ICOS is an inducible T-cell co-stimulator structurally and functionally related to CD28. Nature *397*, 263-266.

Idzko, M., Hammad, H., van Nimwegen, M., Kool, M., Willart, M.A., Muskens, F., Hoogsteden, H.C., Luttmann, W., Ferrari, D., Di Virgilio, F*., et al.* (2007). Extracellular ATP triggers and maintains asthmatic airway inflammation by activating dendritic cells. Nat Med *13*, 913-919.

Iezzi, G., Karjalainen, K., and Lanzavecchia, A. (1998). The duration of antigenic stimulation determines the fate of naive and effector T cells. Immunity *8*, 89-95.

Inaba, K., Witmer-Pack, M., Inaba, M., Hathcock, K.S., Sakuta, H., Azuma, M., Yagita, H., Okumura, K., Linsley, P.S., Ikehara, S*., et al.* (1994). The tissue distribution of the B7-2 costimulator in mice: abundant expression on dendritic cells in situ and during maturation in vitro. J Exp Med *180*, 1849-1860.

Iwashima, M., Irving, B.A., van Oers, N.S., Chan, A.C., and Weiss, A. (1994). Sequential interactions of the TCR with two distinct cytoplasmic tyrosine kinases. Science *263*, 1136-1139.

Jabeen, R., and Kaplan, M.H. (2012). The symphony of the ninth: the development and function of Th9 cells. Curr Opin Immunol *24*, 303-307.

Jacobs, J.F., Nierkens, S., Figdor, C.G., de Vries, I.J., and Adema, G.J. (2012). Regulatory T cells in melanoma: the final hurdle towards effective immunotherapy? Lancet Oncol *13*, e32-42.

Jenkins, M.K., Chen, C.A., Jung, G., Mueller, D.L., and Schwartz, R.H. (1990). Inhibition of antigen-specific proliferation of type 1 murine T cell clones after stimulation with immobilized anti-CD3 monoclonal antibody. J Immunol *144*, 16-22.

Jenkins, M.K., Pardoll, D.M., Mizuguchi, J., Chused, T.M., and Schwartz, R.H. (1987). Molecular events in the induction of a nonresponsive state in interleukin 2-producing helper T-lymphocyte clones. Proc Natl Acad Sci U S A *84*, 5409-5413.

Johnston, R.J., Poholek, A.C., DiToro, D., Yusuf, I., Eto, D., Barnett, B., Dent, A.L., Craft, J., and Crotty, S. (2009). Bcl6 and Blimp-1 are reciprocal and antagonistic regulators of T follicular helper cell differentiation. Science *325*, 1006-1010.

Jones, R.G., and Thompson, C.B. (2007). Revving the engine: signal transduction fuels T cell activation. Immunity *27*, 173-178.

Jutel, M., and Akdis, C.A. (2008). T-cell regulatory mechanisms in specific immunotherapy. Chem Immunol Allergy *94*, 158-177.

Kannan, A., Huang, W., Huang, F., and August, A. (2012). Signal transduction via the T cell antigen receptor in naive and effector/memory T cells. Int J Biochem Cell Biol *44*, 2129-2134.

Kawamura, H., Aswad, F., Minagawa, M., Govindarajan, S., and Dennert, G. (2006). P2X7 receptors regulate NKT cells in autoimmune hepatitis. J Immunol *176*, 2152-2160.

Khong, H.T., Wang, Q.J., and Rosenberg, S.A. (2004). Identification of multiple antigens recognized by tumor-infiltrating lymphocytes from a single patient: tumor escape by antigen loss and loss of MHC expression. J Immunother *27*, 184-190.

Kim, J.W., Tchernyshyov, I., Semenza, G.L., and Dang, C.V. (2006). HIF-1-mediated expression of pyruvate dehydrogenase kinase: a metabolic switch required for cellular adaptation to hypoxia. Cell Metab *3*, 177-185.

Klein Geltink, R.I., O'Sullivan, D., Corrado, M., Bremser, A., Buck, M.D., Buescher, J.M., Firat, E., Zhu, X., Niedermann, G., Caputa, G.*, et al.* (2017). Mitochondrial Priming by CD28. Cell *171*, 385-397 e311.

Kolev, M., Dimeloe, S., Le Friec, G., Navarini, A., Arbore, G., Povoleri, G.A., Fischer, M., Belle, R., Loeliger, J., Develioglu, L.*, et al.* (2015). Complement Regulates Nutrient Influx and Metabolic Reprogramming during Th1 Cell Responses. Immunity *42*, 1033-1047.

Kondrack, R.M., Harbertson, J., Tan, J.T., McBreen, M.E., Surh, C.D., and Bradley, L.M. (2003). Interleukin 7 regulates the survival and generation of memory CD4 cells. J Exp Med *198*, 1797-1806.

Koretzky, G.A., Abtahian, F., and Silverman, M.A. (2006). SLP76 and SLP65: complex regulation of signalling in lymphocytes and beyond. Nat Rev Immunol *6*, 67-78.

Korn, T., Bettelli, E., Gao, W., Awasthi, A., Jager, A., Strom, T.B., Oukka, M., and Kuchroo, V.K. (2007). IL-21 initiates an alternative pathway to induce proinflammatory T(H)17 cells. Nature *448*, 484-487.

Kreslavsky, T., and von Boehmer, H. (2010). gammadeltaTCR ligands and lineage commitment. Semin Immunol *22*, 214-221.

Langenkamp, A., Messi, M., Lanzavecchia, A., and Sallusto, F. (2000). Kinetics of dendritic cell activation: impact on priming of TH1, TH2 and nonpolarized T cells. Nat Immunol *1*, 311-316.

Lanna, A., Henson, S.M., Escors, D., and Akbar, A.N. (2014). The kinase p38 activated by the metabolic regulator AMPK and scaffold TAB1 drives the senescence of human T cells. Nat Immunol *15*, 965-972.

Lanzavecchia, A., and Sallusto, F. (2002). Progressive differentiation and selection of the fittest in the immune response. Nat Rev Immunol *2*, 982-987.

Laurence, A., Tato, C.M., Davidson, T.S., Kanno, Y., Chen, Z., Yao, Z., Blank, R.B., Meylan, F., Siegel, R., Hennighausen, L.*, et al.* (2007). Interleukin-2 signaling via STAT5 constrains T helper 17 cell generation. Immunity *26*, 371-381.

Lee, N., Zakka, L.R., Mihm, M.C., Jr., and Schatton, T. (2016). Tumour-infiltrating lymphocytes in melanoma prognosis and cancer immunotherapy. Pathology *48*, 177-187.

Lenschow, D.J., Walunas, T.L., and Bluestone, J.A. (1996). CD28/B7 system of T cell costimulation. Annu Rev Immunol *14*, 233-258.

Li, M.O., Sanjabi, S., and Flavell, R.A. (2006). Transforming growth factor-beta controls development, homeostasis, and tolerance of T cells by regulatory T cell-dependent and -independent mechanisms. Immunity *25*, 455-471.

Li, W., Whaley, C.D., Mondino, A., and Mueller, D.L. (1996). Blocked signal transduction to the ERK and JNK protein kinases in anergic CD4+ T cells. Science *271*, 1272-1276.

Lind, E.F., Prockop, S.E., Porritt, H.E., and Petrie, H.T. (2001). Mapping precursor movement through the postnatal thymus reveals specific microenvironments supporting defined stages of early lymphoid development. J Exp Med *194*, 127-134.

Longphre, M., Li, D., Gallup, M., Drori, E., Ordonez, C.L., Redman, T., Wenzel, S., Bice, D.E., Fahy, J.V., and Basbaum, C. (1999). Allergen-induced IL-9 directly stimulates mucin transcription in respiratory epithelial cells. J Clin Invest *104*, 1375-1382.

Mackenzie, A.B., Young, M.T., Adinolfi, E., and Surprenant, A. (2005). Pseudoapoptosis induced by brief activation of ATP-gated P2X7 receptors. J Biol Chem *280*, 33968-33976.

Maeurer, M.J., Gollin, S.M., Martin, D., Swaney, W., Bryant, J., Castelli, C., Robbins, P., Parmiani, G., Storkus, W.J., and Lotze, M.T. (1996). Tumor escape from immune recognition: lethal recurrent melanoma in a patient associated with downregulation of the peptide transporter protein TAP-1 and loss of expression of the immunodominant MART-1/Melan-A antigen. J Clin Invest *98*, 1633-1641.

Martinez, G.J., Pereira, R.M., Aijo, T., Kim, E.Y., Marangoni, F., Pipkin, M.E., Togher, S., Heissmeyer, V., Zhang, Y.C., Crotty, S*., et al.* (2015). The transcription factor NFAT promotes exhaustion of activated CD8(+) T cells. Immunity *42*, 265-278.

Martinez, G.J., Zhang, Z., Chung, Y., Reynolds, J.M., Lin, X., Jetten, A.M., Feng, X.H., and Dong, C. (2009). Smad3 differentially regulates the induction of regulatory and inflammatory T cell differentiation. J Biol Chem *284*, 35283-35286.

Meloni, F., Morosini, M., Solari, N., Passadore, I., Nascimbene, C., Novo, M., Ferrari, M., Cosentino, M., Marino, F., Pozzi, E*., et al.* (2006). Foxp3 expressing CD4+ CD25+ and CD8+CD28- T regulatory cells in the peripheral blood of patients with lung cancer and pleural mesothelioma. Hum Immunol *67*, 1-12.

Michaud, M., Martins, I., Sukkurwala, A.Q., Adjemian, S., Ma, Y., Pellegatti, P., Shen, S., Kepp, O., Scoazec, M., Mignot, G*., et al.* (2011). Autophagy-dependent anticancer immune responses induced by chemotherapeutic agents in mice. Science *334*, 1573-1577.

Michie, A.M., and Zuniga-Pflucker, J.C. (2002). Regulation of thymocyte differentiation: pre-TCR signals and beta-selection. Semin Immunol *14*, 311-323.

Mirshahidi, S., Huang, C.T., and Sadegh-Nasseri, S. (2001). Anergy in peripheral memory CD4(+) T cells induced by low avidity engagement of T cell receptor. J Exp Med *194*, 719-731.

Morris, G.P., and Allen, P.M. (2012). How the TCR balances sensitivity and specificity for the recognition of self and pathogens. Nat Immunol *13*, 121-128.

Mueller, D.L., Chiodetti, L., Bacon, P.A., and Schwartz, R.H. (1991). Clonal anergy blocks the response to IL-4, as well as the production of IL-2, in dual-producing T helper cell clones. J Immunol *147*, 4118-4125.

Mueller, S.N., Gebhardt, T., Carbone, F.R., and Heath, W.R. (2013). Memory T cell subsets, migration patterns, and tissue residence. Annu Rev Immunol *31*, 137-161.

Nakano, O., Sato, M., Naito, Y., Suzuki, K., Orikasa, S., Aizawa, M., Suzuki, Y., Shintaku, I., Nagura, H., and Ohtani, H. (2001). Proliferative activity of intratumoral CD8(+) T-lymphocytes as a prognostic factor in human renal cell carcinoma: clinicopathologic demonstration of antitumor immunity. Cancer Res *61*, 5132-5136.

Nicolaou, A., Estdale, S.E., Tsatmali, M., Herrero, D.P., and Thody, A.J. (2004). Prostaglandin production by melanocytic cells and the effect of alpha-melanocyte stimulating hormone. FEBS Lett *570*, 223-226.

Noman, M.Z., Desantis, G., Janji, B., Hasmim, M., Karray, S., Dessen, P., Bronte, V., and Chouaib, S. (2014). PD-L1 is a novel direct target of HIF-1alpha, and its blockade under hypoxia enhanced MDSC-mediated T cell activation. J Exp Med *211*, 781-790.
Nunnari, J., and Suomalainen, A. (2012). Mitochondria: in sickness and in health. Cell *148*, 1145-1159.

Nurieva, R.I., and Chung, Y. (2010). Understanding the development and function of T follicular helper cells. Cell Mol Immunol *7*, 190-197.

Nurieva, R.I., Chung, Y., Martinez, G.J., Yang, X.O., Tanaka, S., Matskevitch, T.D., Wang, Y.H., and Dong, C. (2009). Bcl6 mediates the development of T follicular helper cells. Science *325*, 1001-1005.

Oestreich, K.J., Yoon, H., Ahmed, R., and Boss, J.M. (2008). NFATc1 regulates PD-1 expression upon T cell activation. J Immunol *181*, 4832-4839.

Ono, M., Yaguchi, H., Ohkura, N., Kitabayashi, I., Nagamura, Y., Nomura, T., Miyachi, Y., Tsukada, T., and Sakaguchi, S. (2007). Foxp3 controls regulatory T-cell function by interacting with AML1/Runx1. Nature *446*, 685-689.

Ousingsawat, J., Wanitchakool, P., Kmit, A., Romao, A.M., Jantarajit, W., Schreiber, R., and Kunzelmann, K. (2015). Anoctamin 6 mediates effects essential for innate immunity downstream of P2X7 receptors in macrophages. Nat Commun *6*, 6245.

Ouyang, W., Rutz, S., Crellin, N.K., Valdez, P.A., and Hymowitz, S.G. (2011). Regulation and functions of the IL-10 family of cytokines in inflammation and disease. Annu Rev Immunol *29*, 71-109.

Pages, F., Ragueneau, M., Rottapel, R., Truneh, A., Nunes, J., Imbert, J., and Olive, D. (1994). Binding of phosphatidylinositol-3-OH kinase to CD28 is required for T-cell signalling. Nature *369*, 327-329.

Palmer, E. (2003). Negative selection--clearing out the bad apples from the T-cell repertoire. Nat Rev Immunol *3*, 383-391.

Pardoll, D.M. (2012). The blockade of immune checkpoints in cancer immunotherapy. Nat Rev Cancer *12*, 252-264.

Parronchi, P., De Carli, M., Manetti, R., Simonelli, C., Sampognaro, S., Piccinni, M.P., Macchia, D., Maggi, E., Del Prete, G., and Romagnani, S. (1992). IL-4 and IFN (alpha and gamma) exert opposite regulatory effects on the development of cytolytic potential by Th1 or Th2 human T cell clones. J Immunol *149*, 2977-2983.

Passos, J.F., Nelson, G., Wang, C., Richter, T., Simillion, C., Proctor, C.J., Miwa, S., Olijslagers, S., Hallinan, J., Wipat, A.*, et al.* (2010). Feedback between p21 and reactive oxygen production is necessary for cell senescence. Mol Syst Biol *6*, 347.

Passos, J.F., and Zglinicki, T. (2012). Mitochondrial dysfunction and cell senescence--skin deep into mammalian aging. Aging (Albany NY) *4*, 74-75.

Patterson, H., Nibbs, R., McInnes, I., and Siebert, S. (2014). Protein kinase inhibitors in the treatment of inflammatory and autoimmune diseases. Clin Exp Immunol *176*, 1-10.

Pearce, E.L., Poffenberger, M.C., Chang, C.H., and Jones, R.G. (2013). Fueling immunity: insights into metabolism and lymphocyte function. Science *342*, 1242454.

Pellegatti, P., Raffaghello, L., Bianchi, G., Piccardi, F., Pistoia, V., and Di Virgilio, F. (2008). Increased level of extracellular ATP at tumor sites: in vivo imaging with plasma membrane luciferase. PLoS One *3*, e2599.

Penaloza-MacMaster, P., Teigler, J.E., Obeng, R.C., Kang, Z.H., Provine, N.M., Parenteau, L., Blackmore, S., Ra, J., Borducchi, E.N., and Barouch, D.H. (2014). Augmented replicative capacity of the boosting antigen improves the protective efficacy of heterologous prime-boost vaccine regimens. J Virol *88*, 6243-6254.

Petrie, H.T., Scollay, R., and Shortman, K. (1992). Commitment to the T cell receptor-alpha beta or -gamma delta lineages can occur just prior to the onset of CD4 and CD8 expression among immature thymocytes. Eur J Immunol *22*, 2185-2188.

Petrie, H.T., and Zuniga-Pflucker, J.C. (2007). Zoned out: functional mapping of stromal signaling microenvironments in the thymus. Annu Rev Immunol *25*, 649-679.

Plunkett, F.J., Franzese, O., Belaramani, L.L., Fletcher, J.M., Gilmour, K.C., Sharifi, R., Khan, N., Hislop, A.D., Cara, A., Salmon, M.*, et al.* (2005). The impact of telomere erosion on memory CD8+ T cells in patients with X-linked lymphoproliferative syndrome. Mech Ageing Dev *126*, 855-865.

Plunkett, F.J., Franzese, O., Finney, H.M., Fletcher, J.M., Belaramani, L.L., Salmon, M., Dokal, I., Webster, D., Lawson, A.D., and Akbar, A.N. (2007). The loss of telomerase activity in highly differentiated CD8+CD28-CD27- T cells is associated with decreased Akt (Ser473) phosphorylation. J Immunol *178*, 7710-7719.

Pollizzi, K.N., Patel, C.H., Sun, I.H., Oh, M.H., Waickman, A.T., Wen, J., Delgoffe, G.M., and Powell, J.D. (2015). mTORC1 and mTORC2 selectively regulate CD8(+) T cell differentiation. J Clin Invest *125*, 2090-2108.

Proietti, M., Cornacchione, V., Rezzonico Jost, T., Romagnani, A., Faliti, C.E., Perruzza, L., Rigoni, R., Radaelli, E., Caprioli, F., Preziuso, S.*, et al.* (2014). ATP-gated ionotropic P2X7 receptor controls follicular T helper cell numbers in Peyer's patches to promote host-microbiota mutualism. Immunity *41*, 789-801.

Pulendran, B., and Artis, D. (2012). New paradigms in type 2 immunity. Science *337*, 431-435.

Qin, H., Wang, L., Feng, T., Elson, C.O., Niyongere, S.A., Lee, S.J., Reynolds, S.L., Weaver, C.T., Roarty, K., Serra, R.*, et al.* (2009). TGF-beta promotes Th17 cell development through inhibition of SOCS3. J Immunol *183*, 97-105.

Quezada, S.A., and Peggs, K.S. (2013). Exploiting CTLA-4, PD-1 and PD-L1 to reactivate the host immune response against cancer. Br J Cancer *108*, 1560-1565.

Quezada, S.A., Simpson, T.R., Peggs, K.S., Merghoub, T., Vider, J., Fan, X., Blasberg, R., Yagita, H., Muranski, P., Antony, P.A.*, et al.* (2010). Tumor-reactive CD4(+) T cells develop cytotoxic activity and eradicate large established melanoma after transfer into lymphopenic hosts. J Exp Med *207*, 637-650.

Quill, H., and Schwartz, R.H. (1987). Stimulation of normal inducer T cell clones with antigen presented by purified Ia molecules in planar lipid membranes: specific induction of a long-lived state of proliferative nonresponsiveness. J Immunol *138*, 3704-3712.

Ralevic, V., and Burnstock, G. (1998). Receptors for purines and pyrimidines. Pharmacol Rev *50*, 413-492.

Rambold, A.S., Kostelecky, B., Elia, N., and Lippincott-Schwartz, J. (2011). Tubular network formation protects mitochondria from autophagosomal degradation during nutrient starvation. Proc Natl Acad Sci U S A *108*, 10190-10195.

Rayah, A., Kanellopoulos, J.M., and Di Virgilio, F. (2012). P2 receptors and immunity. Microbes Infect *14*, 1254-1262.

Rissiek, B., Danquah, W., Haag, F., and Koch-Nolte, F. (2014). Technical Advance: a new cell preparation strategy that greatly improves the yield of vital and functional Tregs and NKT cells. J Leukoc Biol *95*, 543-549.

Rissiek, B., Haag, F., Boyer, O., Koch-Nolte, F., and Adriouch, S. (2015). P2X7 on Mouse T Cells: One Channel, Many Functions. Front Immunol *6*, 204.

Roger, S., Jelassi, B., Couillin, I., Pelegrin, P., Besson, P., and Jiang, L.H. (2015). Understanding the roles of the P2X7 receptor in solid tumour progression and therapeutic perspectives. Biochim Biophys Acta *1848*, 2584-2602.

Rolf, J., Bell, S.E., Kovesdi, D., Janas, M.L., Soond, D.R., Webb, L.M., Santinelli, S., Saunders, T., Hebeis, B., Killeen, N.*, et al.* (2010). Phosphoinositide 3-kinase activity in T cells regulates the magnitude of the germinal center reaction. J Immunol *185*, 4042-4052.

Romagnani, S. (1994). Lymphokine production by human T cells in disease states. Annu Rev Immunol *12*, 227-257.

Rosenberg, S.A. (1999). A new era of cancer immunotherapy: converting theory to performance. CA Cancer J Clin *49*, 70-73, 65.

Rudd, C.E., Taylor, A., and Schneider, H. (2009). CD28 and CTLA-4 coreceptor expression and signal transduction. Immunol Rev *229*, 12-26.

Rudensky, A.Y. (2011). Regulatory T cells and Foxp3. Immunol Rev *241*, 260-268.
Sakaguchi, S., Yamaguchi, T., Nomura, T., and Ono, M. (2008). Regulatory T cells and immune tolerance. Cell *133*, 775-787.

Sallusto, F., Geginat, J., and Lanzavecchia, A. (2004). Central memory and effector memory T cell subsets: function, generation, and maintenance. Annu Rev Immunol *22*, 745-763.

Sallusto, F., Lenig, D., Forster, R., Lipp, M., and Lanzavecchia, A. (1999). Two subsets of memory T lymphocytes with distinct homing potentials and effector functions. Nature *401*, 708-712.

Salvador, J.M., Mittelstadt, P.R., Guszczynski, T., Copeland, T.D., Yamaguchi, H., Appella, E., Fornace, A.J., Jr., and Ashwell, J.D. (2005). Alternative p38 activation pathway mediated by T cell receptor-proximal tyrosine kinases. Nat Immunol *6*, 390-395.

Sato, E., Olson, S.H., Ahn, J., Bundy, B., Nishikawa, H., Qian, F., Jungbluth, A.A., Frosina, D., Gnjatic, S., Ambrosone, C.*, et al.* (2005). Intraepithelial CD8+ tumor-infiltrating lymphocytes and a high CD8+/regulatory T cell ratio are associated with favorable prognosis in ovarian cancer. Proc Natl Acad Sci U S A *102*, 18538-18543.

Schaerli, P., Willimann, K., Lang, A.B., Lipp, M., Loetscher, P., and Moser, B. (2000). CXC chemokine receptor 5 expression defines follicular homing T cells with B cell helper function. J Exp Med *192*, 1553-1562.

Scharping, N.E., Menk, A.V., Moreci, R.S., Whetstone, R.D., Dadey, R.E., Watkins, S.C., Ferris, R.L., and Delgoffe, G.M. (2016). The Tumor Microenvironment Represses T Cell Mitochondrial Biogenesis to Drive Intratumoral T Cell Metabolic Insufficiency and Dysfunction. Immunity *45*, 701-703.

Schenk, U., Westendorf, A.M., Radaelli, E., Casati, A., Ferro, M., Fumagalli, M., Verderio, C., Buer, J., Scanziani, E., and Grassi, F. (2008). Purinergic control of T cell activation by ATP released through pannexin-1 hemichannels. Sci Signal *1*, ra6.

Scheuplein, F., Schwarz, N., Adriouch, S., Krebs, C., Bannas, P., Rissiek, B., Seman, M., Haag, F., and Koch-Nolte, F. (2009). NAD+ and ATP released from injured cells induce P2X7-dependent shedding of CD62L and externalization of phosphatidylserine by murine T cells. J Immunol *182*, 2898-2908.

Schreiber, R.D., Old, L.J., and Smyth, M.J. (2011). Cancer immunoediting: integrating immunity's roles in cancer suppression and promotion. Science *331*, 1565-1570.
Schulze-Luehrmann, J., and Ghosh, S. (2006). Antigen-receptor signaling to nuclear factor kappa B. Immunity *25*, 701-715.

Schumacher, T.N., and Schreiber, R.D. (2015). Neoantigens in cancer immunotherapy. Science *348*, 69-74.

Schwartz, R.H. (1990). A cell culture model for T lymphocyte clonal anergy. Science *248*, 1349-1356.

Schwartz, R.H. (2003). T cell anergy. Annu Rev Immunol *21*, 305-334.

Seman, M., Adriouch, S., Scheuplein, F., Krebs, C., Freese, D., Glowacki, G., Deterre, P., Haag, F., and Koch-Nolte, F. (2003). NAD-induced T cell death: ADP-ribosylation of cell surface proteins by ART2 activates the cytolytic P2X7 purinoceptor. Immunity *19*, 571-582.

Sena, L.A., Li, S., Jairaman, A., Prakriya, M., Ezponda, T., Hildeman, D.A., Wang, C.R., Schumacker, P.T., Licht, J.D., Perlman, H.*, et al.* (2013). Mitochondria are required for antigen-specific T cell activation through reactive oxygen species signaling. Immunity *38*, 225-236.

Shankaran, V., Ikeda, H., Bruce, A.T., White, J.M., Swanson, P.E., Old, L.J., and Schreiber, R.D. (2001). IFNgamma and lymphocytes prevent primary tumour development and shape tumour immunogenicity. Nature *410*, 1107-1111.

Sharma, P., Shen, Y., Wen, S., Yamada, S., Jungbluth, A.A., Gnjatic, S., Bajorin, D.F., Reuter, V.E., Herr, H., Old, L.J.*, et al.* (2007). CD8 tumor-infiltrating lymphocytes are predictive of survival in muscle-invasive urothelial carcinoma. Proc Natl Acad Sci U S A *104*, 3967-3972.

Siddiqui, M.S., Francois, M., Fenech, M.F., and Leifert, W.R. (2015). Persistent gammaH2AX: A promising molecular marker of DNA damage and aging. Mutat Res Rev Mutat Res *766*, 1-19.

Sinclair, L.V., Rolf, J., Emslie, E., Shi, Y.B., Taylor, P.M., and Cantrell, D.A. (2013). Control of amino-acid transport by antigen receptors coordinates the metabolic reprogramming essential for T cell differentiation. Nat Immunol *14*, 500-508.

Singer, A., Adoro, S., and Park, J.H. (2008). Lineage fate and intense debate: myths, models and mechanisms of CD4- versus CD8-lineage choice. Nat Rev Immunol *8*, 788-801.

Smith-Garvin, J.E., Koretzky, G.A., and Jordan, M.S. (2009). T cell activation. Annu Rev Immunol *27*, 591-619.

Sommers, C.L., Samelson, L.E., and Love, P.E. (2004). LAT: a T lymphocyte adapter protein that couples the antigen receptor to downstream signaling pathways. Bioessays *26*, 61-67.

Sorensen, A.G., Emblem, K.E., Polaskova, P., Jennings, D., Kim, H., Ancukiewicz, M., Wang, M., Wen, P.Y., Ivy, P., Batchelor, T.T.*, et al.* (2012). Increased survival of glioblastoma patients who respond to antiangiogenic therapy with elevated blood perfusion. Cancer Res *72*, 402-407.

Sotomayor, E.M., Borrello, I., Rattis, F.M., Cuenca, A.G., Abrams, J., Staveley-O'Carroll, K., and Levitsky, H.I. (2001). Cross-presentation of tumor antigens by bone marrow-derived antigen-presenting cells is the dominant mechanism in the induction of T-cell tolerance during B-cell lymphoma progression. Blood *98*, 1070-1077.

Starr, T.K., Daniels, M.A., Lucido, M.M., Jameson, S.C., and Hogquist, K.A. (2003). Thymocyte sensitivity and supramolecular activation cluster formation are developmentally regulated: a partial role for sialylation. J Immunol *171*, 4512-4520.

Stritesky, G.L., Jameson, S.C., and Hogquist, K.A. (2012). Selection of self-reactive T cells in the thymus. Annu Rev Immunol *30*, 95-114.

Surprenant, A., Rassendren, F., Kawashima, E., North, R.A., and Buell, G. (1996). The cytolytic P2Z receptor for extracellular ATP identified as a P2X receptor (P2X7). Science *272*, 735-738.

Taguchi, N., Ishihara, N., Jofuku, A., Oka, T., and Mihara, K. (2007). Mitotic phosphorylation of dynamin-related GTPase Drp1 participates in mitochondrial fission. J Biol Chem *282*, 11521-11529.

Takimoto, T., Wakabayashi, Y., Sekiya, T., Inoue, N., Morita, R., Ichiyama, K., Takahashi, R., Asakawa, M., Muto, G., Mori, T.*, et al.* (2010). Smad2 and Smad3 are redundantly essential for the TGF-beta-mediated regulation of regulatory T plasticity and Th1 development. J Immunol *185*, 842-855.

Taylor, S.R., Gonzalez-Begne, M., Dewhurst, S., Chimini, G., Higgins, C.F., Melvin, J.E., and Elliott, J.I. (2008). Sequential shrinkage and swelling underlie P2X7-stimulated lymphocyte phosphatidylserine exposure and death. J Immunol *180*, 300-308.

Telander, D.G., Malvey, E.N., and Mueller, D.L. (1999). Evidence for repression of IL-2 gene activation in anergic T cells. J Immunol *162*, 1460-1465.

Tinoco, R., Alcalde, V., Yang, Y., Sauer, K., and Zuniga, E.I. (2009). Cell-intrinsic transforming growth factor-beta signaling mediates virus-specific CD8+ T cell deletion and viral persistence in vivo. Immunity *31*, 145-157.

Tognon, C.E., Kirk, H.E., Passmore, L.A., Whitehead, I.P., Der, C.J., and Kay, R.J. (1998). Regulation of RasGRP via a phorbol ester-responsive C1 domain. Mol Cell Biol *18*, 6995-7008.

Tsukishiro, T., Donnenberg, A.D., and Whiteside, T.L. (2003). Rapid turnover of the CD8(+)CD28(-) T-cell subset of effector cells in the circulation of patients with head and neck cancer. Cancer Immunol Immunother *52*, 599-607.

Tumeh, P.C., Harview, C.L., Yearley, J.H., Shintaku, I.P., Taylor, E.J., Robert, L., Chmielowski, B., Spasic, M., Henry, G., Ciobanu, V.*, et al.* (2014). PD-1 blockade induces responses by inhibiting adaptive immune resistance. Nature *515*, 568-571.

Usui, T., Nishikomori, R., Kitani, A., and Strober, W. (2003). GATA-3 suppresses Th1 development by downregulation of Stat4 and not through effects on IL-12Rbeta2 chain or T-bet. Immunity *18*, 415-428.

Usui, T., Preiss, J.C., Kanno, Y., Yao, Z.J., Bream, J.H., O'Shea, J.J., and Strober, W. (2006). T-bet regulates Th1 responses through essential effects on GATA-3 function rather than on IFNG gene acetylation and transcription. J Exp Med *203*, 755-766.

Valitutti, S., Muller, S., Cella, M., Padovan, E., and Lanzavecchia, A. (1995). Serial triggering of many T-cell receptors by a few peptide-MHC complexes. Nature *375*, 148-151.

van der Windt, G.J., Everts, B., Chang, C.H., Curtis, J.D., Freitas, T.C., Amiel, E., Pearce, E.J., and Pearce, E.L. (2012). Mitochondrial respiratory capacity is a critical regulator of CD8+ T cell memory development. Immunity *36*, 68-78.

van der Windt, G.J., O'Sullivan, D., Everts, B., Huang, S.C., Buck, M.D., Curtis, J.D., Chang, C.H., Smith, A.M., Ai, T., Faubert, B.*, et al.* (2013). CD8 memory T cells have a bioenergetic advantage that underlies their rapid recall ability. Proc Natl Acad Sci U S A *110*, 14336-14341.

van Deursen, J.M. (2014). The role of senescent cells in ageing. Nature *509*, 439-446.
Vander Heiden, M.G., Cantley, L.C., and Thompson, C.B. (2009). Understanding the Warburg effect: the metabolic requirements of cell proliferation. Science *324*, 1029-1033.

Veldhoen, M., Hocking, R.J., Atkins, C.J., Locksley, R.M., and Stockinger, B. (2006). TGFbeta in the context of an inflammatory cytokine milieu supports de novo differentiation of IL-17-producing T cells. Immunity *24*, 179-189.

Veldhoen, M., Uyttenhove, C., van Snick, J., Helmby, H., Westendorf, A., Buer, J., Martin, B., Wilhelm, C., and Stockinger, B. (2008). Transforming growth factor-beta 'reprograms' the differentiation of T helper 2 cells and promotes an interleukin 9-producing subset. Nat Immunol *9*, 1341-1346.

Vesely, M.D., and Schreiber, R.D. (2013). Cancer immunoediting: antigens, mechanisms, and implications to cancer immunotherapy. Ann N Y Acad Sci *1284*, 1-5.

Viola, A., Schroeder, S., Sakakibara, Y., and Lanzavecchia, A. (1999). T lymphocyte costimulation mediated by reorganization of membrane microdomains. Science *283*, 680-682.

Virgin, H.W., Wherry, E.J., and Ahmed, R. (2009). Redefining chronic viral infection. Cell *138*, 30-50.

Volpe, E., Servant, N., Zollinger, R., Bogiatzi, S.I., Hupe, P., Barillot, E., and Soumelis, V. (2008). A critical function for transforming growth factor-beta, interleukin 23 and proinflammatory cytokines in driving and modulating human T(H)-17 responses. Nat Immunol *9*, 650-657.

Vuillefroy de Silly, R., Dietrich, P.Y., and Walker, P.R. (2016). Hypoxia and antitumor CD8+ T cells: An incompatible alliance? Oncoimmunology *5*, e1232236.

Wang, R., Dillon, C.P., Shi, L.Z., Milasta, S., Carter, R., Finkelstein, D., McCormick, L.L., Fitzgerald, P., Chi, H., Munger, J.*, et al.* (2011). The transcription factor Myc controls metabolic reprogramming upon T lymphocyte activation. Immunity *35*, 871-882.

Wherry, E.J. (2011). T cell exhaustion. Nat Immunol *12*, 492-499.

Wherry, E.J., Ha, S.J., Kaech, S.M., Haining, W.N., Sarkar, S., Kalia, V., Subramaniam, S., Blattman, J.N., Barber, D.L., and Ahmed, R. (2007). Molecular signature of CD8+ T cell exhaustion during chronic viral infection. Immunity *27*, 670-684.

Wing, K., Onishi, Y., Prieto-Martin, P., Yamaguchi, T., Miyara, M., Fehervari, Z., Nomura, T., and Sakaguchi, S. (2008). CTLA-4 control over Foxp3+ regulatory T cell function. Science *322*, 271-275.

Wolff, M.J., Leung, J.M., Davenport, M., Poles, M.A., Cho, I., and Loke, P. (2012). TH17, TH22 and Treg cells are enriched in the healthy human cecum. PLoS One *7*, e41373.

Wu, L., Multani, A.S., He, H., Cosme-Blanco, W., Deng, Y., Deng, J.M., Bachilo, O., Pathak, S., Tahara, H., Bailey, S.M.*, et al.* (2006). Pot1 deficiency initiates DNA damage checkpoint activation and aberrant homologous recombination at telomeres. Cell *126*, 49-62.

Yamane, H., and Paul, W.E. (2012). Cytokines of the gamma(c) family control CD4+ T cell differentiation and function. Nat Immunol *13*, 1037-1044.

Yegutkin, G.G. (2008). Nucleotide- and nucleoside-converting ectoenzymes: Important modulators of purinergic signalling cascade. Biochim Biophys Acta *1783*, 673-694.

Youle, R.J., and Karbowski, M. (2005). Mitochondrial fission in apoptosis. Nat Rev Mol Cell Biol *6*, 657-663.

Yu, T., Robotham, J.L., and Yoon, Y. (2006). Increased production of reactive oxygen species in hyperglycemic conditions requires dynamic change of mitochondrial morphology. Proc Natl Acad Sci U S A *103*, 2653-2658.

Zaidi, M.R., and Merlino, G. (2011). The two faces of interferon-gamma in cancer. Clin Cancer Res *17*, 6118-6124.

Zha, J., Harada, H., Yang, E., Jockel, J., and Korsmeyer, S.J. (1996). Serine phosphorylation of death agonist BAD in response to survival factor results in binding to 14-3-3 not BCL-X(L). Cell *87*, 619-628.

Zha, Y., Marks, R., Ho, A.W., Peterson, A.C., Janardhan, S., Brown, I., Praveen, K., Stang, S., Stone, J.C., and Gajewski, T.F. (2006). T cell anergy is reversed by active Ras and is regulated by diacylglycerol kinase-alpha. Nat Immunol *7*, 1166-1173.

Zhang, W., Sommers, C.L., Burshtyn, D.N., Stebbins, C.C., DeJarnette, J.B., Trible, R.P., Grinberg, A., Tsay, H.C., Jacobs, H.M., Kessler, C.M.*, et al.* (1999). Essential role of LAT in T cell development. Immunity *10*, 323-332.

Zhang, X., Sun, S., Hwang, I., Tough, D.F., and Sprent, J. (1998). Potent and selective stimulation of memory-phenotype CD8+ T cells in vivo by IL-15. Immunity *8*, 591-599.

Zheng, S.G., Wang, J., and Horwitz, D.A. (2008). Cutting edge: Foxp3+CD4+CD25+ regulatory T cells induced by IL-2 and TGF-beta are resistant to Th17 conversion by IL-6. J Immunol *180*, 7112-7116.

Zheng, Y., Chaudhry, A., Kas, A., deRoos, P., Kim, J.M., Chu, T.T., Corcoran, L., Treuting, P., Klein, U., and Rudensky, A.Y. (2009). Regulatory T-cell suppressor program co-opts transcription factor IRF4 to control T(H)2 responses. Nature *458*, 351-356.

Zhou, L., Chong, M.M., and Littman, D.R. (2009). Plasticity of CD4+ T cell lineage differentiation. Immunity *30*, 646-655.

Zhu, J., Cote-Sierra, J., Guo, L., and Paul, W.E. (2003). Stat5 activation plays a critical role in Th2 differentiation. Immunity *19*, 739-748.

Zhu, J., Yamane, H., Cote-Sierra, J., Guo, L., and Paul, W.E. (2006). GATA-3 promotes Th2 responses through three different mechanisms: induction of Th2 cytokine production, selective growth of Th2 cells and inhibition of Th1 cell-specific factors. Cell Res *16*, 3-10.

Zhu, J., Yamane, H., and Paul, W.E. (2010). Differentiation of effector CD4 T cell populations (*). Annu Rev Immunol *28*, 445-489.

Zou, W., and Chen, L. (2008). Inhibitory B7-family molecules in the tumour microenvironment. Nat Rev Immunol *8*, 467-477.

PAPERS

Nature Communications, in press.

TRPM7 kinase activity is essential for T cell colonization and alloreactivity in the gut

Andrea Romagnani[1,2], Valentina Vettore[3], Tanja Rezzonico-Jost[1], Sarah Hampe[3], Elsa Rottoli[4], Wiebke Nadolni[3], Michela Perotti[1], Melanie A. Meier[3], Constanze Hermanns[3], Sheila Geiger[3], Gunther Wennemuth[5], Camilla Recordati[6], Masayuki Matsushita[7], Susanne Muehlich[3], Michele Proietti[1,9], Vladimir Chubanov[3], Thomas Gudermann[3], Fabio Grassi[1,4,8] and Susanna Zierler[3]

[1]Institute for Research in Biomedicine, Università della Svizzera Italiana, Via Vincenzo Vela 6 - CH-6500 Bellinzona, Switzerland. [2]Graduate School for Cellular and Biomedical Sciences, University of Bern, c/o Theodor Kocher Institute, Freiestrasse 1, P.O. Box 938, CH-3000 Bern 9, Switzerland. [3]Walther Straub Institute of Pharmacology and Toxicology, Ludwig-Maximilians Universität München, Goethestrasse 33, 80336 Munich, Germany. [4]Department of Medical Biotechnology and Translational Medicine (BIOMETRA), Università degli Studi di Milano, Via G.B. Viotti 3/5 - 20133 Milan, Italy. [5]Institute for Anatomy, Universitätsklinikum Essen, Hufelandstrasse 55, 45147 Essen, Germany. [6]Filarete Foundation, Viale Ortles 22/4, 20139 Milan, Italy. [7]Department of Molecular and Cellular Physiology, University of the Ryukyus, 207 Uehara, Okinawa 903-0215, Japan. [8]Istituto Nazionale Genetica Molecolare "Romeo ed Enrica Invernizzi", Via Francesco Sforza, 35 - 20122 Milan, Italy. [9]Present address: Center for Chronic Immunodeficiency, Universitätsklinikum Freiburg, Breisacher Str. 115, 79106 Freiburg, Germany.

Corresponding authors: fabio.grassi@unimi.it, susanna.zierler@lrz.uni-muenchen.de

Abstract

The melastatin-like transient-receptor-potential-7 protein (TRPM7), harboring a cation channel and a serine/threonine kinase, has been implicated in thymopoiesis and cytokine expression. Here we show, by analyzing TRPM7 kinase-dead mutant (*Trpm7*$^{R/R}$) mice, that the enzymatic activity of the receptor is not essential for thymopoiesis, but is required for CD103 transcription and gut-homing of intraepithelial lymphocytes (IEL). Defective T cell gut colonization reduces MHCII expression in intestinal epithelial cells. Mechanistically, TRPM7 kinase activity controls TGF-β-induced CD103 expression and pro-inflammatory T helper 17 cell (T_H17), but not regulatory T cell (Treg), differentiation by modulating SMAD2. Notably, we find that the TRPM7 kinase activity promotes gut colonization by alloreactive T cells in acute graft-versus-host disease. Thus, our results unravel a function of TRPM7 kinase in T cell activity and suggest a therapeutic potential of kinase inhibitors in averting acute graft-versus-host disease.

Introduction

The antigen-rich environment of the gut interrelates with a highly specialized mucosal immune system, mastering the challenge of preventing invasion and systemic spread of microbes while avoiding unnecessary immune reactions to commensal bacteria. Besides representing a physical barrier, the intestinal epithelium constitutes also a dynamic interface between the host immune system and the luminal environment, which harbours potentially harmful microbes. Therefore, maintenance of the protective barrier is essential in mucosal immunity, and intraepithelial lymphocytes (IEL) have an important function in maintaining this barrier function[1]. The intestinal mucosa is composed of a single layer of columnar epithelial cells, the underlying lamina propria and the muscularis mucosa. Tight junctions, components of the apical junctional complex, seal the paracellular space between epithelial cells. IELs are located above the basement membrane, but are subjacent to tight junctions. The lamina propria is located beneath the basement membrane and contains immune cells, including macrophages, dendritic cells and lamina propria lymphocytes (LPL)[2]. Intestinal T cells are highly heterogeneous in phenotype and function and include both conventional and unconventional subpopulations. Conventional mucosal T cells express the $\alpha\ \beta$ T cell receptor (TCR $\alpha\ \beta$) together with CD4 or CD8 $\alpha\ \beta$ as co-receptors, whereas unconventional mucosal T cells express either TCR $\alpha\ \beta$ or TCR $\gamma\ \delta$ together with CD8 $\alpha\ \alpha$ homodimers[1]. During their activation in specialized mesenteric lymph nodes or Peyer's Patches, naïve T cells acquire gut-homing properties through the upregulation of distinct adhesion receptors including the integrins $\alpha_4\beta_7$ and $\alpha_E\beta_7$ (CD103)[3, 4]. Moreover, the resident microbiota regulates the development of specific lymphocyte subsets in the gut. $CD4^+$ T helper 17 (T_H17) cells preferentially accumulate in the intestine, indicating a developmental regulation by gut-intrinsic mechanisms[5]. Forkhead box P3 (FoxP3) expressing regulatory T (T_{reg}) cells represent another $CD4^+$ T helper (T_H) cell subset that preferentially accumulates in the intestine and contributes to gut homeostasis. The regulated induction of pro-inflammatory T_H17 and immunosuppressive T_{reg} cells in the gut illustrates the importance of an equilibrium between effective immunity and tolerance to preserve tissue integrity[1]. However, the mechanisms responsible for this physiologic balance are not well understood. The

induction of both these T_H subsets depends on TGF-β, which is abundantly present in the intestine[6, 7].

Among the mammalian transient receptor potential (TRP) superfamily of unselective cation channels, the TRPM subfamily, named after its founding member melastatin, TRPM1[8], comprises 8 members including the dual-function protein, TRPM7. TRPM7 is a divalent selective cation channel, mainly conducting Mg^{2+}, Ca^{2+} and Zn^{2+}, fused to a C-terminal α-kinase domain[9, 10]. TRPM7 has been implicated in cell survival, proliferation, apoptosis as well as migration and immune cell function. However, the physiologic function of TRPM7 ion channel or enzymatic activity is poorly understood[11, 12]. Unlike conventional kinases, TRPM7 kinase does not recognize known specific amino acid motifs but phosphorylates serines (Ser) and threonines (Thr) located within alpha-helices[10]. TRPM7 contains a Ser/Thr-rich autophosphorylation site, which aids in TRPM7-substrate binding[13]. *In vitro*, TRPM7 kinase phosphorylates annexin A1[10, 14], myosin II isoforms[15], eEF2-k[16] and PLCγ2[17].

Deletion of the ubiquitously expressed TRPM7 protein is embryonic lethal[18, 19]. Deletion of the exons encoding only the TRPM7 kinase domain ($Trpm7^{\Delta K/\Delta K}$) also causes early embryonic death, most probably attributable to reduced channel function in this mutant[19]. However, heterozygous mice ($Trpm7^{+/\Delta K}$) are viable and develop severe hypo-magnesaemia upon Mg^{2+} restriction, causing increased mortality, susceptibility to seizures, and prevalence for allergic hypersensitivity[19]. Interestingly, homozygous mice with genetic inactivation of TRPM7 kinase activity by a point mutation within the active site of the kinase (K1646R, $Trpm7^{R/R}$) have no obvious phenotype[20, 21], indicating that the $Trpm7^{+/\Delta K}$ phenotype, is due to decrease in both channel and kinase activity. Moreover, analysis of these mouse models revealed that TRPM7 kinase activity regulates mast cell degranulation and histamine release, implicating TRPM7 in the hyper-allergic phenotype observed previously[22]. Tissue-specific deletion of *Trpm7* in the T cell lineage disrupts thymopoiesis and results in altered chemokine and cytokine expression profiles[18], indicating that TRPM7 channel and/or kinase are important for T cell function.

Here we show that the ubiquitous kinase-dead mouse model, *Trpm7*$^{R/R}$, with a single point mutation at the active site of the kinase[21] has an exquisite requirement for TRPM7 kinase activity in intra-epithelial T cell homeostasis. We find that gut colonization by alloreactive T cells in acute graft-versus-host disease depends on TRPM7 kinase activity indicating a therapeutic potential of kinase inhibitors in averting this condition.

Results

TRPM7 kinase does not affect channel activity

To investigate the impact of the TRPM7 kinase on T cell function, we utilized a mouse model carrying a point mutation at the active site of the enzyme[21]. Mutating lysine at position 1646 to arginine (*Trpm7*$^{R/R}$) disrupts ATP-binding and thereby kinase activity (Supplementary Fig. 1a)[21]. Using immunoprecipitation and Western Blot analysis, we were able to confirm that the mutation indeed disrupted native kinase activity and thus auto-phosphorylation at serine 1511 in primary splenocytes (Supplementary Fig. 1b). Unlike mice lacking the entire kinase domain[19], homozygous *Trpm7*$^{R/R}$ mice are viable[20, 21]. They are normal in size, weight, and Mendelian inheritance ratio compared to WT[20, 21]. To test whether inactivation of TRPM7 kinase has any effect on Mg^{2+} and Ca^{2+} homeostasis, we used inductively coupled mass spectrometry (ICP-MS), biochemical as well as calcium-imaging techniques. By ICP-MS we observed no changes in serum Mg^{2+} and Ca^{2+} concentrations (Supplementary Fig. 1c,d). Cellular ATP levels are often taken as an estimate for intracellular Mg^{2+} contents[23]. Therefore, we performed a luciferin luciferase assay and found no alterations in intracellular ATP levels between WT and *Trpm7*$^{R/R}$ primary naïve $CD4^+$ T cells (Supplementary Fig. 1e). To determine basal intracellular free Ca^{2+} concentrations ($[Ca^{2+}]_i$), we used ratiometric Fura-Red imaging. No significant differences in $[Ca^{2+}]_i$ between WT and *Trpm7*$^{R/R}$ primary naïve $CD4^+$ T cells were detected (Supplementary Fig. 1f). Further, we assessed the potential function of kinase activity in the regulation of biophysical features of the TRPM7 channel. Whole cell patch-clamp experiments revealed that the channel function is unaltered in primary peritoneal mast cells (Supplementary Fig. 1g,h) as well as in naïve $CD4^+$ T cells (Supplementary Fig. 1j), which is in line with previous reports on peritoneal macrophages

and mast cells, as well as embryonic fibroblasts isolated from *Trpm7*$^{R/R}$ mice[20, 21, 22]. *Trpm7*$^{R/R}$ channels display slightly decreased Mg^{2+}-sensitivity without obvious consequences for the channel activity at physiologic Mg^{2+} levels (Supplementary Fig. 1i). As already shown, serum Mg^{2+} and Ca^{2+} concentrations were unaffected (Supplementary Fig. 1c,d)[21]. This overall constellation allowed us to independently investigate TRPM7 kinase function.

TRPM7 kinase affects serum cytokines but not thymopoiesis

Tissue-specific deletion of *Trpm7* in the T cell lineage was shown to disrupt thymopoiesis and resulted in altered chemokine and cytokine expression profiles[18], indicating that TRPM7 channel and/or kinase are important in T cell development. Our TRPM7 kinase-dead mouse model, *Trpm7*$^{R/R}$, allows us to specifically address the function of TRPM7 kinase activity in T cells. The total numbers of thymocytes, as well as the percentages of double negative (DN, $CD4^-CD8^-$), double positive (DP, $CD4^+CD8^+$) and single positive (SP, $CD4^+CD8^-$, $CD4^-CD8^+$) thymocytes were similar in both genotypes (Fig. 1a-c). Tissue-specific deletion of *Trpm7* in the T cell linage affected thymopoiesis through a block in the transition from the DN3 ($CD25^+CD44^-$) to the DN4 ($CD25^-CD44^-$) stage[18]. However, in the kinase-dead *Trpm7*$^{R/R}$ mutant the distribution of DN3 and DN4 thymocytes was unaltered with respect to WT (Fig. 1d-f), indicating that the kinase activity is not responsible for the thymic phenotype observed previously.

In spite of normal T cell development and similar to T cell specific conditional *Trpm7*$^{-/-}$ mice[18], the *Trpm7*$^{R/R}$ mutant had a significant reduction of pro-inflammatory cytokines in the serum, including G-CSF and IL-17A. Also IL-1ß, IL-3, IL-4, IL-9, IL-10, IL12p70, IL-13, GM-CSF, IFN-γ and TNF were reduced, albeit not significantly (Fig. 1g), thus indicating a function of the TRPM7 kinase in shaping the cytokine secretion profile.

In vitro activation of $CD4^+$ T cells derived from *Trpm7*$^{R/R}$ mice using αCD3/αCD28 coated plates resulted in slightly reduced intracellular Ca^{2+} signalling compared to WT cells (Supplementary Fig. 2a). Although *Trpm7*$^{R/R}$ T cells had similar kinetics of receptor-operated Ca^{2+} entry (ROCE) compared to WT T cells, Ca^{2+} amplitudes in *Trpm7*$^{R/R}$ T cells were significantly different at 150 seconds compared to WT (Supplementary Fig. 2a).

Nonetheless, the proliferation rates were similar between the two genotypes, indicating no primary defect of *Trpm7*$^{R/R}$ mice in T cell activation (Supplementary Fig. 2b,c).

TRPM7 kinase promotes T cell colonization of gut epithelium

While T cell subsets in the spleen and peripheral lymph nodes were distributed normally in *Trpm7*$^{R/R}$ mice (Supplementary Fig. 3a,b), we found a strong reduction of all T cell subsets in the intestinal epithelium (Fig. 2a,c) and the lamina propria (LP) (Fig. 2b,d) by FACS analysis. Notably, LPLs as well as CD4$^+$ TCR$\alpha\beta^+$ IELs were particularly affected by the lack of TRPM7 kinase activity (Fig. 2a,b). In line with these findings, the analysis of the distribution of CD3$^+$ T cells in tissue sections of the small intestine from *Trpm7*$^{R/R}$ mice revealed a significant reduction of IELs compared to WT (Fig. 2e). The presence of IELs correlates with the induction of MHCII expression on epithelial cells[24]. Consistent with the significant reduction of IELs, we detected a dramatic reduction of MHCII expression in EpCAM$^+$ intestinal epithelial cells in *Trpm7*$^{R/R}$ compared to WT mice (Fig 2f). Analysis of the transcriptional profile of the few IELs that were present in *Trpm7*$^{R/R}$ mice revealed no differences in T-bet or FoxP3 expression when compared to WT, indicating a normal T_H1 and T_{reg} polarization, respectively. However, the signature transcription factor for T_H17 cells, Rorc, was significantly reduced in *Trpm7*$^{R/R}$ IELs compared to WT that was also reflected by significantly reduced IL-17 expression (Fig. 2g). These findings were confirmed by intracellular staining via FACS for IFN-γ and IL-17A in IELs isolated from WT and *Trpm7*$^{R/R}$ mice. While IFN-γ secreting cells were comparable between *Trpm7*$^{R/R}$ and WT IELs, IL-17A secreting cells were significantly diminished in *Trpm7*$^{R/R}$ compared to WT IELs (Fig. 2h).

Defect in gut epithelium colonization is T cell intrinsic

In the intestinal epithelium the up-regulation of CD103 is required, specifically integrin $\alpha_E\beta_7$, which in turn interacts with E-cadherin on the epithelial cells and thus facilitates the retention of IELs into the epithelial layer[25, 26]. Interestingly, CD103 and integrin β_7 expressing CD4$^+$ IELs were highly significantly reduced in *Trpm7*$^{R/R}$ mice, while CD8$^+$ IELs were only slightly, albeit significantly, reduced and $\alpha_4\beta_7$ expressing cells were unaffected (Fig. 3a). The analysis of CD4$^+$ and CD8$^+$ LPLs revealed a similar reduction in CD103 expression in *Trpm7*$^{R/R}$ mice compared to WT (Fig. 3b). However, integrin β_7

expressing $CD8^+$ LPLs were unaffected in *Trpm7*$^{R/R}$ mice compared to WT (Fig. 3b). Also the mean fluorescence intensity (MFI) of CD103 expression was significantly reduced in *Trpm7*$^{R/R}$ $CD4^+$ and $CD8^+$ IELs as well as $CD4^+$ and $CD8^+$ LPLs compared to WT cells (Fig. 3c,d). Correspondingly, the MFI of the integrin β_7 was similarly reduced (Fig. 3c,d). At the transcriptional level, analysis of the gene encoding CD103, *Itgae*, via quantitative real-time (qRT)-PCR revealed significantly reduced *Itgae* mRNA expression in lymphocytes isolated from the spleen, LP and intestinal epithelium of *Trpm7*$^{R/R}$ compared to WT mice (Fig. 3e).

To rule out the contribution of other cells to the reduction of IELs and LPLs as well as CD103 expression, we further examined intestinal epithelial as well as dendritic cells. Transmission electron microscopic images of the ileum (upper panel) and the colon (lower panel) of WT and *Trpm7*$^{R/R}$ mice illustrate no changes in overall structure, tight junction, adherens junction or desmosome formation (Fig 4a), indicating no primary difference between the epithelial barrier of WT and *Trpm7*$^{R/R}$ mice. Interestingly, MHCII as well as CD103 surface expression of WT and *Trpm7*$^{R/R}$ dendritic cells was unaltered (Fig. 4b), suggesting that dendritic cell function is not affected by the TRPM7 kinase. Consistently, *Trpm7* mRNA levels were strongly reduced in DCs as well as in epithelial cells, compared to T cells (Supplementary Fig. 3c).

CD103 expression strongly depends on TGF-β stimulation[27]. The analysis of TGF-β1, 2 and 3 mRNA levels in dendritic as well as intestinal epithelial cells, two main sources of TGF-β in the gut, did not reveal significant differences between WT and *Trpm7*$^{R/R}$ mice (Fig. 4c). Moreover, we did not detect any difference in TGF-β serum levels between the different mice (Fig. 4d). Notably, TGF-β1 was the most prominent isoform in serum, while TGF-β3 was not detectable.

To confirm that the reduced number of IELs and LPLs in *Trpm7*$^{R/R}$ mice was T cell intrinsic, we adoptively transferred either WT or *Trpm7*$^{R/R}$ naïve $CD4^+$ cells into congenic *Rag1*$^{-/-}$/*Il2rg*$^{-/-}$ double mutant mice, lacking T- and B- as well as natural killer cells. While both WT and *Trpm7*$^{R/R}$ naïve T cells equally reconstituted the spleen, *Trpm7*$^{R/R}$ T cells exhibited an intrinsic defect in colonizing the intestinal epithelium (Fig. 4e). *Trpm7*$^{R/R}$ $CD4^+$ IELs poorly, if at all, expressed CD103 (Fig. 4f), thereby indicating that the defect of IEL retention within the small intestinal epithelium was T cell autonomous. Moreover,

lymphopenic hosts adoptively transferred with naïve CD4$^+$ T cells from *Trpm7*$^{R/R}$ mice had significantly impaired upregulation of MHCII in intestinal epithelial cells (Fig. 4g).

TRPM7 kinase regulates TGF-β/SMAD pathways

As *Trpm7*$^{R/R}$ IELs displayed a pronounced reduction in Rorc and IL-17 expression while T-bet and FoxP3 were equivalent in *Trpm7*$^{R/R}$ compared to WT IELs (Fig. 2g), we addressed whether *in vitro* differentiation of naïve CD4$^+$ *Trpm7*$^{R/R}$ T cells would reproduce this phenomenon. After polarization of naïve T cells into T_H1 or T_{reg} for 5 days using the respective cytokine and inhibitory-antibody cocktails (see methods), we observed no differences in the percentage of IFN-γ or CD25$^+$FoxP3$^+$ T cells between the two genotypes (Fig. 5a, left and middle panel). Interestingly, *in vitro* polarization of naïve CD4$^+$ T cells into T_H17 cells, using TGF-β, IL-6 and αIFN-γ, was significantly reduced in *Trpm7*$^{R/R}$ compared to WT cells (Fig. 5a, right panel), consistent with the robust reduction of IL-17 concentration in serum from *Trpm7*$^{R/R}$ mice (Fig. 1g) as well as the diminished number of IL17-producing *Trpm7*$^{R/R}$ IELs (Fig. 2h). In contrast, *T-bet* and *Ifn-γ* mRNA levels were not different among *in vitro* differentiated *Trpm7*$^{R/R}$ and WT T_H1 cells (Fig. 5b). Since Rorc and IL-17 mRNA levels were significantly reduced in *in vitro* differentiated *Trpm7*$^{R/R}$ T_H17 cells (Fig. 5b), we analysed STAT3 signalling as a signalling pathway involved in T_H17 differentiation. However, Western Blot analysis of CD4$^+$ T cells treated with IL-6 for 15 and 30 minutes showed no differences in STAT3 phosphorylation at Tyr705 (Fig. 5c).

Next, we asked whether the defect in CD103 expression *in vivo* was also reflected *in vitro*. To this end, naïve CD4$^+$ T cells were treated with TGF-β1, stimulated with αCD3/αCD28 and analyzed for CD103 and integrin β_7 surface expression by FACS. Interestingly, *Trpm7*$^{R/R}$ CD4$^+$ T cells were characterized by a significant reduction in CD103 and integrin β_7 expression (Fig. 5d). While WT naïve CD4$^+$ T cells increased *Itgae* gene expression two fold, *Trpm7*$^{R/R}$ naïve CD4$^+$ T cells were unable to up-regulate *Itgae* expression after 24 hours stimulation (Fig. 5e), suggesting a transcriptional regulation of CD103 via the TRPM7 kinase. Since TGF-β was shown to up-regulate CD103 via SMAD and NFAT pathways in human T cells[28], we addressed whether the TGF-β/SMAD signalling pathway was affected by TRPM7 kinase activity, particularly

as TGF-β/SMAD pathways are also crucial for the polarization of $CD4^+$ T cells into T_H17 cells[29]. Importantly, Western Blot analysis of *Trpm7*$^{R/R}$ naïve $CD4^+$ T cells treated with 5 ng ml^{-1} TGF-β1 for 10 minutes revealed a strong and significant reduction in SMAD2 (Ser465/467) phosphorylation (Fig. 5f, upper row and middle panel), while SMAD3 (Ser423/425) phosphorylation was unaltered (Fig. 5f, middle row and right panel). Consistently, SMAD2 translocation into the nucleus was significantly impaired in *Trpm7*$^{R/R}$ T cells compared to WT (Fig. 6a). Thus, we conclude that the TRPM7 kinase regulates T_H17 differentiation and *Itgae* expression via TGF-β/SMAD2 dependent pathways.

To further clarify the mechanism by which TRPM7 kinase activity controls TGF-β/SMAD2 signalling, we performed an *in vitro* kinase assay using highly purified recombinant TRPM7 kinase, SMAD2-GST, as well as C-terminally truncated SMAD2-GST and GST-tag as controls. Remarkably, TRPM7 phosphorylates SMAD2 in a dose dependent manner. Moreover, TRPM7 fails to phosphorylate the truncated SMAD2 or the GST-tag, thereby identifying the C-terminal SXS-motif of SMAD2 as a substrate for TRPM7 kinase (Fig. 6b). Thus, we conclude that TRPM7 kinase can modulate SMAD2 signalling via direct phosphorylation at the C-terminal Ser465/467 motif (Fig. 5f, 6b), which is essential for its transcriptional activity, while the linker region (Ser245/250/255) is unaffected by TRPM7 kinase (Supplementary Fig. 3d, 6b).

Moreover, we performed a proximity ligation assay (PLA) on purified $CD4^+$ T cells, to characterize the interaction of SMAD2 with TRPM7 kinase in more detail,. Figure 6c depicts a significant increase in SMAD2 co-localization with TRPM7 in WT T cells treated with 5 ng ml^{-1} TGF-β1 ($p<0.0001$, two-tailed Student's t-test), while *Trpm7*$^{R/R}$ T cells fail to recruit SMAD2 into close proximity to TRPM7 kinase (Fig. 6c). SMAD2 has previously been shown to bind to the *Itgae* promoter sequence, thereby facilitating its transcription[25]. To link the observed defect in CD103 expression of *Trpm7*$^{R/R}$ T cells to their defective SMAD2 signalling, we performed a chromatin immunoprecipitation (ChIP) assay on primary murine $CD4^+$ T cells with and without TGF-β1 stimulation (Fig. 6d). Our results show that SMAD2 binds to the *Itgae* promoter regions upon TGF-β1 stimulation in WT T cells, but fails to do so in *Trpm7*$^{R/R}$ T cells in response to TGF-β1

stimulation, underscoring the indispensable requirement of a functional TRPM7 kinase in TGF-β/SMAD2 signalling in T cells.

TRPM7 kinase activity promotes graft-versus-host disease

In acute graft-versus-host disease (GVHD), naïve donor CD4 cells recognize alloantigens on antigen presenting cells in target organs, including skin, intestine and lung. However, the function of different T_H subsets and signalling pathways in the pathogenesis of GVHD in distinct organs is incompletely characterized. We hypothesized that defective intestinal colonization by $CD4^+$ cells lacking TRPM7 kinase activity could affect acute GVHD. To address this hypothesis, BALB/c WT mice were lethally irradiated and transplanted with bone marrow (BM) cells from WT C57BL/6J mice together with WT or *Trpm7*$^{R/R}$ splenocytes. As expected, injection of WT splenocytes resulted in massive intestinal damage as demonstrated by shortening of the colon (Fig. 7a) and most mice died within 35 days after transplantation (Fig. 7b). In contrast, injection of *Trpm7*$^{R/R}$ splenocytes did not cause intestinal damage and shortening of the colon in BALB/c hosts (Fig. 7a). Moreover, we observed a dramatically increased survival of these mice; only about 10 % of mice injected with *Trpm7*$^{R/R}$ splenocytes died within the first 30 days after transplantation (Fig. 7b).

The analysis of intestinal epithelium by FACS with $H2K^B$ (C57BL/6J haplotype) specific mAb revealed a significant reduction of $TCR\alpha\beta^+$ cells derived from *Trpm7*$^{R/R}$ splenocytes with respect to WT cells, suggesting an impairment of T cells lacking TRPM7 kinase activity in the colonization of host intestine (Fig. 7c). Also, the expression of CD103 and integrin β_7 was significantly reduced in $CD4^+$ as well as $CD8^+$ $TCR\alpha\beta^+$ *Trpm7*$^{R/R}$ compared to WT cells (Fig. 7e). The reduction of gut colonization by *Trpm7*$^{R/R}$ T cells correlated with a significantly reduced expression of MHCII in host intestinal epithelial cells with respect to mice injected with WT cells (Fig. 7d). These results indicate that TRPM7 kinase activity in T cells is a decisive factor in the pathogenesis of GVHD by promoting host gut epithelium colonization.

Discussion

Tissue-specific deletion of *Trpm7* in the T cell lineage results in impairment of T cell development in the thymus and altered chemokine as well as cytokine expression profiles[18]. In contrast, mice carrying an inactive TRPM7 kinase (*Trpm7*$^{R/R}$) have unaltered thymopoiesis[21], indicating that the channel but not the kinase activity is important in regulating the progression of T cell progenitors to mature T cells. However, in these mice we observed a significant reduction of pro-inflammatory cytokines, including IL-17 and G-CSF, suggesting that TRPM7 kinase activity might be essential for immune system homeostasis.

While T cells in the spleen and peripheral lymph nodes of *Trpm7*$^{R/R}$ mice were distributed normally, conventional T cells within IELs and LPLs were reduced. In particular, CD4$^+$ T cells were the most significantly reduced IELs and LPLs subsets in *Trpm7*$^{R/R}$ as compared to WT mice. In addition, the analysis of functional subsets in the few CD4$^+$ cells recovered from the gut of *Trpm7*$^{R/R}$ mice revealed a dramatic reduction of T_H17 cells, indicating that TRPM7 kinase activity is important for gut colonization by T cells and T_H17 cell differentiation. In fact, experiments of *in vitro* polarization of naïve CD4$^+$ T cells into T_H1, T_{reg} and T_H17 cells showed a selective defect of *Trpm7*$^{R/R}$ CD4$^+$ T cells to polarize into Rorc and IL-17 expressing cells. STAT3 phosphorylation is important for T_H17 cell differentiation[29] and *Trpm7* silencing was shown to affect STAT3 phosphorylation at Tyr705 in breast cancer cells stimulated with epidermal growth factor[30]. However, IL-6 induced Tyr705 phosphorylation was unaffected in *Trpm7*$^{R/R}$ CD4$^+$ T cells, suggesting that this signalling event is not involved in the defect in T_H17 polarization of *Trpm7*$^{R/R}$ cells; this result also suggests that in breast cancer cells Tyr705 phosphorylation might be conditioned indirectly by the TRPM7 channel rather than kinase moiety.

In *Trpm7*$^{R/R}$ mice, the vascular adhesion molecule integrin $\alpha_4\beta_7$ was not affected in intestinal T cells, whereas CD103 (integrin $\alpha_E\beta_7$) was dramatically reduced. These data indicate that the profound reduction of intestinal T cells that characterizes these mice is due to the impaired retention of T cells mediated by the interaction of CD103 with E-cadherin expressed in epithelial cells rather than emigration from blood vessels into the LP[4]. Mice lacking CD103 have selectively reduced numbers of mucosal T cells and are

more prone to experimentally induced colitis[25, 26]. However, this phenomenon was attributed to lack of CD103 in gut associated CD11c^{high}MHCII^{high} dendritic cells (DCs)[31], a cell population that was not affected by lack of TRPM7 kinase activity. Our observations are consistent with a selective defect of *Trpm7$^{R/R}$* T cells in upregulating CD103 and gut retention, while CD103 expression is not affected in DCs by *Trpm7$^{R/R}$*, pointing to different regulatory mechanism/s in DCs. We demonstrated the T cell intrinsic nature of the intestinal defect due to lack of CD103 upregulation by adoptive transfer of *Trpm7$^{R/R}$* CD4$^+$ cells into lymphopenic hosts. Another important consequence of defective TRPM7 kinase activity in T cells was the significant reduction of MHCII expression in intestinal epithelial cells, a IELs dependent feature essential for proper antigen presentation and immunological function of gut epithelial cells[1, 4].

Both T_H17 cell polarization and CD103 expression depend on TGF-β-signalling[27, 28]. DCs and intestinal epithelial cells (IEL) are the major source for TGF-β in the gut[5]. However, the relative mRNA expressions of *Tgf-β1*, *2* and *3* in DCs and IELs as well as serum concentrations for TGF-β1 and 2 were similar both in *Trpm7$^{R/R}$* and WT mice, indicating no primary defect in TGF-β production or secretion by lack of TRPM7 kinase activity. Conversely, *in vitro* induction of CD103 by TGF-β in naïve *Trpm7$^{R/R}$* CD4$^+$ cells was impaired. This impairment was also evident at the transcriptional level since *Trpm7$^{R/R}$* CD4$^+$ cells failed to upregulate *Itgae*. In fact, according to SMAD dependence of *Itgae* expression[28], we could show a reduction of the phosphorylation of the C-terminal SXS motif of SMAD2 but not of SMAD3 in TGF-β1-stimulated *Trpm7$^{R/R}$* CD4$^+$ cells. Moreover, using ChIP we demonstrated the defective binding of SMAD2 to the *Itgae* promoter region in *Trpm7$^{R/R}$* T cells upon TGF-β1 stimulation. Interestingly, SMAD2 activation was suggested to exquisitely regulate T_H17 cell generation but to be dispensable for T_{reg} cell differentiation[32], consistent with distinct control of T cell functions by SMAD-dependent and -independent TGF-β signalling[33]. However, this notion remains controversial in the literature, as some studies report a dispensable function of SMAD2 in T_H17 cell polarization[34, 35, 36, 37], suggesting the existence of compensatory mechanisms under certain circumstances. As we have not evaluated all possible Ser/Thr phosphorylation sites on SMAD3, we cannot exclude an effect of the TRPM7 kinase deletion on sites other than the C-terminal SXS motif. However, for

SMAD2 we can exclude other direct phosphorylation sites, as the truncated SMAD2 mutant did not have any phosphorylation by TRPM7 kinase in our *in vitro* kinase assay. Nonetheless, our results are in line with a dispensable function of TRPM7 kinase activity in TGF-β mediated differentiation of $CD4^+$ cells into T_{reg} cells.

TGF-β signalling exerts pleiotropic effects on cell physiology via cross-talk with multiple signalling pathways. Imaging of TGF-β1-activated SMAD signalling revealed selective inhibition of SMAD2 phosphorylation by distinct tyrosine kinase inhibitors[38]. TRPM7 kinase appears as a pharmacological target for inhibition of TGF-β1-mediated SMAD2 phosphorylation in T cells, as it is capable to directly phosphorylate SMAD2. In summary, our study demonstrates that TRPM7 kinase contributes to TGF-β-induced SMAD2 phosphorylation at Ser465/467 and translocation into the nucleus. Lack of TRPM7 kinase activity results in impaired transactivation of SMAD2 target genes, including *Itgae* (encoding for CD103), *Il-17* and *Rorc*, thus selectively limiting differentiation of the T cell along the T_H17, but not T_{reg} cell, functional program. The protection of $Trpm7^{R/R}$ mice from GVHD, we have shown, unravels the clinical relevance of TRPM7 kinase as a target for limiting TGF-β-dependent CD103 expression as a pathogenetic mechanism in intestinal destruction during GVHD[27]. Finally, our study demonstrates the importance of developing pharmacological inhibitors for TRPM7 kinase activity to prevent the devastating consequences of acute GVHD without affecting the development of immunosuppressive T_{reg} cells.

Methods

Mice and *in vivo* experiments

Trpm7$^{R/R}$ mice were obtained from RIKEN, Japan[21]. 4-8-weeks-old male and female mice were used for all experiments. For *ex vivo* and *in vitro* experiments mice were euthanized using CO_2 and terminated via cervical dislocation. All experiments involving animals at the Ludwig-Maximilians-Universität München, Munich, Germany were performed in accordance with the EU Animal Welfare Act and were approved by the District Government of Upper Bavaria, Germany, on animal care (permit no. 55.2-1-54-2532-134-13). The use of transgenic animals was approved by the District Government of Upper Bavaria, protocol no. 821–8763.14.718/1210. For *in vivo* experiments C57BL/6J, *Trpm7*$^{R/R}$, BALB/c and *Rag1*$^{-/-}$/*Il2rg*$^{-/-}$ mice were bred in a specific pathogen-free facility at the Institute for Research in Biomedicine, Bellinzona, Switzerland. For adoptive transfer of T naïve, $CD4^+CD8^-CD62L^+CD44^-CD25^-$ cells were sorted at FACSAria (BD Biosciences) from pooled cell suspensions of spleen, inguinal, axillary, brachial, cervical and mesenteric LNs of C57BL/6J and *Trpm7*$^{R/R}$ mice. Eight-week old *Rag1*$^{-/-}$/*Il2rg*$^{-/-}$ mice were injected with $1x10^6$ naïve T cells. Recipient mice were sacrificed 4 weeks after reconstitution. For GVHD experiments lethally irradiated (9 Gy, Cs source) BALB/c (H-2^d) mice were reconstituted within 4–6 h by a single 0.2-ml intravenous inoculum containing 10×10^6 B6 BMC alone or in combination with 10×10^6 C57BL/6J or *Trpm7*$^{R/R}$ splenocytes. All animal experiments were performed in accordance with the Swiss Federal Veterinary Office guidelines and authorized by the Animal Studies Committee of Cantonal Veterinary with authorization numbers TI-10-2013 and TI-17-2015.

Cell isolation and primary cell culture

Lymphocytes infiltrating the intestinal epithelium were isolated as follows: While the small intestine was flushed with PBS, fat and Peyer's patches were removed. The small intestine was divided longitudinally, cut into 2-mm sections and washed twice, in calcium- and magnesium-free HBSS containing 2% FCS (at 4°C) to remove feces. The tissue was placed in 50 ml tubes, washed three-times in HBSS containing 2% FCS at 4°C, transferred to 25 cm tissue culture flasks and incubated at 37°C in HBSS containing 10% FCS, 0.2 mmol l^{-1} EDTA, 1 mmol l^{-1} DTT. After 20 min incubation, the flasks were shaken vigorously for 30 s, and the supernatant containing IELs and the IEC was separated from the tissue fragments using a 40 μm nylon filter. While the supernatant was collected and put on ice, the tissue fragments were retuned to the flasks and the process was repeated. To isolate LPLs, the remaining tissue was washed three-times with RPMI 1640, and intestinal pieces were subsequently incubated with magnetic stirring for 30 minutes at 37°C in cRPMI supplemented with 100 U ml^{-1} collagenase. The epithelial and lamina propria cell suspensions were washed, suspended in RPMI1640 at 4°C and filtered. The cell suspension was collected and suspended in 40% Percoll, which was layered on top of 80% Percoll and centrifuged at 2000 rpm for 20 min at RT. The IELs and LPLs were collected from the interface between the Percoll gradients and prepared for phenotypic analysis by flow cytometry. For mRNA extraction IELs and LPLs were purified by cell sorting as TCR β^+CD4^+Ep-CAM^- cells while IEC cells were sorted as Ep-CAM^+ cells. For isolation of thymocytes, thymi were homogenized and washed in RPMI1640 medium containing 10% (v/v) FBS. For the isolation of $CD4^+$ T cells peripheral lymph nodes were collected, smashed using a 40 μm strain and $CD4^+$ T cells were sorted via MACS ($CD4^+$ isolation kit, Miltenyi Biotec). Purity was assessed via FACS to at least 96% $CD4^+$ T cells before cells were subjected to experiments. For mast cell isolation, cells obtained from the peritoneum of WT or *Trpm7*$^{R/R}$ mice were pelleted and apportioned (Cellgro) into Petri-dishes with PDL-coated glass cover slips. Cells were cultured in 2 ml DMEM containing 10 % FBS (HyClone) and 1 % Penicillin/Streptomycin (Gibco) overnight in a humidified incubator at 37°C and 5% CO_2. For electrophysiological experiments mast cells were identified visually using light microscopy (phase contrast).

Cytokine assays

After blood collection through cardiac puncture using a collector for serum separation and blood cells (Microvette, Sarstedt), samples were separated by 10.000 g centrifugation for 5min; serum was then stored at -80°. Collected samples were prepared for the 23-cytokines assay (BioRad) and TGFß-1, 2, 3 assay (R&D Systems) according to manufacturer's instructions.

Antibodies and Flow Cytometric Analysis

The following mAbs were purchased from BD Biosciences: APC conjugated anti-CD62l (clone:MEL-14, Cat.#: 17-0621-83, working dilution 1:200), Pacific Blue conjugated anti-CD8 β (clone: H35-17.2, Cat.#: 48-0083-80, working dilution 1:200), PERCP-CYANINE5.5 conjugated anti-IL-17A (clone: 17B7, Cat.#: 45-7177-82, working dilution 1:100), FITC conjugated anti-FOXP3 (clone: FJK-16s, Cat.#: 11-5773-82, working dilution 1:100), Pacific Blue conjugated anti-H-2KB (clone: AF6-88.5.5.3, Cat.#: 48-5958-82, working dilution 1:200) APC conjugated anti-CD11C (clone: N418, Cat.#: 17-0114-82, working solution 1:200). The following mAbs were purchased from Biolegend (http://www.biolegend.com/): PE conjugated anti-CD44 (clone:IM7, Cat.#: 103008, working dilution 1:200), PE/Cy7 conjugated anti-CD25 (clone: PC61, Cat.#: 102016 working dilution 1:200), APC/Cy7 conjugated anti-CD4 (clone: RM4-5, Cat.# 100526, working dilution 1:200), FITC conjugated anti-CD8 α (clone: 53-6.7, Cat.# 100706, working dilution 1:200), PE conjugated anti-TCR β (clone: H57-597, Cat.#: 109208, working dilution 1:200), FITC conjugated anti-TCR γ δ (clone: GL3, Cat.#: 118106, working dilution 1:200), PE conjugated anti-CD103 (clone: 2E7, Cat.#: 121406, working dilution 1:200), PE conjugated anti- α 4 β 7 (clone: DATK32, Cat.#: 120606, working dilution 1:200), APC conjugated anti- β 7 (clone: FIB504, Cat.#: 321208, working dilution 1:200), Pacific Blue conjugated anti-MHC-II (clone: M5/114.15.2, Cat.#: 107620, working dilution 1:200), FITC conjugated anti-Ep-CAM (clone: G8.8, Cat.#: 118210, working dilution 1:200), PE conjugated anti-IFN- γ (clone: XMG1.2, Cat.#: 505808, working dilution 1:100). Samples were acquired on a LSRFortessa (BD Biosciences) or Guava (Merck-Millipore) flow cytometer. Data were analysed using FlowJo software (TreeStar, Ashland, OR), FACS Diva software (BD Biosciences) or InCyte (Merck-Millipore) respectively.

Quantitative RT-PCR

Total RNA from FACS sorted cells was precipitated in Trizol (Invitrogen, ThermoFisher) and reverse transcribed to cDNA using Random hexamers (Roche, Cat.#: R 15504) and M-MLV reverse-transcriptase (Invitrogen, Cat.#: 28025-013). For quantification of transcripts, mRNA samples were treated with 2 U per sample of DNase (Applied Biosystems). Transcripts were quantified by real-time PCR on an ABI PRISM 7700 Sequence Detector with predesigned TaqMan Gene Expression Assays and reagents according to the manufacturer's instructions (https://www.lifetechnologies.com). The following probes were used: *Trpm7* (Mm00457998_m1), *Tbx21* (Mm00450960_m1), *Foxp3* (Mm00475162_m1), *Rorc* (Mm01261022_m1), *Il17a* (Mm00439619_m1), *Itgae* (Mm00434443_m1), *Tgfβ1* (Mm01178820_m1), *Tgfβ2* (Mm00436955_m1), *Tgfβ3* (Mm01307950_m1). All reactions were performed in triplicates. The relative amounts of mRNAs were calculated by the ΔΔCT method. 18S and *Hprt* were used as internal housekeeping genes. For *Itgae* gene upregulation $CD4^+$ T cells were treated with 5 ng ml^{-1} of TGF-ß1 (R&D) for 24 hours. Total RNA was precipitated in Trizol (Invitrogen, ThermoFisher) and cDNA synthesis was performed using SuperScript II RT (LifeTech, Invitrogen) and oligo-dT primers (18T, Metabion). Real-time-PCR was performed using a PrimePCR™ SYBR® Green Assay for *Itgae* (BioRad, qMmuCID0039603) and analyzed using LightCycler® 480 SYBR Green I Master (Roche). *Hprt* (Fwd: CTCATGGACTGATTATGGACAGG, Rev: TTAATGTAATCCAGCAGGTCAGC, Metabion) was used as a reference gene. Samples were detected in doublets and the mean CP (Crossing Points) values were analyzed as $2^{-\Delta\Delta CP}$.

***In vitro* T cell polarization and integrin upregulation**

$CD4^+CD8^+CD62L^+CD44^-CD25^-$ naïve T cells were sorted at FACSAria from pooled suspensions of spleen, inguinal, axillary, brachial, cervical and mesenteric LNs of WT and *Trpm7*$^{R/R}$ mice. Cells were seeded in a 96-well, flat-bottomed plate in RPMI supplemented with 10% fetal calf serum (FCS) and 1 % penicillin and streptomycin. For T cell *in vitro* polarization Th1 cells were generated by addition of rmIL-12 at a concentration of 15 ng ml^{-1}, hIL-2 30 U ml^{-1} and anti-IL-4 Ab (clone 11B11) at a concentration of 5 μg ml^{-1} into the culture. For the generation of Th17 cells naïve T cells were cultured with rmIL-6 at a concentration of 20 ng ml^{-1}, rmTGF-β at a concentration of 2 ng ml^{-1}, anti-IFN-γ (clone XMG1.2) and anti IL-4 Ab at a concentration of 5 μg ml^{-1}. For the generation of T_{reg} cells naïve T cells were cultured with rmTGF-β at a concentration of 2 ng ml^{-1} , 30 u ml^{-1} hIL-2, anti-IFN-γ and anti IL-4 Ab at a concentration of 5 μg ml^{-1}. For *in vitro* CD103 upregulation T naïve cells were stimulated in presence or absence of rmTGF-β at a concentration of 1 ng ml^{-1}. After 4 days of stimulation T cells were collected and stained with anti-CD103 and anti-β7 mAbs.

Intracellular cytokine and transcription factor staining

For intracellular staining of FOXP3, after surface antigens staining, cells were fixed and permeabilized using the Foxp3 / Transcription Factor Staining Buffer Set (eBioscience) according to the manufacturer's recommendations, followed by staining with anti-FOXP3. For intracellular staining of IFN-γ and IL-17A, cells were stimulated for 4 hr with PMA (100 nM, Sigma-Aldrich) and ionomycin (1 μM, Sigma-Aldrich). Brefeldin A (BFA) was included during the last 4 hours of activation to inhibit intracellular transport. After surface antigens staining cells were fixed and permeabilized using the BD Cytofix/Cytoperm Fixation/Permeabilization Solution Kit (BD Biosciences) according to the manufacturer's recommendations, followed by staining with anti-IFN-γ and anti- IL-17A mAbs.

Immunohistochemistry and digital image analysis

To assess the number of infiltrating T cells, 4 μm sections from each formalin-fixed paraffin embedded small intestinal sample were immunostained with a primary goat polyclonal antibody against CD3 epsilon antigen (Santa Cruz Biotechnology; #Sc-1127). A biotinylated rabbit anti-goat IgG antibody (BA-5000, Vector Laboratories, Burlingame, CA, USA) was added for 30 min and sections were then labeled by the avidin-biotin-peroxidase (ABC) procedure with a commercial immunoperoxidase kit (VECTASTAIN Elite ABC HRP Kit, PK-6100, Vector Laboratories, Burlingame, CA, USA). The immunoreaction was visualized with 3,3'-diaminobenzidine (Peroxidase DAB Substrate Kit, VC-SK-4100-KI01, Vector Laboratories, Burlingame, CA, USA) substrate and sections were counterstained with Mayer's haematoxylin. For each sample, serial sections incubated with a 10% solution of normal rabbit serum served as negative controls. The number of CD3 epsilon$^+$ cells and the area of the intestinal mucosa were evaluated using the ImageJ analysis program (http://rsb.info.nih.gov/ij/) in 4 200x microscopic fields. The number of T cells per mm^2 of intestinal mucosa was then calculated.

Transmission Electron Microscopy

Electron microscopy was preformed as follows: mice ileum and colon was washed with phosphate buffer (0.1M; pH 7.2). Tissue was fixed in 2.5% glutaraldehyde in PB for 3 h, followed by washing the samples in phosphate buffer three-times for 3 h. Samples were treated for 1.5 h with 1% osmium in H_2O and increasing alcohol concentrations for dehydration. Finally samples were embedded in EPON™ and propylenoxid (propylenoxide: EPON™ = 3:1, 1:1, 1:3; 60 min each) followed by pure EPON™ for two days by 60°C. Ultrathin sections were analysed in a Zeiss transmission electron microscope (EM902A).

Western Blot Analysis

$CD4^+$ T cells were seeded in 24-well plates and stimulated with 10 ng ml^{-1} IL-6 or 5 ng ml^{-1} TGF-ß1 (PeproTech or R&D Systems) for the indicated time frames. For detection of phosphorylated proteins following antibodies were used: pSTAT3 (Tyr705, Cat.#: 9131, Cell Signaling, MW 86 kDa, working dilution 1:2500), pSMAD2 (Ser465/467, Cat.#: 138D4, Cell Signaling, MW 60 kDa, working dilution 1:200) and pSMAD3 (Ser423/425, Cat.#: C25A9, Cell Signaling, MW 52 kDa, working dilution 1:200).

Total proteins were used as loading controls and stained for STAT3 (Cat.#: 9132, Cell Signaling, MW 86 kDa, working dilution 1:5000) and SMAD2/3 (Cat.#: D7G7, Cell Signaling, MW 60 kDa and 52 kDa, working dilution 1:1000). Cells were lysed with RIPA buffer. Lysates were subjected to SDS-PAGE, and proteins were transferred to nitrocellulose by Western blotting. The first antibody was incubated overnight at 4°C. After washing three times with TBS-T for 5 min, the membrane was incubated with a HRP-conjugated secondary antibody diluted in TBS-T and incubated for 45-60 min at RT. Immune reactivity was quantified by densitometry, ratios between p-SMAD2 or 3 and total SMAD2 or 3 signals, respectively, were calculated, and TGF- ß1-induced SMAD phosphorylation was normalized to that of unstimulated cells. Data analysis was performed with the ImageJ analysis program (http://rsb.info.nih.gov/ij/). For analysis of the intensity of TGF-ß1-induced SMAD phosphorylation compared to untreated controls a one-way ANOVA was used. Values of $p < 0.05$ (#) were considered significant. $CD4^+$ T cells were seeded in 24-well plates and stimulated with 10 ng ml^{-1} IL-6, 5 ng mL^{-1} TGF-ß1 (PeproTech or R&D Systems) and anti-CD3/anti-CD28 coated beads (Invitrogen) for 10 min[39]. For detection of phosphorylated proteins following antibody was used: pSMAD2 (Ser245/250/255, no. 3104, Cell Signaling, MW 60 kDa, working dilution 1:200). Total proteins were used as loading controls and stained for SMAD2 (D43B4, Cell Signaling, MW 60 kDa, working dilution 1:1000). Cells were lysed with RIPA buffer. Lysates were subjected to SDS-PAGE, and proteins were transferred to nitrocellulose by Western blotting. The first antibody was incubated overnight at 4°C. After washing three times with TBS-T for 5 min, the membrane was incubated with an HRP-conjugated secondary antibody diluted in TBS-T and incubated for 45-60 min at RT.

***In vitro* kinase assay**

Highly purified recombinant human SMAD2-GST, C-terminally truncated SMAD2-GST and GST were purchased from SignalChem (Richmond, BC, Canada, S11-30G-250, CUSTOM S11-30G-250, G52-30U-250). The *in vitro* kinase assay was performed by Reaction Biology Corp. (Woodbridge, CT, USA) following the RBC HotSpot Kinase Assay Protocol. RBC Standard reaction buffer contained: 20 mM Hepes (pH 7.5), 10 mM $MgCl_2$, 1 mM EGTA, 2 nM $MnCl_2$, 0.02% Brij35, 0.02 mg ml^{-1} BSA, 0.1 mM Na_3VO_4, 2 mM DTT, 1% DMSO. Reactions were carried out at 4 µM ATP in duplicates and measured at 1h and 2h, respectively. 4 μM rhSMAD2-GST was used as substrate, and 4 μM rh-trSMAD2-GST as well as the 4 μM GST-tag alone were used as control substrates, while the TRPM7 kinase was titrated in a serial dilution starting at 50 nM. Kinase alone was subtracted as background. RBC standard substrate (MBP) was used as a positive and substrate alone as an additional negative control. Data acquired at 2h were converted to nM substrate phosphorylation after background subtraction, averaged and plotted as mean values ± s.e.m.

***In situ* Proximity ligation assay**

MACS sorted $CD4^+$ T cells from *TRPM7*$^{R/R}$ or WT mice were seeded on fibronectin coated coverslips (Carl Roth GmbH + Co. KG, Cat.#: H873.2) in a 6-well plate. After stimulation with 5 ng ml^{-1} TGF-β1 (R&D systems) for 10 min cells were fixed with 4% paraformaldehyde for 10 min and permeabilised with 0.2% Triton X-100 in PBS for 7 min. Blocking and the proximity ligation assay were performed with the DuoLink® In situ Red Starter kit mouse/rabbit (Sigma Aldrich, Cat.#: DUO92101) according to the manufacturer`s instructions (http://www.sigmaaldrich.com/technical-documents/protocols/biology/duolink-fluorescence-user-manual.html). T cells were stained with anti-TRPM7 (self made, Dr. Chubanov, working dilution 1:100) and anti-SMAD2 (Santa Cruz, Cat.#: sc-101153, working solution 1:100) for 1 h at room temperature. DuoLink® In situ PLA® Probe anti-mouse PLUS and DuoLink® In situ PLA® Probe anti-rabbit MINUS were used for labelling anti-SMAD2 and anti-TRPM7 antibodies. Data acquisition was done on a Leica SP5 confocal microscope with a 63 × NA 1.4 PL APO objective (both Leica, Mannheim, Germany) by producing z-stacks of five randomly selected fields. Analysis of the data was done by production of maximum peak projections of the z-stacks and counting the PLA signals per cell manually. The mean number of PLA signals per cell was calculated per field. For comparison of two different sample groups, two-tailed unpaired Student's t-test was performed in Prism 6 (GraphPad Software, La Jolla, CA, USA).

Chromatin Immunoprecipitation

MACS sorted CD4$^+$ T cells from *Trpm7$^{R/R}$* or WT mice were treated with or without 5 ng ml^{-1} TGF-β1 (R&D systems) for 10 min. In total 7 mice per genotype were used. Cells were cross-linked with 1% methanol-free formaldehyde and quenched with 0.125 M glycine. Nuclei were pelleted and lysed for 10 min on ice. After washings, lysates were sonicated four times for 30 sec into DNA fragments of 200-2000 bp. Immunoprecipitation of the sheared chromatin was performed using an anti-SMAD2 (Cell Signaling Technology, Cat.#: 5339S.) antibody coupled to Dynabeads Protein G overnight at 4°C. 1% of the sonicated chromatin was set aside as input without antibody. After washings of immune complexes and elution of DNA of both input and ChIP samples, qRT-PCR with specific primers for the *Itgae* (Fwd: CCTCCACAGCCCTATGTGTT, Rev: GCCTCACAGGTAGGAACTGG) and the *Gapdh* (Fwd: CCCTGCTTATCCAGTCCTAGCTCA AGG, Rev: CTCGGGAAGCAGCATTCAGGTCTCTGG) promoters for normalization was performed. For comparison of two different sample groups, one-way ANOVA was performed in Prism 6 (GraphPad Software, La Jolla, CA, USA).

Determination of magnesium and calcium

Content of main elements in serum samples was determined by inductively coupled plasma mass spectrometry (ICP-MS) by ALS Scandinavia (Sweden). Therefore, serum was collected using a collector for serum separation and blood cells (Microvette, Sarstedt), samples were separated by 10.000 g centrifugation for 5 min; serum was then stored at -80°. Collected samples were shipped on dry ice for further analysis via ICP-MS.

Immunoprecipitation and Western Blotting

Spleens were collected, smashed using a 100 μ m strain, washed in PBS and subjected to red blood cell lysis. The red blood cell lysis buffer contained in mM: 160 NH4Cl, 10 KHCO3, 0.1 EDTA. After washing twice in PBS, splenocytes were lysed using a 1x Lysis-Buffer containing: 0.5% (v/v) Igepal 0.5% (v/v) PMSF 1% (v/v) Protease & Phosphatase inhibitor 5 mM NaF. Lysates were incubated with a total TRPM7 antibody (ProScientifica, working dilution 1:50) and rotated for 2h at 4°C. Afterwards, Protein G sepharose beads (Dynabeads®, Invitrogen) equilibrated with lysis buffer were added at a working ratio 1:18 and rotated overnight at 4°C. Immuno-precipitated lysates were subjected to SDS-PAGE, and proteins were transferred to nitrocellulose by Western blotting. Following antibodies were used for detection: total TRPM7 (ProScientifica, working dilution 1:1000) pTRPM7Ser1511, working dilution 1:60). The first antibody was incubated overnight at 4°C. After washing three times with TBS-T for 5 min, the membrane was incubated with a HRP-conjugated secondary antibody diluted in TBS-T and incubated for 45-60 min at R, and after subsequent washing steps, the chemiluminescent signal was detected.

Generation of pTRPM7Ser1511-specific antibody

To generate a polyclonal pTRPM7Ser1511-specific antibody, rabbits were immunized with a phosphorylated peptide H2N-DSPEVD(**p**)SKAALLPC-NH2 coupled via its C-terminal cystein residue to keyhole limpet hemacyanin (Phospho-peptide immunization program Eurogentec, Belgium). The generated serum was subjected to two rounds of peptide affinity chromatography. First, a fraction of antibody was purified using the phosphorylated peptide. Second, the isolated antibody was followed by an additional round of chromatography using a non-phosphorylated variant of the peptide (H2N-DSPEVDSKAALLPC-NH2) in order to deplete a fraction of antibody with cross-reactivity to a non-phosphorylated TRPM7. The final fraction of anti-pTRPM7Ser1511 antibody was aliquoted and stored at -80 ºC

ATP detection

Detection of ATP was performed using a conventional lucifern/luciferase assay, following manufacturer's instructions (ATP Determination Kit, Invitrogen, Molecular Probes). Luminescence was monitored at ~560 nm using a microplate luminometer, FLUOstar OMEGA, by BMG.

Electrophysiology

Patch clamp experiments in whole-cell configuration were performed as follows: Currents were elicited by a ramp protocol from –100 mV to +100 mV over 50 ms acquired at 0.5 Hz and a holding potential of 0 mV. Inward current amplitudes were extracted at –80 mV, outward currents at +80 mV and plotted versus time. Data were normalized to cell size as pA pF^{-1}. Capacitance was measured using the automated capacitance cancellation function of the EPC-9/10 (HEKA, Lambrecht, Germany). Values over time were normalized to the cell size measured immediately after whole-cell break-in. Standard extracellular solution contained (in mM): 140 NaCl, 1 $CaCl_2$, 2.8 KCl, 2 $MgCl_2$, 10 HEPES-NaOH, 11 Gluc (pH 7.2, 300 mOsm). Nominally Mg^{2+}-free extracellular solution contained (in mM): 140 NaCl, 3 $CaCl_2$, 2.8 KCl, 10 HEPES-NaOH, 11 Gluc (pH 7.2, 300 mOsm). Divalent-free extracellular solution contained (in mM): 140 NaCl, 2.8 KCl, 10 HEPES-NaOH, 0.5 mM EDTA, 11 Gluc (pH 7.2, 300 mOsm). Standard intracellular solution contained (in mM): 120 Cs-glutamate, 8 NaCl, 10 HEPES, 10 Cs-EGTA, 5 EDTA (pH 7.2, 300 mOsm). For $MgCl_2$ dose response intracellular solution contained (in mM): 120 Cs-glutamate, 8 NaCl, 10 Cs-BAPTA + appropriate amount of $MgCl_2$ was added, as calculated with WebMaxC (stanford.edu).

Calcium Imaging

Intracellular calcium measurements were performed with freshly isolated naïve $CD4^+$ T cells. Measurements of intracellular Ca^{2+} levels with Fura-Red were made using dual excitation wavelengths of 420 nm and 470 nm (Invitrogen). $CD4^+$ cells were loaded with 1 μM Fura-Red-AM in external solution for 30 min at room temperature. After incubation cells were centrifuged at 1.500 rpm for 5 min at room temperature and resuspended in external solution containing (in mM) 140 NaCl, 2 $CaCl_2$, 2.8 KCl, 1 $MgCl_2$, 10 HEPES-NaOH, 11 Gluc (pH 7.2, 300 mOsm). Cells were transferred into a cell culture dish with glass bottom and kept in the dark at room temperature for 20 min. Then the dish was positioned in in the recording chamber. For basal Ca^{2+} concentrations, the mean of 5 ratio values recorded within the first minute after establishing a baseline was calculated. Images were analyzed via the ZEN Software. Alternatively, naïve $CD4^+$ T cells were loaded with 2 μM Fura-2-AM, 1% BSA and 0.02% Pluronic® F-127 in external solution for 15 min at room temperature in the dark. Cells were transferred into a cell culture dish with glass bottom, and stimulated with plate bound anti-CD3ε and anti-CD28 (5 μg ml^{-1} and 2μg ml^{-1} respectively). Images were analysed with TILLvisION software.

***In vitro* T cell proliferation**

$CD4^+$ naïve T cells were seeded in a 96-well, flat-bottomed plate in RPMI supplemented with 10% fetal calf serum (FCS) and 1 % penicillin and streptomycin. In proliferation assays cells were labelled with the Thermo Fisher CellTrace violet (#C34557) and stimulated by plate-bound anti-CD3ε (2µg ml^{-1}) mAb with or without co-immobilized anti-CD28 mAb (2µg ml^{-1}) (eBioscence). CellTrace dilution was measured in truly live cells through the exclusion of dead cells by electronic gate of Propidium Iodide negative cells. FACS acquisitions were standardized by fixed numbers of calibration beads (BD Biosciences). Alternatively, 0.5 x10^6 $CD4^+$ T cells per mL were seeded into 96-round-bottom-well plates coated with anti-CD3 (5 μg ml^{-1}) as well as anti-CD28 (5 μ g mL^{-1}). Every day cells were resuspended in medium and 50 μL were analysed via FACS analysis (Guava, Merck-Millipore) using the ViaCount dye (Merck-Millipore) to count live cells.

Statistical analysis

Unless stated otherwise, a two-tailed unpaired Student's t-test was used to determine the significance of differences between mean values (GraphPad or IgorPro). Data are presented as mean values ± s.e.m. of at least 3 mice. Values of $p < 0.05$ were considered significant with * $p<0.05$, ** $p<0.01$ and *** $p<0.001$.

Data availability

The authors declare that the data supporting the findings of this study are available within the paper and its supplementary information file.

References

1. van Wijk F, Cheroutre H. Mucosal T cells in gut homeostasis and inflammation. *Expert review of clinical immunology* 2010, **6**(4)**:** 559-566.

2. Turner JR. Intestinal mucosal barrier function in health and disease. *Nature reviews Immunology* 2009, **9**(11)**:** 799-809.

3. Campbell DJ, Butcher EC. Rapid acquisition of tissue-specific homing phenotypes by CD4(+) T cells activated in cutaneous or mucosal lymphoid tissues. *The Journal of experimental medicine* 2002, **195**(1)**:** 135-141.

4. Habtezion A, Nguyen LP, Hadeiba H, Butcher EC. Leukocyte Trafficking to the Small Intestine and Colon. *Gastroenterology* 2016, **150**(2)**:** 340-354.

5. Kamada N, Nunez G. Role of the gut microbiota in the development and function of lymphoid cells. *Journal of immunology* 2013, **190**(4)**:** 1389-1395.

6. Chen W, Jin W, Hardegen N, Lei KJ, Li L, Marinos N*, et al.* Conversion of peripheral CD4+CD25- naive T cells to CD4+CD25+ regulatory T cells by TGF-beta induction of transcription factor Foxp3. *The Journal of experimental medicine* 2003, **198**(12)**:** 1875-1886.

7. Veldhoen M, Hocking RJ, Atkins CJ, Locksley RM, Stockinger B. TGFbeta in the context of an inflammatory cytokine milieu supports de novo differentiation of IL-17-producing T cells. *Immunity* 2006, **24**(2)**:** 179-189.

8. Venkatachalam K, Montell C. TRP channels. *Annual review of biochemistry* 2007, **76:** 387-417.

9. Monteilh-Zoller MK, Hermosura MC, Nadler MJ, Scharenberg AM, Penner R, Fleig A. TRPM7 provides an ion channel mechanism for cellular entry of trace metal ions. *The Journal of general physiology* 2003, **121**(1)**:** 49-60.

10. Ryazanova LV, Dorovkov MV, Ansari A, Ryazanov AG. Characterization of the protein kinase activity of TRPM7/ChaK1, a protein kinase fused to the transient receptor potential ion channel. *The Journal of biological chemistry* 2004, **279**(5)**:** 3708-3716.

11. Fleig A, Chubanov V. Trpm7. *Handbook of experimental pharmacology* 2014, **222:** 521-546.

12. Paravicini TM, Chubanov V, Gudermann T. TRPM7: a unique channel involved in magnesium homeostasis. *The international journal of biochemistry & cell biology* 2012, **44**(8)**:** 1381-1384.

13. Matsushita M, Kozak JA, Shimizu Y, McLachlin DT, Yamaguchi H, Wei FY*, et al.* Channel function is dissociated from the intrinsic kinase activity and autophosphorylation of TRPM7/ChaK1. *The Journal of biological chemistry* 2005, **280**(21)**:** 20793-20803.

14. Dorovkov MV, Kostyukova AS, Ryazanov AG. Phosphorylation of annexin A1 by TRPM7 kinase: a switch regulating the induction of an alpha-helix. *Biochemistry* 2011, **50**(12)**:** 2187-2193.

15. Clark K, Middelbeek J, Dorovkov MV, Figdor CG, Ryazanov AG, Lasonder E*, et al.* The alpha-kinases TRPM6 and TRPM7, but not eEF-2 kinase, phosphorylate the assembly domain of myosin IIA, IIB and IIC. *FEBS Lett* 2008, **582**(20)**:** 2993-2997.

16. Perraud AL, Zhao X, Ryazanov AG, Schmitz C. The channel-kinase TRPM7 regulates phosphorylation of the translational factor eEF2 via eEF2-k. *Cell Signal* 2011, **23**(3)**:** 586-593.

17. Deason-Towne F, Perraud AL, Schmitz C. Identification of Ser/Thr phosphorylation sites in the C2-domain of phospholipase C gamma2 (PLCgamma2) using TRPM7-kinase. *Cell Signal* 2012, **24**(11)**:** 2070-2075.

18. Jin J, Desai BN, Navarro B, Donovan A, Andrews NC, Clapham DE. Deletion of Trpm7 disrupts embryonic development and thymopoiesis without altering Mg2+ homeostasis. *Science* 2008, **322**(5902)**:** 756-760.

19. Ryazanova LV, Rondon LJ, Zierler S, Hu Z, Galli J, Yamaguchi TP*, et al.* TRPM7 is essential for Mg(2+) homeostasis in mammals. *Nature communications* 2010, **1:** 109.

20. Ryazanova LV, Hu Z, Suzuki S, Chubanov V, Fleig A, Ryazanov AG. Elucidating the role of the TRPM7 alpha-kinase: TRPM7 kinase inactivation leads to magnesium deprivation resistance phenotype in mice. *Scientific reports* 2014, **4:** 7599.

21. Kaitsuka T, Katagiri C, Beesetty P, Nakamura K, Hourani S, Tomizawa K*, et al.* Inactivation of TRPM7 kinase activity does not impair its channel function in mice. *Scientific reports* 2014, **4:** 5718.

22. Zierler S, Sumoza-Toledo A, Suzuki S, Duill FO, Ryazanova LV, Penner R*, et al.* TRPM7 kinase activity regulates murine mast cell degranulation. *The Journal of physiology* 2016, **594**(11)**:** 2957-2970.

23. Feeney KA, Hansen LL, Putker M, Olivares-Yanez C, Day J, Eades LJ*, et al.* Daily magnesium fluxes regulate cellular timekeeping and energy balance. *Nature* 2016, **532**(7599)**:** 375-379.

24. Scott H, Sollid LM, Fausa O, Brandtzaeg P, Thorsby E. Expression of major histocompatibility complex class II subregion products by jejunal epithelium in patients with coeliac disease. *Scandinavian journal of immunology* 1987, **26**(5)**:** 563-571.

25. Schon MP, Arya A, Murphy EA, Adams CM, Strauch UG, Agace WW*, et al.* Mucosal T lymphocyte numbers are selectively reduced in integrin alpha E (CD103)-deficient mice. *Journal of immunology* 1999, **162**(11)**:** 6641-6649.

26. Gorfu G, Rivera-Nieves J, Ley K. Role of beta7 integrins in intestinal lymphocyte homing and retention. *Curr Mol Med* 2009, **9**(7)**:** 836-850.

27. El-Asady R, Yuan R, Liu K, Wang D, Gress RE, Lucas PJ*, et al.* TGF-{beta}-dependent CD103 expression by CD8(+) T cells promotes selective destruction of the host intestinal epithelium during graft-versus-host disease. *The Journal of experimental medicine* 2005, **201**(10)**:** 1647-1657.

28. Mokrani M, Klibi J, Bluteau D, Bismuth G, Mami-Chouaib F. Smad and NFAT pathways cooperate to induce CD103 expression in human CD8 T lymphocytes. *Journal of immunology* 2014, **192**(5)**:** 2471-2479.

29. Yang XO, Panopoulos AD, Nurieva R, Chang SH, Wang D, Watowich SS*, et al.* STAT3 regulates cytokine-mediated generation of inflammatory helper T cells. *The Journal of biological chemistry* 2007, **282**(13)**:** 9358-9363.

30. Davis FM, Azimi I, Faville RA, Peters AA, Jalink K, Putney JW, Jr.*, et al.* Induction of epithelial-mesenchymal transition (EMT) in breast cancer cells is calcium signal dependent. *Oncogene* 2014, **33**(18)**:** 2307-2316.

31. Annacker O, Coombes JL, Malmstrom V, Uhlig HH, Bourne T, Johansson-Lindbom B*, et al.* Essential role for CD103 in the T cell-mediated regulation of experimental colitis. *The Journal of experimental medicine* 2005, **202**(8)**:** 1051-1061.

32. Martinez GJ, Zhang Z, Reynolds JM, Tanaka S, Chung Y, Liu T*, et al.* Smad2 positively regulates the generation of Th17 cells. *The Journal of biological chemistry* 2010, **285**(38)**:** 29039-29043.

33. Gu AD, Wang Y, Lin L, Zhang SS, Wan YY. Requirements of transcription factor Smad-dependent and -independent TGF-beta signaling to control discrete T-cell functions. *Proceedings of the National Academy of Sciences of the United States of America* 2012, **109**(3)**:** 905-910.

34. Biswas PS, Gupta S, Chang E, Song L, Stirzaker RA, Liao JK*, et al.* Phosphorylation of IRF4 by ROCK2 regulates IL-17 and IL-21 production and

the development of autoimmunity in mice. *The Journal of clinical investigation* 2010, **120**(9)**:** 3280-3295.

35. Lu L, Wang J, Zhang F, Chai Y, Brand D, Wang X*, et al.* Role of SMAD and non-SMAD signals in the development of Th17 and regulatory T cells. *Journal of immunology* 2010, **184**(8)**:** 4295-4306.

36. Ichiyama K, Sekiya T, Inoue N, Tamiya T, Kashiwagi I, Kimura A*, et al.* Transcription factor Smad-independent T helper 17 cell induction by transforming-growth factor-beta is mediated by suppression of eomesodermin. *Immunity* 2011, **34**(5)**:** 741-754.

37. Hasan M, Neumann B, Haupeltshofer S, Stahlke S, Fantini MC, Angstwurm K*, et al.* Activation of TGF-beta-induced non-Smad signaling pathways during Th17 differentiation. *Immunology and cell biology* 2015, **93**(7)**:** 662-672.

38. Nyati S, Schinske K, Ray D, Nyati MK, Ross BD, Rehemtulla A. Molecular imaging of TGFbeta-induced Smad2/3 phosphorylation reveals a role for receptor tyrosine kinases in modulating TGFbeta signaling. *Clinical cancer research : an official journal of the American Association for Cancer Research* 2011, **17**(23)**:** 7424-7439.

39. Yoon JH, Sudo K, Kuroda M, Kato M, Lee IK, Han JS*, et al.* Phosphorylation status determines the opposing functions of Smad2/Smad3 as STAT3 cofactors in TH17 differentiation. *Nature communications* 2015, **6:** 7600.

Author contributions

A.R., F.G. and S.Z. designed experiments. A.R., E.R. and T.R-J. performed mice immune-phenotyping, *in vitro* and *in vivo* experiments with contribution by M.Pr. V.V. performed *in vitro* experiments, electrophysiology, imaging and cytokine secretion analysis. S.H. performed electrophysiology, IP and Western Blotting. W.N. performed Western Blotting and imaging. M.Pe. performed gene expression analysis on purified T cell subsets, C.R. performed histological analysis, G.W. performed transmission electron microscopy. M.M. performed the PLA assay and C.H. the ChIP assay under the supervision of S.M. and S.Z. S.G. performed gene expression analysis on stimulated T cells with contribution by V.V. and S.H., and V.C. performed assessments of Ca^{2+} and Mg^{2+} serum levels, provided antibodies and scientific advice. M.M. provided the mouse model. T.G. provided expertise and feedback and revised the manuscript. F.G. and S.Z. supervised the study and wrote the manuscript.

Acknowledgements

We thank Andreas Breit (Walther-Straub-Institute, LMU Munich) for scientific advice, David Jarossay (Institute for Research in Biomedicine) for cell sorting and Jan Weber (Walther-Straub-Institute, LMU Munich) for technical assistance. EM images were acquired at the Imaging Center Essen (IMCES). This work was supported by the European Commission (FP7, ERA.netRUS STProjects-184) to F.G. and S.Z., Fondazione Gelu, Fondazione per la Ricerca sulla Trasfusione

e sui Trapianti and grant 310030_15949 of the Swiss National Science Foundation to F.G. S.Z. was supported by a Marie-Curie Career-Integration-grant (no. 322185). S.Z., V.C. and T.G. were supported by the Deutsche Forschungsgemeinschaft (TRR 152/1).

Competing financial interests

The authors declare no competing financial interests.

Figure Legends

Figure 1 Normal T cell development in *Trpm7*$^{R/R}$ mice but altered cytokine secretion.

(**a**) Total WT or *Trpm7*$^{R/R}$ cell recovery from thymus. (**b**) Representative dot plot analysis of thymocytes from WT or *Trpm7*$^{R/R}$ thymi stained with CD4 and CD8 mAb. Percentages are shown in each gate. (**c**) Dot charts comparing the total number of thymocytes in the double negative (DN), double positive (DP), CD4$^+$, and CD8$^+$ thymocytes are shown (mean ± s.e.m. n=5). (**d**) Representative dot plot analysis of thymocytes gated on DN cells from WT or *Trpm7*$^{R/R}$ thymi stained with CD44 and CD25 mAbs. Percentages are shown in each gate. (**e**) Representative histogram overlay of cell surface *CD25* in WT or *Trpm7*$^{R/R}$ thymocytes. (**f**) Dot charts showing the number of total cells (mean ± s.e.m. n=5) of DN population found in the DN1, DN2, DN3, and DN4 stages. Data are representative results of 2 independent experiments with 5 mice per experiment. (**g**) Basal cytokine levels evaluated in serum of WT (black, n=3-7) and *Trpm7*$^{R/R}$ (grey, n=3-7) mice, respectively, and shown as pg ml^{-1}. Bar charts indicate mean ± s.e.m. A total number of 7 mice were used for each genotype. Note a significant reduction of serum levels of IL-17 and G-CSF in *Trpm7*$^{R/R}$. A two-tailed Student's t-test was used with * $p<0.05$; ** $p<0.01$ and *** $p<0.001$.

Figure 2 Selectively reduced intraepithelial lymphocytes in *Trpm7*$^{R/R}$ mice.

(**a**) Dot plot (left) and statistical analyses (right) of intraepithelial lymphocytes (IEL) from WT or *Trpm7*$^{R/R}$ mice stained as indicated. Percentages are shown in each gate, bar charts show mean percentages ± s.e.m. (WT, n=6; *Trpm7*$^{R/R}$, n=7). (**b**) Dot plot (left) and statistical analyses (right) of LPLs from WT or *Trpm7*$^{R/R}$ mice stained as indicated. Percentages are shown in each gate, bar charts show mean percentages ± s.e.m. (n=7). (**c**) Absolute numbers (WT, n=6; *Trpm7*$^{R/R}$, n=7) of the indicated IELs subsets. Bar charts show mean percentages ± s.e.m. (**d**) Absolute numbers (mean ± s.e.m. n=7) of the indicated LPLs subsets. (**e**) CD3 immunohistochemical staining of small intestine sections of WT or *Trpm7*$^{R/R}$ mice and relative quantification (right). Scale bars indicate 100 μm. (**f**) Dot blots and statistical analyses of MHCII expression in EpCAM$^+$ intestinal epithelial cells (IEC). Percentages are shown in each gate, bar charts show mean percentages ± s.e.m. (n=3). (**g**) Quantitative real-time PCR of *T-bet*, *Foxp3*, *Rorc* and *Il-17a* expression in purified TCR $\alpha\beta^+$CD4$^+$ IELs from WT or *Trpm7*$^{R/R}$ mice. (**h**) Dot plot and statistical analyses of IFN-γ and IL-17A staining in WT or *Trpm7*$^{R/R}$ TCR $\alpha\beta^+$CD4$^+$ IELs. Percentages are shown in each gate, bar charts show mean percentages ± s.e.m. (WT, n=5; *Trpm7*$^{R/R}$, n=8). Data are representative results of at least 3 independent experiments. A two-tailed Student's t-test was used with * $p<0.05$; ** $p<0.01$ and *** $p<0.001$.

Figure 3 *Trpm7*$^{R/R}$ mutation affects $\alpha_E\beta_7$ expression in T cells.

(**a**) Representative histogram overlay of cell surface CD103, β_7 and $\alpha_4\beta_7$ expression of intraepithelial lymphocytes (IEL, left) and relative statistical analysis (right). Percentages are shown in each gate, bar charts show mean percentages ± s.e.m. (n=4). (**b**) Representative histogram overlay of cell surface CD103, β_7 and $\alpha_4\beta_7$ expression of lamina propria lymphocytes (LPL, left) and relative statistical analysis (right). Percentages are shown in each gate, bar charts show mean percentages ± s.e.m. (n=4). (**c**) Surface CD103, β_7, and $\alpha_4\beta_7$ expression in IELs, bar charts show Mean Fluorescence Intensity ± s.e.m. (n=5). (**d**) Surface CD103, β_7 and $\alpha_4\beta_7$ expression of LPLs, bar charts show Mean Fluorescence Intensity ± s.e.m. (n=5). (**e**) Quantitative real-time PCR of *Itgae* expression in purified TCR $\alpha\beta^+$CD4$^+$ lymphocytes from spleen (SPL), lamina propria (LPL) or intraepithelium (IEL). Data are representative results of at least 3

independent experiments. A two-tailed Student's t-test was used with * p<0.05; ** p<0.01 and *** p<0.001.

Figure 4 TRPM7 kinase dead T cell autonomous defect in *in vivo* CD103 expression and intraepithelial localization.

(**a**) Transmission electron microscopic (TEM) images of small intestine (upper panel) and colon (lower panel) sections from WT or *Trpm7*$^{R/R}$ mice. Note no changes in tight junction, adherens junction or desmosome formation between the two genotypes. Scale bars indicate 500 nm and 200 nm, respectively. (**b**) Dot plot (left) and statistical analyses (right) of CD11c^{+}MHCII^{+} DC and relative CD103 expression. Percentages are shown in each gate, bar charts show mean percentages ± s.e.m. (n=3). (**c**) Quantitative real-time PCR of *Tgf-β1*, *Tgf-β2* and *Tgf-β3* expression in WT or *Trpm7*$^{R/R}$ purified CD11c^{+}MHCII^{+} DC cells (left) or in EpCAM^{+} IEC (right). (**d**) TGF-β 1 and TGF-β 2 levels measured in serum harvested from WT or *Trpm7*$^{R/R}$ mice (n=4). Data are shown as mean ± s.e.m. (**e**) Dot plot and statistical analyses of spleen (SPL), lamina propria (LPL) and intraepithelial (IEL) TCRαβ^{+} CD4^{+} lymphocytes from *Rag1*$^{-/-}$/*Il2rg*$^{-/-}$ mice reconstituted with purified WT or *Trpm7*$^{R/R}$ naïve CD4 cells. (**f**) Cells were gated for surface CD4 and TCRαβ and were analyzed for CD103 expression. Percentages are shown in each gate, bar charts show mean percentages ± s.e.m. (n=4). (**g**) Dot plots and statistical analyses of MHCII expression in EpCAM^{+} intestinal epithelial cells (IEC) from *Rag1*$^{-/-}$/*Il2rg*$^{-/-}$ mice reconstituted with purified WT or *Trpm7*$^{R/R}$ naïve T cells. Percentages are shown in each gate, bar charts show mean percentages ± s.e.m. (n=4). Data are representative results of at least 3 independent experiments. A two-tailed Student's t-test was used with * p<0.05; ** p<0.01 and *** p<0.001.

Figure 5 *Trpm7*$^{R/R}$ T cells have autonomous defect in *in vitro* Th17 polarization and CD103 up-regulation.

(**a**) Representative dot plots and statistical analyses of IFN-γ, IL-17A, CD25 and FOXP3 expression in stimulated naïve T cells under Th1, T_{reg} or Th17-polarizing conditions after 5 days of *in vitro* culture. Percentages are shown in each gate, bar charts show mean percentages ± s.e.m. (n = 4) (**b**) Quantitative real-time PCR of T-bet, IFN-γ, Rorc, and IL-17A expression in naïve T cells stimulated under Th1 or Th17-polarizing conditions after 5 days of culture *in vitro*. (n = 3) (**c**) Western Blot analysis of STAT3 phosphorylation (Tyr705) of control and IL-6 treated WT and *Trpm7*$^{R/R}$ (*R/R*) naïve T cells, respectively. Blots are representatives of at least 3 independent experiments. (**d**) Histogram overlays and statistical analyses of CD103 and β7 staining by flow cytometry in WT or *Trpm7*$^{R/R}$ naïve T cells stimulated with anti-CD3ε/anti-CD28 in the absence or presence of TGF-β (10 ng ml^{-1}) for 4 d. Histograms show Mean Fluorescence Intensity (MFI) ± s.e.m. (n=4). Data are representative results of at least 3 independent experiments. (**e**) Quantitative real-time PCR of *Itgae* (CD103) in control (CTRL) and WT or *Trpm7*$^{R/R}$ naïve T cells stimulated with anti-CD3ε/anti-CD28 in the presence of TGF-β (5 ng ml^{-1}) for 24 h. Data are shown as $2^{-\Delta\Delta CP}$ ± s.e.m. (n=3). (**f**) Western Blot and statistical analysis of SMAD2 (Ser465/467) and SMAD3 (Ser423/425) phosphorylation. Blots are representatives of at least 4 independent experiments. The semi-quantitative analysis was done via ImageJ software and plotted as percent increase in intensity of pSMAD/total SMAD compared to control. Bar charts show mean percentages ± s.e.m. for SMAD2 and SMAD3 (n=4-5). A two-tailed Student's t-test was used with * p<0.05; ** p<0.01 and *** p<0.001. To demonstrate a significant increase in TGF-β-induced SMAD phosphorylation compared to untreated controls a one-way ANOVA was used with # p<0.05.

Figure 6 TRPM7 kinase affects SMAD2 translocation via direct phosphorylation.

(**a**) Analysis of pSMAD2 translocation into the nucleus. WT and *Trpm7*$^{R/R}$ naïve CD4^{+} T cells were co-stimulated with αCD3/αCD28 and 5 ng ml^{-1} TGF-β1 for 10 min. Representative Western Blot images depicting that pSMAD2 and total SMAD2 in the nuclear fraction (right panel) were strongly reduced in *Trpm7*$^{R/R}$ T cells compared to WT. In the respective cytosolic fraction (left panel) the pSMAD2 was not detectable, however amounts of total SMAD2 were comparable between *Trpm7*$^{R/R}$ and WT. (**b**) Concentration dependent phosphorylation of human recombinant SMAD2-GST by TRPM7 kinase. Data have been obtained via RBC hotspot *in vitro* kinase assay using 4 μM ATP and 4 μM substrate at 2 h. RBC standard substrate was used as a positive control, substrate alone as a negative control and kinase activity alone was subtracted as background. Data have been converted to nM substrate phosphorylation and are plotted as mean ± s.e.m. Truncated recombinant SMAD2 (trun. SMAD2-GST) as well as the GST-tag alone were not phosphorylated, suggesting specific phosphorylation of SMAD2 at the c-terminal SXS motif. (**c**) Analysis of interaction between SMAD2 and TRPM7 in CD4^{+} T cells via Proximity Ligation Assay (PLA). Scale bar indicates 10 μm. Note a significant increase in SMAD2 co-localization with TRPM7 in WT T cells treated with 5 ng ml^{-1} TGF-β1 (#### p<0.0001; two-tailed Student's t-test). *Trpm7*$^{R/R}$ T cells fail to recruit SMAD2 into close proximity to the TRPM7 kinase upon TGF-β1 stimulation compared to WT (**** p<0.0001; two-tailed Student's t-test). Bar graphs show mean PLA signals per cell counted in five fields of vision ± s.e.m. (**d**) ChIP assay was performed in untreated and TGF-β1 (5 ng ml^{-1}) stimulated CD4^{+} T cells using a specific antibody against SMAD2 for immunoprecipitation. Primers for *Itgae* and *Gapdh* were used for qRT-PCR; *Gapdh* was used for normalization. Note a significant increase in -fold enrichment in TGF-β1-treated WT T cells compared to untreated controls (#, p<0.05, one-way ANOVA) as well as a reduction in -fold enrichment of TGF-β1-treated *Trpm7*$^{R/R}$ T cells compared to WT (* p<0.05, one-way ANOVA). Bar graphs show mean ± s.e.m.

Figure 7 TRPM7 kinase activity promotes destruction of the host intestinal epithelium by T cells during GVHD.

(**a**) Representative picture of colon specimens at day 25 after BMT in recipients of WT or *Trpm7*$^{R/R}$ splenocytes or (CTRL) bone marrow cells alone (left) and relative statistical analyses showing colon length (right). Bars represent mean ± s.e.m. (n=5) (**b**) Survival of lethally irradiated BALB/c recipients of C57BL/6J bone marrow cells (BMC) alone (Ctrl, triangle, dashed line) or in combination with WT (black circles) or *Trpm7*$^{R/R}$ (*R*/*R*, grey squares) splenocytes (n=10). (**c**) Dot plot and statistical analyses of TCR $\alpha\ \beta^{+}$H-2^{b+} IELs cells from BALB/c mice reconstituted with WT or *Trpm7*$^{R/R}$ splenocytes. Percentages are shown in each gate, bar charts show mean percentages ± s.e.m. (n=3). (**d**) Dot plot and statistical analyses of MHCII expression in EpCAM^{+} IEC from BALB/c mice reconstituted with WT or *Trpm7*$^{R/R}$ splenocytes. Percentages are shown in each gate, bar charts show mean percentages ± s.e.m. (n=3). (**e**) Dot plot and statistical analyses of CD103 and β7 expression in electronically gated H-2^{b+}TCR $\alpha\ \beta^{+}$CD4^{+} or H-2^{b+}TCR $\alpha\ \beta^{+}$CD8^{+} IELs. Percentages are shown within each gate, bar charts show mean percentages ± s.e.m. (n=3).

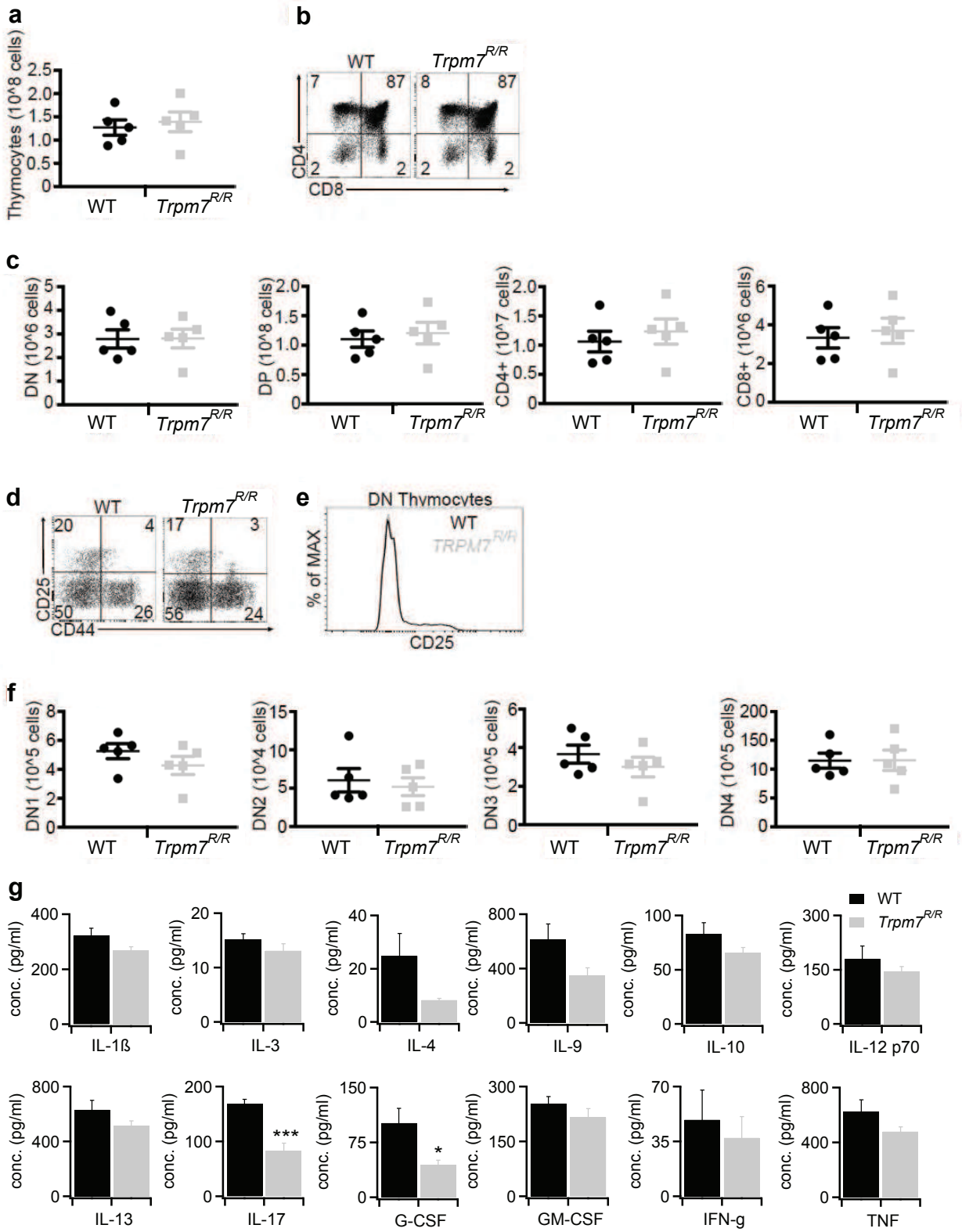
a
Thymocytes (10^8 cells)
WT
Trpm7R/R
b
WT
Trpm7R/R
CD4
CD8
c
DN (10^6 cells)
DP (10^8 cells)
CD4+ (10^7 cells)
CD8+ (10^6 cells)
d
CD25
CD44
e
DN Thymocytes
% of MAX
CD25
f
DN1 (10^5 cells)
DN2 (10^4 cells)
DN3 (10^5 cells)
DN4 (10^5 cells)
g
conc. (pg/ml)
IL-1ß
IL-3
IL-4
IL-9
IL-10
IL-12 p70
IL-13
IL-17
G-CSF
GM-CSF
IFN-g
TNF

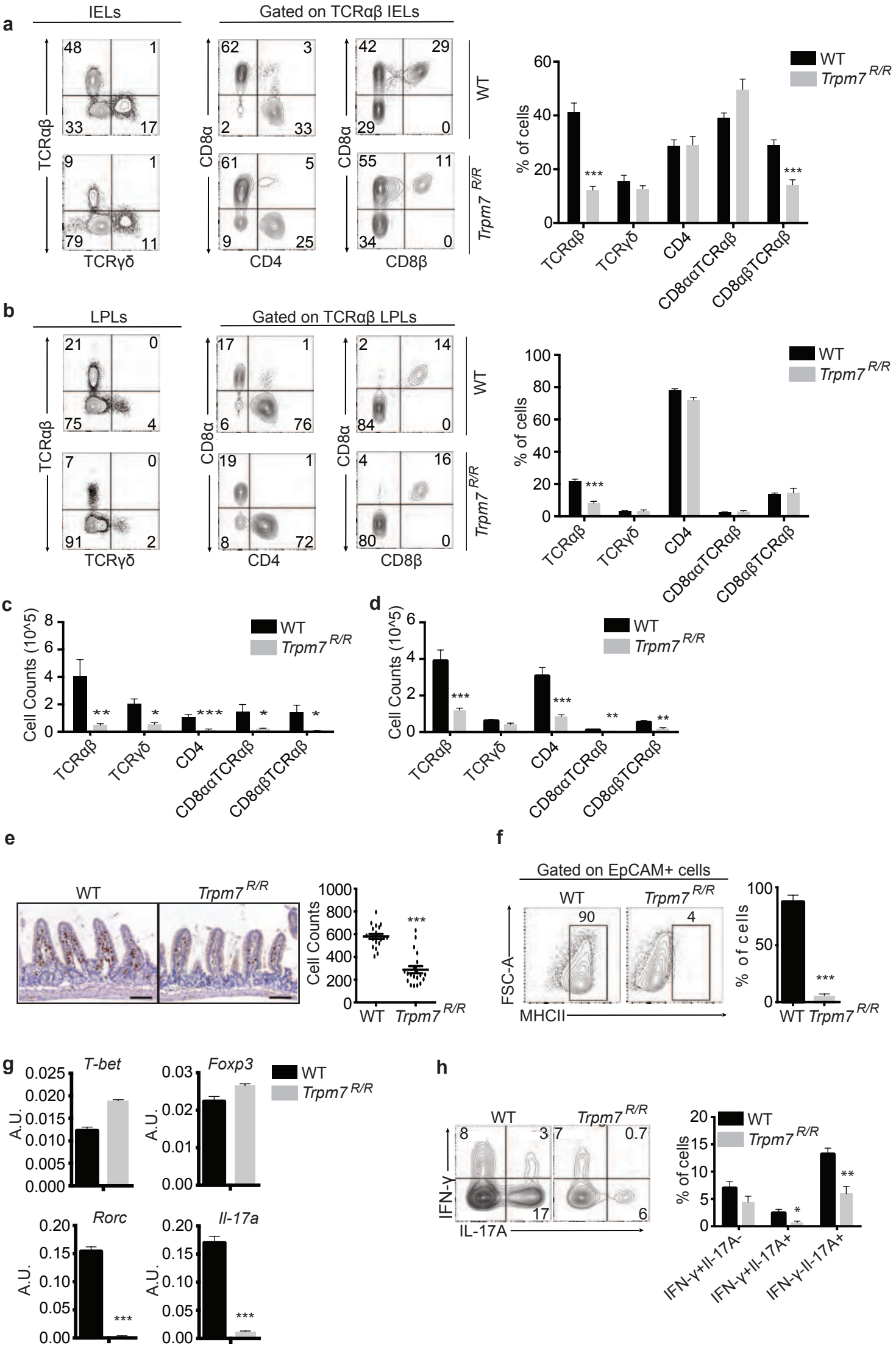
a
IELs
Gated on TCRαβ IELs
TCRαβ
TCRγδ
CD8α
CD4
CD8β
WT
Trpm7 R/R
% of cells
TCRαβ
TCRγδ
CD4
CD8αα TCRαβ
CD8αβ TCRαβ
b
LPLs
Gated on TCRαβ LPLs
c
Cell Counts (10^5)
d
e
WT
Trpm7 R/R
Cell Counts
f
Gated on EpCAM+ cells
FSC-A
MHCII
% of cells
g
T-bet
Foxp3
Rorc
Il-17a
A.U.
h
IFN-γ
IL-17A
IFN-γ+Il-17A-
IFN-γ+Il-17A+
IFN-γ-Il-17A+

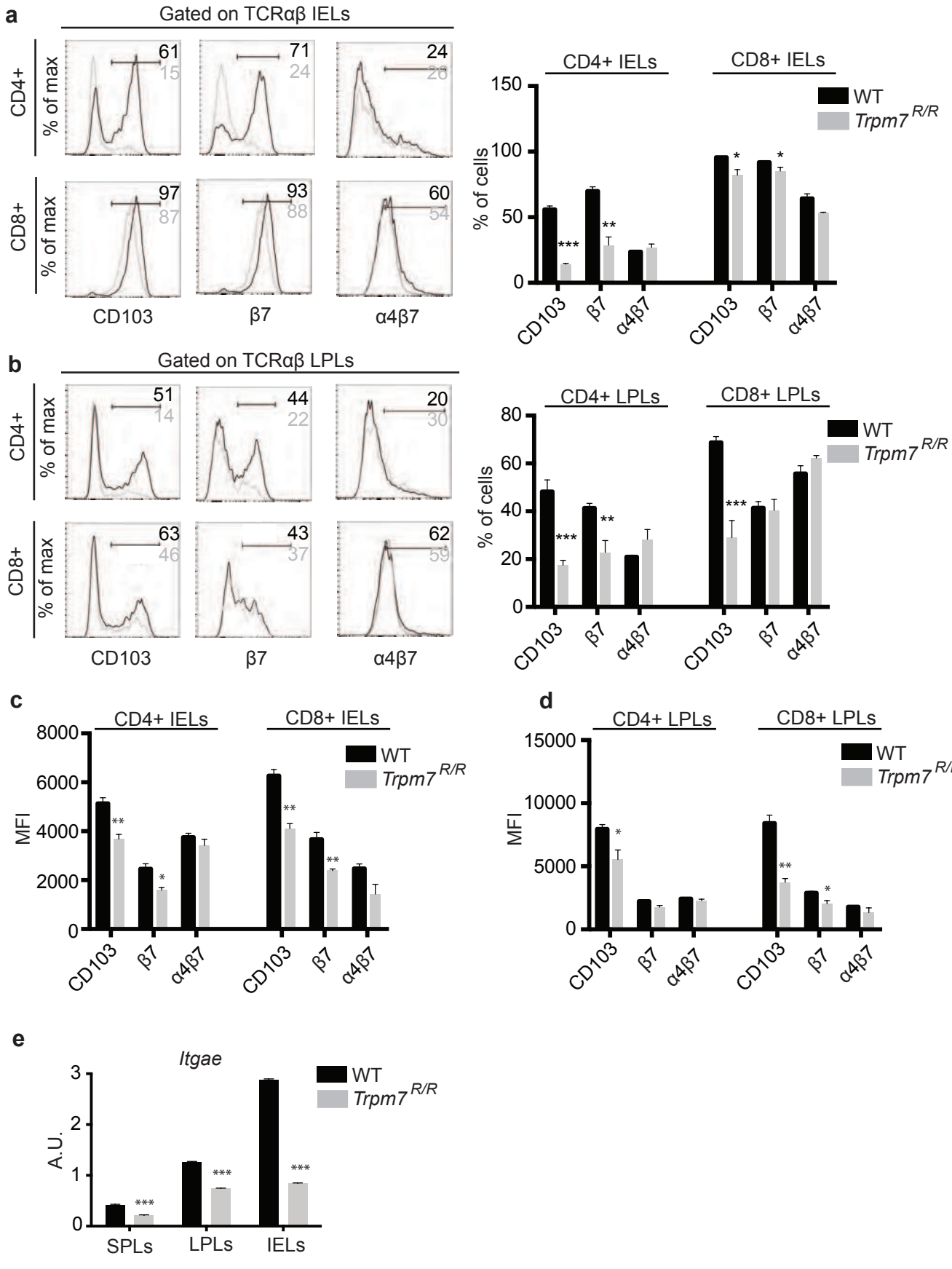
a
Gated on TCRαβ IELs
CD4+
CD8+
% of max
61
15
71
24
24
28
97
87
93
88
60
54
CD103
β7
α4β7
CD4+ IELs
CD8+ IELs
WT
Trpm7 R/R
% of cells
150
100
50
0
b
Gated on TCRαβ LPLs
51
14
44
22
20
30
63
46
43
37
62
59
CD4+ LPLs
CD8+ LPLs
c
CD4+ IELs
CD8+ IELs
MFI
8000
6000
4000
2000
0
d
CD4+ LPLs
CD8+ LPLs
15000
10000
5000
e
Itgae
A.U.
3
2
1
SPLs
LPLs
IELs

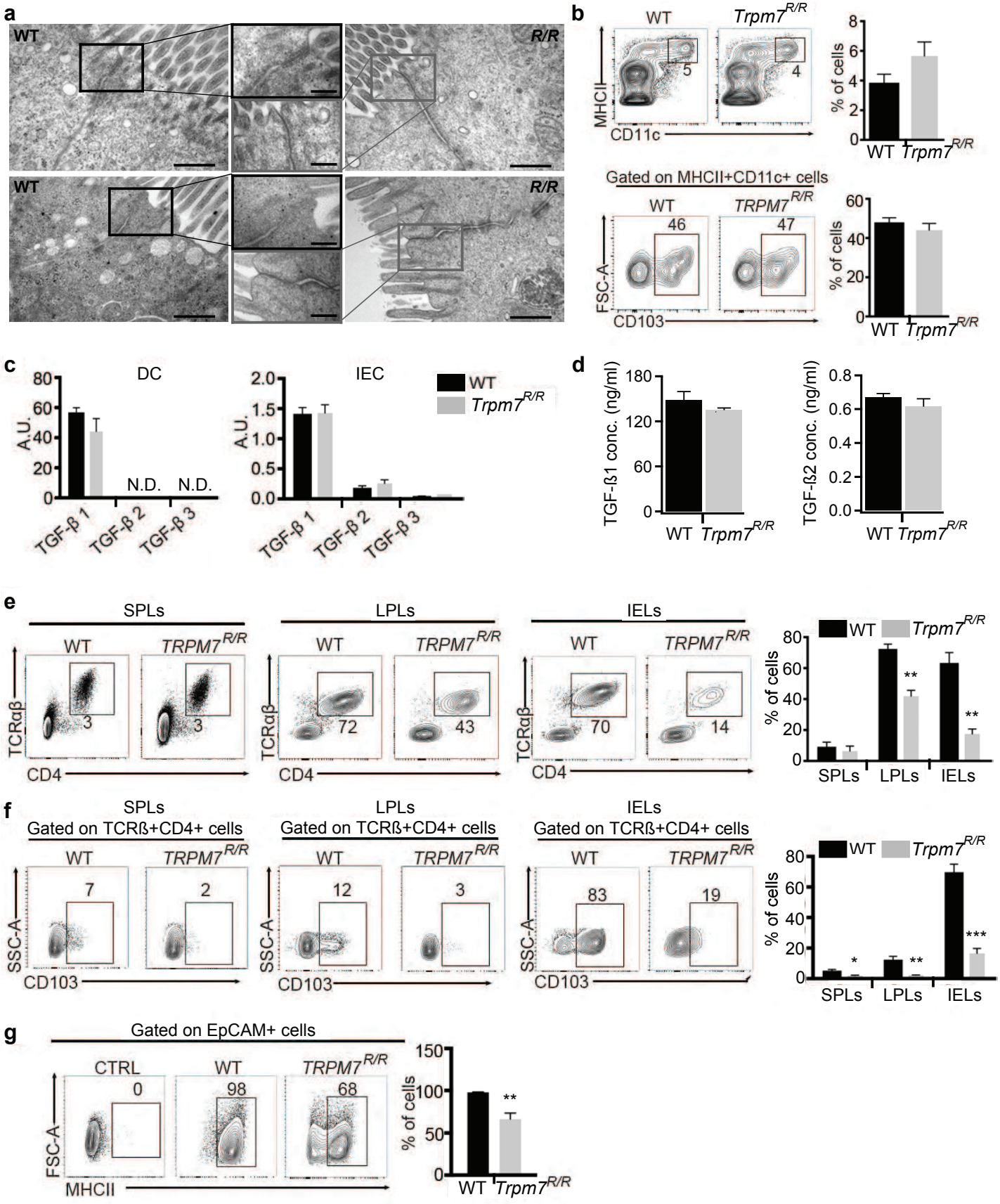
a
WT
R/R
WT
R/R
b
WT
Trpm7R/R
MHCII
CD11c
5
4
% of cells
WT Trpm7R/R
Gated on MHCII+CD11c+ cells
WT
TRPM7R/R
46
47
FSC-A
CD103
% of cells
WT Trpm7R/R
c
DC
IEC
WT
Trpm7R/R
A.U.
N.D.
N.D.
TGF-β 1
TGF-β 2
TGF-β 3
d
TGF-ß1 conc. (ng/ml)
TGF-ß2 conc. (ng/ml)
WT Trpm7R/R
e
SPLs
LPLs
IELs
WT
TRPM7R/R
TCRαβ
CD4
3
3
72
43
70
14
% of cells
WT
Trpm7R/R
SPLs
LPLs
IELs
f
SPLs
LPLs
IELs
Gated on TCRß+CD4+ cells
WT
TRPM7R/R
SSC-A
CD103
7
2
12
3
83
19
% of cells
WT
Trpm7R/R
SPLs
LPLs
IELs
g
Gated on EpCAM+ cells
CTRL
WT
TRPM7R/R
0
98
68
FSC-A
MHCII
% of cells
WT Trpm7R/R

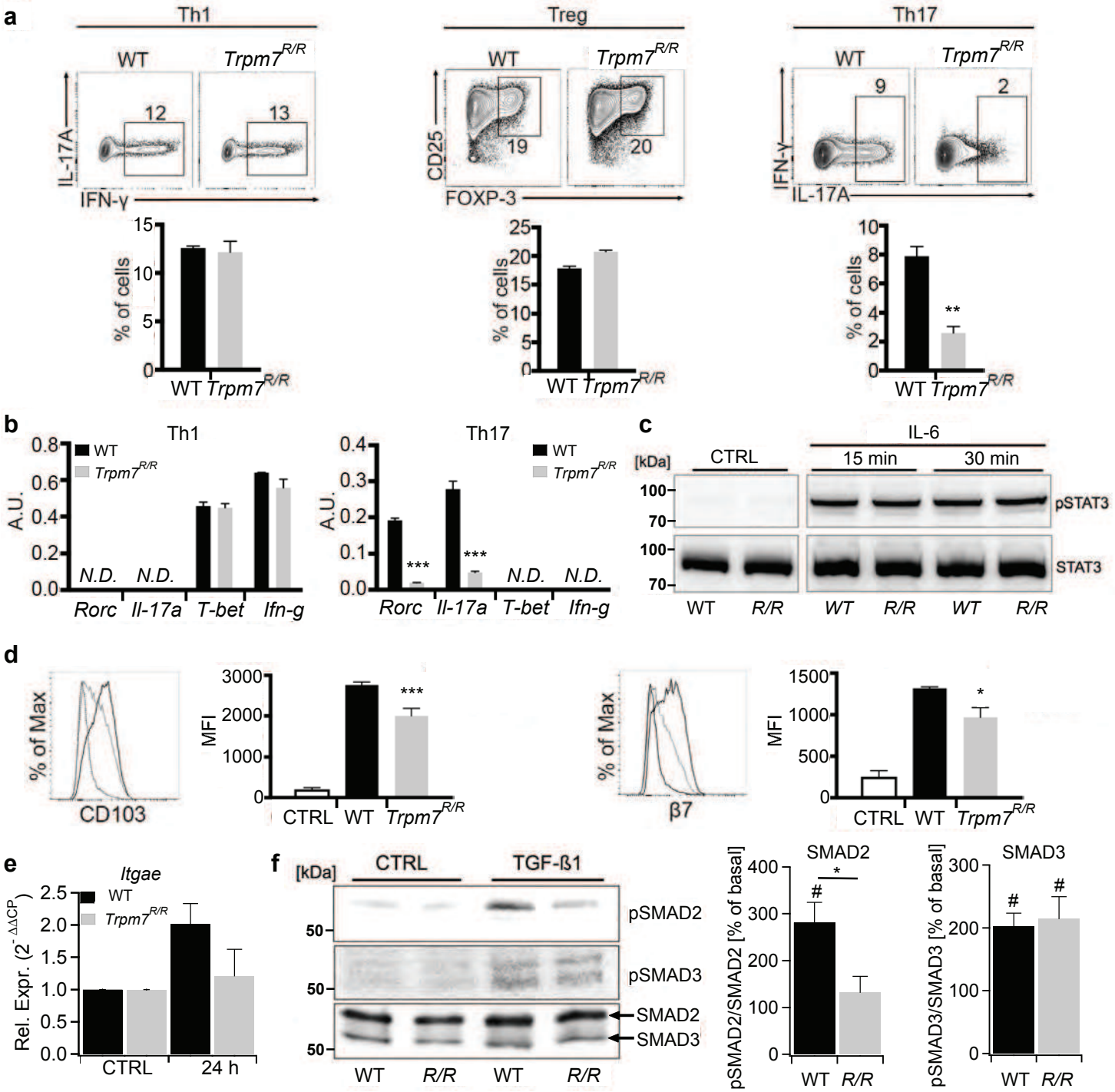
a
Th1
Treg
Th17
WT
Trpm7R/R
IL-17A
IFN-γ
CD25
FOXP-3
% of cells
WT Trpm7R/R
b
Th1
Th17
A.U.
N.D.
Rorc
Il-17a
T-bet
Ifn-g
c
IL-6
CTRL
15 min
30 min
[kDa]
pSTAT3
STAT3
d
% of Max
CD103
β7
MFI
CTRL
e
Itgae
Rel. Expr. (2-ΔΔCP)
24 h
f
TGF-ß1
pSMAD2
pSMAD3
SMAD2
SMAD3
pSMAD2/SMAD2 [% of basal]
pSMAD3/SMAD3 [% of basal]

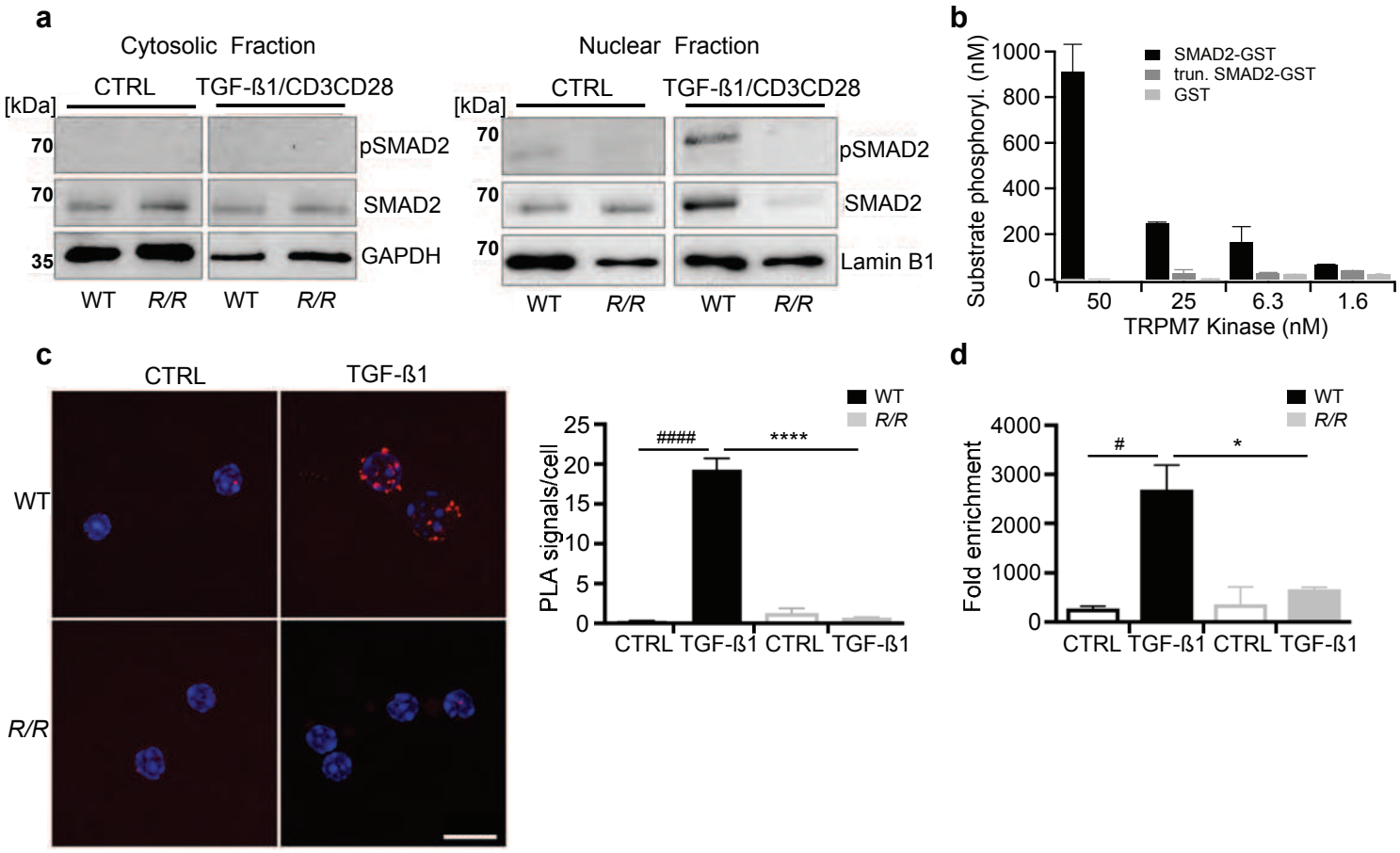
a
Cytosolic Fraction
Nuclear Fraction
CTRL
TGF-ß1/CD3CD28
[kDa]
70
pSMAD2
SMAD2
35
GAPDH
Lamin B1
WT
R/R
b
Substrate phosphoryl. (nM)
SMAD2-GST
trun. SMAD2-GST
GST
TRPM7 Kinase (nM)
c
CTRL
TGF-ß1
PLA signals/cell
####
****
d
Fold enrichment
#
*

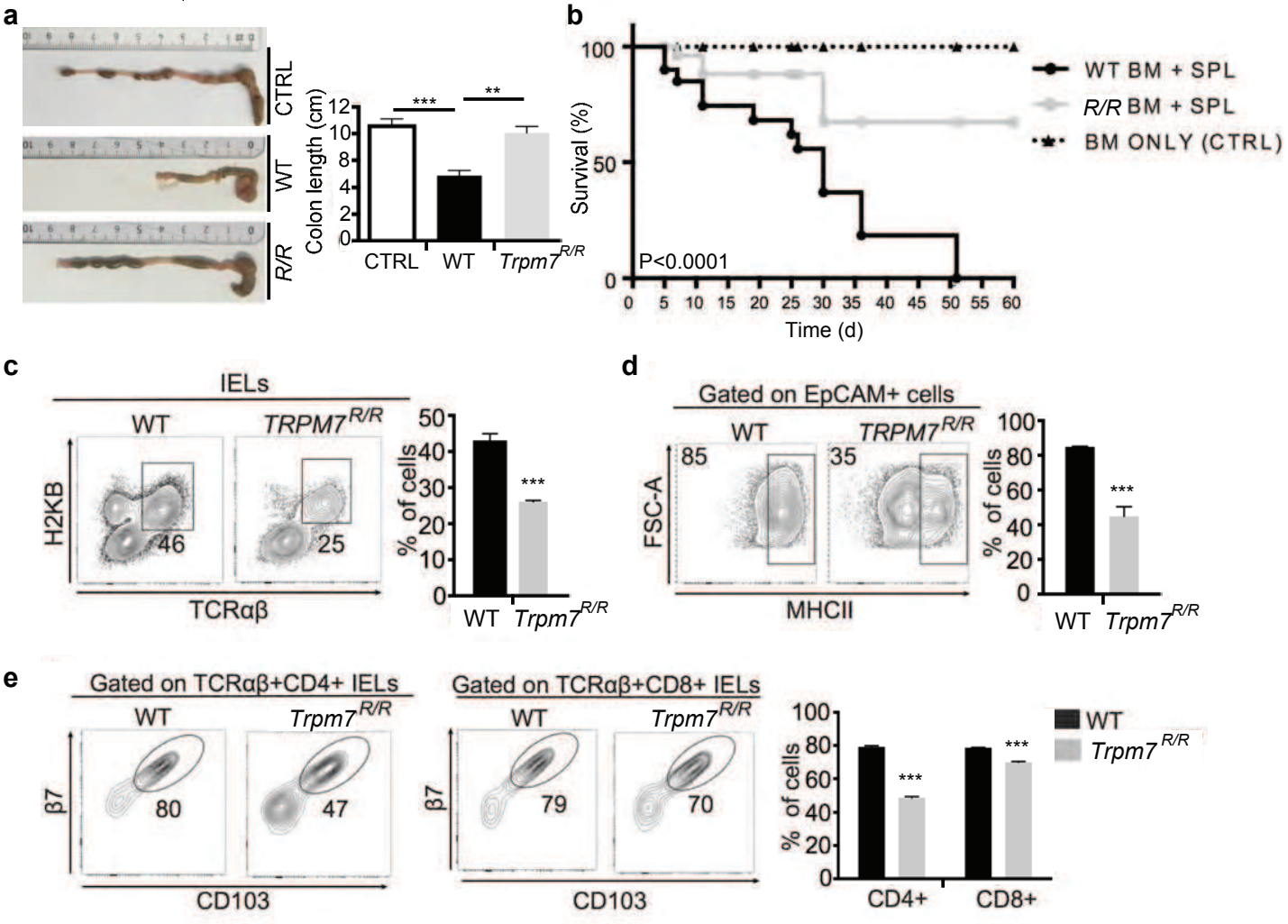
a
CTRL
WT
R/R
Colon length (cm)
***
**
CTRL
WT
Trpm7R/R
b
Survival (%)
P<0.0001
Time (d)
WT BM + SPL
R/R BM + SPL
BM ONLY (CTRL)
c
IELs
WT
TRPM7R/R
H2KB
TCRαβ
46
25
% of cells
***
WT
Trpm7R/R
d
Gated on EpCAM+ cells
WT
TRPM7R/R
FSC-A
MHCII
85
35
% of cells
***
WT
Trpm7R/R
e
Gated on TCRαβ+CD4+ IELs
Gated on TCRαβ+CD8+ IELs
WT
Trpm7R/R
β7
CD103
80
47
79
70
% of cells
***
***
CD4+
CD8+
WT
Trpm7R/R

Supplementary Information

Supplementary Figures and Figure Legends
Supplementary Western Blot Images
Supplementary Table

Supplementary Figures and Figure Legends

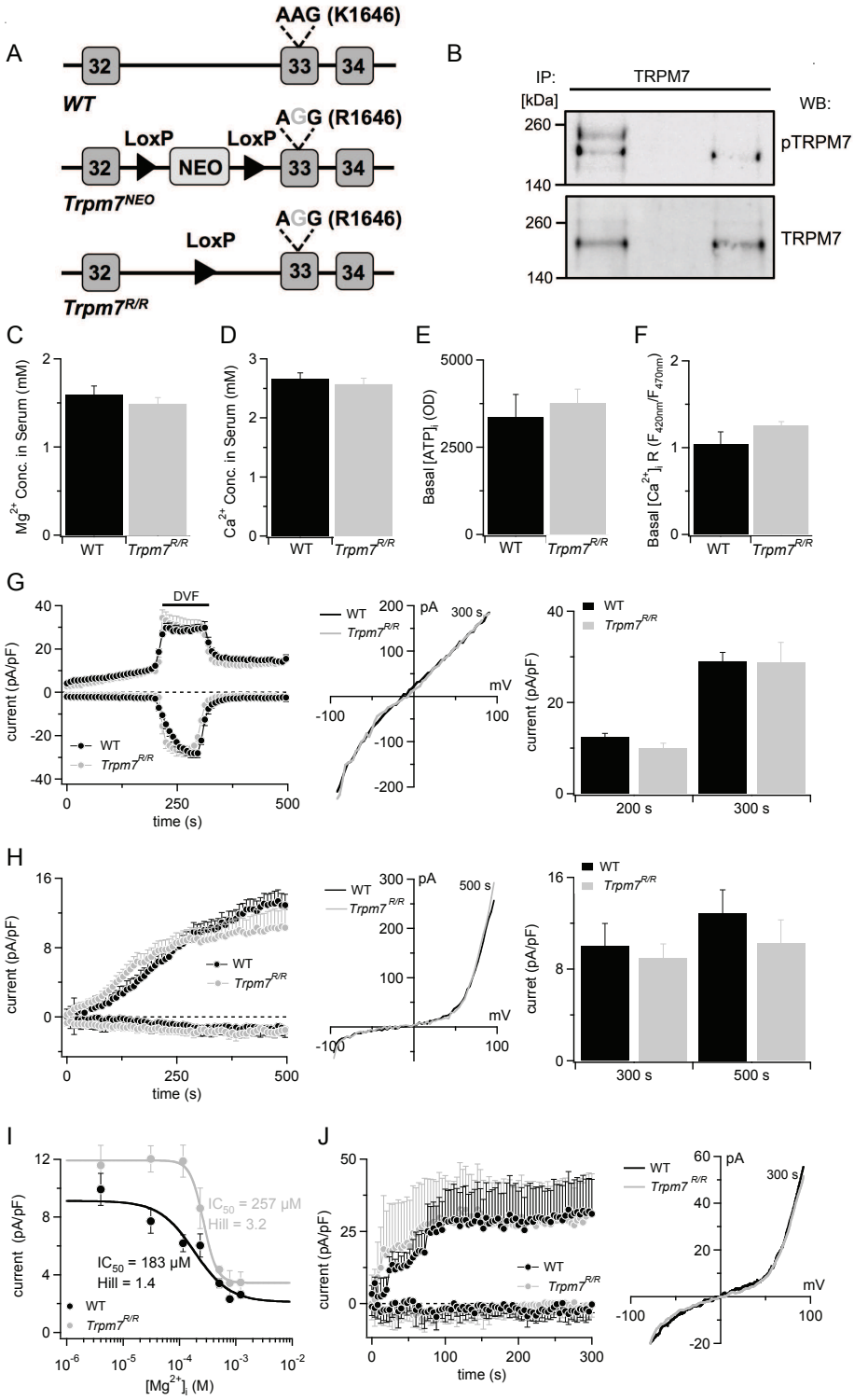

Supplementary Figure 1

Phenotype of *Trpm7*$^{R/R}$ mutant mice (**a**) Targeting strategy for the generation of *Trpm7*$^{R/R}$ mutant mice. (**b**) Immuno-precipitation (IP) and Western Blot (WB) analysis of primary splenocytes isolated from WT or *Trpm7*$^{R/R}$ mice, respectively. (**c,d**) Mg^{2+} and Ca^{2+} concentrations in WT and *Trpm7*$^{R/R}$ sera. Ions in the serum of individual mice were measured with inductively coupled plasma mass spectrometry (ICP-MS). Data are shown as average concentrations in mM (WT: black, Mg: n = 7, Ca: n = 13 and *Trpm7*$^{R/R}$: grey, Mg: n = 8, Ca: n = 14). Error bars indicate s.e.m. (**e**) Bar graph showing averages of luciferase luminescence detecting ATP levels in cell lysates of $CD4^+$ T cells. Averages of

WT (black, n = 4) and *Trpm7*$^{R/R}$ (grey, n = 4) are shown and error bars indicate s.e.m. (**f**) Bar graphs comparing average Fura-Red ratios of WT (black, n = 28) and *Trpm7*$^{R/R}$ (grey, n = 31) CD4^{+} T cells indicating cellular, free Ca^{2+} concentrations at rest. Error bars indicate s.e.m. (G-J) Electrophysiological characterization of TRPM7 in WT and *Trpm7*$^{R/R}$ derived immune cells. Whole-cell currents were recorded in freshly isolated primary peritoneal mast cells, or CD4^{+} T lymphocytes. Voltage ramps were elicited from −100 to +100 mV over 50 ms, acquired at 0.5 Hz and recorded at an interval of 2 s. TRPM7 current amplitudes were assessed at +80 mV for outward currents and at -80 mV for inward currents, averaged and normalized to cell size (pF). Error bars indicate s.e.m. (**g**) Whole-cell patch clamp analysis of TRPM7 current development in WT (black, n = 6) and *Trpm7*$^{R/R}$ (grey, n = 8) mast cells. In the left panel the current densities at +80 and -80 mV are plotted versus time of the experiment in seconds (s). Representative current-voltage relationships extracted at 500 seconds of WT (black) and *Trpm7*$^{R/R}$ (grey) cells are shown in the middle panel. Bar graphs of current densities at +80 mV extracted at 300 and 500 seconds (right panel). Measurements have been conducted in absence of extracellular and intracellular Mg^{2+} to elicit maximal TRPM7 currents. (**h**) To estimate functional channel expression, we perfused WT (black, n = 12) and *Trpm7*$^{R/R}$ (grey, n = 9) mast cells with divalent-free solution (DVF, left panel). Current densities were plotted *versus* time of the experiment. Representative current-voltage relationships extracted at 300 s (middle panel). Bar graphs of mean current densities at +80mV extracted at 200 s and 300 s. WT (black, n = 5-12) and *Trpm7*$^{R/R}$ (grey, n = 6-12). (**i**) Mg^{2+}-dose-response curve of outward current densities plotted against different $[Mg^{2+}]_i$ concentrations. (**j**) Experiments and analysis were performed as in (**g,h**), using, WT (black, n = 5) and *Trpm7*$^{R/R}$ (grey, n = 5) primary, murine CD4^{+} T cells.

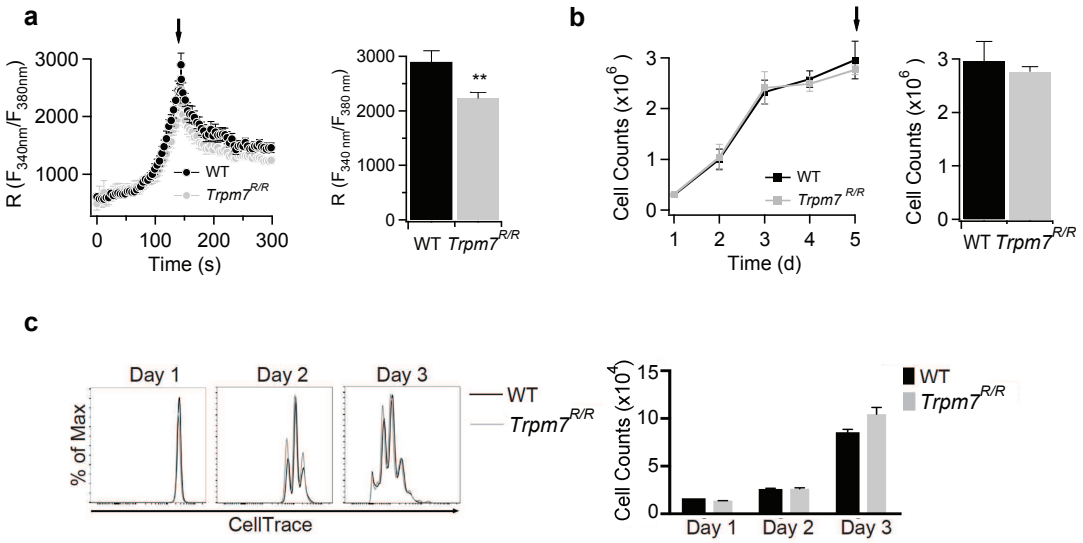

Supplementary Figure 2

Ca^{2+} signaling and proliferation of $CD4^+$ T cells. (**a**) Ratiometric Ca^{2+} measurements of WT (black, n = 28) and *Trpm7*$^{R/R}$ (grey, n = 31) $CD4^+$ T cells stimulated with αCD3/αCD28 were plotted over time (s). In total 3 WT and 3 *Trpm7*$^{R/R}$ mice were used. A bar graph extracted at 150 s shows mean values ± s.e.m. (right panel). (**b**) T cell proliferation shown in cell numbers plotted *versus* time (days). $CD4^+$ T cells isolated from WT (black, n = 3-4) and *Trpm7*$^{R/R}$ (grey, n = 3-4) were stimulated with αCD3/αCD28 antibodies. A total number of 5 animals were used each. In the right panel data at day 5 are shown as average cell numbers ± s.e.m. (**c**) Representative overlay (left) showing the CellTrace profile of WT or *Trpm7*$^{R/R}$ naïve T cells stimulated for 3 days with αCD3/αCD28 and statistical analysis (right) of the total number of recovered cells at the indicated day. Data are representative results of at least 3 independent experiments. * p<0.05; ** p<0.01 and *** p<0.001.

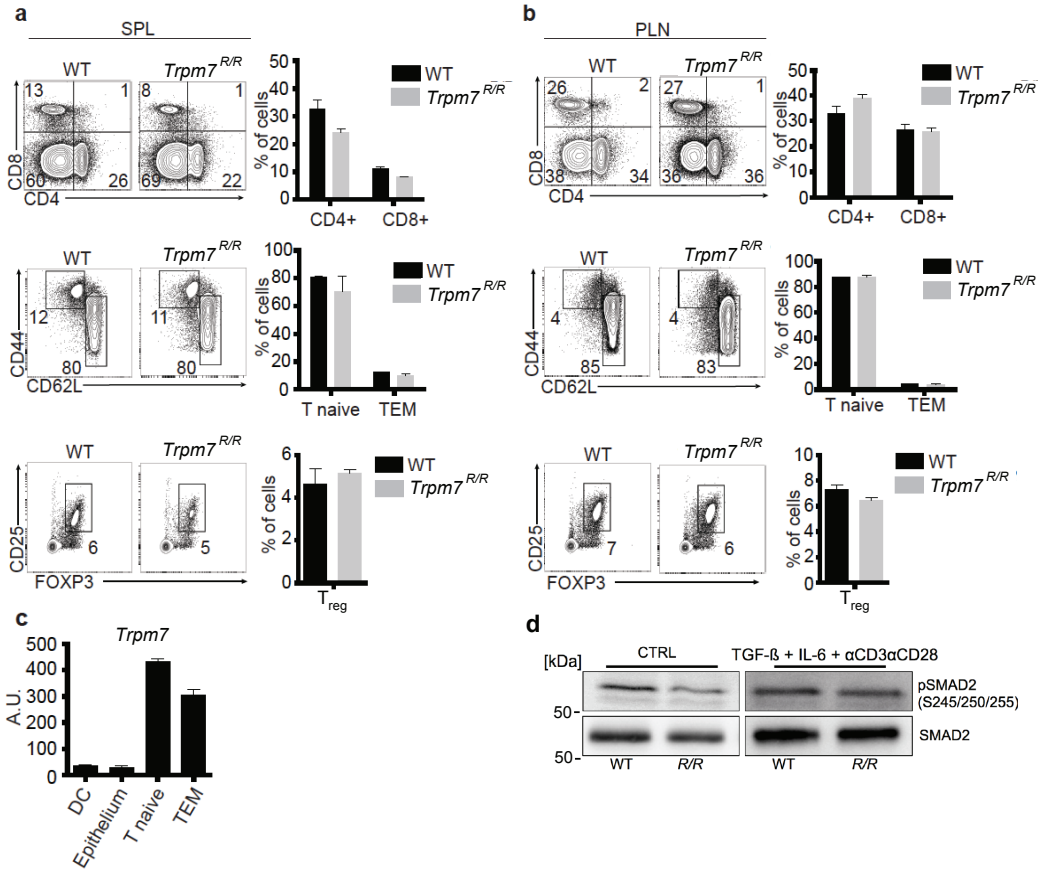

Supplementary Figure 3

Lymphocyte distribution in peripheral lymphoid organs and TRPM7 expression. (**a**) Dot plot and statistical analyses of lymphocytes derived from spleen (SPL) of WT or *Trpm7*$^{R/R}$ mice stained as indicated. Percentages are shown in each gate, histograms show mean percentages ± s.e.m. (WT, n=5; *Trpm7*$^{R/R}$, n=5). (**b**) Dot plot and statistical analyses of lymphocytes from peripheral lymph nodes (PLN) of WT or *Trpm7*$^{R/R}$ mice stained as indicated. Percentages are shown in each gate, histograms show mean percentages ± s.e.m. (WT, n=5; *Trpm7*$^{R/R}$, n=5). Data are representative results of at least 3 independent experiments. (**c**) Quantitative real-time PCR of TRPM7 expression in WT purified CD11c^{+}MHCII^{+} dendritic cells (DC), EpCAM^{+} epithelial cells (EC), naïve T cells as well as effector memory T cells (TEM) (n=3). Note that T cells express substantially more TRPM7 transcripts compared to DC or EC. (**d**) Representative Western Blot analysis of SMAD2 phosphorylation at the linker region (Ser245/250/255) induced via co-stimulation of naïve T cells with 5 ng ml^{-1} TGF-β1, 10 ng ml^{-1} IL-6 and αCD3/αCD28 for 10 min.

Supplementary Full Blots

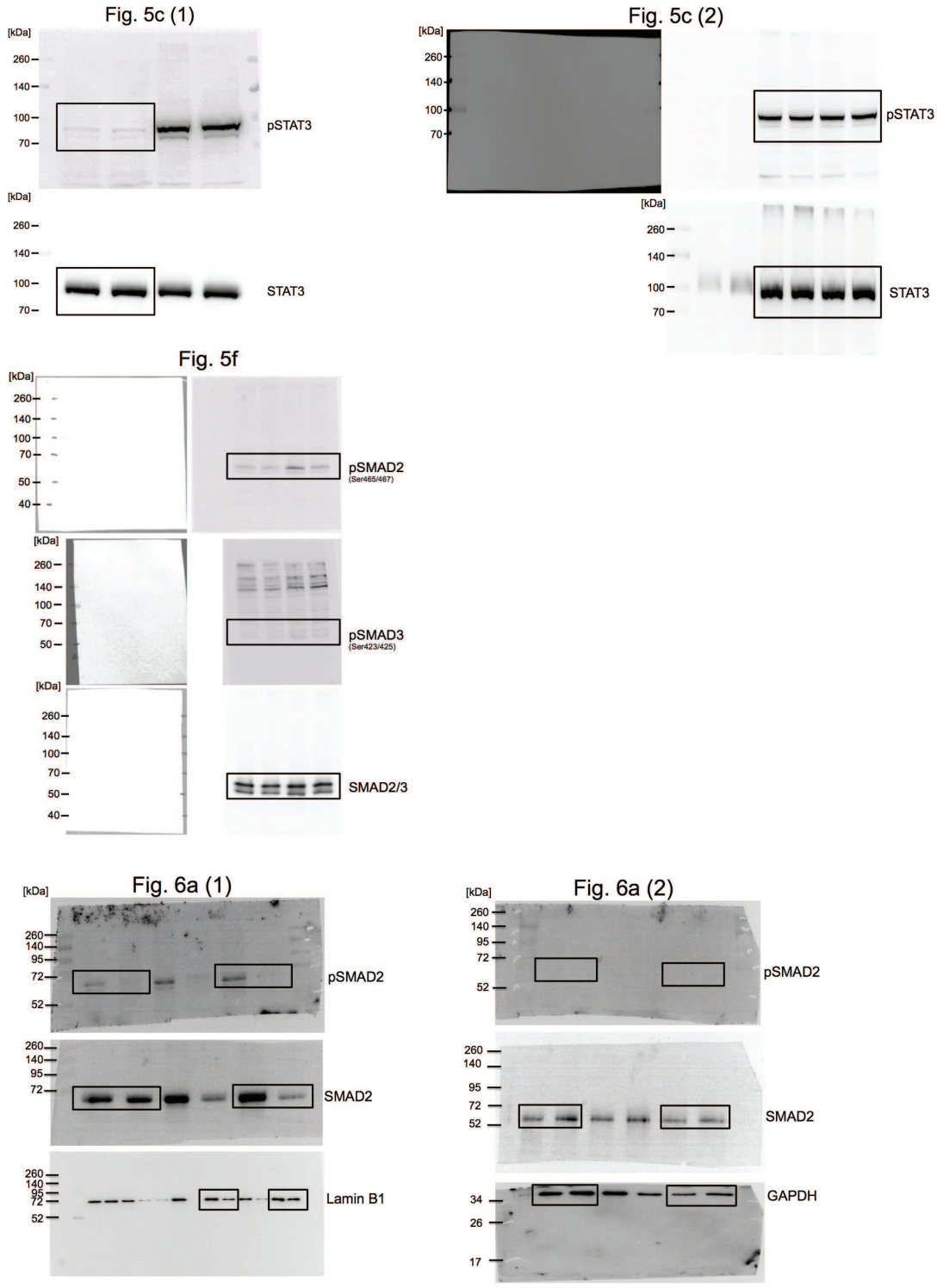

Supplementary Figure 4
Original data of immunoblots of Figures 3, 5 and 6.

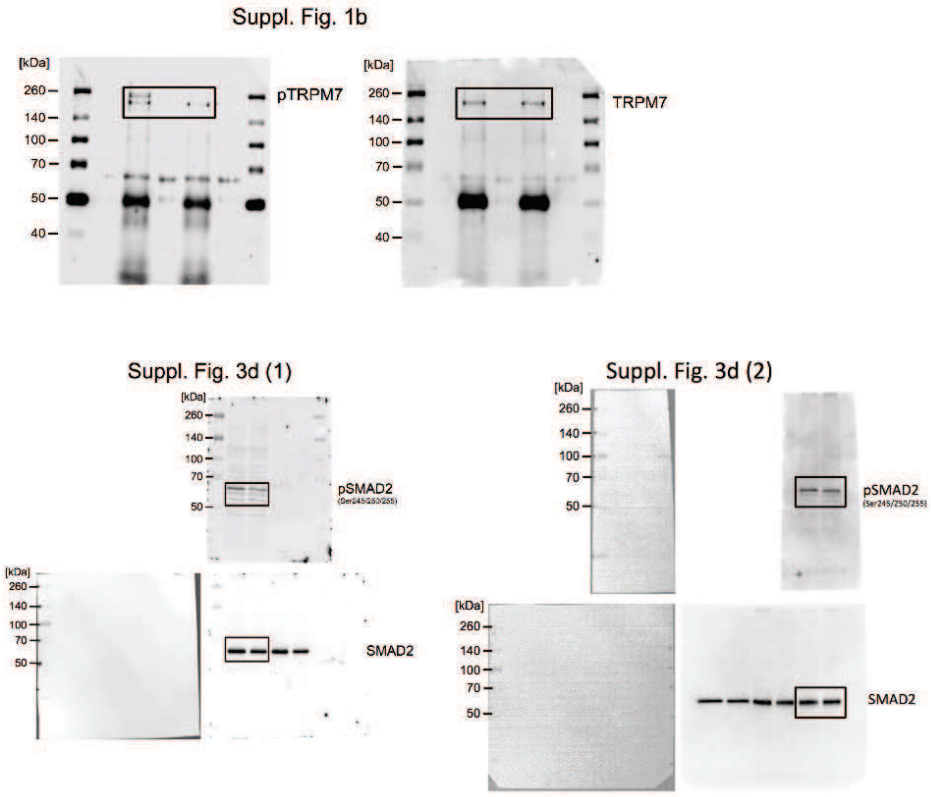

Supplementary Figure 5
Original data of immunoblots of Supplementary Figures 1 and 3.

Supplementary Table

Gene Name	species	Oligonucleotide sequence or catalogue number
Trpm7	mouse	Assay ID: Mm00457998_m1
Tbx21	mouse	Assay ID: Mm00450960_m1
Foxp3	mouse	Assay ID: Mm00475162_m1
Rorc	mouse	Assay ID: Mm01261022_m1
Il17a	mouse	Assay ID: Mm00439619_m1
Itgae	mouse	Assay ID: Mm00434443_m1
Itgae	mouse	Assay ID: qMmuCID0039603
Itgae	mouse	Fwd: CCTCCACAGCCCTATGTGTT Rev: GCCTCACAGGTAGGAACTGG
Tgfβ1	mouse	Assay ID: Mm01178820_m1
Tgfβ2	mouse	Assay ID: Mm00436955_m1
Tgfβ3	mouse	Assay ID: Mm01307950_m1
Hprt	mouse	Fwd: CTCATGGACTGATTATGGACAGG, Rev: TTAATGTAATCCAGCAGGTCAGC
Gapdh	mouse	Fwd:CCCTGCTTATCCAGTCCTAGCTCAAGG Rev:CTCGGGAAGCAGCATTCAGGTCTCTGG

Supplementary Table 1
List of all oligonucleotide sequences or catalogue numbers used in qRT-PCR or ChIP-PCR.

The Journal of Experimental Medicine, submitted.

Impaired P2X7 receptor activity promotes the expansion of T follicular helper cells in systemic lupus erythematosus

Caterina E. Faliti[1,2], Roberta Gualtierotti[3,4], Elsa Rottoli[1,5], Maria Gerosa[3,4], Lisa Perruzza[1,2], Andrea Romagnani[1,2], Giovanni Pellegrini[6], Riccardo L. Rossi[7], Emilia M.C. Mazza[8], Silvio Bicciato[8], Elisabetta Traggiai[9], Pier Luigi Meroni[3,4,10,*] and Fabio Grassi[1,5,7,*]

[1]Institute for Research in Biomedicine, Università della Svizzera Italiana, Bellinzona, Switzerland.
[2]Graduate School for Cellular and Biomedical Sciences, University of Bern, Bern, Switzerland.
[3]Department of Clinical Science and Community Health, University of Milan, Milan, Italy.
[4] Lupus Clinic, IASST-Istituto Gaetano Pini, Milan, Italy.
[5]Department of Medical Biotechnology and Translational Medicine, University of Milan, Milan, Italy.
[6]Laboratory for Animal Model Pathology, Institute of Veterinary Pathology, Vetsuisse Faculty, University of Zurich, Zurich, Switzerland.
[7]Istituto Nazionale Genetica Molecolare "Romeo ed Enrica Invernizzi", Milan, Italy.
[8]Department of Life Sciences, University of Modena and Reggio Emilia, Modena, Italy
[9]Novartis Institute for Biomedical Research, Basel, Switzerland.
[10]Istituto Auxologico Italiano, Milan, Italy.

[*]Corresponding authors: fabio.grassi@irb.usi.ch; pierluigi.meroni@unimi.it

ABSTRACT

Altered control of T follicular helper (Tfh) cells can lead to generation of autoantibodies and autoimmune manifestations. Signaling pathways that selectively limit pathogenic responses without affecting the protective function of Tfh cells are unknown. Here we show that the ATP-gated ionotropic P2X7 receptor restricts the expansion and B cell helper activity of Tfh cells in mice with pristane-induced lupus but does not affect Tfh cells response to conventional foreign antigens, such as ovalbumin. P2X7 stimulation promotes caspase-mediated pyroptosis of Tfh cells and controls the development of pathogenic ICOS$^+$ IFN-γ-secreting cells. Circulating Tfh cells from patients with systemic lupus erythematosus (SLE) but not primary anti-phospholipid syndrome (PAPS), a non-lupus systemic autoimmune disease, were hyporesponsive to P2X7 stimulation and resistant to P2X7-mediated inhibition of cytokine-driven expansion. Moreover,

in vitro generated Tfh cells from SLE were less sensitive to P2X7-mediated control. These data suggest that restoring P2X7 activity in SLE patients could selectively limit the progressive amplification of pathogenic autoantibodies, which deteriorate patients' conditions.

INTRODUCTION

T follicular helper cells are a specialized subset of effector CD4 T cells that play a crucial role in the generation of protective antibody responses against pathogens. However, dysfunctional Tfh cells can activate autoantibody-producing B cells that cause autoimmunity (Craft, 2012; Crotty, 2014; Yu and Vinuesa, 2010). Understanding the regulatory mechanisms that ensure the homeostatic control of Tfh cell activation can provide insight for manipulating T cell dependent antibody responses in autoimmune conditions. The Tfh cell differentiation program is implemented by upregulation of inducible T-cell costimulator (ICOS) that induces the transcription factor Bcl6 (Choi et al., 2011; Nurieva et al., 2008). Bcl6 in turn promotes CXCR5 expression and migration of the developing Tfh cell to the B cell follicle (Choi et al., 2011; Pepper et al., 2011). The concomitant downregulation of CCR7 and P-selectin glycoprotein ligand 1 (PSGL-1) allows the T cell to exit the T cell zone and colocalize with B cells. The ICOS/ICOSL interaction is important in mediating Tfh cell migration to the B cell follicle (Xu et al., 2013). Antigen presentation and ICOSL expression by B cells are instrumental to the expansion of Tfh cells, resulting in GC formation.

Adenosine triphosphate (ATP) is a ubiquitous extracellular messenger, which activates purinergic receptors in the plasma membrane termed P2 receptors. The P2X7 receptor subtype is an ATP-gated nonselective cationic channel characterized by dual gating: whereas P2X7 stimulation with ATP in the hundreds micromolar range leads to opening of a cytolytic pore and cell death, receptor exposure to low concentrations of ATP (e.g. micromolar range) results in small-amplitude currents (Khadra et al., 2013). Tfh cells express high levels of P2X7 in the plasma membrane; in the Peyer's patches (PPs) of the small intestine they are exposed to extracellular concentrations of ATP that promote cell death via

P2X7. Consequently, Tfh cells with deletion of *P2rx7*, encoding for P2X7, show resistance to extracellular ATP induced pore opening and cell death. The improved helper activity of *P2rx7*$^{-/-}$ Tfh cells results in enhanced germinal center reaction, IgA secretion and binding to commensals (Proietti et al., 2014).

It is not clear whether extracellular ATP might influence Tfh cells at inflammatory sites, where it is present at high concentrations (Wilhelm et al., 2010). We addressed this issue in chronic inflammation elicited by pristane-injection that causes a lupus-like syndrome in mice (Reeves et al., 2009; Satoh and Reeves, 1994). We show that lack of P2X7 in Tfh cells significantly worsened the disease by enhancing the generation of autoantibodies. Notably, circulating Tfh cells from patients with SLE were almost insensitive to P2X7-mediated control. In contrast, Tfh cells from patients with PAPS were inhibited by P2X7 stimulation suggesting that impaired P2X7 activity selectively contributes to the immunopathogenesis of SLE.

RESULTS

P2rx7 deletion exacerbates immunopathology in pristane induced lupus (PIL)

Several key features of SLE can be induced in mice by a single i.p. injection of the hydrocarbon oil 2,6,10,14-Tetramethylpentadecane (TMPD, commonly known as "pristane") (Reeves et al., 2009; Satoh and Reeves, 1994), which provokes peritoneal inflammation, production of antinuclear antibodies (ANAs) and glomerulonephritis. *P2rx7*$^{-/-}$ mice showed a significantly increased mortality with respect to WT mice after pristane administration (**Fig. 1A**) and more severe splenomegaly (**Fig. 1B**). PIL is characterized by peritoneal lipogranulomas, ectopic lymphoid structures that sustain autoantibodies production (Nacionales et al., 2009; Weinstein et al., 2013). We observed more widespread lipogranulomas (data not shown) and enhanced glomerular damage in *P2rx7*$^{-/-}$ compared to WT mice (**Fig. 1D**). Consistent with these findings, proteinuria levels (**Fig. 1C**), IgG immunocomplexes as well as complement C3 deposits in the glomeruli (**Fig. 1E**) were markedly

increased in mice lacking P2X7. Overall, these results indicate that *P2rx7* deletion exacerbates pristane-induced immunopathology.

***P2rx7* deletion leads to enhanced GC reaction and generation of autoantibodies in PIL**

Administration of pristane results in hypergammaglobulinemia and production of ANAs, a hallmark of SLE (Reeves et al., 2009; Satoh and Reeves, 1994). Serum concentrations of IgG_1 and IgG_{2B} subtypes were significantly augmented in *P2rx7*$^{-/-}$ with respect to WT mice, whereas IgG_{2C}, IgM and T-independent IgG_3 were comparable in the two groups of animals (**Fig. 2A**). Immunofluorescence of HEp-2 cells revealed dominant homogenous and mixed homogeneous/nucleolar staining patterns with sera from *P2rx7*$^{-/-}$ mice, suggesting robust generation of autoantibodies directed against nuclear components, whereas sera from WT mice preferentially showed cytoplasmic and mixed cytoplasmic/nucleolar patterns (**Fig. 2B**). Semi-quantitative detection of IgG reactive to SLE-specific self-antigens showed significant increases in sera from *P2rx7*$^{-/-}$ mice, which showed values more similar to those of autoimmune-prone MRL/*lpr* than to WT mice (**Fig. 2C**).

The analysis of splenic B cell compartment at 8 months after pristane administration did not reveal differences in the distribution of follicular and marginal zone B cells between WT and *P2rx7*$^{-/-}$ mice (**Fig. S1A**). Conversely, splenic plasma cells (**Fig. S1B**) as well as IgG secreting cells (**Fig. 3B**) were more abundant in *P2rx7*$^{-/-}$ mice. Splenic PNA^+Fas^+ GC B cells were unaltered in pristane treated WT mice with respect to untreated animals at this time after pristane administration. However, these cells were significantly increased in *P2rx7*$^{-/-}$ mice (**Fig. 3A**), as were GCs detected in immunofluorescence staining on spleen cryosections (**Fig. 3C**). These experiments suggest that protracted GC reaction could be responsible for the enrichment of autoreactive IgG in *P2rx7*$^{-/-}$ mice.

P2X7 activity limits Tfh cells expansion and kidney infiltration

Pristane administration induced a significant expansion of effector/memory CD4 cells in *P2rx7*$^{-/-}$ mice as compared to WT mice (**Fig. S2A, B**). Tfh cells expressing ICOS and PD-1 were dramatically increased both as frequency and absolute number (**Fig. 4**). ICOS amplification results in spontaneous

autoimmune manifestations in *sanroque* mice (Vinuesa et al., 2005) and increased IgG production as well as multi-organ inflammation in autoimmune-prone MRL/lpr mice (Odegard et al., 2008; Teichmann et al., 2015). ICOS-expressing CD4 cells promote nephritis in lupus-prone mice (Odegard et al., 2009) and were detected in renal biopsy of patients with lupus nephritis (Cohen et al., 2008; Hutloff et al., 2004). In *P2rx7*$^{-/-}$ mice, kidney-infiltrating ICOS^{+} CD4 cells were significantly increased following pristane administration (**Fig. S3A, B**). The expansion of ICOS^{+} cells in *P2rx7*$^{-/-}$ mice was associated with decreased frequency of ICOSL^{+} GC B cells and ICOSL mean fluorescence intensity (MFI) (**Fig. S1C**), as described both in murine (Iwai et al., 2003) and human (Her et al., 2009; Hutloff et al., 2004) lupus. These findings suggest that P2X7 activity exerts a crucial function in controlling ICOS^{+} Tfh cells to prevent autoimmune responses.

Immunosuppressive T regulatory cells (Tregs) limit the expansion of autoreactive cells and their defect might contribute to lupus pathogenesis, albeit a specific role in human SLE is debated (Ohl and Tenbrock, 2015). We did not detect differences in Tregs representation in the spleen between pristane injected WT and *P2rx7*$^{-/-}$ mice (**Fig. S2C**). We addressed whether T follicular regulatory (Tfr) cells, which represent specialized Tregs controlling GC reaction (Chung et al., 2011; Linterman et al., 2011; Wollenberg et al., 2011) were affected in *P2rx7*$^{-/-}$ mice. However, we did not detect differences in Tfh/Tfr cells or GC B/Tfr cells ratios in the spleen of treated animals (**Fig. S2D**), suggesting that *P2rx7*$^{-/-}$ Tfr cells efficiently expanded concomitantly to enhanced Tfh and GC B cells expansion.

Specific defect of P2X7 in Tfh cells enhances the generation of autoantibodies

We addressed whether *P2rx7*$^{-/-}$ Tfh but not other cells contributed to the phenotype of pristane-treated *P2rx7*$^{-/-}$ mice by analyzing the impact of the treatment in *Icos*$^{-/-}$*P2rx7*$^{-/-}$ mice, which are devoid of Tfh cells (Proietti et al., 2014). In double knock-out mice we did not detect variations in GC B cells abundance with respect to untreated animals (**Fig. 5A**), while we observed a slight but significant increase in serum autoantibodies, likely representing Tfh and GC independent responses. Nevertheless, the concentration of autoreactive IgG in *Icos*$^{-/-}$*P2rx7*$^{-/-}$ mice was markedly reduced with respect to

P2rx7$^{-/-}$ mice, indicating that P2X7 deficient Tfh cells are important for the enhanced autoreactive response observed in *P2rx7*$^{-/-}$ mice (**Fig. 5B**). Consistent with a pathogenic role of Tfh cells in lupus nephritis, *Icos*$^{-/-}$*P2rx7*$^{-/-}$ mice showed significantly reduced proteinuria with respect to *P2rx7*$^{-/-}$ mice (**Fig. 5C**).

Bcl6 dependent downregulation of P-selectin glycoprotein ligand-1 (PSGL-1) is part of the Tfh cell differentiation program (Poholek et al., 2010). In MRL/*lpr* mice, ICOS-dependent interaction with B cells was shown to promote PSGL-1 downregulation and autoantibodies production (Odegard et al., 2008). Analogously, we found a significant increase of PSGL-1$^{lo/-}$ cells in pristane-treated *P2rx7*$^{-/-}$ mice (**Fig. 5D**). Concomitant ICOS deletion abolished PSGL-1 downregulation in these mice and resulted in unaltered PSGL-1$^{lo/-}$ CD4 cells with respect to untreated mice (**Fig. 5D**), suggesting ICOS dependent and protracted functional activity of *P2rx7*$^{-/-}$ Tfh cells.

Augmented IFN-γ secretion by PSGL-1$^{lo/-}$ committed Tfh cells in pristane-treated *P2rx7*$^{-/-}$ mice

Expression of IL-21 is considered a key feature of normal (Nurieva et al., 2008) as well as pathogenic Tfh cells (Kim et al., 2015; McGuire et al., 2011; Yang et al., 2013). However, other proinflammatory cytokines such as IFN-γ (Domeier et al., 2016; Jackson et al., 2016; Lee et al., 2012) or IL-17 (Ding et al., 2013) were implicated in aberrant Tfh cell function. Intracellular staining for IL-21, IL-17 and IFN-γ showed a preferential increase in the percentage of IFN-γ secreting CD4 cells in pristane treated *P2rx7*$^{-/-}$ mice that was abolished by *Icos* deletion (**Fig. S3C**). Accordingly, we observed a selective enrichment of IFN-γ secreting cells in ICOS^{+} and PSGL-1$^{lo/-}$ CD4 cells (**Figure 5E and Fig. S3D**). According to previous data showing the relative resistance of *P2rx7*$^{-/-}$ CD4^{+} T cells to differentiate along the Th17 pathway (Schenk et al., 2011), we detected decreased percentages of IL-17 secreting cells in pristane-treated *P2rx7*$^{-/-}$ mice as well as decreased percentages of IL-21 secreting cells with respect to WT mice (**Fig. S3C**). These observations are consistent with the reported role of IFN-γ secreting Tfh cells in contributing to lupus pathology (Lee et al., 2012).

P2X7 mediated pyroptosis of Tfh cells via caspase-mediated activation of Gasdermin D

Online monitoring of cell permeability to YO-PRO-1 at FACS upon stimulation with the P2X7 agonist 3'-*O*-(4-benzoyl)benzoyl ATP (BzATP) is used to assess cellular sensitivity to death mediated by cytolytic pore opening. Tfh cells from spleen of WT but not *P2rx7*$^{-/-}$ mice were sensitive to P2X7 stimulation in this assay (**Fig. 6A**). In T cells, P2X7 mediated pore opening and cell death was associated to features characteristic of pyroptosis (Taylor et al., 2008), a form of death executed by gasdermin D (Gsdmd) upon caspase mediated cleavage and relieve of autoinhibition of the pore forming N-terminus (Kayagaki et al., 2015; Shi et al., 2015). A search of gene-expression profiles in public data sets revealed Gsdmd as the most widely represented member among Gasdermin family in CD4 naïve and Tfh cells (**Fig. 6B**). The analysis of caspase expression in CD4 naïve versus Tfh cells revealed the selective upregulation of caspase-1 and -4 in Tfh cells (**Fig. 6C**). Since Gsdmd is a substrate of caspase-1 and -4, this observation suggests Tfh cells could be sensitive to Gsdmd pore-forming activity and execute pyroptosis in Tfh cells upon exposure to BzATP. Accordingly, treatment of WT but not *P2rx7*$^{-/-}$ Tfh cells with BzATP resulted in caspase activation (**Fig. 6D**) and generation of cleaved Gsdmd (**Fig. 6E**), suggesting that P2X7 limits Tfh cells survival in extracellular ATP-rich microenvironment via Gsdmd-mediated pyroptotic cell death.

P2X7 limits expansion of Tfh cells in PIL but not during conventional immunization

To address whether the selective lack of P2X7 in CD4 cells was sufficient to induce Tfh cells expansion in PIL, we transferred CD90.2 WT or *P2rx7*$^{-/-}$ CD4 cells from untreated mice into congenic CD90.1 WT animals. The analysis of donors Tfh cells at 1, 2 and 4 months after pristane injection revealed the significant increase of *P2rx7*$^{-/-}$ Tfh cells with respect to WT cells (**Fig. 7A**). This result suggests that P2X7 limits Tfh cells expansion upon inflammation and chronic exposure to self-antigens. Notably, Tfh cells expansion significantly correlated with GC B cells abundance (**Fig. 7B**). To address whether P2X7 mediated control of Tfh cells expansion was peculiar for the inflammatory environment elicited by pristane administration but not immunization with a conventional antigen, we

immunized WT and *P2rx7*$^{-/-}$ mice with NP_{16}-OVA in MF59, a potent ATP-releasing adjuvant (Vono et al., 2013). In contrast to the enhanced response to pristane, we detected an impaired expansion of Tfh cells and OVA-peptide$_{329-337}$ specific CD4 cells (**Fig. 8A**) as well as NP-specific GC B cells (**Fig. 8B**) in *P2rx7*$^{-/-}$ mice at 7 d post-immunization. Recall immunization at 14 d and analysis after 7 d showed the persistent reduction of antigen-specific B cells in the spleen of mutant animals (**Fig. 8C**) concomitant to significantly reduced abundance of both high and low affinity IgG secreting B cells specific for NP-4 and NP-41 antigen, respectively (**Fig. 8D**). Since P2X7 is important in promoting the proinflammatory activation of APCs during antigen priming of adaptive immunity (Wilhelm et al., 2010), the defective antigen responsiveness of *P2rx7*$^{-/-}$ mice could be due to impaired APCs activation. To rule out an intrinsic defect of *P2rx7*$^{-/-}$ Tfh cells during antigen priming, we transferred either WT or *P2rx7*$^{-/-}$ TCR transgenic CD90.2 OT-II CD4 cells (specific for OVA peptide 323-339) into congenic CD90.1 WT mice and immunized mice with NP_{16}-OVA in MF59. The analysis of primary as well as re-activated memory response revealed undistinguishable frequencies of antigen-specific CD4 cells in mice adoptively transferred with WT or *P2rx7*$^{-/-}$ OT-II cells (**Fig. 7C**). Altogether, these results are consistent with the function of P2X7 in APCs in ensuring effective antigen priming of T cells (Wilhelm et al., 2010). Conversely, P2X7 in Tfh cells does not influence responsiveness within a prophylactic immunization protocol, likely due to its robust down-regulation during TCR stimulation by cognate antigen (Proietti et al., 2014). Importantly, these data show that P2X7 in Tfh cells plays an exquisite role in limiting the expansion of potentially pathogenic cells in chronic inflammatory conditions.

Phenotypic and functional distinction of circulating Tfh cells in SLE and PAPS donors

As previously shown (He et al., 2013), we observed significantly increased frequencies of the CCR7$^{lo/-}$ PD-1^{hi} subset of circulating Tfh (cTfh) cells in SLE patients (**Fig. 9A**). The same phenotype was used to define immunopathogenic Tfh cells in lupus-prone sanroque mice (He et al., 2013). Analogously, CCR7$^{lo/-}$PD-1^{hi} Tfh cells were significantly increased in the spleen of pristane-treated *P2rx7*$^{-/-}$ with respect to WT mice (**Fig. S4A**). Interestingly, the analysis of these cells in patients suffering from

another systemic autoantibody-mediated disease, namely PAPS, did not reveal differences with respect to healthy donors (**Fig. 9A**). Moreover, quantification of CXCL13 in the blood as a Tfh cells derived biomarker of GC activity in humans (Havenar-Daughton et al., 2016) showed the significant increase in SLE but not PAPS with respect to HD (**Fig. 9B**). These results support a role for deregulated Tfh cells in autoantibodies generation and pathogenesis in SLE, but not PAPS (where SLE features are not observed even in the presence of anti-phospholipid antibodies, including lupus anticoagulant, anti-cardiolipin or anti-β2-glycoprotein-I antibodies) (Ruiz-Irastorza et al., 2010). To investigate possible differences in cTfh cells function in SLE and PAPS, we used a chemokine receptors signature, which classifies these cells into three majors subsets: efficient B cell helper cells, defined as cTfh2 ($CXCR3^-CCR6^-$) and cTfh17 ($CXCR3^-CCR6^+$) cells, which are increased in some autoimmune disorders, including SLE, and non-efficient B cell helper cTfh1 ($CXCR3^+CCR6^-$) cells (Blanco et al., 2016; Ueno et al., 2015). As expected, we detected a significant increase in cTfh2 concomitant to a decrease in cTfh1 cells in SLE patients. In contrast, PAPS patients were characterized by the increase in a cTfh1/Tfh17 hybrid cell subset that was negatively associated with disease activity in SLE (Choi et al., 2015) (**Fig. S4B**). SLE and PAPS patients showed an opposite trend of the ratio between the sum of cTfh2 and cTfh17 cells with cTfh1 cells compared to healthy donors. Whereas SLE patients showed a significant increase of this value, as previously described (Le Coz et al., 2013), PAPS patients displayed a significant reduction, thereby defining a functional distinction of cTfh cells in these two auto-antibody mediated pathological conditions (**Fig. S4C**).

Impaired P2X7 receptor activity unleashes Tfh cells expansion in SLE

To address possible differences in sensitivity to extracellular ATP via P2X7 in cTfh cells from SLE versus PAPS, we tested YO-PRO-1 permeability at FACS upon stimulation with BzATP. These experiments revealed the significant reduction of BzATP sensitive cells and impairment of YO-PRO-1 permeability in SLE patients with respect to both healthy and PAPS subjects (**Fig. 9C**). The analysis of *P2RX7* mRNA in sorted $CXCR5^+$ circulating T cells revealed significantly reduced levels in cells from

SLE with respect to both healthy and PAPS donors, suggesting *P2RX7* is selectively downregulated in SLE (**Fig. S4D**). YO-PRO-1 permeability by P2X7 stimulation inversely correlated with the frequency of $CCR7^{lo/-}PD\text{-}1^{hi}$ cTfh cells (**Fig. 9D**). Principal component analysis (PCA) for the frequencies of $CCR7^{lo/-}PD\text{-}1^{hi}$ and YO-PRO-1^{+} cells as well as YO-PRO-1 uptake at 450 sec identified two main clusters: while HD and PAPS segregated close to each other, SLE samples were clearly differentiated along the first component (**Fig. 9D**). These results indicate that impaired P2X7 activity might be responsible for the increase in cTfh cells in SLE. The propensity of effector CD4 cells to expand in an antigen-independent fashion can be scored *in vitro* by the analysis of cell proliferation in response to cytokines (Geginat et al., 2001). Upon stimulation with IL-7 and IL-15 $CXCR5^{+}$ circulating T cells from SLE patients proliferated more robustly than cells isolated from healthy or PAPS subjects and were significantly more resistant to inhibition of proliferation by BzATP (**Fig. 9E**). Analogous defective inhibition was observed also in purified $CCR7^{lo/-}PD\text{-}1^{hi}$ cells (**Fig. S4E**).

It was recently shown that CD4 naïve T cells can differentiate into Tfh cells and expand *in vitro* upon exposure to activin A and IL-12 (Locci et al., 2016). The generation and expansion of Tfh cells in this assay was significantly inhibited by addition of BzATP (**Fig. 9F**). However, CD4 cells from SLE donors generated Tfh cells with the same efficiency irrespective to the presence of BzATP, suggesting Tfh cells in SLE are poised to be defective in sensing extracellular ATP as an inflammatory cue that should limit their function (**Fig. 9F**). Altogether, these results point to a role for P2X7 as a checkpoint regulator for Tfh cells that appears to be compromised in SLE.

DISCUSSION

The identification of the *sanroque* mutation (that disrupts a repressor of ICOS) unraveled the causal role of deregulated Tfh cells and GCs in developing high titres of autoantibodies and lupus pathology (Vinuesa et al., 2005). We hypothesize P2X7-mediated regulation of Tfh cells can limit potentially

pathogenic GC activity. The abundance of $CCR7^{lo/-}PD\text{-}1^{hi}$ cTfh cells in the blood correlates with active Tfh cells differentiation (He et al., 2013). These cells were selectively enriched and resistant to P2X7-mediated cell death in SLE but not PAPS patients. Excessive IFN-γ promotes Tfh cells accumulation and lupus-associated pathology (Lee et al., 2012). Our results indicate that P2X7 activity might contribute to inhibition of IFN-γ secretion and offset the risk of GC-driven autoimmunity by chronic Tfh cells stimulation. Notably, IFN-γ deficiency did not impair Tfh cell response against immunization with foreign antigen (Lee et al., 2012). According to a dichotomy of P2X7 in regulating Tfh cells function in acute stimulation by cognate antigen versus chronic exposure to inflammatory environments, immunization with OVA did not result in any difference in the expansion of OT-II Tfh cells both in primary and secondary response. Whereas P2X7 activity does not affect Tfh cells response to "physiological" stimulation by exogenous antigens it appears to crucially limit immunopathological responses. Therefore, restoring P2X7 competence in Tfh cells might improve immunopathology in systemic autoimmunity.

The progressive nature of SLE is characterized by the accumulation of new type of autoantibodies up to the clinical onset of the disease. Moreover, the appearance of specific autoantibodies, namely anti-Sm and anti–nuclear ribonucleoprotein antibodies, tends to coincide with the clinical manifestations of SLE. These observations led to the modeling of disease evolution into three distinct phases of benign autoimmunity, pathogenic autoimmunity and clinical illness (Arbuckle et al., 2003). The genetic as well as environmental factors influencing the development of pathogenic autoimmunity in SLE are not defined. SLE is a polygenic disease; strong candidate/s that may cause the disease seem to be located across chromosomal bands 12q24.1 to 12q24.3 (Nath et al., 2004). Together with other potential candidate genes in SLE pathogenesis, *P2RX7* is located within this chromosomal region. Human *P2RX7* is highly polymorphic and contains a large set of single nucleotide polymorphisms (SNPs) that affect P2X7 activity. Haplotypes containing the Ala348>Thr polymorphism (rs1718119) are characterized by a gain-of-function effect (Stokes et al., 2010). Interestingly, this polymorphism was

associated with lower risk of SLE in a Chinese population (Chen et al., 2013). CD4 cells from patients with SLE, but not rheumatoid arthritis, exhibited diminished P2X7 dependent ATP-mediated cell death compared with healthy controls (Portales-Cervantes et al., 2010). We have shown a profoundly diminished sensitivity of Tfh cells from SLE but not PAPS patients to cytolytic pore opening by P2X7 pharmacological agonist, suggesting that downregulation of P2X7 might contribute to a selective Tfh cells dysfunction associated with SLE. Notably, aging Fas-deficient MRL/*lpr* mice, which develop a lupus-like syndrome, show a drastically reduced sensitivity to ATP-mediated stimulation of P2X7 in T cells associated with progressive lymphoproliferation (Le Gall et al., 2012). In innate immune system P2X7 has a well-established role as a trigger for inflammatory cytokines release, a feature that fostered the development of P2X7 inhibitors to be used as therapeutic drugs in autoimmune diseases (Ferrari et al., 2006). Our results suggest P2X7 inhibition in chronic inflammatory conditions where GC activity is enhanced might promote the inappropriate expansion of potentially pathogenic Tfh cells.

MATERIALS AND METHODS

Mice

C57/BL6J, *P2rx7*$^{-/-}$ (B6.129P2-P2rx7tm1Gab/J), *Icos*$^{-/-}$ (B6.129P2-Icostm1Mak/J), OT-II [B6.Cg-Tg(TcraTcrb)425Cbn/J], CD45.1 (B6.SJL-Ptprca Pepcb/BoyJ) and CD90.1 (B6.PL-Thy1a/CyJ) mice from Jackson Lab were bred in the specific pathogen-free (SPF) facility at IRB, Bellinzona, Switzerland. All animal experiments were performed in accordance with the Swiss Federal Veterinary Office guidelines and authorized by the Cantonal Veterinary.

Pristane-induced lupus (PIL)

SLE was induced by a single i.p. injection of 0.5 ml pristane to 8-week-old WT or *P2rx7*$^{-/-}$ female mice. Mice were monitored for clinical signs of SLE until the end of the study (33 weeks post dosing) and examined for lesions consistent with SLE by kidney histology and immunofluorescence, presence

of serum autoantibodies by ELISA and cell subsets composition by flow cytometry. Proteinuria was measured using Bayer Albustix reagent strips on collected fresh spots of urine from each mouse. Score from 0 to 4+ was applied as follows: 0 - none, 1+ trace, 2+ 30 mg/ml, 3+ 100 mg/ml, 4+ ≥ 500 mg/ml.

Immunization and adoptive transfer of CD4 cells

Eight week-old female mice were subcutaneously injected with 50 μg of $NP_{(16)}$-Ovalbumin (BIOSEARCH Technologies) in MF59 (AddaVaxTM, InvivoGen). Draining lymph nodes and spleen were collected 1 wk post-injection and cells analysed by flow cytometry. For the analysis of secondary response, the same immunogen was administered and cells analysed after 1 wk. For adoptive transfer of OT-II cells, $CD4^+$ cells were enriched with anti-CD4 coated magnetic beads (Miltenyi) and sorted as $CD4^+CD8^-CD25^-CD44^-CD62L^+$ naïve cells at FACSAria. Eight-week old CD90.1 mice were injected intravenously with 2.5 $x10^5$ sorted cells containing at least 90% $OT\text{-}II^+$ cells. Recipient mice were immunized 24 h later with a subcutaneous injection of 50 μg of NP(16)-Ovalbumin (BIOSEARCH Technologies) 1:1 in MF59 (AddaVaxTM, InvivoGen). For retransfer of activated OT II effector cells, CD4 enriched cells were sorted for CD90.2 cells and $5x10^4$ cells were injected intravenously into naïve CD90.1 hosts. To re-activate memory OT-II cells, recipient mice received a subcutaneous injection of 50 μg of NP(16)-Ovalbumin in MF59 28 days after secondary transfer and draining lymph nodes were analyzed 1 week later. For adoptive transfer of polyclonal $CD4^+$ T cells from either WT or *P2rx7*$^{-/-}$ mice, spleens were collected, $CD4^+$ cells enriched with anti-CD4 coated magnetic beads (Miltenyi) and then sorted as $CD4^+CD8^-CD19^-B220^-CD11c^-CD11b^-$ cells at FACSAria. $3.5x10^6$ cells were injected into CD90.1 WT mice and 24 h later mice were injected i.p. with 0.5 ml pristane. Spleens were collected and analyzed after 1, 2 or 4 months post-injection.

Histochemistry and Immunohistochemistry

All animals were euthanatized with CO_2, followed by exsanguination. For histological evaluation, the kidneys were removed, fixed in 10% neutral buffered formalin for 48 h, trimmed, dehydrated and

embedded in paraffin wax. Sections of 3-5 μm thickness were prepared, mounted on glass slides, deparaffinized in xylene and rehydrated through graded alcohols, before staining with hematoxylin and eosin (HE) or the periodic-acid-Schiff (PAS) reagent. Slides were evaluated in a blinded fashion by a board-certified veterinary pathologist (G.P.). Glomerular injury was assessed by light microscopy on 50 consecutive glomeruli/mouse using a histopathological scoring system modified from Wang et al. (Wang et al., 1999). Briefly, a grade of 0 indicated normal glomerular histology; scores 1 to 3 indicated progressive severe glomerular injury, i.e.: score 1, mildly thickened and hypereosinophilic mesangium, multiple clusters of nuclei, mild reduction in the number of glomerular capillaries; score 2: moderately thickened and hypereosinophilic mesangium, moderate diffuse hypercellularity, marked reduction in the number of glomerular capillaries, occasional inflammatory cells, mostly neutrophils; score 3: noticeable enlargement of the glomerular tuft, abnormal glomerular shape (irregular rather than round), severely thickened and hypereosinophilic mesangium, occasional adhesions of the glomerular tuft to the Bowman's capsule (synechiae), severe diffuse hypercellularity, loss of capillaries, occasional inflammatory cells, mostly neutrophils. To detect glomerular immune complexes (ICs) by immunofluorescence, kidneys were removed and immediately frozen in OCT (Tissue TeK). Cryostat sections (4 μm) were stained with the following antibodies: AF488 goat anti-mouse IgG (highly cross-adsorbed, Southern Biotech), rat anti-mouse C3 (RmC11H9) followed by AF647 labeled goat anti-rat IgG (cross-adsorbed against mouse IgG, Southern Biotech). To detect renal infiltrating CD4 T lymphocytes, the following antibodies were applied to the sections: rat anti-mouse CD4 (clone: GK1.5; BD Pharmingen) followed by AF488 goat anti-rat IgG (Invitrogen), hamster anti-mouse ICOS (clone: C398.4A**;** eBioscience) followed by AF594 goat anti-hamster IgG (Invitrogen). Slides were mounted with Gelvatol Mounting Media and stained with DAPI for the detection of nuclei. Images were acquired using a Leica TCS SP5 confocal microscope, with a HCX PL APO 40x/1.25 N.A. oil immersion objective. Quantification was performed with ImageJ open-source software (Schindelin et al., 2012): regions of interests (ROIs) containing the glomeruli were manually defined, and the

background was excluded by applying a threshold on the intensity; the area above the threshold in these ROIs was measured in 3 different fields of view for each sample, and is expressed as percentage of the total glomerulus area. For histological analysis of GCs, spleens were frozen in OCT (Tissue TeK). Cryostat sections (4 μm) were stained with the following antibodies: AF594 anti-mouse IgD (clone: 11-26c.2a**;** Biolegend), AF647 anti-mouse GL-7 (clone: GL-7; Biolegend), BV405 anti-mouse CD4 (clone: GK1.5; Biolegend), unconjugated goat anti-mouse PD-1 Ig (Novusbio) followed by AF488 rabbit anti-goat Ig (Invitrogen). Images were collected on a laser-scanning confocal microscope with a HCX PL APO 40x/1.25 N.A. oil immersion objective. GC area was measured using ImageJ open-source software (Schindelin et al., 2012). To score GCs frequency, total GC numbers were quantitated in three separate 10x field of view of 2.4 mm^2 (1550 μm x 1550 μm) per spleen section.

Preparation of single-cell suspension from kidney

Kidneys were removed, minced, and digested with Liberase (0.14 mg/ml; Roche) and DNase I (0.03 mg/ml; Sigma-Aldrich) in HBSS medium, for 30-40 min at 37°C. Tissue pieces were then pressed through a 70 μm strainer to obtain single-cell suspensions. Cells were enriched in leukocytes using an 80/20 Percoll gradient and centrifuged at 800 g for 20 min at room temperature. Lymphoid fractions were collected at the interphase of the Percoll gradient and used for flow cytometry.

Mouse cell isolation and flow cytometry

Single cell suspensions were prepared by passing spleens through a 70 μm nylon mesh . After centrifugation at 1500 rpm for 5 min, red blood cells were lysed in ACK-lysis buffer for 7 min. Lysis buffer was neutralized by washing once in staining buffer. Cells were stained with the following monoclonal antibodies: biotin-conjugated anti-CXCR5 (clone: 2G8; BD), PE-labeled anti ICOS (clone: 7E.17G9; BD) or PerCPCy5-labeled anti-ICOS (clone: C398.4A; Biolegend), APC-labeled anti PD-1 (clone: RMPI-30; Biolegend), Percp-eFluor710-labeled anti-CD3 (Clone: 17A2; eBioscience), AF488-labeled TCRβ (clone: H57-597; Biolegend), APC-Cy7-labeled anti-CD4 (clone: RM4-5; Biolegend),

BV421 anti-CD162 (PSGL1) (clone 2PH1; BD), PeCy7-labeled anti-CD25 (clone: PC61; Biolegend), PE-labeled anti-CD44 (clone: IM7; Biolegend), APC-labeled CD62L (clone: MEL-14; eBiosceince), BV421-labeled anti-CD197 (CCR7) (clone: 4B12; Biolegend). APC-Cy7-labeled anti-CD19 (clone: 6D5; Biolegend), BV405-labeled B220 (clone: RA3-6B2; Biolegend), PE-labeled anti-Fas (clone: Jo2; BD), Fluorescein labelled Peanut Agglutinin (PNA) (Cat. #: FL-10-71; Vectorlabs), biotinylated anti-CD275 (ICOSL) (clone: HK5.3; Biolegend), PE-labeled anti-CD138 (clone: 281-2; BD) APC-labeled anti-CD11c (clone: N418; eBioscience), APC-eFluor780-labeled CD45.2 (clone: 104; eBioscience), APC-Cy7-labeled anti-CD90.2 (clone: 30-H12; Biolegend). APC-labeled streptavidin was purchased from Biolegend and efluo405-labeled streptavidin from eBioscience. Intracellular staining was performed using the BD Cytofix/Cytoperm and Perm/Wash buffers or, for intracellular FoxP3 (FITC-labeled, clone: FJK-16s; eBioscience) staining, the eBioscience FoxP3 staining buffer set. For intra-cellular staining of IL-21 (R&D systems), IFN-γ (PeCy7-labeled, clone: XMG1.2; eBioscience) and IL-17A (PerCP-Cy5-labeled, clone: eBio17B7; eBioscience) 5 x 10^6 splenocytes were cultured for 5 h at 37 °C in 24-well plates in 2 ml culture medium containing ionomycin (750 ng/ml) and PMA (20 ng/ml). For the last 4 h Monensin (eBioscience, 1000X Solution) was added to the cultures. IL-21 was detected with a recombinant mouse IL-21R subunit/human IgG1 Fc chimera (R&D systems) with goat anti-human Fcγ conjugated to AF488 (Jackson ImmunoResearch). For detection of activated caspases, Tfh cells were incubated with FITC-VAD-FMK (CaspGlow Fluorescein Active Caspase Staining Kit; BioVision) for 30-45 min at 37 °C in RPMI-1640 medium according to the manufacturer's protocol. Cells were then washed and resuspended in PBS for FACS analysis. Samples were acquired on a LSRFortessa (BD Biosciences) flow cytometer. Data were analysed using FlowJo software (TreeStar).

Tetramer staining

Tetramers were kindly provided by the NIH Tetramer Core Facility. Cells were stained for 2 h at 37℃ with the following APC-labeled Tetramers: I-A^b chicken $OVA_{329-337}$ AAHAEINEA, I-A^b chicken

$OVA_{328-337}$ HAAHAEINEA, I-A^b chicken $OVA_{259-277}$ IINFEKLTEWTSSNVMEER and I-A^b human $CLIP_{87-101}$ PVSKMRMATPLLMQA. All OVA tetramers gave comparable results in flow cytometry.

ELISA and ELISPOT assays

For total immunoglobulin isotype determination, ELISA plates (Corning® 96 Well Half Area Flat Bottom Polystyrene High Bind) were coated for 3 h at room temperature with purified goat anti-mouse IgG, IgM and IgA antibodies (Southern Biotech) used at a concentration of 10 μg/ml . After 4 washes with PBS 0.025% Tween20 and blocking with PBS 1% BSA for 1h at room temperature, samples and standards (relative unlabeled mouse Ig, Southern Biotech) were diluted and incubated at room temperature for 4 h. Specific secondary goat-anti mouse Ig conjugated with alkaline-phosphatase were added after 4 washes with PBS, 0.025% Tween20 and incubated for 2 h at room temperature. Plates were washed again and the assay developed with Sigma 104 phosphatase substrate. Plates were read at 405 nm. IgG secreting cells (ISCs) were detected using ELISPOT assay: 96-well plates (Millipore, MSIPS4510 Sterile, hydrophobic high protein binding immobilion-P membrane) were coated with 10 μg/ml purified goat anti-mouse IgG (Southern Biotech) for 2 h at room temperature. After 3 washes with PBS solution, plates were blocked with PBS, 1% BSA and incubated for 30 min at 37 °C. Serial dilutions of splenocytes were added in a final volume of 200 μL of B cell medium (RPMI, 10% Hyclone serum) and left at 37 °C for 16 h. Subsequently, plates were washed 3 times with PBS, 0.25% Tween20, and 4 times with PBS and incubated for 2 h at room temperature with biotinylated goat anti-mouse IgG (Southern Biotech). After washing, avidin-peroxidase (horseradish peroxidase, HRP, from Sigma-Aldrich) was added and left for 1 h at room temperature. The assay was developed with AEC (Sigma-Aldrich). For quantification of ISCs, plates were acquired, counted and quality controlled using an ELISPOT reader and ImmunoSpot 5.1 software (CTL, Europe GmbH). For ANAs detection, both IFA ANA-Hep-2 fixed cells (Orgentec, ORG 870) and microwell ELISA plates coated with highly purified individual antigens plus extracts from Hep-2 nuclei and nucleoli (QUANTA LiteTM, Inova

Diagnostics) were used. Briefly, fixed Hep-2 cells were incubated with mouse sera (diluted 1:100) and ANAs detected with AF488-labeled goat anti-mouse IgG (Southern Biotech). Slides were stained with DAPI and captured with a Nikon Eclipse E800 upright microscope, with a 20X/0.75 N.A. objective. Images were analyzed with ImageJ open-source software for pattern recognition (Schindelin et al., 2012). The kit ELISA (QUANTA LiteTM) for the semi-quantitative detection of ANAs in human serum was used and adapted for the detection of mouse ANAs. The antigens include chromatin (dsDNA and histones), Sm/RNP, SS-A, SS-B, Scl-70, centromere, PCNA, Jo-1, mitochondria (M-2) and ribosomal-P protein, as well as the extracts. Sera were diluted at 1:200 in ANA sample diluent and detected with HRP-conjugated goat anti-mouse IgG (Southern Biotech). Plates were read for the absorbance (O.D.) at 450 nm within one hour after addiction of the Stop Solution, as described in the protocol.

Western Blot

Tfh cells were isolated from mesenteric lymph nodes and PPs, washed with ice cold PBS and lysed with RIPA buffer 1x (Sigma) supplemented with protease inhibitor cocktail (Roche). Samples were centrifuged at 14.000 rpm for 10 min at 4°C and snap frozen. Cleared protein lysate was denaturated with loading buffer supplemented with 0.1 μM DTT for 10 min at 65°C. Samples were run on precast 4-12% bis-tris protein gels (BioRad) and then transferred onto PVDF membranes using Trans-Blot Turbo Transfer System (BioRad). Membranes were blocked with 10% (wt/vol) nonfat dry milk (Bio-Rad), 0.1% Tween-20 in TBS and incubated with appropriate antibodies in TBS with 0.1% Tween-20 16 h at 4°C. The following antibodies were used: anti-GSDMDC1 (clone: A-7, cat. #sc-393656, Santa Cruz Biotechnology), anti-actin (Cat. #A2066, Sigma). Bound antibodies were revealed by incubation with secondary HRP-conjugated anti-mouse (Cat. #7076, Cell Signaling Technology) or anti-rabbit (Cat. #7074, Cell Signaling Technology) IgG antibodies in TBS with 0.1% Tween-20. Membranes were developed using the Pierce ECL Western blotting substrate (Thermo Scientific, Cat.# 32209),

signals were detected with the ImageQuant LAS 4000 system in the standard acquisition mode (GE Healthcare Life Sciences), and bands were quantified using the Multi Gauge Analysis tool (Fujifilm).

Human samples and patients

Peripheral blood samples from patients with SLE and PAPS were obtained after providing informed consent (Local Ethics Committee approval n. 192_2016bis) during regular follow-up visits at the Lupus Clinic, IASST-Istituto Gaetano Pini, University of Milan, Italy. Inclusion criteria were: age >18 years, fulfillment of the American College of Rheumatology 1997 classification criteria for SLE (Hochberg, 1997) and 2006 classification criteria for APS (Miyakis et al., 2006) (**Supplementary Table 1**). Exclusion criteria were: treatment with B-cell depleting agents or experimental drugs. Disease activity was determined with SLE disease activity index (SLEDAI-2K) (Gladman et al., 2002); clinical and laboratory data were obtained during the routine follow-up. Patients were characterized for anti-phospholipid antibodies (Lupus Anticoagulant, anticardiolipin IgG and IgM and anti-beta2GPI IgG and IgM) (Andreoli et al., 2015) as well as ANA, anti-ENA and anti-dsDNA antibodies (Ingegnoli et al., 2014). Blood samples from healthy donors were obtained upon providing informed consent from the IRCCS Policlinico Ospedale Maggiore, Milan, Italy.

Human cell isolation and flow cytometry

Peripheral blood mononuclear cells (PBMCs) were isolated from blood by density-gradient centrifugation using Ficoll-Paque™ Plus gradient (GE-Healthcare). $CD4^+$ T cells were enriched by positive selection using human CD4 MicroBeads (Miltenyi Biotec) and then $CD4^+$ T cell subsets were sorted to 99% purity with a FACSAria (BD). PBMCs were stained with the following antibodies: (PE-Texas Red)-labeled anti-CD4 (clone: MHCD0417; Life Technologies), QD655-labeled anti-CD45RA (clone: MEM-56; Life Technologies), PE-labeled anti-CCR7 (clone: G043H7; Biolegend), purified mouse monoclonal IgG_{2b} anti-CXCR5 (BRL-1, clone: 51505; R&D System) revealed by FITC-labeled anti-mouse IgG_{2b} (Southern Biotech), PE-cyanine 5 (PeCy5)–labeled anti-CD183 (CXCR3) (clone: 1C6/CXCR3; BD), PE-labeled anti-CD196 (CCR6) (clone: 11A9; BD), BV785-labeled anti-CD279

(PD-1) (clone: EH12.2H7; Biolegend). PeCy5–labeled anti-CD56 (clone: A07789; Beckman Coulter), anti-CD14 (clone: A07765; Beckman Coulter), anti-CD19 (clone: HIB19; Biolegend), anti-CD25 (clone: BC96; Biolegend), and anti-CD8 (clone: HIT8a; Biolegend) were included as a dump channel to exclude contaminant cells.

Time monitoring of YO-PRO-1 uptake

$1x10^6$ human PBMCs were stained with the appropriate antibodies, washed, resuspended in RPMI 1640 complete medium and loaded with YO-PRO-1 iodide (Life technologies) at a final concentration of 5 μM. The YO-PRO-1 uptake following cell stimulation with 1 mM BzATP (Sigma) was monitored at LSRFortessa for 480 sec, and the kinetics analyzed using FlowJo software (TreeStar). Murine splenocytes ($1x10^6$) were stimulated with 0.1 mM BzATP.

In vitro cytokine-driven proliferation assay

For cytokine-driven proliferation assay, sorted $CXCR5^+$ or $CCR7^{lo/-}PD\text{-}1^{hi}$ CD4 T cells were labeled with 5 μM Cell Trace Violet (CTV, Life Technologies) in PBS for 20 min at 37°C; staining was blocked by adding an equal volume of filtered pre-warmed FBS. Cells were centrifuged at 1500 rpm for 5 min and plated at a minimal density of 25'000 cells/well in RMPI 1640 complete medium. Plated cells were stimulated with recombinant IL-7 and IL-15 (R&D System) at 25 ng/ml, with BzATP at a final concentration of 100 μM when indicated. Cell proliferation and viability were assessed after 7 days using LSRFortessa.

***In vitro* CD4 cell differentiation to Tfh cell**

$CD4^+$ cells were enriched from PBMCs by positive selection with anti-CD4 MicroBeads (Miltenyi Biotec). Naive T cells were sorted at FACSAria (BD) to 99% purity as $CD8^-CD25^-CD14^-CD19^-CD4^+CD45RA^+CCR7^+$ cells, activated by Dynabeads Human T-Activator CD3/CD28 (Life Technologies) and cultured with recombinant activin A (100 ng/ml), human IL-12 (5 ng/ml), IL-7 (4 ng/ml) (all from R&D System) and BzATP where indicated, in AIM-V medium (Life Technologies), as

described (Locci et al., 2016). After 5 d, cells were stained with Zombie Aqua™ dye (BioLegend) to exclude dead cells, anti-human CXCR5 and PD-1 antibodies and analysed at LSRFortessa.

Real-time quantitative PCR

$CXCR5^+$ CD4 cells were sorted at FACSAria (BD) from PBMCs. RNA was extracted using the RNeasy Mini Kit (Qiagen) and converted to cDNA. Random primers and MMLV Reverse Transcriptase (Invitrogen) were used for cDNA synthesis. Transcripts were quantified by real-time quantitative PCR on an ABI PRISM 7900HT with Applied Biosystem predesigned TaqMan Gene expression Assays and reagents according to the manufacturer's instructions. The following probe was used (identified by Applied Biosystem assay identification number): *P2RX7* (Hs00175721_m1). For each sample, mRNA abundance was normalized to the amount of TBP (TAT-box binding protein, Hs00427620_m1), used as gene reference, and expressed as arbitrary units (A.U.).

Meta-analysis of gene-expression data in CD4 cells

All data were measured on Affymetrix arrays and have been downloaded from Gene Expression Omnibus (GEO) (http://www.ncbi.nlm.nih.gov/geo). The following series of GEO data were used: GSE46892 (Huang et al., 2014), GSE49314 (Weber et al., 2015), GSE56883 (Moriyama et al., 2014), GSE21381 (Yusuf et al., 2010), GSE24574 (Kitano et al., 2011). Microarray probe fluorescence signals were converted to log2 expression values using the Robust Multiarray Average procedure (Irizarry et al., 2003) of the affy Bioconductor package. Fluorescence intensities were background-adjusted and normalized using quantile normalization, and expression values were calculated using median polish summarization and custom chip definition files for a total of 18139 custom probe sets for Mouse Genome 430 2.0 Array based on Entrez genes (Mouse4302_Mm_ENTREZG version 21.0.0). All data analyses were performed in R version 3.3.3 using Bioconductor libraries and R statistical packages. The expression change of any caspase was quantified as the difference between its log2 expression level in any sample of Tfh cells and its average log2 gene expression signal in naïve CD4 cells (log2 fold-change).

Principal component analysis (PCA)

Principal component analysis was performed using the "prcomp{stats}" method in R, and visualized with ggplot2 library. Datasets were pruned for missing values before analysis, thus a total of 77 samples were used for PCA (28 HD, 14 PAPS, 35 SLE). The percent contributions of each variable to the segregation process were determined as cumulative sum of absolute values of the PCA loadings, which are an estimate of how much each variable used in the PCA analysis contribute to each of the new variables (the principal components) after the PCA transformation.

Statistical analysis

Statistical analysis was performed with the Prism software (GraphPad). Results were analyzed using the nonparametric Mann Whitney test, Student's unpaired t test and two-way ANOVA with Bonferroni post-test analysis, as indicated. Results are presented as mean ± SEM. Values of p were indicated throughout as *: $p < 0.05$, **: $p < 0.01$, ***: $p < 0.001$ and ****: $p < 0.0001$; ns: non-significant.

Online supplemental material

Fig. S1 shows the phenotypic analysis of B cells in WT and *P2rx7*$^{-/-}$ mice. Fig. S2 shows the distribution of CD4^{+} T cells for CD44 and CD62L as well as frequencies of Tregs and Tfr in untreated and treated WT and *P2rx7*$^{-/-}$ mice. Fig. S3 shows the increase of ICOS^{+} CD4 T cells in kidneys and IFN-γ secreting CD4 cells selectively within ICOS^{+} cells in pristane treated *P2rx7*$^{-/-}$ mice. Fig. S4 shows the increased representation of CCR7$^{lo/-}$PD-1^{hi} CD4 cells in pristane treated *P2rx7*$^{-/-}$ mice, the distribution of functional cTfh cell subsets and *P2RX7* mRNA levels in CXCR5^{+} cells from HD, SLE and PAPS patients, and the inhibition of CCR7$^{lo/-}$PD-1^{hi} Tfh cells proliferation by BzATP. Table S1 lists the demographic, clinical and laboratory characteristics of SLE and PAPS patients and healthy donors

ACKNOWLEDGMENTS

We thank David Jarrossay (IRB) for cell sorting and helpful discussion, Rocco D'Antuono (IRB) for help with confocal microscopy and generation of images, Bianca Calí (University of Padua, Italy) for advice on immunofluorescence and discussion, the NIH Tetramer Core Facility for providing tetramers. The work was supported by grant 310030-159491 of the Swiss National Science Foundation and grant of Fondazione per la Ricerca sulla Trasfusione e sui Trapianti to F.G. R.G. was supported by a fellowship from Società Italiana di Reumatologia. The PhD fellowship of L.P. was supported by Signora Alessandra.

The authors declare non competing financial interests.

Author contributions: F.G., C.E.F., E.T. and P.L.M. designed experiments. C.E.F. performed most experiments. E.R., L.P. and A.R. performed experiments. F.G. and C.E.F. analysed data. G.P. performed histopathological analysis. M.G. and R.G. selected and provided human samples. R.R. performed PCA. E.M.C.M. and S.B. performed meta-analysis of gene expression. C.E.F. prepared the figures. F.G. supervised the study and wrote the paper with contribution by C.E.F.

REFERENCES

Andreoli, L., C.B. Chighizola, C. Nalli, M. Gerosa, M.O. Borghi, F. Pregnolato, C. Grossi, A. Zanola, F. Allegri, G.L. Norman, M. Mahler, P.L. Meroni, and A. Tincani. 2015. Clinical characterization of antiphospholipid syndrome by detection of IgG antibodies against beta2 - glycoprotein i domain 1 and domain 4/5: ratio of anti-domain 1 to anti-domain 4/5 as a useful new biomarker for antiphospholipid syndrome. *Arthritis & rheumatology* 67:2196-2204.

Arbuckle, M.R., M.T. McClain, M.V. Rubertone, R.H. Scofield, G.J. Dennis, J.A. James, and J.B. Harley. 2003. Development of autoantibodies before the clinical onset of systemic lupus erythematosus. *The New England journal of medicine* 349:1526-1533.

Blanco, P., H. Ueno, and N. Schmitt. 2016. T follicular helper (Tfh) cells in lupus: Activation and involvement in SLE pathogenesis. *European journal of immunology* 46:281-290.

Chen, G.M., C.C. Feng, Q.L. Ye, J.H. Tao, R. Li, H. Peng, M. Zhou, R.X. Leng, J. Li, H. Cen, Y.G. Fan, H.F. Pan, and D.Q. Ye. 2013. Association of P2X7R gene polymorphisms with systemic lupus erythematosus in a Chinese population. *Mutagenesis* 28:351-355.

Choi, J.Y., J.H. Ho, S.G. Pasoto, V. Bunin, S.T. Kim, S. Carrasco, E.F. Borba, C.R. Goncalves, P.R. Costa, E.G. Kallas, E. Bonfa, and J. Craft. 2015. Circulating follicular helper-like T cells in systemic lupus erythematosus: association with disease activity. *Arthritis & rheumatology* 67:988-999.

Choi, Y.S., R. Kageyama, D. Eto, T.C. Escobar, R.J. Johnston, L. Monticelli, C. Lao, and S. Crotty. 2011. ICOS receptor instructs T follicular helper cell versus effector cell differentiation via induction of the transcriptional repressor Bcl6. *Immunity* 34:932-946.

Chung, Y., S. Tanaka, F. Chu, R.I. Nurieva, G.J. Martinez, S. Rawal, Y.H. Wang, H. Lim, J.M. Reynolds, X.H. Zhou, H.M. Fan, Z.M. Liu, S.S. Neelapu, and C. Dong. 2011. Follicular regulatory T cells expressing Foxp3 and Bcl-6 suppress germinal center reactions. *Nat Med* 17:983-988.

Cohen, R.A., G. Bayliss, J.C. Crispin, G.F. Kane-Wanger, C.A. Van Beek, V.C. Kyttaris, I. Avalos, C.Y. Yu, G.C. Tsokos, and I.E. Stillman. 2008. T cells and in situ cryoglobulin deposition in the pathogenesis of lupus nephritis. *Clinical immunology* 128:1-7.

Craft, J.E. 2012. Follicular helper T cells in immunity and systemic autoimmunity. *Nature reviews. Rheumatology* 8:337-347.

Crotty, S. 2014. T follicular helper cell differentiation, function, and roles in disease. *Immunity* 41:529-542.

Ding, Y., J. Li, Q. Wu, P. Yang, B. Luo, S. Xie, K.M. Druey, A.J. Zajac, H.C. Hsu, and J.D. Mountz. 2013. IL-17RA is essential for optimal localization of follicular Th cells in the germinal center light zone to promote autoantibody-producing B cells. *Journal of immunology* 191:1614-1624.

Domeier, P.P., S.B. Chodisetti, C. Soni, S.L. Schell, M.J. Elias, E.B. Wong, T.K. Cooper, D. Kitamura, and Z.S. Rahman. 2016. IFN-gamma receptor and STAT1 signaling in B cells are central to spontaneous germinal center formation and autoimmunity. *The Journal of experimental medicine* 213:715-732.

Ferrari, D., C. Pizzirani, E. Adinolfi, R.M. Lemoli, A. Curti, M. Idzko, E. Panther, and F. Di Virgilio. 2006. The P2X7 receptor: a key player in IL-1 processing and release. *Journal of immunology* 176:3877-3883.

Geginat, J., F. Sallusto, and A. Lanzavecchia. 2001. Cytokine-driven proliferation and differentiation of human naive, central memory, and effector memory CD4(+) T cells. *The Journal of experimental medicine* 194:1711-1719.

Gladman, D.D., D. Ibanez, and M.B. Urowitz. 2002. Systemic lupus erythematosus disease activity index 2000. *The Journal of rheumatology* 29:288-291.

Havenar-Daughton, C., M. Lindqvist, A. Heit, J.E. Wu, S.M. Reiss, K. Kendric, S. Belanger, S.P. Kasturi, E. Landais, R.S. Akondy, H.M. McGuire, M. Bothwell, P.A. Vagefi, E. Scully, I.P.C.P. Investigators, G.D. Tomaras, M.M. Davis, P. Poignard, R. Ahmed, B.D. Walker, B. Pulendran, M.J. McElrath, D.E. Kaufmann, and S. Crotty. 2016. CXCL13 is a plasma biomarker of germinal center activity. *Proceedings of the National Academy of Sciences of the United States of America* 113:2702-2707.

He, J., L.M. Tsai, Y.A. Leong, X. Hu, C.S. Ma, N. Chevalier, X. Sun, K. Vandenberg, S. Rockman, Y. Ding, L. Zhu, W. Wei, C. Wang, A. Karnowski, G.T. Belz, J.R. Ghali, M.C. Cook, D.S. Riminton, A. Veillette, P.L. Schwartzberg, F. Mackay, R. Brink, S.G. Tangye, C.G. Vinuesa, C.R. Mackay, Z. Li, and D. Yu. 2013. Circulating precursor CCR7(lo)PD-1(hi) CXCR5(+) CD4(+) T cells indicate Tfh cell activity and promote antibody responses upon antigen reexposure. *Immunity* 39:770-781.

Her, M., D. Kim, M. Oh, H. Jeong, and I. Choi. 2009. Increased expression of soluble inducible costimulator ligand (ICOSL) in patients with systemic lupus erythematosus. *Lupus* 18:501-507.

Hochberg, M.C. 1997. Updating the American College of Rheumatology revised criteria for the classification of systemic lupus erythematosus. *Arthritis and rheumatism* 40:1725.

Huang, W., Q. Qi, J. Hu, F. Huang, T.M. Laufer, and A. August. 2014. Dendritic cell-MHC class II and Itk regulate functional development of regulatory innate memory CD4+ T cells in bone marrow transplantation. *Journal of immunology* 192:3435-3441.

Hutloff, A., K. Buchner, K. Reiter, H.J. Baelde, M. Odendahl, A. Jacobi, T. Dorner, and R.A. Kroczek. 2004. Involvement of inducible costimulator in the exaggerated memory B cell and plasma cell generation in systemic lupus erythematosus. *Arthritis and rheumatism* 50:3211-3220.

Ingegnoli, F., R. Gualtierotti, T. Schioppo, A. Orenti, P. Boracchi, C. Lubatti, C. Mastaglio, V. Galbiati, A. Murgo, S. Zeni, C. Grossi, O. Borghi, W. Rosenberg, L. Castelnovo, and L. Meroni Pier. 2014. Fibrosis biomarkers in isolated Raynaud's phenomenon: too little, too soon? *Annals of the rheumatic diseases* 73:940-941.

Irizarry, R.A., B. Hobbs, F. Collin, Y.D. Beazer-Barclay, K.J. Antonellis, U. Scherf, and T.P. Speed. 2003. Exploration, normalization, and summaries of high density oligonucleotide array probe level data. *Biostatistics* 4:249-264.

Iwai, H., M. Abe, S. Hirose, F. Tsushima, K. Tezuka, H. Akiba, H. Yagita, K. Okumura, H. Kohsaka, N. Miyasaka, and M. Azuma. 2003. Involvement of inducible costimulator-B7 homologous protein costimulatory pathway in murine lupus nephritis. *Journal of immunology* 171:2848-2854.

Jackson, S.W., H.M. Jacobs, T. Arkatkar, E.M. Dam, N.E. Scharping, N.S. Kolhatkar, B. Hou, J.H. Buckner, and D.J. Rawlings. 2016. B cell IFN-gamma receptor signaling promotes autoimmune germinal centers via cell-intrinsic induction of BCL-6. *The Journal of experimental medicine* 213:733-750.

Kayagaki, N., I.B. Stowe, B.L. Lee, K. O'Rourke, K. Anderson, S. Warming, T. Cuellar, B. Haley, M. Roose-Girma, Q.T. Phung, P.S. Liu, J.R. Lill, H. Li, J. Wu, S. Kummerfeld, J. Zhang, W.P. Lee, S.J. Snipas, G.S. Salvesen, L.X. Morris, L. Fitzgerald, Y. Zhang, E.M. Bertram, C.C. Goodnow, and V.M. Dixit. 2015. Caspase-11 cleaves gasdermin D for non-canonical inflammasome signalling. *Nature* 526:666-671.

Khadra, A., M. Tomic, Z. Yan, H. Zemkova, A. Sherman, and S.S. Stojilkovic. 2013. Dual gating mechanism and function of P2X7 receptor channels. *Biophysical journal* 104:2612-2621.

Kim, Y.U., H. Lim, H.E. Jung, R.A. Wetsel, and Y. Chung. 2015. Regulation of autoimmune germinal center reactions in lupus-prone BXD2 mice by follicular helper T cells. *PloS one* 10:e0120294.

Kitano, M., S. Moriyama, Y. Ando, M. Hikida, Y. Mori, T. Kurosaki, and T. Okada. 2011. Bcl6 protein expression shapes pre-germinal center B cell dynamics and follicular helper T cell heterogeneity. *Immunity* 34:961-972.

Le Coz, C., A. Joublin, J.L. Pasquali, A.S. Korganow, H. Dumortier, and F. Monneaux. 2013. Circulating TFH subset distribution is strongly affected in lupus patients with an active disease. *PloS one* 8:e75319.

Le Gall, S.M., J. Legrand, M. Benbijja, H. Safya, K. Benihoud, J.M. Kanellopoulos, and P. Bobe. 2012. Loss of P2X7 receptor plasma membrane expression and function in pathogenic B220+ double-negative T lymphocytes of autoimmune MRL/lpr mice. *PloS one* 7:e52161.

Lee, S.K., D.G. Silva, J.L. Martin, A. Pratama, X. Hu, P.P. Chang, G. Walters, and C.G. Vinuesa. 2012. Interferon-gamma excess leads to pathogenic accumulation of follicular helper T cells and germinal centers. *Immunity* 37:880-892.

Linterman, M.A., W. Pierson, S.K. Lee, A. Kallies, S. Kawamoto, T.F. Rayner, M. Srivastava, D.P. Divekar, L. Beaton, J.J. Hogan, S. Fagarasan, A. Liston, K.G. Smith, and C.G. Vinuesa. 2011. Foxp3+ follicular regulatory T cells control the germinal center response. *Nat Med* 17:975-982.

Locci, M., J.E. Wu, F. Arumemi, Z. Mikulski, C. Dahlberg, A.T. Miller, and S. Crotty. 2016. Activin A programs the differentiation of human TFH cells. *Nature immunology* 17:976-984.

McGuire, H.M., A. Vogelzang, C.S. Ma, W.E. Hughes, P.A. Silveira, S.G. Tangye, D. Christ, D. Fulcher, M. Falcone, and C. King. 2011. A subset of interleukin-21+ chemokine receptor CCR9+ T helper cells target accessory organs of the digestive system in autoimmunity. *Immunity* 34:602-615.

Miyakis, S., M.D. Lockshin, T. Atsumi, D.W. Branch, R.L. Brey, R. Cervera, R.H. Derksen, D.E.G. PG, T. Koike, P.L. Meroni, G. Reber, Y. Shoenfeld, A. Tincani, P.G. Vlachoyiannopoulos, and S.A. Krilis. 2006. International consensus statement on an update of the classification criteria for definite antiphospholipid syndrome (APS). *Journal of thrombosis and haemostasis : JTH* 4:295-306.

Moriyama, S., N. Takahashi, J.A. Green, S. Hori, M. Kubo, J.G. Cyster, and T. Okada. 2014. Sphingosine-1-phosphate receptor 2 is critical for follicular helper T cell retention in germinal centers. *The Journal of experimental medicine* 211:1297-1305.

Nacionales, D.C., J.S. Weinstein, X.J. Yan, E. Albesiano, P.Y. Lee, K.M. Kelly-Scumpia, R. Lyons, M. Satoh, N. Chiorazzi, and W.H. Reeves. 2009. B cell proliferation, somatic hypermutation, class switch recombination, and autoantibody production in ectopic lymphoid tissue in murine lupus. *Journal of immunology* 182:4226-4236.

Nath, S.K., A.I. Quintero-Del-Rio, J. Kilpatrick, L. Feo, M. Ballesteros, and J.B. Harley. 2004. Linkage at 12q24 with systemic lupus erythematosus (SLE) is established and confirmed in Hispanic and European American families. *American journal of human genetics* 74:73-82.

Nurieva, R.I., Y. Chung, D. Hwang, X.O. Yang, H.S. Kang, L. Ma, Y.H. Wang, S.S. Watowich, A.M. Jetten, Q. Tian, and C. Dong. 2008. Generation of T follicular helper cells is mediated by interleukin-21 but independent of T helper 1, 2, or 17 cell lineages. *Immunity* 29:138-149.

Odegard, J.M., L.D. DiPlacido, L. Greenwald, M. Kashgarian, D.H. Kono, C. Dong, R.A. Flavell, and J. Craft. 2009. ICOS controls effector function but not trafficking receptor expression of kidney-infiltrating effector T cells in murine lupus. *Journal of immunology* 182:4076-4084.

Odegard, J.M., B.R. Marks, L.D. DiPlacido, A.C. Poholek, D.H. Kono, C. Dong, R.A. Flavell, and J. Craft. 2008. ICOS-dependent extrafollicular helper T cells elicit IgG production via IL-21 in systemic autoimmunity. *The Journal of experimental medicine* 205:2873-2886.

Ohl, K., and K. Tenbrock. 2015. Regulatory T cells in systemic lupus erythematosus. *European journal of immunology* 45:344-355.

Pepper, M., A.J. Pagan, B.Z. Igyarto, J.J. Taylor, and M.K. Jenkins. 2011. Opposing signals from the Bcl6 transcription factor and the interleukin-2 receptor generate T helper 1 central and effector memory cells. *Immunity* 35:583-595.

Poholek, A.C., K. Hansen, S.G. Hernandez, D. Eto, A. Chandele, J.S. Weinstein, X. Dong, J.M. Odegard, S.M. Kaech, A.L. Dent, S. Crotty, and J. Craft. 2010. In vivo regulation of Bcl6 and T follicular helper cell development. *Journal of immunology* 185:313-326.

Portales-Cervantes, L., P. Nino-Moreno, L. Doniz-Padilla, L. Baranda-Candido, M. Garcia-Hernandez, M. Salgado-Bustamante, R. Gonzalez-Amaro, and D. Portales-Perez. 2010. Expression and function of the P2X(7) purinergic receptor in patients with systemic lupus erythematosus and rheumatoid arthritis. *Human immunology* 71:818-825.

Proietti, M., V. Cornacchione, T. Rezzonico Jost, A. Romagnani, C.E. Faliti, L. Perruzza, R. Rigoni, E. Radaelli, F. Caprioli, S. Preziuso, B. Brannetti, M. Thelen, K.D. McCoy, E. Slack, E. Traggiai, and F. Grassi. 2014. ATP-gated ionotropic P2X7 receptor controls follicular T helper cell numbers in Peyer's patches to promote host-microbiota mutualism. *Immunity* 41:789-801.

Reeves, W.H., P.Y. Lee, J.S. Weinstein, M. Satoh, and L. Lu. 2009. Induction of autoimmunity by pristane and other naturally occurring hydrocarbons. *Trends in immunology* 30:455-464.

Ruiz-Irastorza, G., M. Crowther, W. Branch, and M.A. Khamashta. 2010. Antiphospholipid syndrome. *Lancet* 376:1498-1509.

Satoh, M., and W.H. Reeves. 1994. Induction of lupus-associated autoantibodies in BALB/c mice by intraperitoneal injection of pristane. *The Journal of experimental medicine* 180:2341-2346.

Schenk, U., M. Frascoli, M. Proietti, R. Geffers, E. Traggiai, J. Buer, C. Ricordi, A.M. Westendorf, and F. Grassi. 2011. ATP inhibits the generation and function of regulatory T cells through the activation of purinergic P2X receptors. *Sci Signal* 4:ra12.

Schindelin, J., I. Arganda-Carreras, E. Frise, V. Kaynig, M. Longair, T. Pietzsch, S. Preibisch, C. Rueden, S. Saalfeld, B. Schmid, J.Y. Tinevez, D.J. White, V. Hartenstein, K. Eliceiri, P. Tomancak, and A. Cardona. 2012. Fiji: an open-source platform for biological-image analysis. *Nature methods* 9:676-682.

Shi, J., Y. Zhao, K. Wang, X. Shi, Y. Wang, H. Huang, Y. Zhuang, T. Cai, F. Wang, and F. Shao. 2015. Cleavage of GSDMD by inflammatory caspases determines pyroptotic cell death. *Nature* 526:660-665.

Stokes, L., S.J. Fuller, R. Sluyter, K.K. Skarratt, B.J. Gu, and J.S. Wiley. 2010. Two haplotypes of the P2X(7) receptor containing the Ala-348 to Thr polymorphism exhibit a gain-of-function effect and enhanced interleukin-1beta secretion. *FASEB journal : official publication of the Federation of American Societies for Experimental Biology* 24:2916-2927.

Taylor, S.R., M. Gonzalez-Begne, S. Dewhurst, G. Chimini, C.F. Higgins, J.E. Melvin, and J.I. Elliott. 2008. Sequential shrinkage and swelling underlie P2X7-stimulated lymphocyte phosphatidylserine exposure and death. *Journal of immunology* 180:300-308.

Teichmann, L.L., J.L. Cullen, M. Kashgarian, C. Dong, J. Craft, and M.J. Shlomchik. 2015. Local triggering of the ICOS coreceptor by CD11c(+) myeloid cells drives organ inflammation in lupus. *Immunity* 42:552-565.

Ueno, H., J. Banchereau, and C.G. Vinuesa. 2015. Pathophysiology of T follicular helper cells in humans and mice. *Nature immunology* 16:142-152.

Vinuesa, C.G., M.C. Cook, C. Angelucci, V. Athanasopoulos, L. Rui, K.M. Hill, D. Yu, H. Domaschenz, B. Whittle, T. Lambe, I.S. Roberts, R.R. Copley, J.I. Bell, R.J. Cornall, and C.C. Goodnow. 2005. A RING-type ubiquitin ligase family member required to repress follicular helper T cells and autoimmunity. *Nature* 435:452-458.

Vono, M., M. Taccone, P. Caccin, M. Gallotta, G. Donvito, S. Falzoni, E. Palmieri, M. Pallaoro, R. Rappuoli, F. Di Virgilio, E. De Gregorio, C. Montecucco, and A. Seubert. 2013. The adjuvant MF59 induces ATP release from muscle that potentiates response to vaccination. *Proceedings of the National Academy of Sciences of the United States of America* 110:21095-21100.

Wang, B., Y. Yamamoto, N.S. El-Badri, and R.A. Good. 1999. Effective treatment of autoimmune disease and progressive renal disease by mixed bone-marrow transplantation that establishes a stable mixed chimerism in BXSB recipient mice. *Proceedings of the National Academy of Sciences of the United States of America* 96:3012-3016.

Weber, J.P., F. Fuhrmann, R.K. Feist, A. Lahmann, M.S. Al Baz, L.J. Gentz, D. Vu Van, H.W. Mages, C. Haftmann, R. Riedel, J.R. Grun, W. Schuh, R.A. Kroczek, A. Radbruch, M.F. Mashreghi, and A. Hutloff. 2015. ICOS maintains the T follicular helper cell phenotype by down-regulating Kruppel-like factor 2. *The Journal of experimental medicine* 212:217-233.

Weinstein, J.S., M.J. Delano, Y. Xu, K.M. Kelly-Scumpia, D.C. Nacionales, Y. Li, P.Y. Lee, P.O. Scumpia, L. Yang, E. Sobel, L.L. Moldawer, and W.H. Reeves. 2013. Maintenance of anti-Sm/RNP autoantibody production by plasma cells residing in ectopic lymphoid tissue and bone marrow memory B cells. *Journal of immunology* 190:3916-3927.

Wilhelm, K., J. Ganesan, T. Muller, C. Durr, M. Grimm, A. Beilhack, C.D. Krempl, S. Sorichter, U.V. Gerlach, E. Juttner, A. Zerweck, F. Gartner, P. Pellegatti, F. Di Virgilio, D. Ferrari, N. Kambham, P. Fisch, J. Finke, M. Idzko, and R. Zeiser. 2010. Graft-versus-host disease is enhanced by extracellular ATP activating P2X7R. *Nat Med* 16:1434-1438.

Wollenberg, I., A. Agua-Doce, A. Hernandez, C. Almeida, V.G. Oliveira, J. Faro, and L. Graca. 2011. Regulation of the germinal center reaction by Foxp3+ follicular regulatory T cells. *Journal of immunology* 187:4553-4560.

Xu, H., X. Li, D. Liu, J. Li, X. Zhang, X. Chen, S. Hou, L. Peng, C. Xu, W. Liu, L. Zhang, and H. Qi. 2013. Follicular T-helper cell recruitment governed by bystander B cells and ICOS-driven motility. *Nature* 496:523-527.

Yang, X., J. Yang, Y. Chu, J. Wang, M. Guan, X. Zhu, Y. Xue, and H. Zou. 2013. T follicular helper cells mediate expansion of regulatory B cells via IL-21 in Lupus-prone MRL/lpr mice. *PloS one* 8:e62855.

Yu, D., and C.G. Vinuesa. 2010. Multiple checkpoints keep follicular helper T cells under control to prevent autoimmunity. *Cellular & molecular immunology* 7:198-203.

Yusuf, I., R. Kageyama, L. Monticelli, R.J. Johnston, D. Ditoro, K. Hansen, B. Barnett, and S. Crotty. 2010. Germinal center T follicular helper cell IL-4 production is dependent on signaling lymphocytic activation molecule receptor (CD150). *Journal of immunology* 185:190-202.

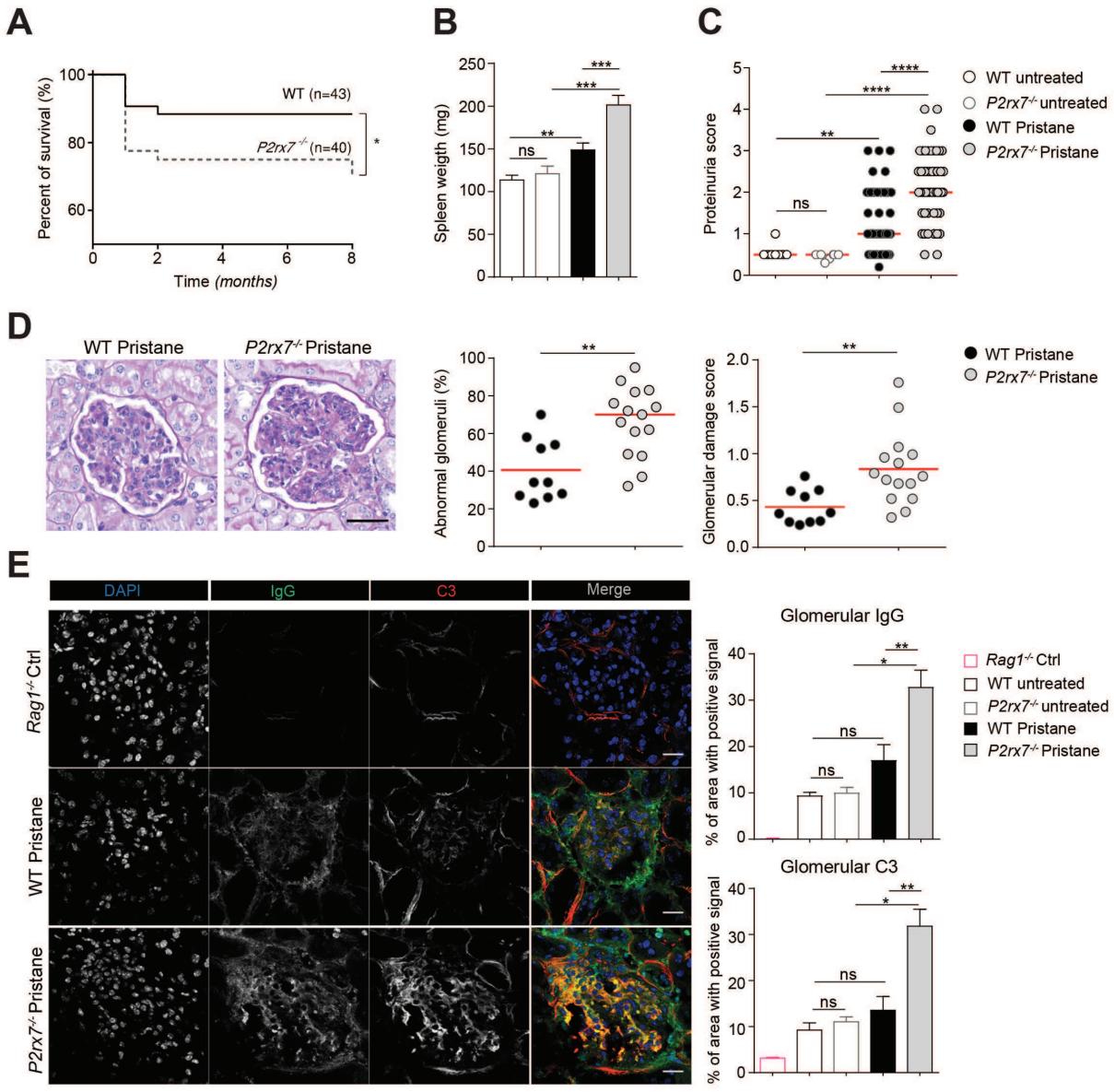

Figure 1. Increased mortality and lupus nephritis severity in *P2rx7*$^{-/-}$ mice. (**A**) WT (black line) and *P2rx7*$^{-/-}$ (grey dashed line) mice were observed until the time of sacrifice. *p=0.0403 by log-rank test. (**B**) Spleen weight of untreated WT (n=7), *P2rx7*$^{-/-}$ (n=6), pristane-treated WT (n=19) and *P2rx7*$^{-/-}$ (n=18) mice. (**C**) Proteinuria score of pristane-treated WT and *P2rx7*$^{-/-}$ mice. Each dot represents an individual mouse and horizontal lines median values. (**D**) Representative pristane-induced glomerular injury in PAS-stained kidney sections (scale bar: 50 µm) with proportion of affected glomeruli (left graph) and glomerular injury score (right graph). (**E**) Confocal microscopy of kidneys stained for IgG (green) and complement C3 (red) to detect glomerular immune deposits. *Rag1*$^{-/-}$ mice were used as negative control for IgG staining (scale bar: 20 µm). Histograms show means ± SEM for glomerular IgG (top) and C3 depositions (bottom) of 3 independent experiments. All data are from mice at 33 weeks post-injection. Two-tailed Mann-Whitney U test. *p<0.05, **p<0.01, ***p < 0.001, ****p < 0.0001.

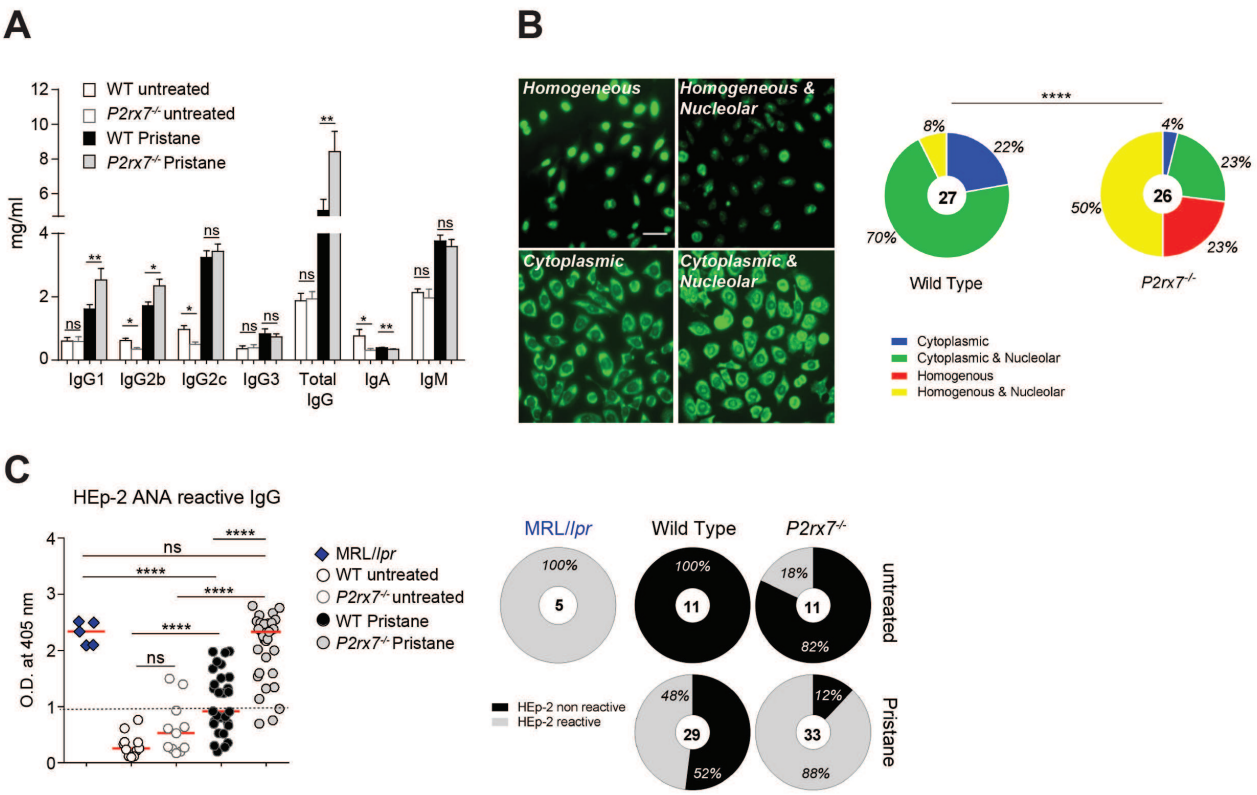

Figure 2. Increased serum autoantibodies in *P2rx7*$^{-/-}$ mice. (**A**) Serum Ig isotype concentrations in untreated (n=6 for IgM and IgA, n=16 for total IgG, n=12 for IgG subclasses) and pristane treated (n=15 for IgM and IgA, n=40 for total IgG, n=15 for IgG subclasses) mice determined by ELISA. Data are represented as mean ± SEM. Two-tailed nonparametric Mann-Whitney U test. (**B**) Representative immunofluorescence of HEp-2 cells and relative distribution of ANA IgG staining patterns with sera from pristane-treated WT and *P2rx7*$^{-/-}$ mice. Scale bar: 50 µm. The number in the circle indicates the number of analyzed mice. Fisher's exact test with Chi-square. (**C**) ELISA (QUANTA-Lite ANA) for the semi-quantitative detection of self-reactive IgG. Each dot represents an individual mouse. MRL/*lpr* sera were used as positive controls. Two-tailed Mann-Whitney U test. Distribution of sera from the indicated mice as non-reactive or reactive in the assay is shown.

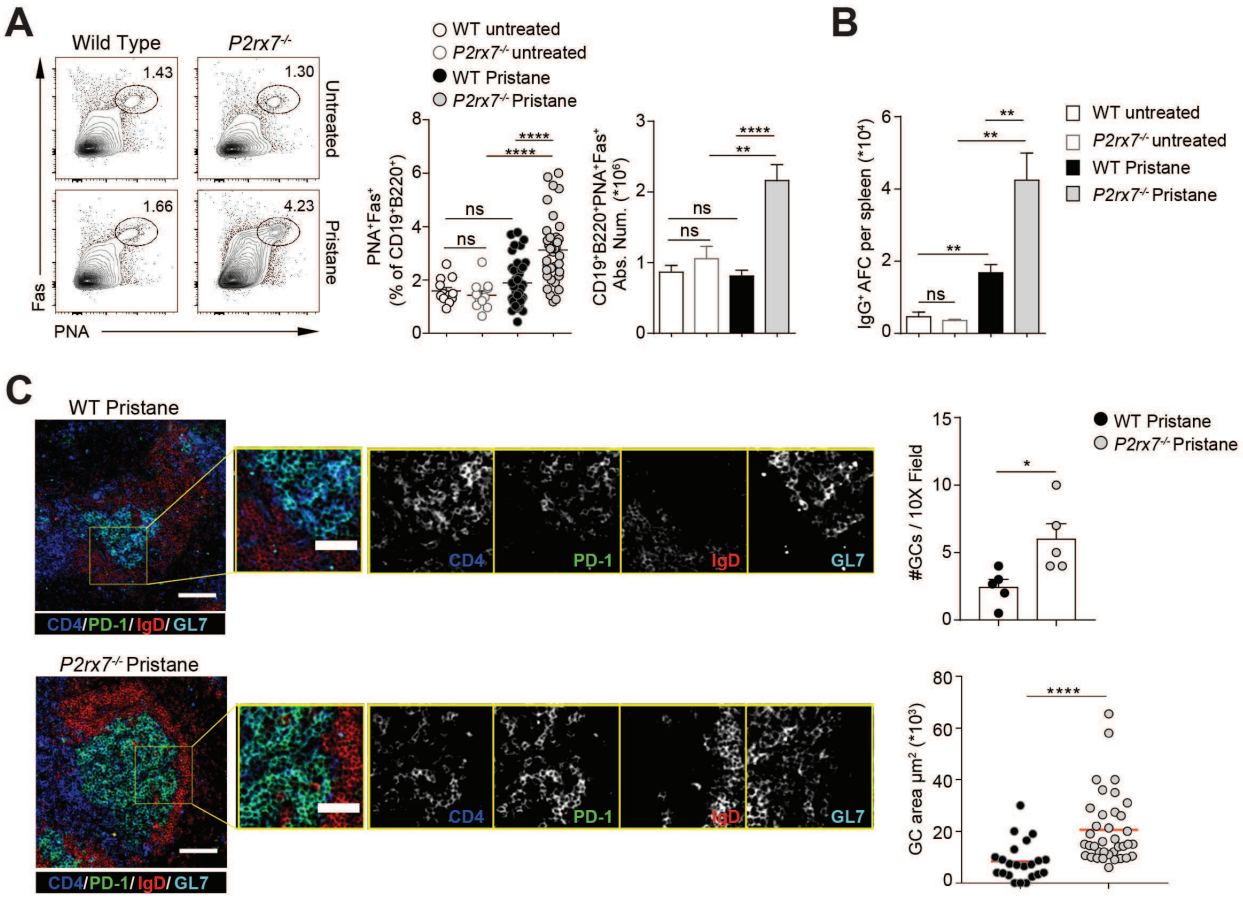

Figure 3. Increased germinal center reaction and splenic plasma cells in *P2rx7*$^{-/-}$ mice. (**A**) Representative contour plots for PNA and Fas staining on gated CD19^{+}B220^{+} splenocytes, frequency and absolute number in untreated (n=12) and treated (n=37) WT as well as *P2rx7*$^{-/-}$ mice. (**B**) Absolute number of IgG-secreting cells by ELISpot assay in spleens from the indicated mice. Mean ± SEM of 3 independent experiments. (**C**) Representative images of spleen sections from pristane treated WT and *P2rx7*$^{-/-}$ mice stained with anti-IgD, -CD4, -GL-7 and -PD-1 antibodies (scale bar: 100 µm) and inset zooming on GC cells (scale bar: 50 µm). The number of GCs per field at 10-fold magnification in individual mice and GC areas in WT and *P2rx7*$^{-/-}$ mice are shown in right panels. Two-tailed Mann-Whitney U test. Mean ± SEM are shown in bar graphs. *p < 0.05, **p<0.01, ****p < 0.0001.

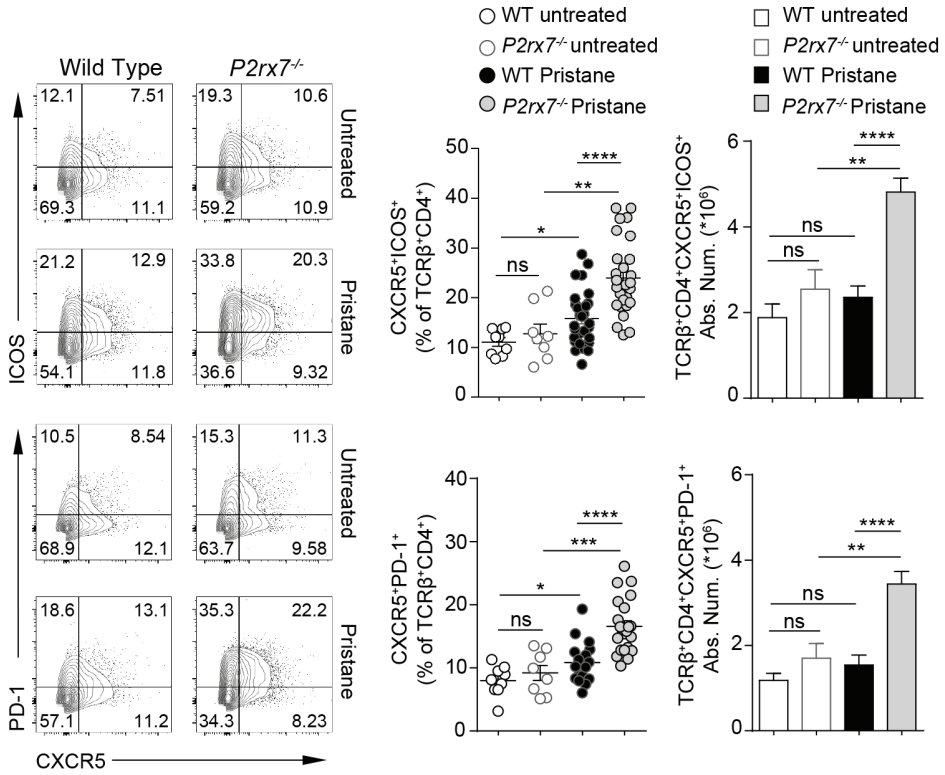

Figure 4. Enhanced CD4 cells activation in *P2rx7*$^{-/-}$ mice. Representative contour plots, frequency and absolute number of CXCR5^{+}ICOS^{+} and CXCR5^{+}PD-1^{+} cells [untreated WT (n=10), *P2rx7*$^{-/-}$ (n=9), treated WT (n=30) and *P2rx7*$^{-/-}$ (n=34) mice] and PD-1 [untreated WT (n=9), *P2rx7*$^{-/-}$ (n=8), treated WT (n=17) and *P2rx7*$^{-/-}$ (n=22) mice] within gated TCRβ^{+}CD4^{+} splenocytes. Bar graphs: mean ± SEM. Two-tailed Mann-Whitney U test. *p<0.05; **p<0.01; ***p<0.001; ****p<0.0001.

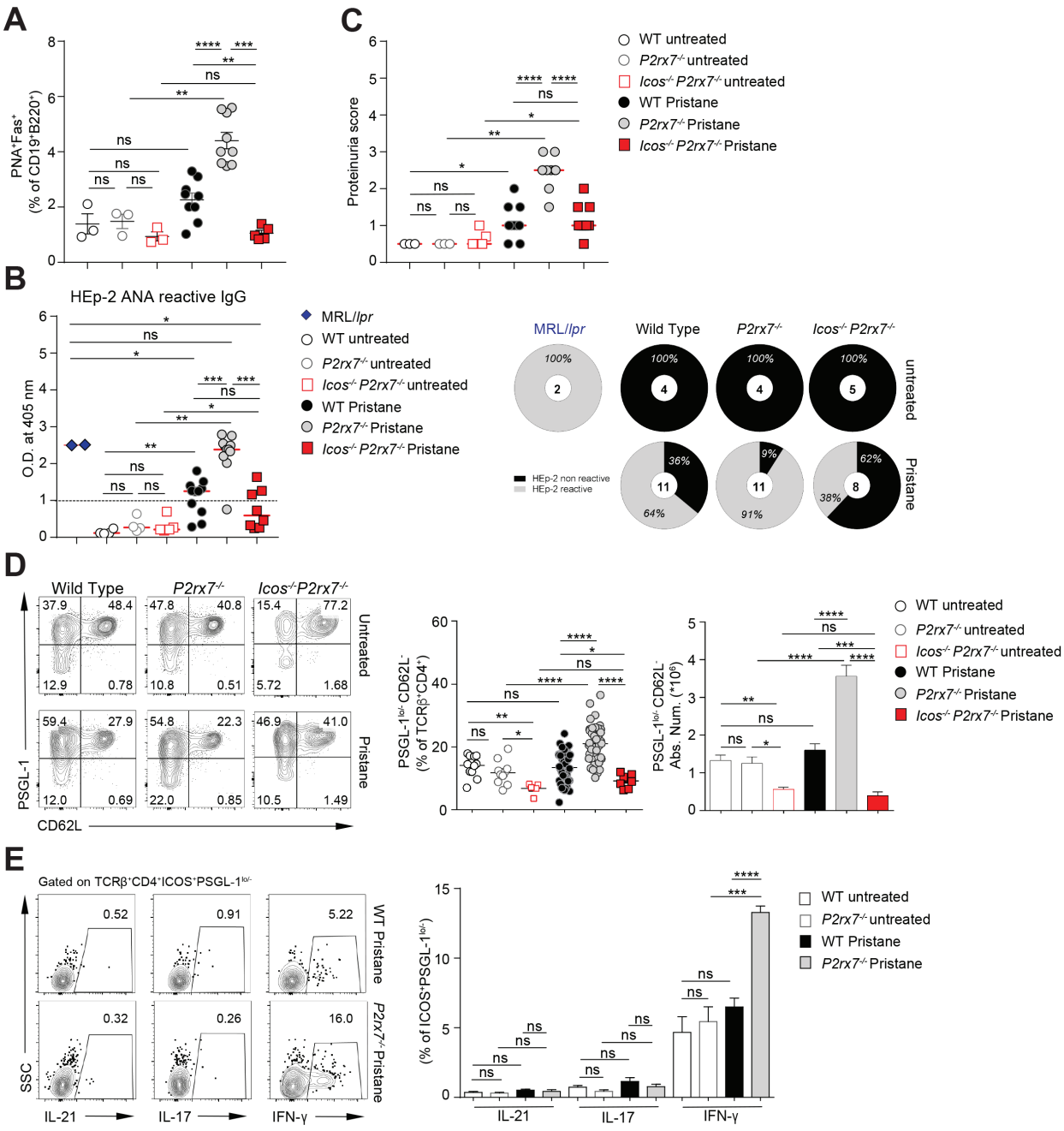

Figure 5. P2X7-mediated control of PSGL-1 downregulation and IFN-γ secretion in pristane treated mice. (**A**) Frequency of $PNA^{+}Fas^{+}$ GC splenic B cells, (**B**) serum ANA IgG detection by ELISA and (**C**) proteinuria score in the indicated mice at 33 wk after pristane injection. (**D**) Representative contour plots for PSGL-1 and CD62L on splenic $CD4^{+}$ T cells, frequency and absolute number (mean ± SEM) of $PSGL1^{lo/-}CD62L^{-}$ cells from untreated WT (n=12), *P2rx7*$^{-/-}$ (n=10), *Icos*$^{-/-}$ *P2rx7*$^{-/-}$ (n=5), treated WT (n=38), *P2rx7*$^{-/-}$ (n=37) and *Icos*$^{-/-}$*P2rx7*$^{-/-}$ (n=8) mice. (**E**) Contour plots show representative intracellular staining for IL-21, IL-17 and IFN-γ on gated $CD4^{+}ICOS^{+}PSGL1^{lo/-}$ cells from spleens of treated WT and *P2rx7*$^{-/-}$ mice. Statistics from three independent experiments is shown (mean ± SEM, untreated mice, n= at least 4; treated mice, n= at least 8). Two-tailed Mann-Whitney U test. *p<0.05; **p<0.01; ***p<0.001; ****p<0.0001.

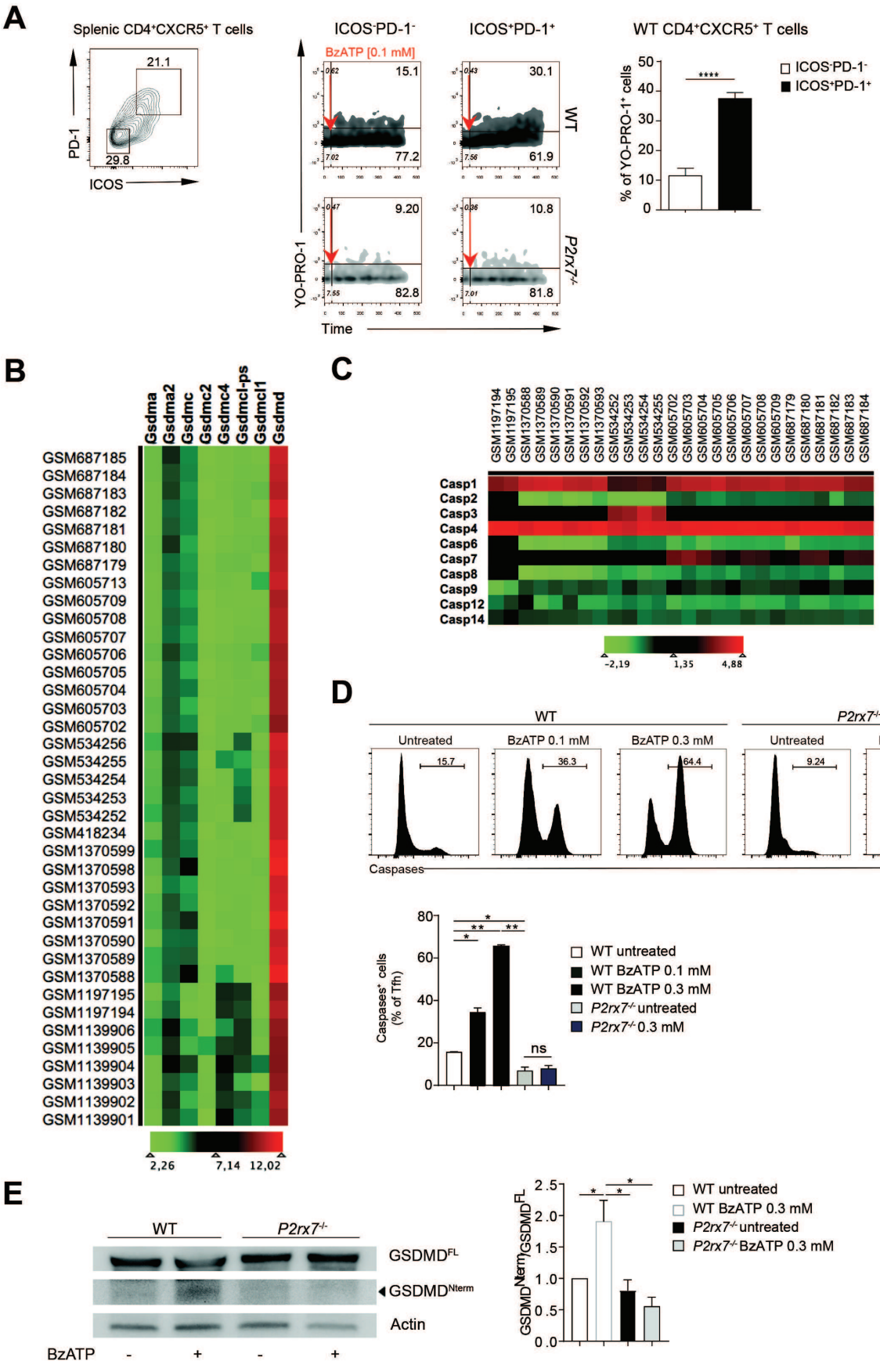
A
Splenic CD4+CXCR5+ T cells
21.1
29.8
PD-1
ICOS
ICOS-PD-1-
ICOS+PD-1+
BzATP [0.1 mM]
15.1
77.2
30.1
61.9
WT
9.20
82.8
10.8
81.8
P2rx7-/-
YO-PRO-1
Time
WT CD4+CXCR5+ T cells
% of YO-PRO-1+ cells
****
ICOS-PD-1-
ICOS+PD-1+
B
Gsdma
Gsdma2
Gsdmc
Gsdmc2
Gsdmc4
Gsdmcl-ps
Gsdmcl1
Gsdmd
GSM687185
GSM687184
GSM687183
GSM687182
GSM687181
GSM687180
GSM687179
GSM605713
GSM605709
GSM605708
GSM605707
GSM605706
GSM605705
GSM605704
GSM605703
GSM605702
GSM534256
GSM534255
GSM534254
GSM534253
GSM534252
GSM418234
GSM1370599
GSM1370598
GSM1370593
GSM1370592
GSM1370591
GSM1370590
GSM1370589
GSM1370588
GSM1197195
GSM1197194
GSM1139906
GSM1139905
GSM1139904
GSM1139903
GSM1139902
GSM1139901
2,26
7,14
12,02
C
GSM1197194
GSM1197195
GSM1370588
GSM1370589
GSM1370590
GSM1370591
GSM1370592
GSM1370593
GSM534252
GSM534253
GSM534254
GSM534255
GSM605702
GSM605703
GSM605704
GSM605705
GSM605706
GSM605707
GSM605708
GSM605709
GSM687179
GSM687180
GSM687181
GSM687182
GSM687183
GSM687184
Casp1
Casp2
Casp3
Casp4
Casp6
Casp7
Casp8
Casp9
Casp12
Casp14
-2,19
1,35
4,88
D
WT
P2rx7-/-
Untreated
BzATP 0.1 mM
BzATP 0.3 mM
Untreated
BzATP 0.3 mM
15.7
36.3
64.4
9.24
11.6
Caspases
Caspases+ cells (% of Tfh)
ns
WT untreated
WT BzATP 0.1 mM
WT BzATP 0.3 mM
P2rx7-/- untreated
P2rx7-/- 0.3 mM
E
WT
P2rx7-/-
GSDMDFL
GSDMDNterm
Actin
BzATP
GSDMDNterm/GSDMDFL
WT untreated
WT BzATP 0.3 mM
P2rx7-/- untreated
P2rx7-/- BzATP 0.3 mM

Figure 6. P2X7 mediated caspase activation and Gsdmd cleavage in Tfh cells. (**A**) Time-monitoring of YO-PRO-1 uptake after stimulation with BzATP in $ICOS^{-}PD\text{-}1^{-}$ and $ICOS^{+}PD\text{-}1^{+}$ cells within $CXCR5^{+}$ $CD4^{+}$ T cells from spleen of WT and *P2rx7*$^{-/-}$ mice, and frequency of responding cells in the two subsets from WT mice (n=13). (**B**) Heat-map representing the log2 expression levels of genes encoding mouse gasdermins in CD4 naïve and Tfh cells based on data derived from publicly available gene expression data sets (numbers on the left are accession codes). (**C**) Heat-map showing fold changes of caspases in Tfh compared to naïve CD4 cells (accession codes on top). (**D**) FACS analysis and statistics of caspase activation in purified WT and *P2rx7*$^{-/-}$ Tfh cells upon stimulation with BzATP as indicated (n=4). (**E**) Representative WB of full length and caspase cleaved Gsdmd (FL and Nterm, respectively), and actin on WT and *P2rx7*$^{-/-}$ Tfh cells either untreated or stimulated with BzATP. Histograms show the statistics of $Gsdmd^{Nterm}$/ $Gsdmd^{FL}$ ratio in the indicated conditions (n=4). Bar graphs: mean ± SEM. Two-tailed Mann-Whitney U test. *p<0.05; **p<0.01; ****p<0.0001.

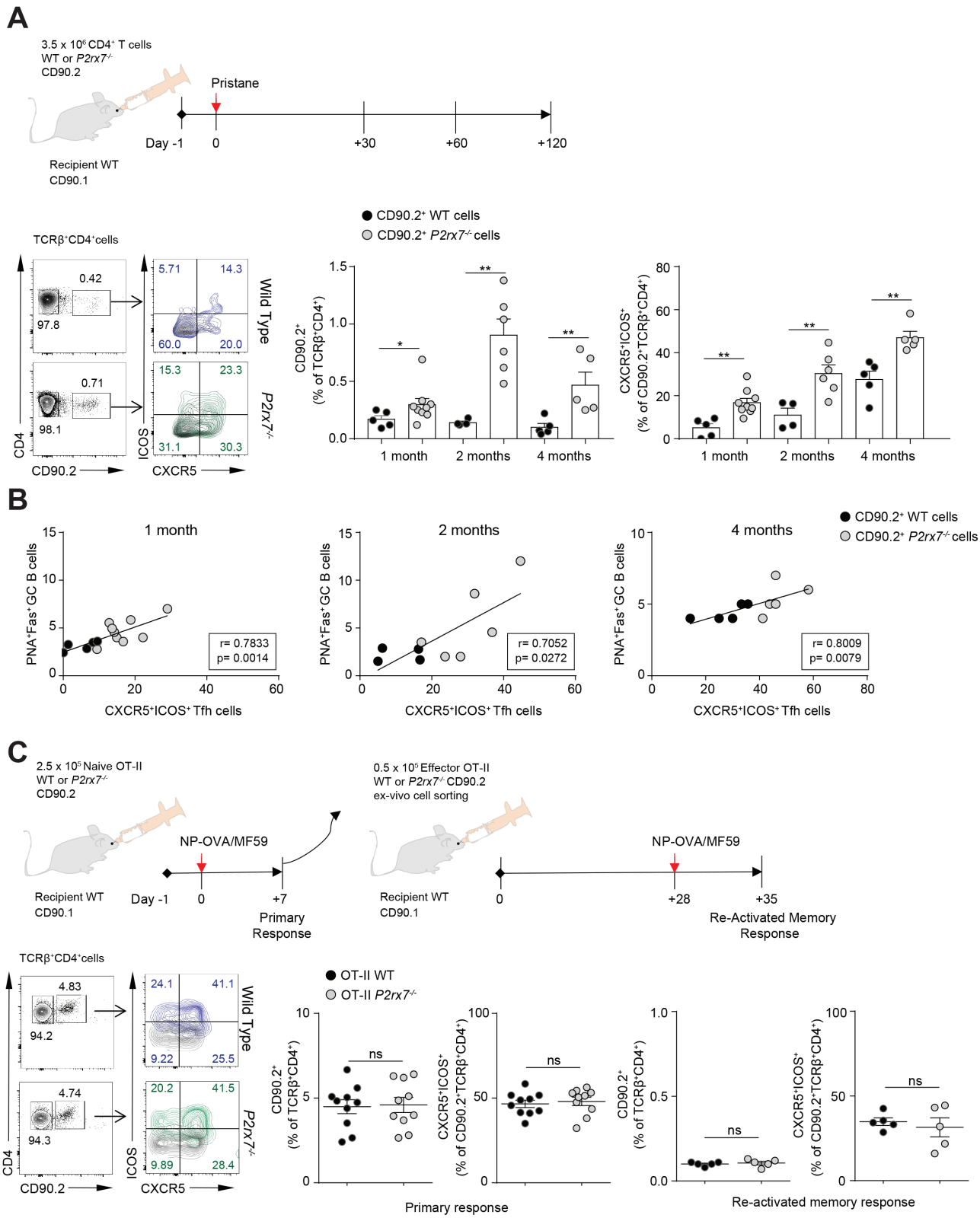
A
3.5 x 10⁶ CD4⁺ T cells
WT or P2rx7⁻/⁻
CD90.2
Pristane
Day -1
0
+30
+60
+120
Recipient WT
CD90.1
TCRβ⁺CD4⁺cells
0.42
97.8
0.71
98.1
5.71
14.3
60.0
20.0
15.3
23.3
31.1
30.3
Wild Type
P2rx7⁻/⁻
CD4
CD90.2
ICOS
CXCR5
CD90.2⁺ WT cells
CD90.2⁺ P2rx7⁻/⁻ cells
CD90.2⁺ (% of TCRβ⁺CD4⁺)
CXCR5⁺ICOS⁺ (% of CD90.2⁺TCRβ⁺CD4⁺)
1 month
2 months
4 months
B
1 month
2 months
4 months
PNA⁺Fas⁺ GC B cells
CXCR5⁺ICOS⁺ Tfh cells
r= 0.7833
p= 0.0014
r= 0.7052
p= 0.0272
r= 0.8009
p= 0.0079
C
2.5 x 10⁵ Naive OT-II
WT or P2rx7⁻/⁻
CD90.2
NP-OVA/MF59
Recipient WT
CD90.1
Day -1
0
+7
Primary
Response
0.5 x 10⁵ Effector OT-II
WT or P2rx7⁻/⁻ CD90.2
ex-vivo cell sorting
Recipient WT
CD90.1
0
+28
+35
Re-Activated Memory
Response
TCRβ⁺CD4⁺cells
4.83
94.2
4.74
94.3
24.1
41.1
9.22
25.5
20.2
41.5
9.89
28.4
Wild Type
P2rx7⁻/⁻
CD4
CD90.2
ICOS
CXCR5
OT-II WT
OT-II P2rx7⁻/⁻
CD90.2⁺ (% of TCRβ⁺CD4⁺)
CXCR5⁺ICOS⁺ (% of CD90.2⁺TCRβ⁺CD4⁺)
ns
Primary response
Re-activated memory response

Figure 7. Selective expansion of *P2rx7*$^{-/-}$ Tfh cells upon pristane injection but not conventional immunization. (**A**) Scheme of the adoptive transfer and pristane administration experiment, representative plots of CD90.2^{+} donor CD4^{+} T cells from spleen at 2 months post-transfer, frequency of recovered donor CXCR5^{+}ICOS^{+} CD4^{+} T cells within individual mice at 1, 2 and 4 months post-injection of pristane (mean ± SEM). (**B**) Correlation between GC B cells and donor Tfh cell frequencies at the indicated time points. The correlation coefficient r and the respective p value were calculated with nonparametric Spearman test. (**C**) Scheme of the adoptive transfer and immunization experiment, representative plots of donor CD4^{+} and CXCR5^{+}ICOS^{+} T cells within transgenic cells recovered from the draining lymph nodes of recipient mice 1 week after primary immunization and frequency of recovered donor cells within individual mice after primary immunization and secondary response (mean ± SEM). Two-tailed Mann-Whitney U test. *p<0.05; **p<0.01; ***p<0.001.

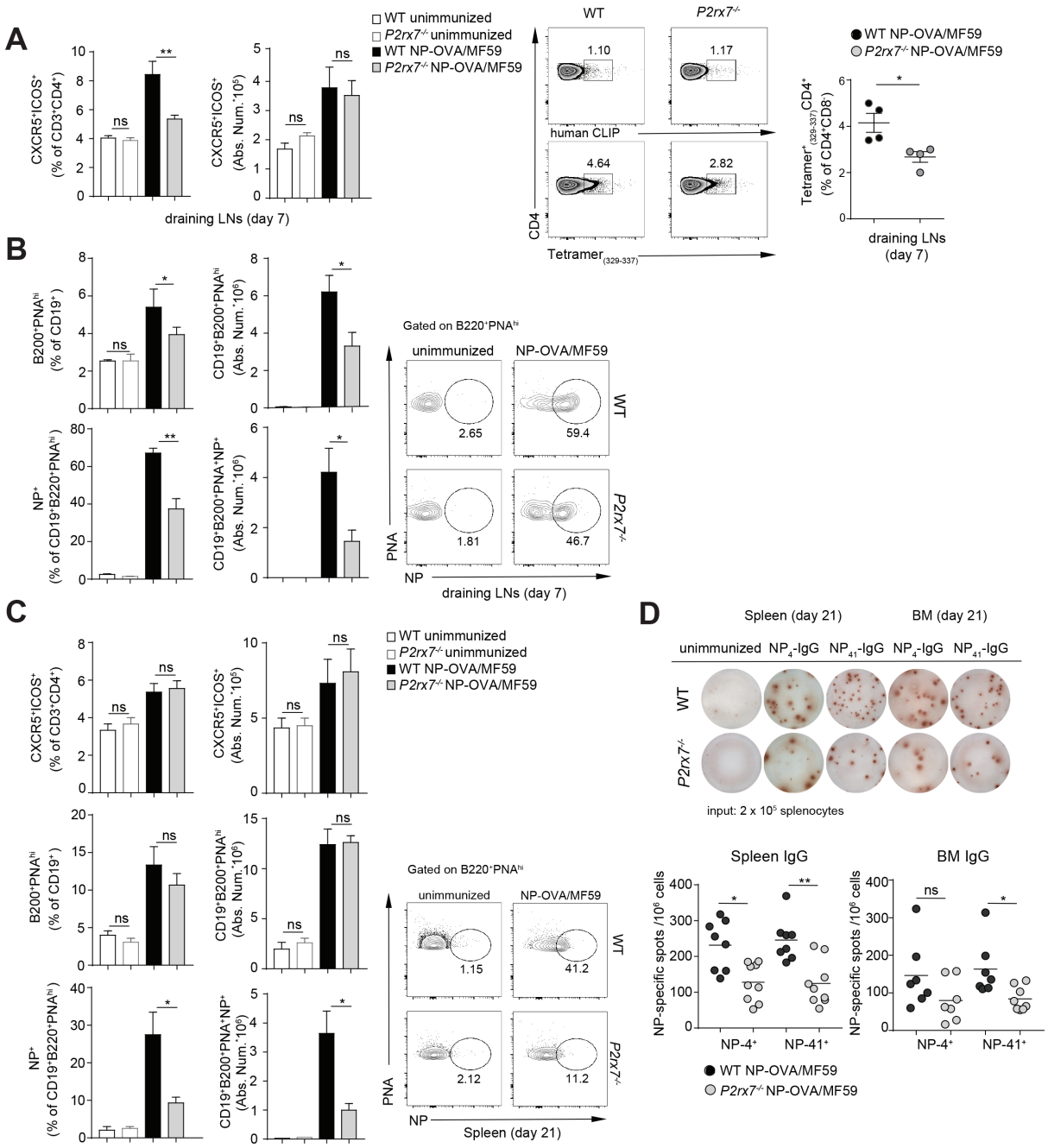

Figure 8. Impaired primary and secondary responses to NP-Ovalbumin in *P2rx7*$^{-/-}$ mice. (**A**) Frequency and absolute number of CXCR5^{+}ICOS^{+} Tfh cells in the draining lymph nodes from untreated or immunized WT and *P2rx7*$^{-/-}$ mice at 1 wk after s.c. injection of NP-OVA in MF59, representative contour plots of staining with human CLIP and OVA tetramers, and statistics of OVA tetramer positive cells. (**B**) Frequency and absolute number of GC B cells (same samples as above) gated as PNA^{hi}B220^{+} among CD19^{+} B cells (upper bar graphs) and of NP-positive GC B cells (lower bar graphs) with representative contour plots. (**C**) Frequency and absolute number of CXCR5^{+}ICOS^{+} Tfh cells (upper bar graphs), GC B cells (middle bar graphs) and NP-positive GC B cells (lower bar graphs) in the spleen of the indicated mice within secondary response to NP-OVA. (**D**) Representative ELISpot assay for antigen specific IgG secreting cells in the spleen and bone marrow of immunized mice during secondary response and statistics (lower panel). Unpaired Student T test. *p<0.05; **p<0.01.

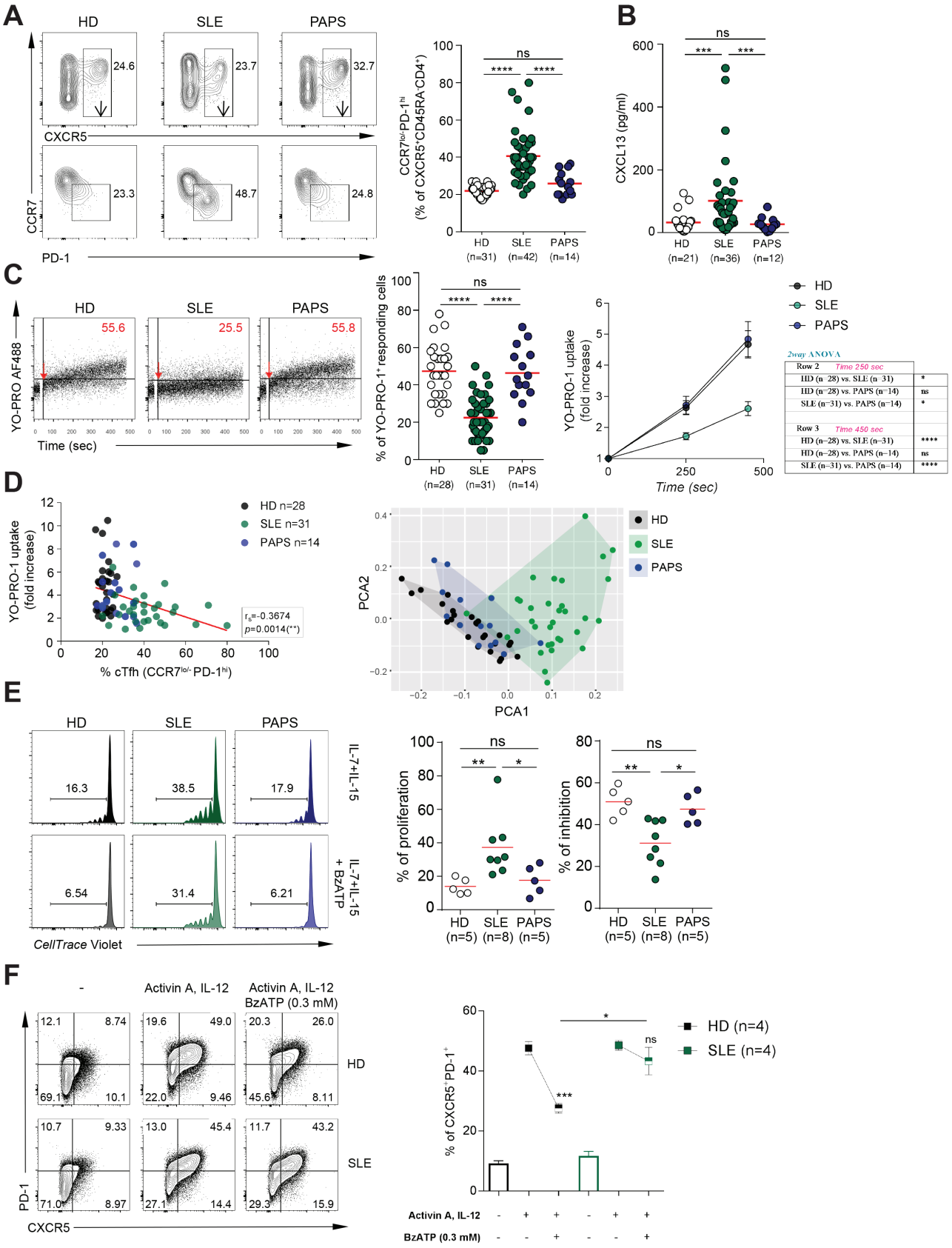
A
HD
SLE
PAPS
24.6
23.7
32.7
CXCR5
23.3
48.7
24.8
CCR7
PD-1
CCR7lo/-PD-1hi (% of CXCR5+CD45RA-CD4+)
ns
****
HD (n=31)
SLE (n=42)
PAPS (n=14)
B
CXCL13 (pg/ml)
***
HD (n=21)
SLE (n=36)
PAPS (n=12)
C
YO-PRO AF488
55.6
25.5
55.8
Time (sec)
% of YO-PRO-1+ responding cells
HD (n=28)
SLE (n=31)
PAPS (n=14)
YO-PRO-1 uptake (fold increase)
Time (sec)
2way ANOVA
Row 2 Time 250 sec
HD (n=28) vs. SLE (n=31) *
HD (n=28) vs. PAPS (n=14) ns
SLE (n=31) vs. PAPS (n=14) *
Row 3 Time 450 sec
HD (n=28) vs. SLE (n=31) ****
HD (n=28) vs. PAPS (n=14) ns
SLE (n=31) vs. PAPS (n=14) ****
D
YO-PRO-1 uptake (fold increase)
HD n=28
SLE n=31
PAPS n=14
rs=-0.3674
p=0.0014(**)
% cTfh (CCR7lo/-PD-1hi)
PCA2
PCA1
E
IL-7+IL-15
IL-7+IL-15 + BzATP
16.3
38.5
17.9
6.54
31.4
6.21
CellTrace Violet
% of proliferation
% of inhibition
HD (n=5)
SLE (n=8)
PAPS (n=5)
F
-
Activin A, IL-12
Activin A, IL-12 BzATP (0.3 mM)
12.1
8.74
69.1
10.1
19.6
49.0
22.0
9.46
20.3
26.0
45.6
8.11
10.7
9.33
71.0
8.97
13.0
45.4
27.1
14.4
11.7
43.2
29.3
15.9
PD-1
CXCR5
% of CXCR5+PD-1+
HD (n=4)
SLE (n=4)
Activin A, IL-12
BzATP (0.3 mM)

Figure 9. Frequency of cTfh cells and P2X7-mediated regulation in healthy subjects, SLE and PAPS patients. (**A**) Representative dot plots for $CXCR5^{+}$ cells and $CCR7^{lo/-}PD\text{-}1^{hi}$ cells within cTfh cells of the indicated subjects and frequency of $CCR7^{lo/-}PD\text{-}1^{hi}$ cells within cTfh cells in HD, SLE and PAPS subjects. Two-tailed Mann-Whitney U test. (**B**) Serum CXCL13 concentration in HD, SLE and PAPS subjects. (**C**) Representative time-monitoring of YO-PRO-1 uptake in $CD14^{-}CD4^{+}CD45RA^{-}CXCR5^{+}CCR7^{lo/-}PD\text{-}1^{hi}$ cTfh cells from PBMCs of the indicated subjects after stimulation with BzATP. Statistics of YO-PRO-1 permeable cells (two-tailed Mann-Whitney U test) and YO-PRO-1 uptake expressed as fold increase of mean fluorescence intensity at 250 and 450 sec (two-way ANOVA multiple comparisons, with Bonferroni's correction) are shown. (**D**) Correlation of fold increase in YO-PRO-1 uptake at 450 sec and percentage of cTfh cells. The correlation coefficient r and the respective p value were calculated with nonparametric Spearman test (upper graph). PCA of HD, SLE and PAPS patients according to % cTfh cells, % YO-PRO-1^{+} cTfh cells and YO-PRO-1 uptake at 450 sec. Areas of spreading are highlighted to better visualize segregation of groups of subjects (lower graph). (**E**) Representative histograms of CellTrace Violet (CTV) dilution in purified $CXCR5^{+}CD4^{+}$ cells from the indicated subjects after 7 d culture in the presence of IL-7 and IL-15 either without or with BzATP. Percentages of proliferating cells within the marker are indicated. Statistics for proliferation and inhibition of proliferation by BzATP (two-tailed Mann-Whitney U test). (**F**) Representative contour plots for *in vitro* differentiation of naïve CD4 cells from HD and SLE donors into Tfh cells in the presence of the indicated stimuli and statistics (Student T test). *$p<0.05$; **$p<0.01$; ***$p<0.001$; ****$p<0.0001$.

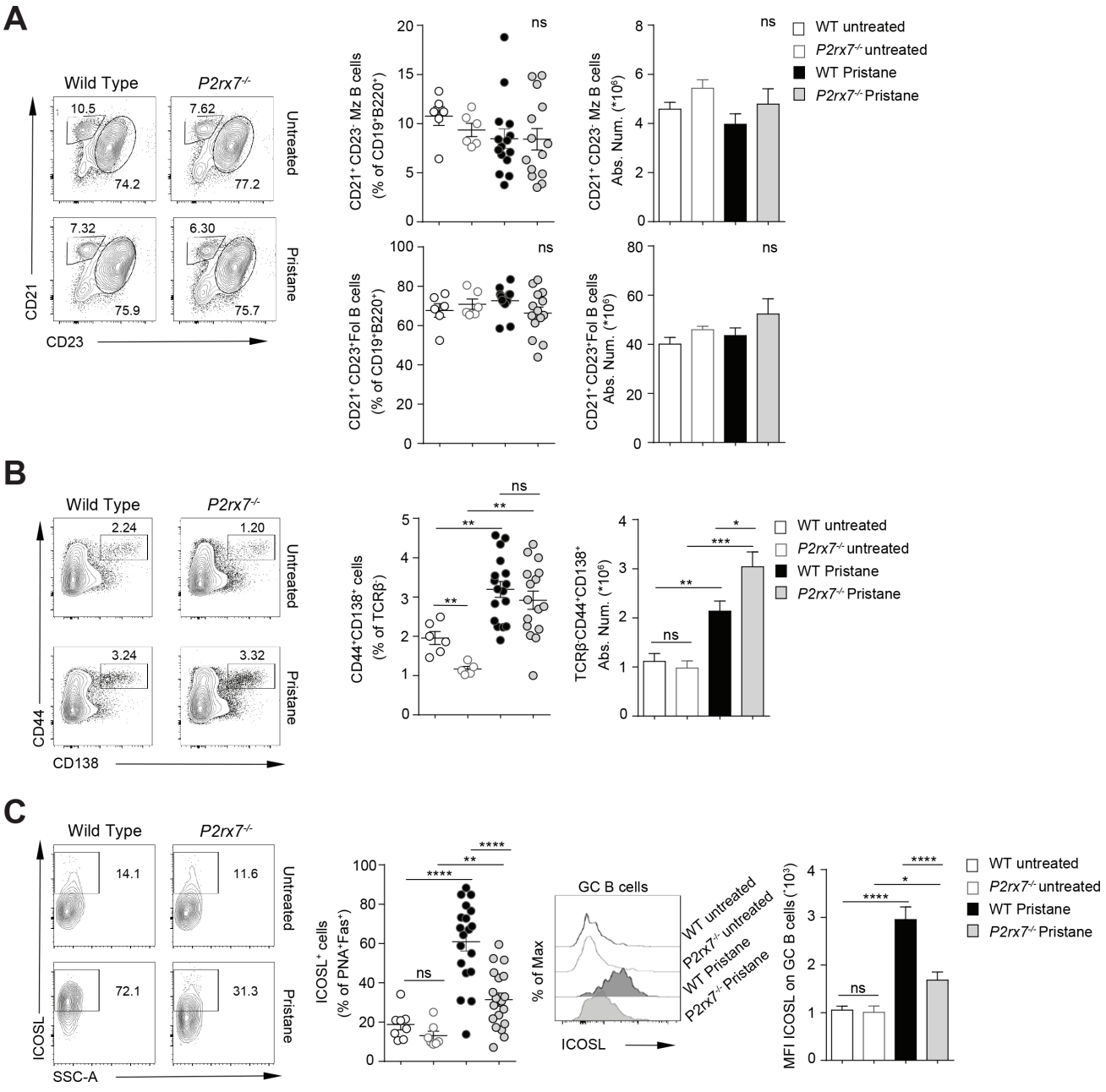

Figure S1. Phenotypic analysis of B cells in WT and *P2rx7*$^{-/-}$ mice. (**A**) Representative contour plots of B2 B cells in the spleen of WT and *P2rx7*$^{-/-}$ mice. Frequencies and absolute numbers from untreated WT (n=6) and *P2rx7*$^{-/-}$ (n=6) mice and treated WT (n=15) and *P2rx7*$^{-/-}$ (n=14) mice of marginal zone (Mz) and follicular (Fol) B cells gated as CD21^{+}CD23^{-} and CD21^{lo}CD23^{+} cells (as depicted in dot plots), respectively, among CD19^{+}B220^{+} total B cells. (**B**) Representative contour plots, relative frequency and absolute number of splenic plasma cells gated as TCRβ^{-}CD138^{+}CD44^{+} cells from untreated WT (n=6) and *P2rx7*$^{-/-}$ (n=5) mice and treated WT (n=17) and *P2rx7*$^{-/-}$ (n=16) mice. (**C**) Representative dot plots and statistics of ICOSL^{+} cells frequency within PNA^{+}Fas^{+} GC B cells from untreated WT (n=8) and *P2rx7*$^{-/-}$ (n=7) mice and treated WT (n=19) and *P2rx7*$^{-/-}$ (n=19) mice, representative histograms and statistics of ICOSL MFI. Two-tailed Mann-Whitney U test. Data in bar graphs are represent as mean ± SEM . *p<0.05; **p<0.01; ***p<0.001; ****p<0.0001.

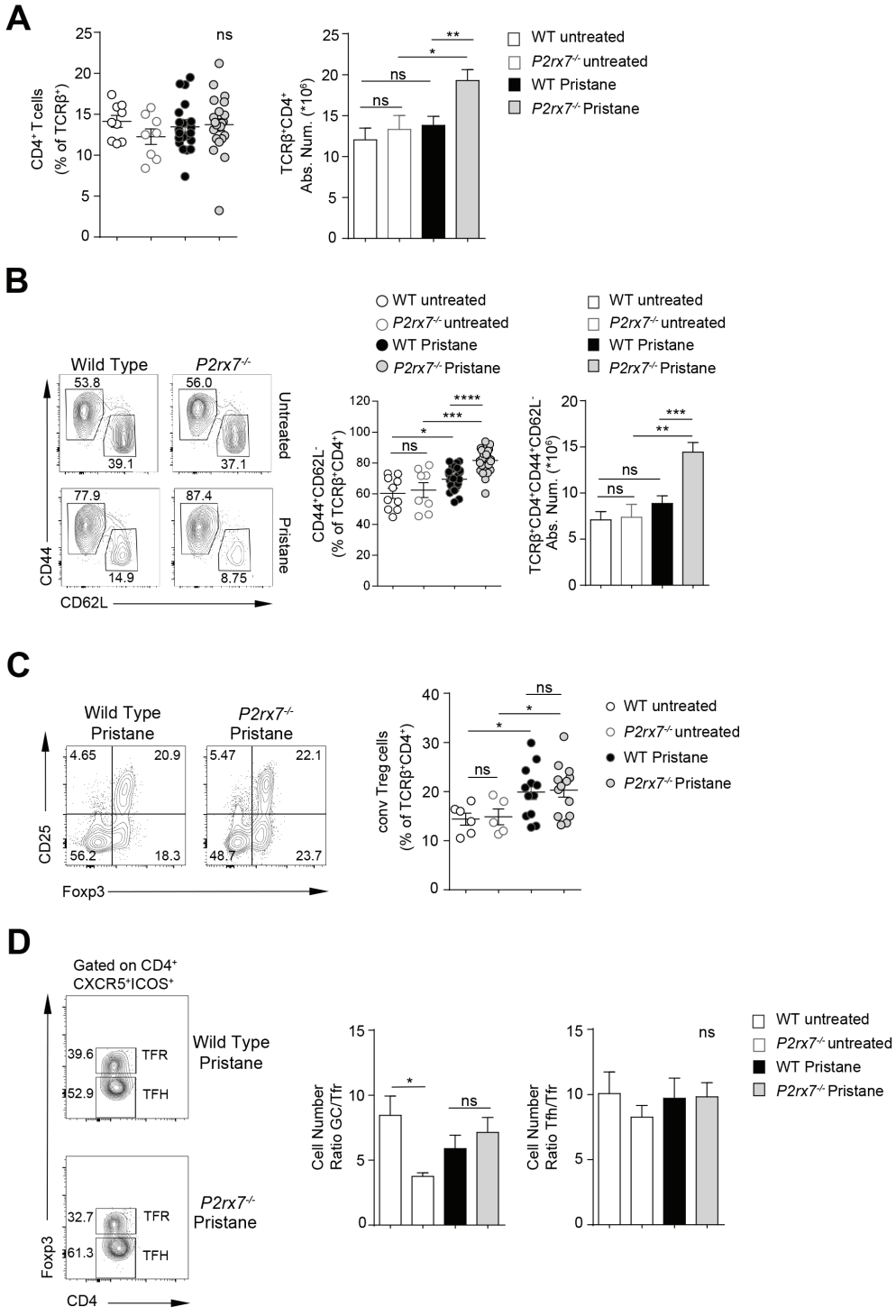

Figure S2. Distribution of CD4$^+$ T cells in untreated and treated WT and *P2rx7*$^{-/-}$ mice. (**A**) Frequency and absolute number of splenic CD4$^+$ T cells from untreated WT (n=9), *P2rx7*$^{-/-}$ (n=8), treated WT (n=23) and *P2rx7*$^{-/-}$ (n=22) mice. (**B**) CD44 and CD62L staining of TCRβ$^+$CD4$^+$ cells. Numbers indicate percentages of CD44$^+$CD62L$^-$ (effector) and CD44$^-$ CD62L$^+$ (naïve) cells within displayed quadrants; untreated WT (n=10), *P2rx7*$^{-/-}$ (n=8), treated WT (n=29) and *P2rx7*$^{-/-}$ (n=29). (**C**) Representative contour plots for CD25 and Foxp3 on gated CD4$^+$ T cells and frequency of conventional Tregs in the spleen of the indicated mice. (**D**) Representative contour plots used to define Tfh and Tfr cells on gated CXCR5$^+$ICOS$^+$ CD4$^+$ T cells. Bar graphs (mean± SEM) represent ratios of GC B/Tfr (left) and Tfh/Tfr (right) cells in the spleen of the indicated mice. Two-tailed Mann-Whitney U test. *p<0.05; **p<0.01; ***p<0.001.

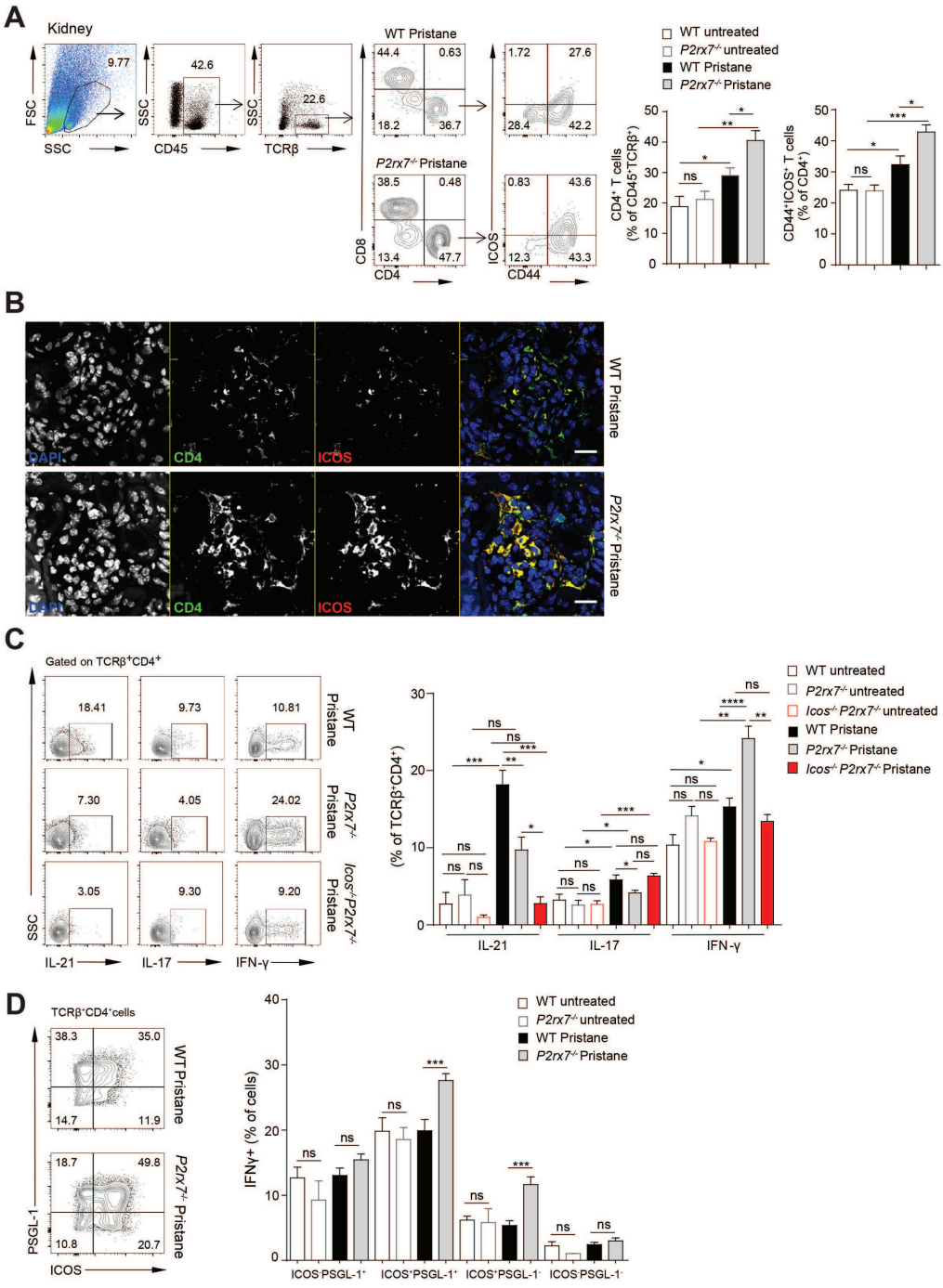

Figure S3. Increase of ICOS$^+$ CD4 T cells in kidneys and IFN-γ secreting CD4 cells selectively within ICOS$^+$ cells in pristane treated *P2rx7*$^{-/-}$ mice. (**A**) Gating strategy for quantifying kidney-infiltrating CD44$^+$ICOS$^+$ effector CD4 T cells, and frequency of CD4$^+$ and CD44$^+$ICOS$^+$ T cells from at least 5 animals. Mean ± SEM, two-tailed Mann-Whitney U test. (**B**) Representative confocal immunofluorescence images of fixed kidney cryosection stained with anti-CD4 (green), anti-ICOS (red) antibodies and DAPI (blue) showing ICOS$^+$ T cells within glomeruli of WT and *P2rx7*$^{-/-}$ mice. Scale bar corresponds to 20 µm. (**C**) Representative contour plots for intracellular staining of IL-21, IL-17 and IFN-γ in CD4$^+$ T cells from spleen of pristane treated WT, *P2rx7*$^{-/-}$ and *Icos*$^{-/-}$*P2rx7*$^{-/-}$ mice and frequencies. (**D**) Representative contour plots for ICOS and PSGL-1 staining among CD4$^+$ T cells from spleen of pristane treated WT and *P2rx7*$^{-/-}$ mice, and frequency of IFN-γ secreting cells within the indicated subsets. Mean ± SEM (n= 2 independent experiments with at least 5 mice). Student T test. *p<0.05; **p<0.01; ***p<0.001; ****p<0.0001.

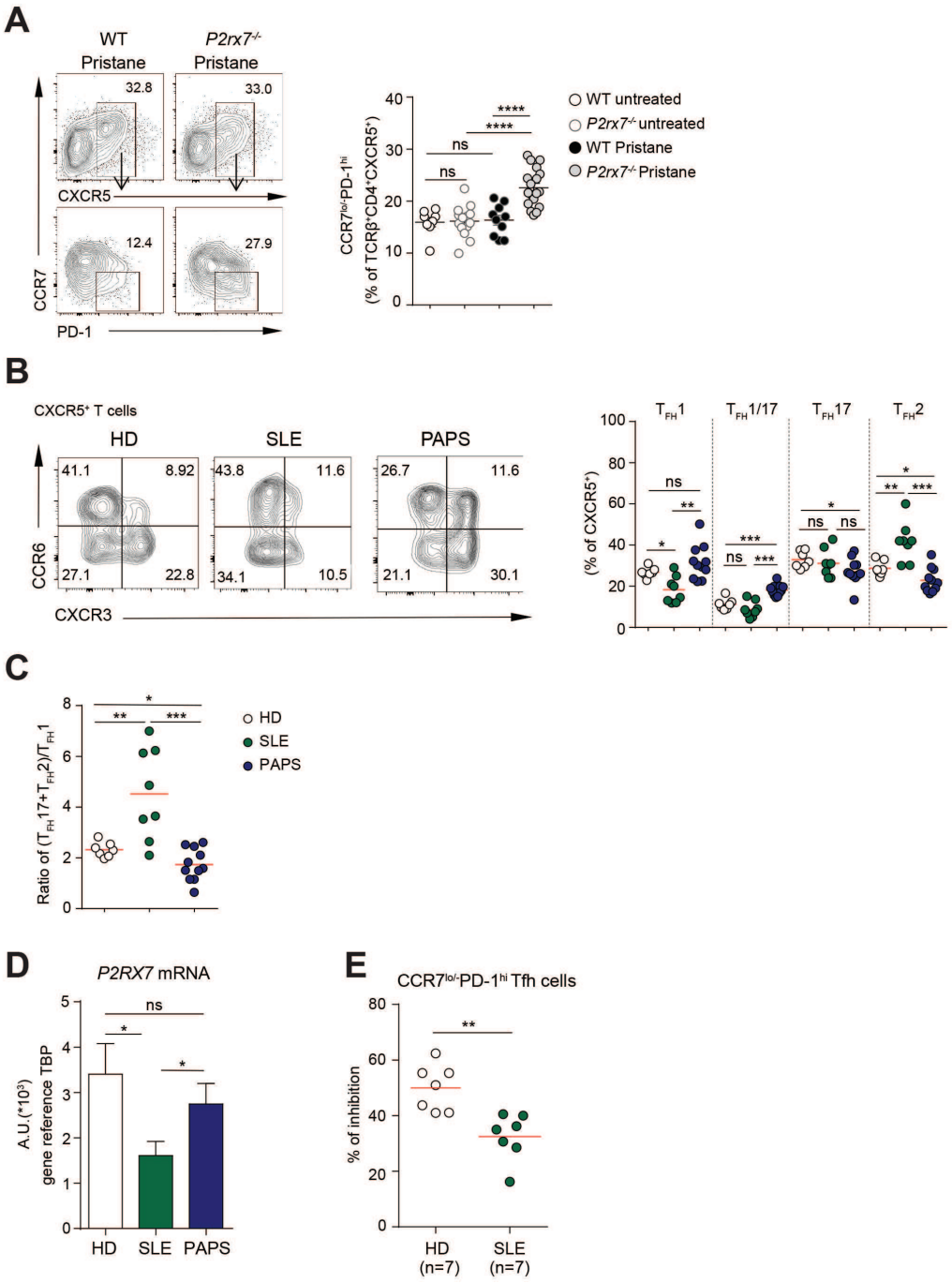

Figure S4. Increased representation of CCR7$^{lo/-}$PD-1^{hi} CD4 cells in pristane treated *P2rx7*$^{-/-}$ mice, distribution of functional cTfh cell subsets and *P2RX7* mRNA levels in CXCR5^{+} cells from HD, SLE and PAPS patients, inhibition of CCR7$^{lo/-}$PD-1^{hi} Tfh cells proliferation by BzATP. (**A**) Representative contour plots for CXCR5 as well as CCR7 and PD-1 among CXCR5^{+} CD4 T cells, and frequency of CCR7$^{lo/-}$PD-1^{hi} CD4 Tfh cells in the spleen of indicated mice. (**B**) Representative contour plots of CXCR5^{+} cTfh cells from HD, SLE and PAPS subjects for CCR6 and CXCR3, and distribution of Tfh1, Tfh1/17, Tfh17 and Tfh2 cells in individual subjects from different groups (see Results for details). (**C**) Ratio between (Tfh17+Tfh2) and Tfh1 cells in different subjects. (**D**) Semi-quantitative RT-PCR analysis of *P2RX7* transcripts in sorted CXCR5^{+} CD4 T cells from HD, SLE and PAPS donors (n=10, A.U.: arbitrary units). (**E**) Percentage inhibition of proliferation by BzATP in sorted CCR7$^{lo/-}$PD-1^{hi} Tfh cells from HD and SLE individual subjects at day 7 of stimulation with IL-7 and IL-15. Mean ± SEM are shown in bar graph. Two-tailed Mann-Whitney U test. *p<0.05; **p<0.01; ***p<0.001; ****p<0.0001.

Table S1. Demographic, clinical and laboratory characteristics of SLE and PAPS patients and healthy donors

Characteristics	SLE (n=42)	PAPS (=14)	HD (=31)
Female/Male, n	41/1	8/6	29/2
Age, years, median (range)	43 (26-76)	51 (39-68)	41 (25-62)
Disease duration, years, median (range)	17 (0.5-48)	13.65 (2-24)	na
Onset <18 years, n (%)	12 (28)	0 (0)	na
Laboratory tests			
ANA positivity (%)	40 (95)	6 (42.8)	na
anti-ENA positivity	19 (45)	0 (0)	na
anti-SSA/Ro, n (%)	13 (30.9)	na	na
anti-Sm, n (%)	6 (14.3)	na	na
anti-RNP, n (%)	6 (14.3)	na	na
*anti-dsDNA positivity, n (%)	22 (52.4)	1 (7.14)	na
low titre, n (%)	7 (16.7)	1 (7.14)	na
medium/high titre, n (%)	15 (36)	0 (0)	na
LA, n (%)	12 (28.5)	13 (93)	na
[ç]anti-β2GPI IgG, n (%)	5 (11.9)	12 (85.7)	na
[ç]anti-β2GPI IgM, n (%)	2 (4.7)	5 (35.7)	na
[ç]anti-CL IgG, n (%)	7 (16.6)	13 (92.8)	na
[ç]anti-CL IgM, n (%)	2 (4.7)	2 (14.3)	na
°Low C3, n (%)	19 (45.2)	4 (28.6)	na
°Low C4, n (%)	27 (64.3)	7 (50)	na
[§]Hypergammaglobulinemia, n (%)	14 (33)	3 (21)	na
Clinical manifestations (ever)			
SLEDAI-2K, median (IQR)	4 (2-6)	na	na
Skin rash,n (%)	9 (21.4)	na	na
Alopecia, n (%)	2 (4.76)	na	na
^Haematological involvement, n (%)	12 (28.6)	na	na
Arthritis, n (%)	11 (26)	na	na
Myositis, n (%)	1 (2.4)	na	na
Glomerulonephritis, n (%)	2 (4.76)	na	na
Thrombotic APS, n (%)	6 (14)	11 (78.6)	na
Obstetric APS, (%)	0 (0)	14 (28.6)	na
Therapy			
Equivalent prednisone dose			
cumulative dose, mg, median (IQR)	36.5 (15-58.4)	na	na
daily dose, mg/die, median (IQR)	5 (2.5-10)	na	na
Ongoing DMARDs			
Hydroxychloroquine, n (%)	28 (66.7)	9 (64)	na
Mycophenolate Mofetil, n (%)	8 (19)	1 (7)	na
Azathioprine, n (%)	5 (11.9)	0 (0)	na
Methotrexate, n (%)	3 (7)	0 (0)	na
Cyclosporine, n (%)	5 (11.9)	0 (0)	na

anti-CL: anti-cardiolipin, anti-β2GPI: anti-β2glycoprotein I, ANA: anti-nuclear antibodies, APS: anti-phospholipid syndrome, anti-ENA: anti-extractable anti-nuclear antigens; IQR: inter-quartile range; DMARDs (Disease-Modifying Anti-rheumatic Drugs); na: not applicable.
[§]Hypergammaglobulinemia: >20% of total serum proteins
[ϛ]Anti-β2GPI and anti-CL positivity was defined as medium/high titre according to 2006 revised classification criteria for APS (>99° percentile for anti-β2GPI and >40 GPL/MPL for anti-CL) (Miyakis et al., 2006)
GPL/MPL refers to IgG/IgM anti-Phospholipid Units

°Low C3 was defined as <80 mg/dL; low C4 as <15 mg/dL
^Haematological involvement: leukopenia, thrombocytopenia, Coombs positive haemolytic anemia based on SLEDAI-2K definitions (Gladman et al., 2002). LA: lupus anticoagulans, PAPS: primary APS
*anti-dsDNA have been detected as previously reported (Ingegnoli et al., 2014). anti-dsDNA titres were defined as low if <40 UI/mL, medium/high if >40 UI/mL.